Custom-made receiver mixer MMIC front-end for X-band radars

Michaelsen, Rasmus Schandorph

Publication date:
2016

Document Version
Publisher's PDF, also known as Version of record

Custom-made receiver mixer MMIC front-end for X-band radars

Ph.D. Thesis

Rasmus Schandorph Michaelsen

February 2016

The present work was carried out at DTU Elektro and Weibel Scientific A/S in partial fulfilment of the requirements for the Ph.D. degree from the Technical University of Denmark.

Supervisors:

Tom Keinicke Johansen
Electromagnetic Systems, DTU Elektro, Technical University of Denmark.

Kjeld M. Tamborg
Weibel Scientific A/S.

To my lovely girls.

Abstract

Monolithic Microwave Integrated Circuit (MMIC) Mixers in Silicon-Germanium (SiGe) technology for direct conversion suitable for X-band Doppler radars have been investigated. The mixers are passive double balanced diode mixers, as these have the properties of good linearity and low noise, together with isolation between all ports.

An investigation into how Local Oscillator (LO)-leakage and DC-level influences the flicker noise of the mixers was conducted. It showed that the DC level is critical in regard to minimize the flicker noise, where a zero volt DC level gives minimum noise. And that the DC-level is a function of LO-leakage due to self-mixing.

This led to the idea of mixers where the LO-leakage can be controlled. It is proposed to use a balun with tunable phase balance to control the LO-leakage. A novel Marchand balun configuration which allows this is described. Experimental results showed a tuning range from -183° to -175.8°. This circuit is used as the crucial building block in an experiment comparing three mixers. Two mixers with tunable balun on the LO port, one with diode connected HBTs and the other with Schottky diodes. And a reference mixer for comparison, with diode connected Heterojunction Bipolar Transistor (HBT)s, but without the tuning circuit. These are all manufactured in a SiGe technology. Unfortunately the diode connected HBT mixer was short circuited on the control voltage, only allowing comparison between the Schottky mixer with tuning and the HBT mixer without this option implemented. It is shown that by tuning the balun one can enhance linearity and isolation of the mixer, but not 1/f noise. They both have a conversion loss around 9 dB. The HBT mixer has a flicker noise corner around 10 kHz while the Schottky mixer has one around 250 kHz.

The low Quality factor (Q) inductors used for the Marchand baluns and matching have rather high loss. Techniques to overcome this loss are investigated. Suggestions for an active balun and a novel Marchand balun with complex matching are given, and two mixers are designed with these, with promising results for Doppler radar applications.

Resumé

MMIC miksere til direkte konvertering brugbare i X-bånds Doppler radarer er blevet undersøgt. Mikserne er passive dobbelt balancerede diode miksere, da disse har egenskaberne: god linearitet og lav støj sammen med isolation mellem alle porte.

Det er blevet undersøgt hvordan LO-læk og DC-niveau har indflydelse på 'flicker' støjen i mikserne. Den viste at DC-niveauet er kritisk i forhold til at minimere 'flicker' støjen. Samt at DC-niveauet er en funktion af LO-lækken.

Dette førte til ideen om miksere hvor LO-lækken kan blive styret. Styringskredsløbet er en 'balun' med tunbar fasebalance. En ny Marchand 'balun' struktur, der tillader dette, er beskrevet, sammen med en grundig beskrivelse af 'lumped element' implementeringen af Marchand 'balun'en. Eksperimenelle resultater viser at det er muligt at opnå tuning fra $-183°$ til $-175.8°$. To miksere er fremstillet med tunbar 'balun' på LO porten, en med diode forbundne HBTer og en med Schottky dioder. Endnu en mikser med diode forbundne HBTer, men uden tuningskredsløb, er fremstillet til at sammenligne op imod. Uheldigvis er mikseren med diode forbundne HBTer kortsluttet på kontrolspændingen, således at det kun er muligt at sammenligne Schottky mikseren med tuning og den diode forbundne HBT mikser uden. Det er vist at ved at tune 'balun'en, kan man forbedre lineariteten og isolationen for mikseren. Med hensyn til konverteringstab er de to miksere ens, det ligger omkring 9 dB. Tilgengæld har HBT mikseren et 'flicker' støj hjørne omkring 10 kHz imens Schottky mikseren har et omkring 250 kHz.

Induktorerne med lav Q-værdi, der bliver brugt i Marchand 'balun'erne og til tilpasningskredsløb, har relativt højt tab. Derfor er teknikker til at undgå dette undersøgt. Design foreslag til en aktiv 'balun' og en ny Marchand 'balun' der tillader kompleks tilpasning er givet. Der er designet to miksere med disse og de viser lovende resultater for brug i Doppler radarer.

Preface

The PhD study presented in this thesis was carried out partly at Weibel Scientific and partly at the Electromagnetics Systems (EMS) group at the Department of Electrical Engineering at the Technical University of Denmark (DTU) between November 2011 and May 2015. The effective study period has been 36 months + 3 months extension. Financial support for the study was provided by Weibel Scientific and the Danish Industrial Ph.D. program. Associate Professor Tom Keinicke Johansen from DTU acted as project supervisor, with Kjeld Tamborg from Weibel Scientific as co-supervisor.

Acknowledgement

A lot of thanks to all people involved in the work.

I would like to thank my supervisors, Associate Prof. Tom K. Johansen and Kjeld M. Tamborg for the support and many good inputs throughout the entire project. A profound thank you to Associate Prof. Vitaliy Zhurbenko, for guiding and helping with the probestation and measurements.

Also a thanks to Peder Pedersen, president of Weibel, for believing in this project and my skills to carry it out. Thanks to all the good people at Weibel, especially Morten Aarøe, for helping me with design programs and stuff, and for interesting discussions somewhat related to my research.

Thanks to Lei Yan for sharing his office and helping me in the beginning of my Ph.D, and Öncel Acar for sharing thoughts and food, both helped me expand my view on specific matters or the world as a whole. Johan Mohr and Ulrik Nielsen for the swimming, sauna talks, about things related to the life of a Ph.D, and help with setting up a suitable LaTeX environment for this thesis.

Bo Brændstrup for fixing broken equipment, with short notice, during measurements.

To friends and family for support and encouragement. And last to my wonderful wife, Ann, who made every day a joy and blessed my life with two lovely daughters, Kastanje and Nova, one in the beginning and one in the end of this work. I have cherished every moment with the three of you.

List of publications

The following publications have been prepared during the study. The papers [JP1–JP3, CP1–CP5] are included at the end of the thesis, starting on page 79.

[JP1] R. Michaelsen, T. Johansen, K. Tamborg, and V. Zhurbenko, "A modified Marchand balun configuration with tunable phase balance", *IEEE Microwave and Wireless Components Letters*, vol. 23, no. 2, pp. 66–68, 2013.

[JP2] R. Michaelsen, T. Johansen, K. Tamborg, and V. Zhurbenko, "Design of a broadband passive X-band double-balanced mixer in SiGe HBT technology", *International Journal of Microwave and Wireless Technologies*, vol. 6, no. 3-4, pp. 235–242, 2014.

[JP3] R. Michaelsen, T. Johansen, L. Yan, K. Tamborg, and V. Zhurbenko, "A X-band Schottky diode mixer in SiGe technology with tunable balun", *Submitted to IEEE Transactions on Microwave Theory and Techniques*, 2015.

[CP1] R. Michaelsen, T. Johansen, and K. Tamborg, "Investigation of LO-leakage cancellation and DC-offset influence on flicker-noise in X-band mixers", in *Proceedings of the 7th European Microwave Integrated Circuit Conference*, 2012, pp. 99–102.

[CP2] R. Michaelsen, T. Johansen, K. Tamborg, and V. Zhurbenko, "A passive X-band double balanced mixer utilizing diode connected SiGe HBTs", in *Proceedings of the 8th European Microwave Integrated Circuits Conference*. IEEE, 2013, pp. 188–191.

[CP3] R. Michaelsen, T. Johansen, and K. Tamborg, "Analysis and design of complex impedance transforming Marchand baluns", in *Proceedings of 20th International Conference on Microwaves, Radar, and Wireless Communications*. IEEE, 2014.

[CP4] R. Michaelsen, T. Johansen, K. Tamborg, and M. Squartecchia, "Flicker noise comparison of direct conversion mixers using Schottky and HBT dioderings in SiGe:C BiCMOS technology", in *To be published at The International Workshop on Integrated Nonlinear Microwave and Millimetre-wave Circuits (INMMiC)*, IEEE, 2015.

[CP5] R. Michaelsen, T. Johansen, K. Tamborg, and V. Zhurbenko, "A SiGe BiCMOS double-balanced mixer with active balun for X-band doppler radar", in *Submitted to SBMO/IEEE MTT-S International Microwave and Optoelectronics Conference*, IEEE, 2015.

The publications [OP1, OP2] are based on work and results, which are obtained before the PhD project started, but the publications has been written and is published during the period of the PhD work.

[OP1] R. Michaelsen, T. Johansen, and V. Krozer, "Design of a x4 subharmonic submillimeter wave diode mixer, based on an analytic expression for small-signal conversion admittance parameters", in *2013 Microwave & Optoelectronics Conference (IMOC)*, IEEE, 2013.

[OP2] L. Yan, V. Krozer, R. Michaelsen, T. Djurhuus, and T. Johansen, "Physical based Schottky barrier diode modeling for THz applications", in *Proceedings of the 2013 IEEE International Wireless Symposium*. IEEE, 2013.

Contents

List of Figures

List of Tables

Acronyms

ADS Keysight's *Advanced Design System*.

BiCMOS Bipolar and Complementary Metal Oxide Semiconductor.

CMOS Complementary Metal Oxide Semiconductor.

$\mathbf{f_{max}}$ maximum oscillation frequency.

$\mathbf{f_t}$ unit current gain frequency.

FMCW Frequency Modulated Continous Wave.

HBT Heterojunction Bipolar Transistor.

I/Q In-phase and Quadrature.

IF Intermediate Frequency.

$\mathbf{IIP_2}$ input referred second order intercept point.

$\mathbf{IIP_3}$ input referred third order intercept point.

LNA Low Noise Amplifier.

LO Local Oscillator.

LVS Layout versus schematic.

MIM Metal-insulator-metal.

MMIC Monolithic Microwave Integrated Circuit.

MOS metal-oxide-semiconductor.

Q Quality factor.

RF Radio Frequency.

SiGe Silicon-Germanium.

SiGe:C Silicon-Germanium with Carbon doped base.

SMA SubMiniature version A connector.

1

Introduction

Doppler radars can be used for a lot of different purposes, among these defense and space applications [1], for measuring human vital signs [2] or in the automotive industry for different types of driving assistance [3, 4].

The Weibel Doppler radars are used for tracking ballistic targets. In Figure 1.1 a picture of one of the radars is shown. They employ Frequency Modulated Continous Wave (FMCW) for the tracking algorithm, this needs at least four receiver channels, each with two In-phase and Quadrature (I/Q) mixers operating at slightly different frequencies. That totals to at least sixteen mixers in the receiver front-end. Current generation of Weibel Doppler radar front-ends rely on hybrid mounting of devices, such as diodes and transistors. Furthermore, some of these components require custom bonding and tuning which is time-consuming and requires an experienced worker. Using MMIC technology makes mass production a possibility and gives good uniformity between any two circuits. The size of such circuitry is also much smaller than the one made with hybrid mounted devices, making it possible to have a large number of receivers on a single circuit board, as depicted in figure 1.2. If next generation Weibel Doppler radars are to utilize large phased array antennas, mass production and re-

Figure 1.1. Weibel radar

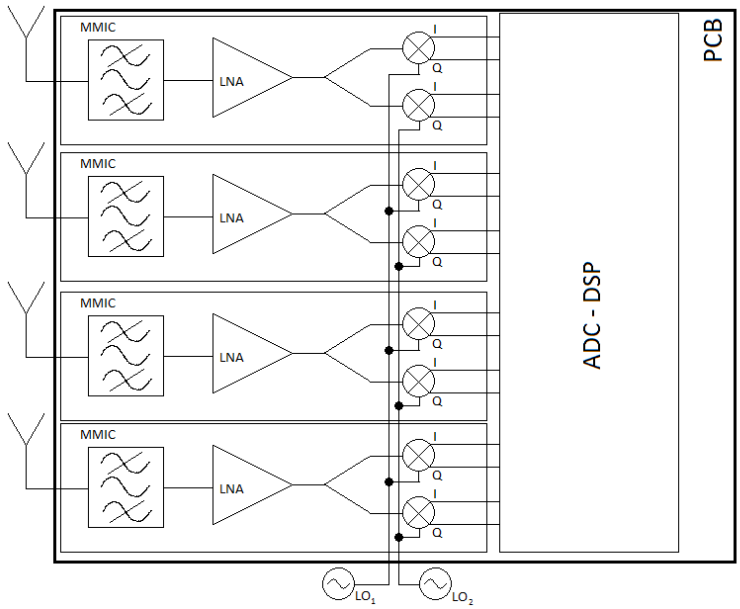

Figure 1.2. Radar receiver block diagram

liability is even more important. Due to the possibility of large integration density, together with high performance bipolar transistors a SiGe technology is chosen for the MMIC circuits.

A Doppler radar calculates the velocity of the target by measuring the Doppler shift of the returned radar signal. In these applications using direct conversion gives the Doppler shift and thus the speed measurement directly from the received frequency. Direct conversion receivers, is not only used for Doppler radars, they are also used in communication circuits to avoid complex image rejection structures [5].

Direct-conversion systems comes with drawbacks. One significant drawback is leakage, since the LO signal and Radio Frequency (RF) signal is at the same frequency and isolation between those is in many applications an important criteria. Another drawback is that, due to the low Intermediate Frequency (IF), it has an increased noise level due to low frequency noise. The low frequency noise is also called flicker noise and is caused by generation-recombination processes in the solid-state devices.

The key element in a direct conversion receiver is the mixer. Two fundamental types of direct conversion mixers exists, active and passive. Active mixers have the advantage of providing conversion gain, whereas passive mixers have the advantage of higher linearity and less noise. Structures for increasing linearity of active mixers have been proposed [6], but then suffers from increased noise. Thus the dynamic range remains largest for a passive mixer design. The main disadvantage of the passive mixer is the loss in the signal path. Passive mixers are recognized for their excellent low frequency noise performance.

The low frequency noise is influenced by the LO pump signal in a non-linear manner [7] and is generally believed to be present in passive mixers only if a non-zero net

average current flows through the mixing core. Bipolar devices are bulk conduction devices which have an order of magnitude lower 1/f noise compared to the surface channel conduction of Complementary Metal Oxide Semiconductor (CMOS) devices [8]. In general, Schottky diodes is preferred for implementing passive mixers because they are majority carrier devices and hence leads to lower conversion loss at higher frequencies than mixers built using pn-junction diodes [9]. Schottky diodes, however, are not standard elements in high performance Silicon technologies. Structures with low reverse leakage current have been proposed in a SiGe Bipolar and Complementary Metal Oxide Semiconductor (BiCMOS) technology [10], but little information is generally available about their noise performance at low frequencies.

The double balanced mixer ideally provides infinite isolation between all ports and is therefore a good choice to use as a mixer for direct conversion. Other benefits of the double balanced mixer is rejection of LO noise and high linearity [9]. These are all desired characteristics for mixers to be used in Doppler radars. Having built-in isolation in the mixer structure is important, as normal filtering is difficult due to the proximity of the RF and LO frequencies. The drawbacks are increased circuit complexity, higher LO-power requirement, and higher conversion loss. In double balanced mixers, flicker noise is believed to be caused by unavoidable asymmetries in the diode ring and balun structures.

In this thesis the focus will be on double balanced mixers for direct conversion. A technique for reduction of low frequency noise will be investigated. Novel balun configurations to reduce manufacturing uncertainties and loss in matching circuits will be suggested. Several mixers for direct conversion will be designed and measured.

1.1 Technology

All circuits are fabricated using a Silicon-Germanium with Carbon doped base (SiGe:C) BiCMOS process from Innovations for High Performance Microelectronics (IHP). It is a 0.25 μm technology, featuring high performance npn-HBTs having a unit current gain frequency (f_t) of 110 GHz and a maximum oscillation frequency (f_{max}) of 180 GHz. The process has Metal-insulator-metal (MIM)-capacitors, metal-oxide-semiconductor (MOS)-varactors and five metal layers of which the upper two are extra thick, intended for passives or low loss interconnects [11].

1.2 Thesis overview

In Chapter 2 an experiment is described, where the LO signal leakage is cancelled. It is investigated how this influences the DC-level and the 1/f-noise. This investigation leads to the belief that circuit techniques can improve the low frequency noise of SiGe:C circuits. In Chapter 3 one such circuit technique is investigated. Three passive mixers are designed and manufactured in IHPs SiGe:C technology, one without any enhancements with diode connected HBT's, another diode connected HBT mixer with a tunable balun and a Schottky diode mixer with tunable balun. To make this experiment the Marchand Balun is investigated and a modified version invented, which allows for phase-balance tuning. The passive structures are rather lossy in SiGe:C technology, so in Chapter 4 mixers with alternative balun structures is investigated.

One solution is an active balun, the other a Marchand balun with arbitrary impedance matching. Finally in Chapter 5 a conclusion is given together with suggestions for future work.

2 Investigations of LO leakage and DC level on $1/f$ noise

In this chapter an investigation on how LO leakage and the DC level in the mixer influences the 1/f noise is presented.

There have been many proposals to reduce 1/f noise in active mixers, common for many is that the steps used to reduce 1/f noise is to reduce the DC-bias current through the switching transistors. This either through a static principle [12] or using dynamic current injection [13, 14]. Also in passive transistor mixers a DC-offset results in an increased 1/f noise [15, 16]. In passive mixers where no bias is applied there still will be a DC-offset due to self mixing of the LO-signal that leak to the RF port.

In [17] a LO-leakage and DC-offset cancellation techniques is presented for direct conversion systems, and tested at 2.4 GHz. In this chapter the idea of this technique is expanded and used at X-band and tested using a 10.5 GHz system. There will be derived conditions for when LO-leakage cancellation is obtained and when zero DC-offset is obtained. With this knowledge improved direct-conversion designs can be a possibility. This chapter has previously been published in [CP1].

2.1 LO cancellation and DC offset

In a direct conversion system the LO and RF signal is at roughly the same frequencies. As the isolation between the LO an RF port of the mixer in practice will be finite, there will be some leakage from one to the other. In passive mixers, the LO drive level is typically quite high (many operates with a LO power of 7dBm or above [9]), this leads to a significant component of the LO signal at the RF-port. Instead of mixing the RF with the LO signal, actually it will be a sum of the RF and a leakage signal that is mixed with the LO signal. This self-mixing of the LO signal will give higher harmonic components and a DC offset.

It is proposed in [17], to use a cancellation signal to remove the leakage signal. Figure 2.1 shows a block diagram of the method and defines the signals. The output signal, due to leakage and cancellation signals, at the IF port will then be given by

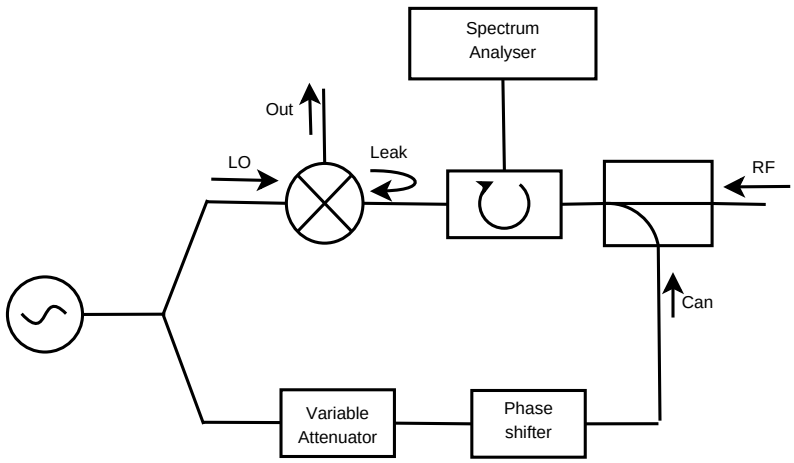

Figure 2.1. Block diagram of the LO-leakage cancellation setup.

(2.1)

$$\begin{aligned} S_{\text{out}} = & A_{\text{LO}} \cos(\omega t) \cdot \left[A_{\text{Leak}} \cos(\omega t + \phi_{\text{Leak}}) \right. \\ & \left. + A_{\text{Can}} \cos(\omega t + \phi_{\text{Can}}) \right] \qquad (2.1) \\ = & \frac{A_{\text{LO}} A_{\text{Leak}}}{2} \left(\cos(\phi_{\text{Leak}}) + \cos(2\omega t + \phi_{\text{Leak}}) \right) \\ & + \frac{A_{\text{LO}} A_{\text{Can}}}{2} \left(\cos(\phi_{\text{Can}}) + \cos(2\omega t + \phi_{\text{Can}}) \right) \qquad (2.2) \end{aligned}$$

From (2.2) it is seen that the output is a signal with a DC part and a part with the frequency of the second harmonic. The second harmonic parts of (2.2) is easily removed by low pass filtering, and the output is then given as (2.3)

$$S_{\text{out, lowpass}} = \frac{A_{\text{LO}}}{2} \Big(A_{\text{Leak}} \cos(\phi_{\text{Leak}}) + A_{\text{Can}} \cos(\phi_{\text{Can}}) \Big) \qquad (2.3)$$

The criteria for cancellation of the leakage signal at the RF port is found from the part of (2.1) with the brackets. When this sum to zero, the cancellation signal will remove the leakage signal.

$$A_{\text{Leak}} \cos(\omega t + \phi_{\text{Leak}}) + A_{\text{Can}} \cos(\omega t + \phi_{\text{Can}}) = 0 \Leftrightarrow \qquad (2.4)$$

$$A_{\text{Leak}} = A_{\text{Can}} \qquad (2.5)$$

and

$$\phi_{\text{Leak}} - \phi_{\text{Can}} = \pm\pi \qquad (2.6)$$

The criteria for a DC offset of zero can be found by setting (2.3) equal to zero.

$$\frac{A_{\text{LO}}}{2} \left(A_{\text{Leak}} \cos(\phi_{\text{Leak}}) + A_{\text{Can}} \cos(\phi_{\text{Can}}) \right) = 0 \Leftrightarrow \qquad (2.7)$$

$$-\frac{A_{\text{Leak}}}{A_{\text{Can}}} = \frac{\cos(\phi_{\text{Can}})}{\cos(\phi_{\text{Leak}})} \qquad (2.8)$$

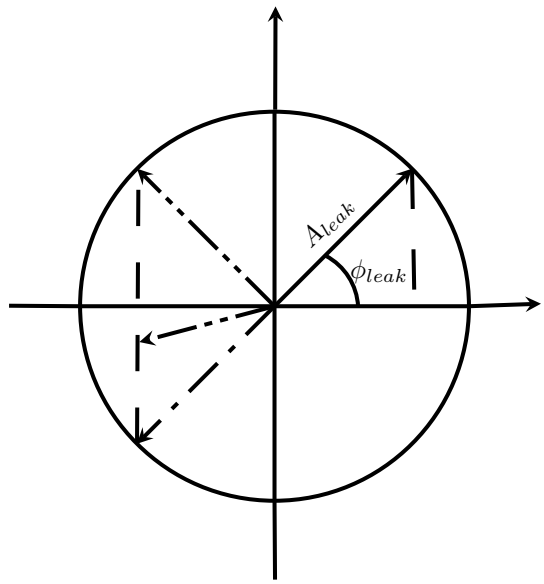

Figure 2.2. Phasor representation of leakage signal (solid arrow) and three possibilities of cancellation signals (dashed arrows). Only the single dotted cancels the leakage, whereas all cancels the DC-offset.

Observe that to cancel the leakage the cancellation signal must have the exact same amplitude as the leakage signal and be 180° out of phase, whereas to cancel the DC offset there is no such strict limit. Even when the amplitudes are equal there are two choices for the phase of the cancellation signal, such that the DC offset will be zero. Figure 2.2 illustrates this with phasors.

2.2 Measurements

2.2.1 Measurement setup

To test the cancellation technique two double balanced mixers each utilizing a commercial MACOM MA4E2532L diode ring is used. One denoted 'Mixer 1' and the other 'Mixer 2', the difference between the two is in the matching circuitry. The X-band LO source is a custom made 10.52GHz oscillator. To measure the noise, a spectrum analyzer is used with a calibrated noise-diode, this setup uses the Y-factor method to measure the noise figure for the mixer [9].

In figure 2.3 the experimental setup is shown. The LO-signal is split in two parts using a matched T-split, one part is used to drive the mixer (the actual LO signal), the other part is used to generate the cancellation signal. To control the phase and amplitude of the cancellation signal a variable attenuator and phase shifter is used. The cancellation signal is coupled to the RF/Noise signal from the noise source, using a directional coupler with coupling of -15dB.

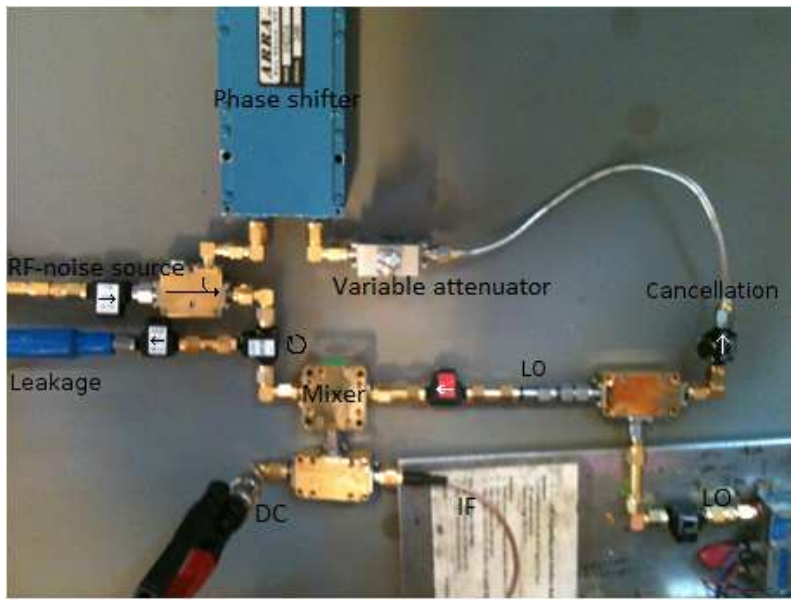

Figure 2.3. Measurement setup

The DC offset is measured using a voltmeter, which is disconnected during noise measurements, to ensure that instrument noise is not influencing the measurement. A circulator is placed at the RF port of the mixer, this allows to measure the LO-leakage during measurements. After the circulator an isolator is used to ensure that reflections or noise from the instrument is not coupled to the setup. Isolators is used between all critical components to remove reflections and limit unwanted coupling in the system.

When starting a measurement the attenuator and phase shifter is tuned such that the measured leakage is as low as possible. This is done to set the cancellation amplitude equal to the leakage amplitude, which is the case when they cancel, as was predicted in (2.5). When the amplitude is set, the phase is swept to see the change in DC-offset, leakage, and noise figure.

2.2.2 Results

The mixer is measured to have an LO-RF isolation of 18dB and a noise figure of 14.3dB and 6.2dB at frequencies 10KHz and 1MHz, respectively. Using the LO-cancellation technique the LO-RF isolation could be improved to 60dB. Figure 2.4 shows the LO-RF isolation and the DC-offset as a function of phase change in the cancellation signal. As was predicted in section 2.1 only one phase gives a leakage minima while there is two phases which gives a DC-offset of zero. The leakage minima and DC-offset is not located at the same phase, which according to (2.5), (2.6) and (2.8) is the case when the amplitudes are equal. After the full sweep there was measured an amplitude difference of 1.5dB between the cancellation signal and the leakage signal, this is the reason for the difference in phase of the DC-offset zero and leakage minima.

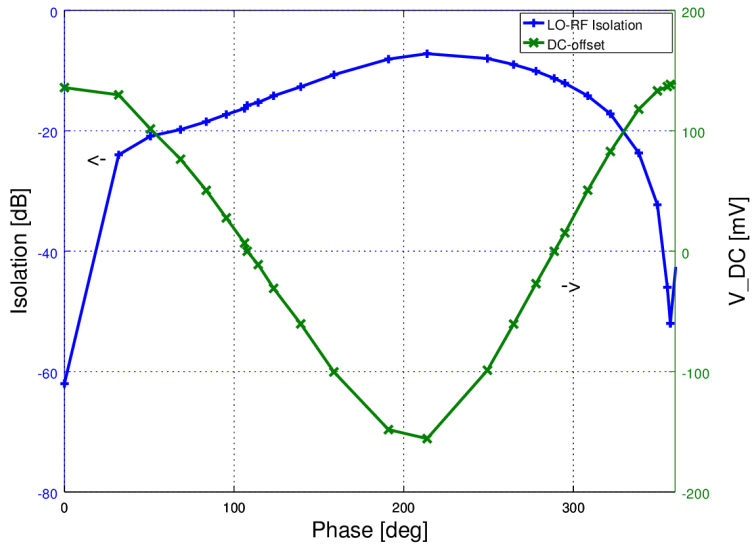
LO-RF Isolation
DC-offset
Isolation [dB]
V_DC [mV]
Phase [deg]
0
-20
-40
-60
-80
200
100
0
-100
-200
0
100
200
300
<-
->

Figure 2.4. LO-RF Isolation and DC-offset vs phase change.

If one wants the minimum LO leakage while achieving a DC-offset of zero, special care should be taken to match the cancellation signal amplitude to the leakage amplitude.

Using this technique can reduce the noise figure from 14.3dB to 12.1dB at 10KHz. In figures 2.5 and 2.6, the noise figure and DC-offset is plotted as a function of phase change in the cancellation signal. It can be observed that the noise figure is proportional to the magnitude of the DC offset, having minima when the DC offset is zero. Using the cancellation signal with a wrong phase will severely damage the mixers noise figure.

While the noise figure can be improved with 2dB at 10KHz there is no significant improvement at 1MHz. Rather at one of the zeros the noise figure is worse. In figures 2.7 and 2.8 the noise figure is plotted as a function of phase change in the cancellation signal for IF frequencies of 10KHz, 20KHz, 100KHz and 1MHz. It can be seen that for the low frequencies the improvement is largest, thus there must be a correspondence between the DC-offset and the 1/f noise. This is what is expected as increased DC level leads to increased 1/f noise [15, 16]. Comparing figure 2.5 and 2.7 it is clearly seen that the DC-offset increases the 1/f noise, thus one should try to avoid the DC-offset to get better mixers regarding 1/f noise. Comparing figure 2.4 and 2.7 there is observed no correspondence between the noise figure and the leakage, thus it is concluded that the leakage has no influence on the 1/f noise except to generate the DC-offset.

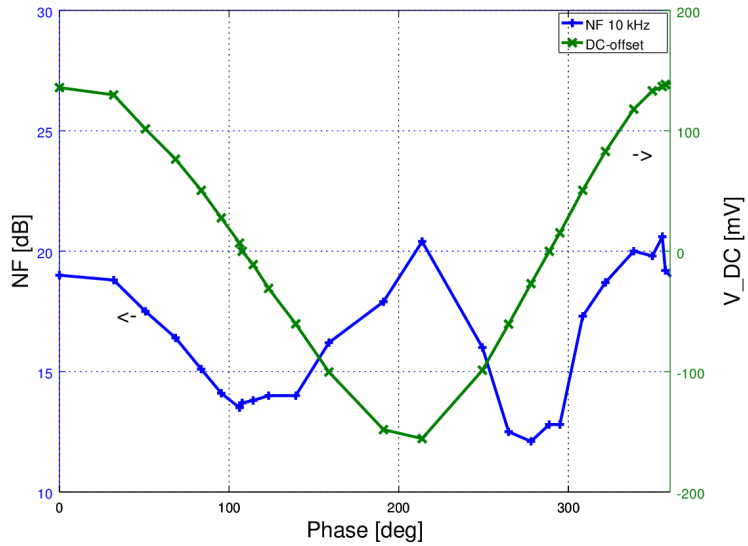

Figure 2.5. Noise figure (10KHz) and DC-offset vs phase change, 'Mixer 1'.

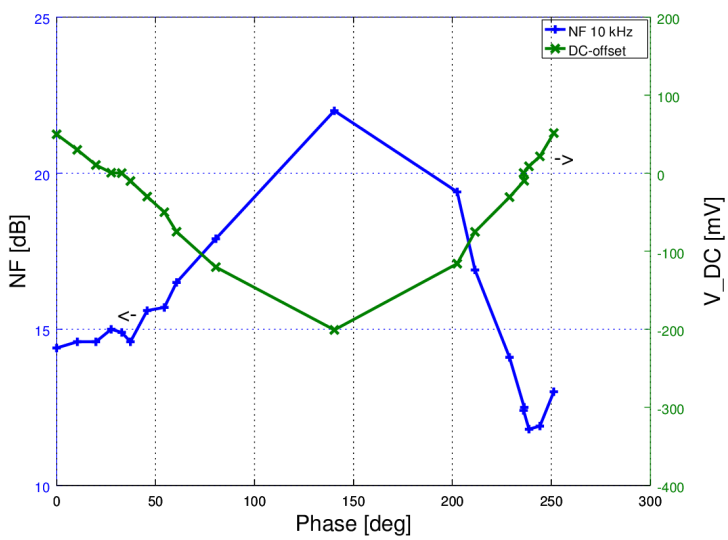

Figure 2.6. Noise figure (10KHz) and DC-offset vs phase change, 'Mixer 2'.

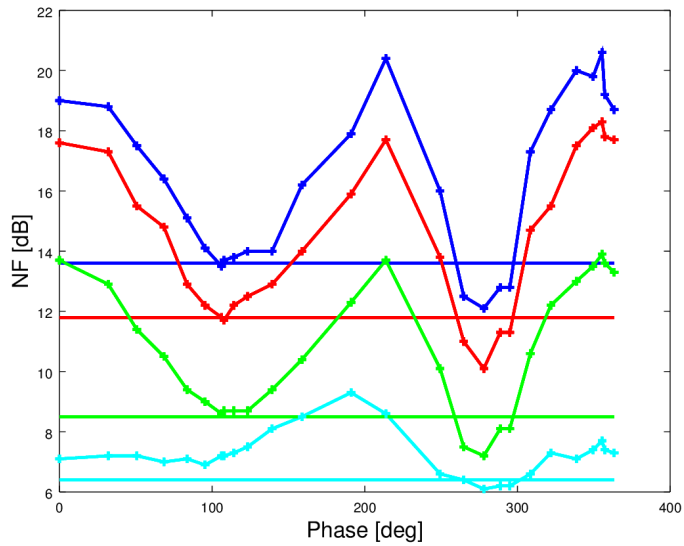

Figure 2.7. Noise figure at different frequencies vs phase change, 'Mixer 1'. From top to bottom: Blue @10KHz, Green @20KHz, Red @100KHz, Cyan @1MHz (Straight lines are without cancellation signal applied).

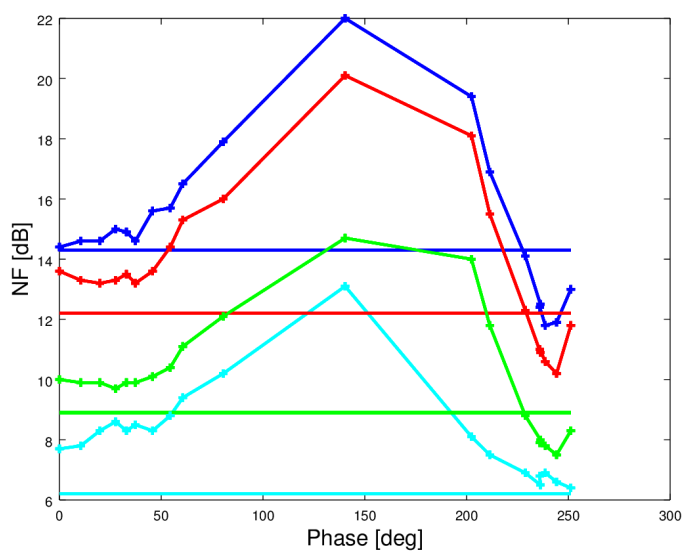

Figure 2.8. Noise figure at different frequencies vs phase change, 'Mixer 2'. From top to bottom: Blue @10KHz, Green @20KHz, Red @100KHz, Cyan @1MHz (Straight lines are without cancellation signal applied.)

2.3 Conclusion

A investigation on how LO-leakage and DC-offset affects 1/f-noise was conducted, using a LO-leakage cancellation method. For this method conditions for LO-leakage cancellation was derived together with conditions for zero DC-offset. It was shown that for leakage cancellation only one amplitude and phase will give full cancellation, whereas for zero DC-offset there is no strict limit to what the amplitude should be and there can be up to two phases for a given amplitude which gives the desired result.

The cancellation method was tested using a double balanced ring diode mixer. LO-RF isolation was improved from 18dB to 60dB. Noise figure could be improved from 14.3dB to 12.1dB at 10KHz, while maintaining a noise figure of 6.2dB at 1MHz. It was shown that the 1/f noise increases as the absolute DC-offset is increased. While the LO-leakage does not affect the 1/f noise.

LO-RF isolation and zero DC-offset was not obtained in the measurement using the same cancellation signal. This was due to a amplitude mismatch between the cancellation signal and the leakage signal. In future designs utilizing this method, if it is wanted to have zero DC-offset together with no leakage, one should take special care to match the amplitudes.

These findings leads to the hypothesis; that by making a mixer which has a tunable LO-balun, it is possible to reduce the flicker noise, as it is possible to compensate for manufacturing mismatches with the balun, leaving no LO-leakage to cause self-mixing. In the following chapter we will investigate this hypothesis.

3

Passive diode ring mixers with tunable balun

Low frequency noise generated in the mixer core, is increased with the DC current through the core. This DC level can come from the self-mixing of the LO signal, as we saw in Chapter 2. So if one wants to make a low flicker noise mixer, LO leakage must be reduced. This could be by compensating from manufacturing mismatches, by making a mixer which has a tunable LO-balun.

In this chapter three mixers will be designed and compared. Two with a tunable balance on the LO-balun, one of which is with a core of Schottky diodes and the other with a core of diode-connected HBTs. The third mixer is a reference mixer without a tunable balun using diode-connected HBTs for the mixer core. By comparing these three mixers insight in technology choice (diode connected HBTs or Schottky diodes) and circuit topology (how does the phase of the balun matter for mixer performance) should be gained.

In section Section 3.1 the design of the novel modified Marchand balun with tunable phase is discussed. This is followed by the three mixer designs in Section 3.2, Section 3.3 and Section 3.4 discussing the reference HBT-mixer, tunable HBT-mixer and tunable Schottky diode mixer, respectively. Then Section 3.5 shows a comparison and low frequency noise measurement of the mixers. Some concluding remarks follows in Section 3.6.

3.1 Tuneable Marchand balun

Baluns are used to transform an unbalanced input signal into a balanced output signal. Baluns are essential components in many microwave circuits, e.g., balanced mixers and push-pull amplifiers. Baluns can be split into active and passive types. Active baluns use transistors to overcome losses found in passive baluns and allow for compact circuits in MMIC processes. The main drawback of active baluns is that they limit the dynamic range of the balanced mixer or amplifier significantly.

Passive baluns can be realized using either lumped components, like capacitors and inductors or distributed elements such as transmission lines. Due to its wide band properties, the Marchand type balun finds widespread applications. Several modifications of this circuit have been reported including techniques for impedance scaling [18], tuning of center frequency [19], bandwidth enhancements [20, 21] and different types of miniaturization [19, 22–25].

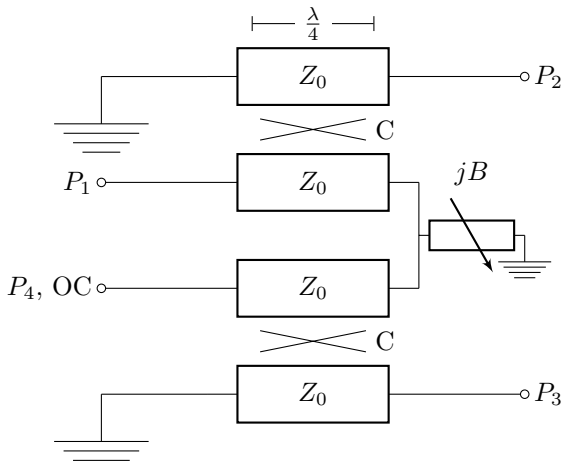

Figure 3.1. Modified Marchand balun configuration, with tunable phase balance, utilizing a variable susceptance.

Practical baluns suffer from imperfect phase and magnitude balance due to layout asymmetries and production variations. Only perfect phase matched baluns make it possible to exploit the full benefits of balanced configurations, i.e., for a double balanced mixer you obtain complete port-to-port isolation, rejection of LO-AM noise, spurious signals, and certain intermodulation products [9]. Therefore it would be an advantage with a balun having a tunable phase balance, allowing to correct any imbalance. Tuning of the phase balance has previously been reported for active baluns only [26].

The purpose of this section is to introduce a novel configuration of the Marchand balun with tunable phase balance. First the general theory of the modified Marchand balun will be developed. This will be followed by the design and experimental results to verify the proposed configuration. The experimental results are obtained by producing a lumped element Marchand balun, utilizing this principle, in a SiGe BiCMOS technology. This section was published in [JP1] and is, to the best knowledge of the author, the first published demonstration of a Marchand balun with tunable phase balance. Later attempts include [27], which tune the balun by varying a load on port 4.

3.1.1 Theory

In this section, it will be shown that by placing a shunt susceptive element between the two couplers in the Marchand balun, it is possible to tune the phase difference between Port 2 and 3 while maintaining an almost constant magnitude balance. Fig. 3.1 shows the proposed configuration. For an ideal coupled line of length $\frac{\lambda}{4}$ the S-parameters is given as [18]

$$S_{\text{coupler}} = \begin{bmatrix} 0 & C & -j\sqrt{1-C^2} & 0 \\ C & 0 & 0 & -j\sqrt{1-C^2} \\ -j\sqrt{1-C^2} & 0 & 0 & C \\ 0 & -j\sqrt{1-C^2} & C & 0 \end{bmatrix}, \tag{3.1}$$

where C is the coupling factor. Then by using the S-parameters for the two couplers and a shunted susceptance, B, the transmission from Port 1 to Port 2 and 3, respectively, can be derived to be:

$$S_{21} = S_{12} = \frac{j2C(jBZ_0C^2+1)\sqrt{1-C^2}}{1+C^2+jBZ_0C^2} \tag{3.2}$$

$$S_{31} = S_{13} = \frac{j2C\sqrt{1-C^2}}{1+C^2+jBZ_0C^2} \tag{3.3}$$

where Z_0 is the reference impedance for the S-parameters. The derivation can be found in appendix A. Taking the magnitude and phase of S_{21} and S_{31} from (3.2) and (3.3) gives:

$$|S_{21}| = \frac{2C\sqrt{C^4Z_0^2B^2+1}\sqrt{1-C^2}}{\sqrt{C^4Z_0^2B^2+2C^2+C^4+1}} \approx \frac{2C\sqrt{1-C^2}}{C^2+1} \tag{3.4}$$

$$|S_{31}| = \frac{2C\sqrt{1-C^2}}{\sqrt{C^4Z_0^2B^2+2C^2+C^4+1}} \approx \frac{2C\sqrt{1-C^2}}{C^2+1} \tag{3.5}$$

$$\angle S_{21} = -\arctan\left(\frac{C^4Z_0^2B^2+C^2+1}{C^4Z_0B}\right) + \begin{cases} \pi \text{ for } B\geq 0 \\ 0 \text{ for } B<0 \end{cases} \tag{3.6}$$

$$\approx \frac{1}{2}\pi + \frac{C^4Z_0}{C^2+1}B$$

$$\angle S_{31} = \arctan\left(\frac{C^2+1}{C^2Z_0B}\right) - \begin{cases} \pi \text{ for } B\geq 0 \\ 0 \text{ for } B<0 \end{cases} \tag{3.7}$$

$$\approx -\frac{1}{2}\pi - \frac{C^2Z_0}{C^2+1}B \tag{3.8}$$

where the approximations are first order Taylor expansions valid for small B.

From (3.4) and (3.5) it is seen that the magnitude is independent to changes in the susceptance and is similar to what is given in [18]. This is not the case for the phase, where both (3.6) and (3.7) shows that there is a linear relationship between the susceptance and the phase. It is thus possible to tune the phase balance of the Marchand balun by insertion of a shunt tunable susceptance. In Fig. 3.2 the magnitude imbalance and phase difference calculated from (3.4), (3.5), (3.6), and (3.7) are plotted together with simulation of a circuit with ideal couplers from ADS. The ADS simulation results for the phase is hardly discernible from the theoretical results obtained with the Taylor expansion. The amplitude imbalance is seen to deviate from the approximation by 0.5 dB for a phase change of $\pm 20°$.

3.1.2 Design

The design procedure for a miniaturized Marchand balun utilizing lumped elements is described in section 3.2.1, it uses offset coupled broadside spiral inductors together with capacitors to realize the coupled transmission lines. This configuration lend itself to easy integration of a shunt susceptance, due to the capacitor already placed as part of the couplers. This allows an effective negative susceptance by reducing this capacitance. A MOS-capacitive varactor is chosen to implement the variable susceptance with a size that allows the tuning range to be centered around 180°. The

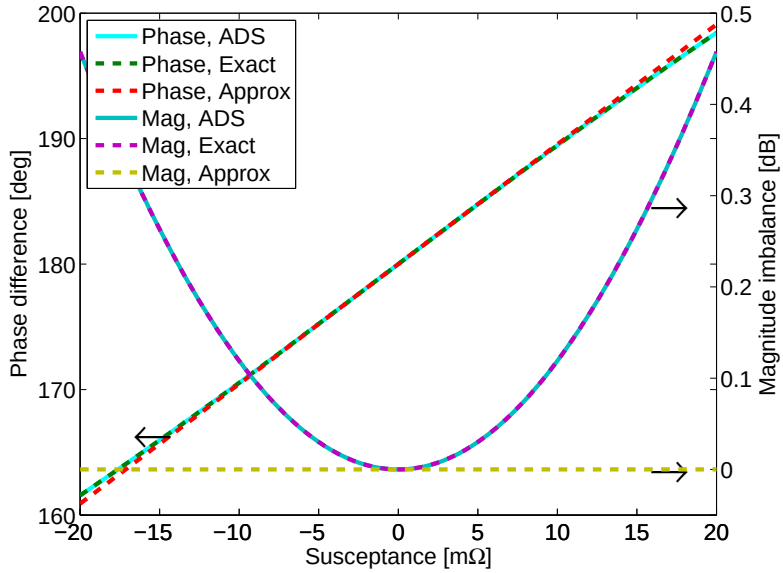

Figure 3.2. The phase difference and magnitude imbalance calculated using (3.6) and (3.7) are plotted together with an ADS simulation using perfect couplers.

MOS-varactor, can be adjusted within a voltage range from −2.5 V to 2.5 V, and the circuit is designed such that 0 V corresponds to a 180° phase difference. Fig. 3.3 shows a microphotograph of the fabricated circuit.

3.1.3 Experimental results

In this section, the experimental results obtained by on wafer measurements are discussed. Measurements of insertion loss, input matching, and isolation between output ports, for the full range of tuning voltages, are plotted in Fig. 3.4 together with the simulation results for $V_t = 0$ V, all simulations are done using Momentum in ADS. The insertion loss at the design frequency of 9.4 GHz is 6.0 dB, and remains better than 8.5 dB from 7 GHz to 11 GHz. The rather large insertion loss is a consequence of the low Q of the rectangular broadside coupled spiral structure. The measured performance of the balun is well predicted by EM simulations. The input matching stays better than −15 dB in this band and the output matching is better than −6 dB and isolation between ports 2 and 3 is better than 8 dB. Fig. 3.5 shows the measured magnitude imbalance versus frequency. Observe that within the band from 7.0 GHz to 11.0 GHz the magnitude balance is better than 0.6 dB and only changes ±0.25 dB with the bias voltage. The measured phase difference, shown in Fig. 3.6, can be tuned to 180° in this band. At the design frequency the phase difference can be varied from −183° to −175.8° while maintaining an almost constant magnitude imbalance of 0.3 ± 0.05 dB. As the shunted susceptance is realized by a MOS-varactor the tuning is frequency dependent. At 7 GHz it is only possible to tune the balun from −183.2° to −178.4° while at 11 GHz it can be tuned from −183.8° to −174.4°.

The nonlinearity in the phase response comes from the nonlinear relationship

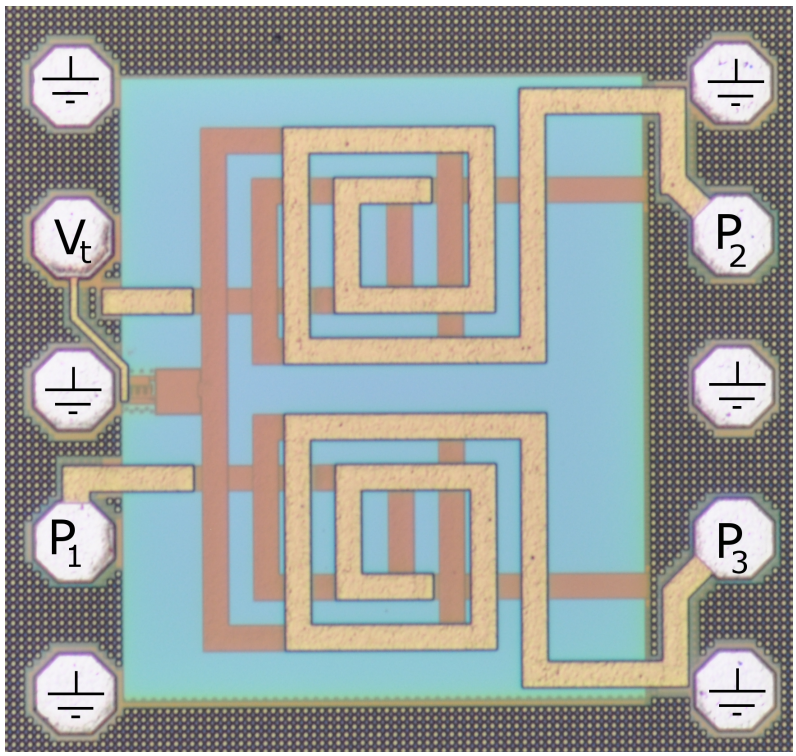

Figure 3.3. Microphotograph of fabricated circuit. The size is 750 µm × 800 µm.

between the tuning voltage and the capacitance of the varactor. In Table 3.1, this work is compared to other Marchand balun configurations recently reported in the literature. While being the only one with a tunable phase and thus the only with a zero phase imbalance, it also exhibits the state-of-the-art magnitude balance. The high insertion loss can be improved by using higher Q spiral transformers.

3.2 HBT reference mixer design

In this section the reference HBT mixer design is described. The purpose is to compare this mixer with the mixers having a tunable balun. It is a direct conversion mixer operating at X-band which has characteristics optimized for Doppler radar applications. These characteristics include state-of-the-art linearity, together with good 1/f-noise performance and reasonable conversion loss. To meet these requirements a double balanced passive mixer architecture is chosen.

As the SiGe HBT process used for implementation do not offer suitable diodes for mixing, diode connected HBTs as in [30] are used. The content of this section has been published in [JP2].

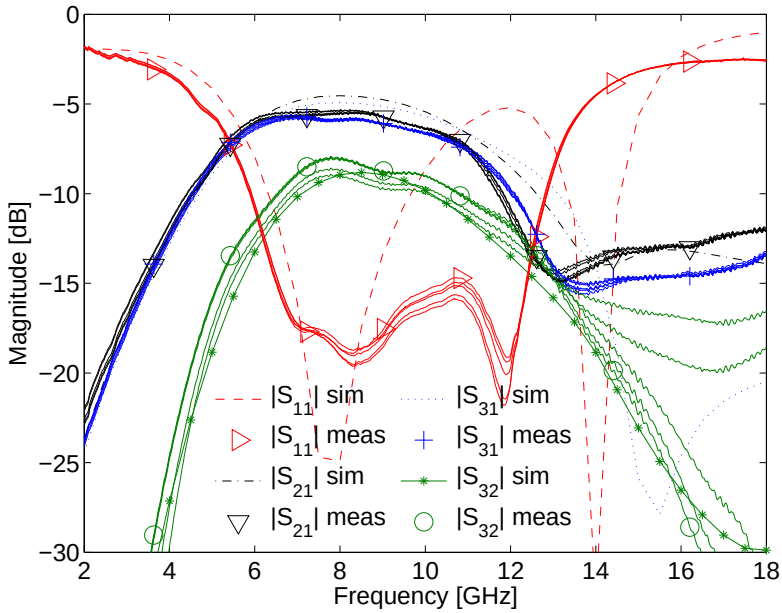

Figure 3.4. Insertion loss and input matching measured with tuning voltages ranging from −2.5 V to 2.5 V and simulation with tuning voltage at 0 V.

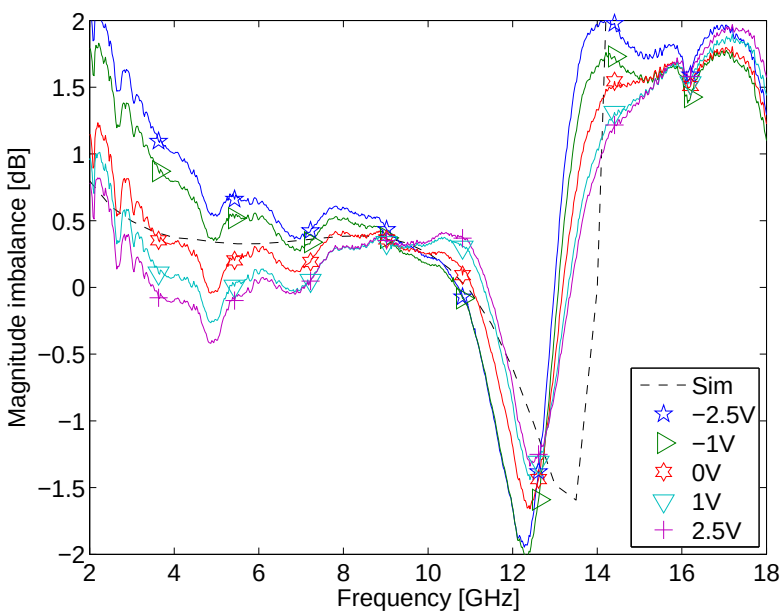

Figure 3.5. Measurement of magnitude imbalance with tuning voltages ranging from −2.5 V to 2.5 V and simulation with tuning voltage at 0 V.

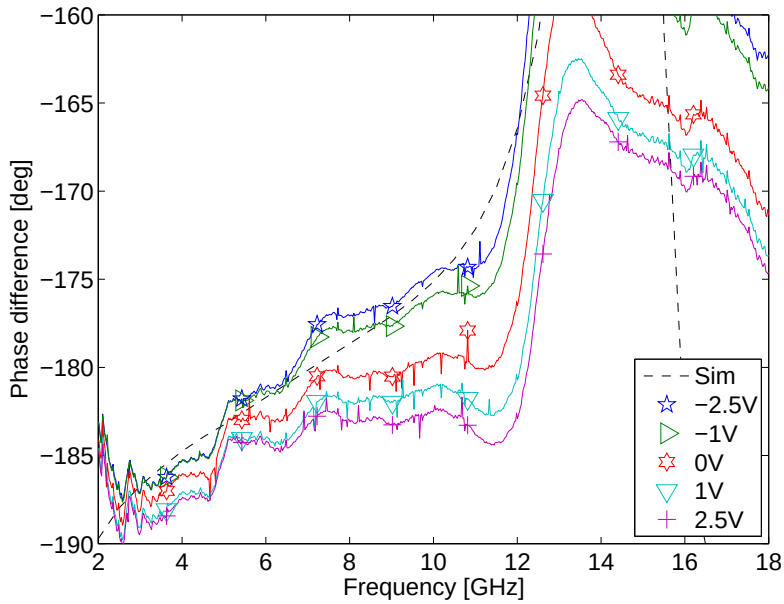

Figure 3.6. Measurement of phase difference between output ports with tuning voltages ranging from −2.5 V to 2.5 V and simulation with tuning voltage at 0 V.

Table 3.1. Performance comparison of published Marchand baluns and this work

Ref.	Freq [GHz]	Band-width [GHz]	IL [dB]	Phase/Mag balance [°/dB]	Phase tune [°]
[20]	1.11-2.93	1.8	3.3	1.4 / 0.7	N/A
[21]	0.5-3.6	3.1	< 5	< 10 / < 1	N/A
[23]	23.6	24.5	5.9	< 10 / 1.5	N/A
[24]	2.09-3.06	0.97	3.8	1.6 / 0.4	N/A
[28]	4-9	5	< 4	5 / 0.5	N/A
[29]	55	10	4.14	0.9 / 1.2	N/A
This work	9.4	4	6.0	0 / 0.3	7.2

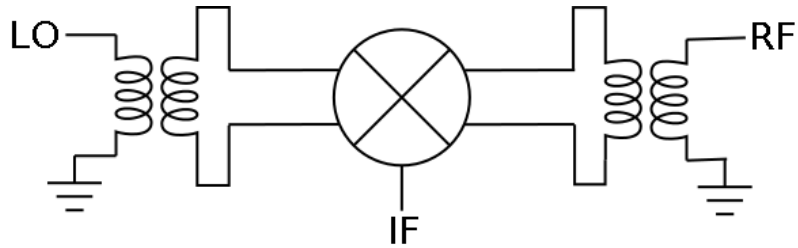

Figure 3.7. Block diagram of balanced mixer circuit. Showing LO and RF balun together with center tapped IF extraction.

3.2.1 Design

This section describes the design of the proposed double balanced ring diode mixer. Diodes are desired for the implementation of low-noise mixers in direct conversion receivers. In many SiGe HBT technologies there are no dedicated mixer diodes available. Using the base-emitter junction of the high-speed HBTs available as a pn-junction diode [30], it is possible to have good mixer diodes in a SiGe HBT technology. The design description is divided into three parts covering the design of the balun, the IF extraction and the mixer core. Figure 3.7 shows a block diagram of the mixer circuit.

Marchand balun

The balun of the double balanced mixer is implemented in the form of a lumped element Marchand balun. The Marchand balun is chosen due to its broadband properties. The lumped element implementation allows compact size and straightforward design procedure for good phase and magnitude balance [22, 31]. The lumped element implementation uses offset broadside coupled spiral inductors together with capacitors to realize the coupled transmission lines, normally used in Marchand baluns. The schematic of the balun is shown in Figure 3.8, where it is depicted as a symmetrical four port, together with the corresponding even- and odd-mode circuits. For normal operation port four is open circuited.

For a circuit to behave like an ideal balun it must have S-parameters given as

$$S_{21} = -S_{31} \tag{3.9}$$

$$S_{11} = 0. \tag{3.10}$$

For a symmetrical four port circuit, (3.9) and (3.10) is fulfilled if the fourth port is terminated in an open circuit to give [32]

$$T_{\text{even}} = 0 \tag{3.11}$$

$$Z_{\text{in}_{\text{even}}} + Z_{\text{in}_{\text{odd}}} = 2Z_{\text{P1}}, \tag{3.12}$$

where T_{even} is the transmission coefficient in the even-mode circuit, Z_{P1} is the system impedance at port 1, $Z_{\text{in}_{\text{even}}}$ and $Z_{\text{in}_{\text{odd}}}$ are the input impedance of the even mode and odd mode circuit, respectively.

The synthesis of this type of lumped balun is based on the coupled line Marchand balun [22]. Thus the synthesis starts by selecting the even- and odd-mode charac-

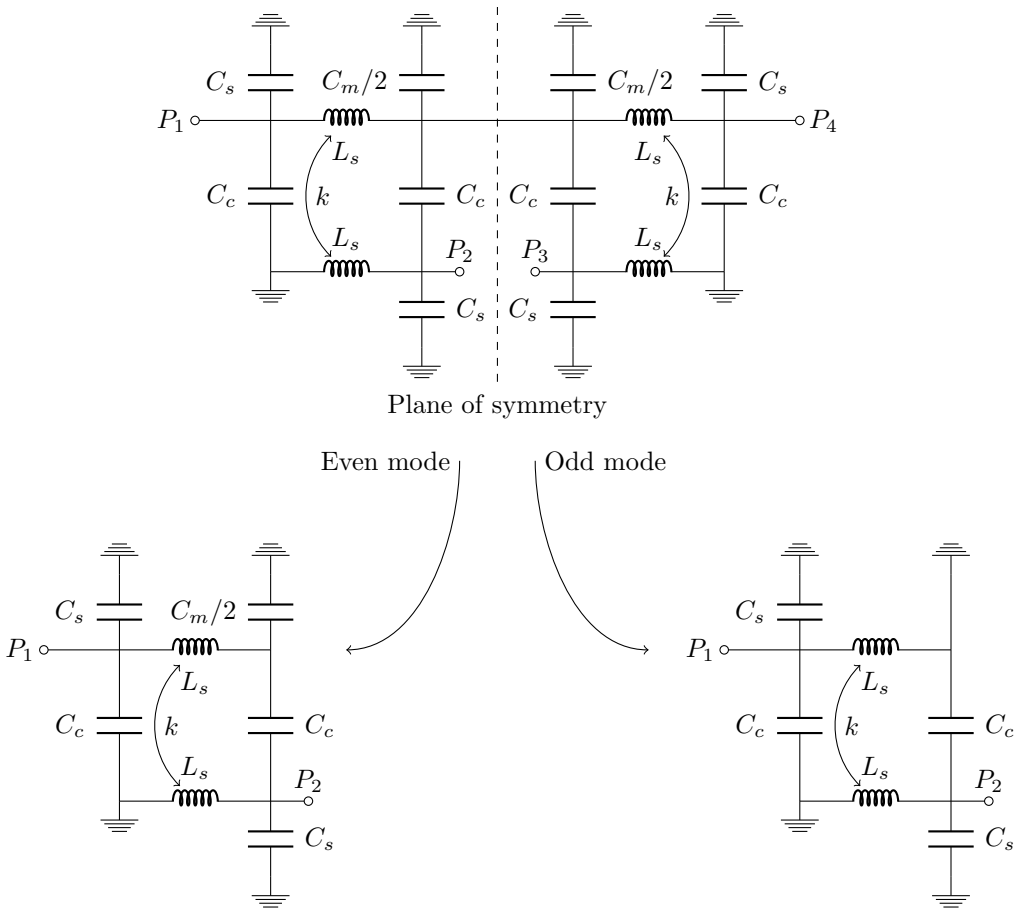

Figure 3.8. Circuit diagram for the lumped Marchand balun, showing it as a symmetrical four port. Normal operation requires P_4 to be open circuited.

teristic impedance of the lines. For a real valued impedance scaling, $\alpha = \frac{Z_{\mathrm{P2,3}}}{Z_{\mathrm{P1}}}$ the relation giving the even and odd mode impedance is [33]

$$\frac{1}{Z_{0_{\mathrm{odd}}}} - \frac{1}{Z_{0_{\mathrm{even}}}} = \frac{1}{Z_{\mathrm{P1}}}\sqrt{\frac{2}{\alpha}}, \tag{3.13}$$

where $Z_{0_{\mathrm{even}}}$ and $Z_{0_{\mathrm{odd}}}$ are the even- and odd-mode characteristic impedance of the coupled line, respectively.

From the even- and odd-mode characteristic impedance the circuit parameters for the lumped element balun can be found. This procedure was described in [22] and

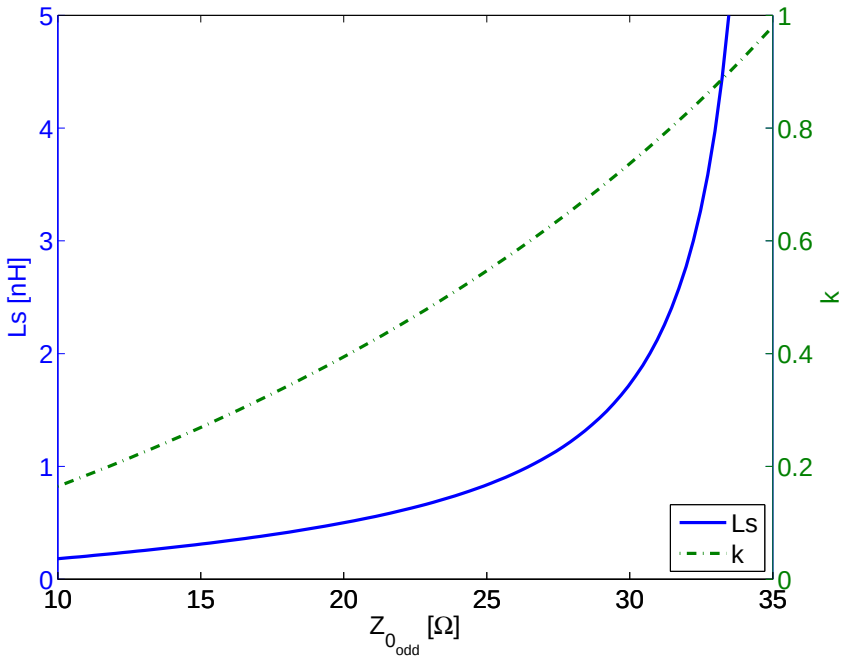

Figure 3.9. Design curves for L_s and k as function of $Z_{0_{odd}}$.

the design equations are repeated here

$$L_s = \frac{Z_{0_{even}} + Z_{0_{odd}}}{2\omega} \tag{3.14}$$

$$k = \frac{Z_{0_{even}} - Z_{0_{odd}}}{2\omega L_s} \tag{3.15}$$

$$C_c = \frac{1}{2\omega}\left(\frac{1}{Z_{0_{odd}}} - \frac{1}{Z_{0_{even}}}\right) \tag{3.16}$$

$$C_s = \frac{1}{\omega Z_{0_{even}}}, \tag{3.17}$$

where k and C_c are the inductive coupling coefficient and the capacitive coupling, respectively, of the coupled spiral pairs. The center capacitors are given as $C_m = 2C_s$.

From (3.13) it is evident that there are several values of $Z_{0_{\mathrm{odd}}}$ and $Z_{0_{\mathrm{even}}}$ which fulfills the requirement. A higher $Z_{0_{\mathrm{odd}}}$ gives larger bandwidth, but gives larger inductors in the realization of the lumped element balun, so a trade off between bandwidth and desired balun size must be made. In Figures 3.9 and 3.10 are the design curves plotted for a 50Ω environment at a frequency of 10.5 GHz, without scaling.

The coupled broadside spiral inductor design is limited in the realization, as it is often not possible to obtain values as dictated by equations (3.14)-(3.16). Further investigation of the structure is therefore required to reveal possible solutions or trade offs for this problem. For the even mode circuit, shown in Figure 3.8, the requirement for the transmission coefficient being zero is the same as the Y-parameter Y_{21e} become

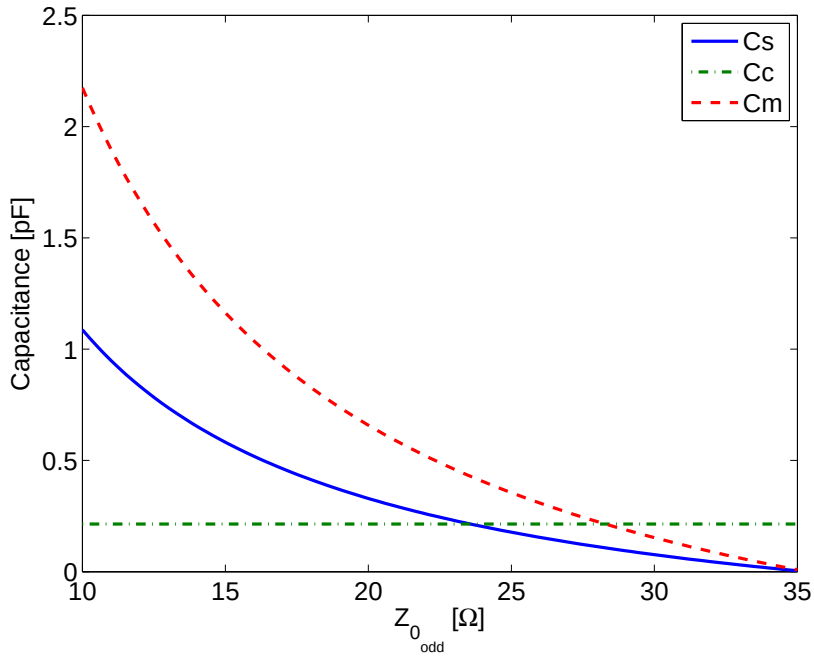

Figure 3.10. Design curves for C_s, C_c and C_m as function of $Z_{0_{odd}}$.

zero [31]. Thus for (3.9) to be fulfilled we have

$$Y_{21e}{=}-\frac{(1-k)\,s\,(C_m/2+C_c)-sC_m/2}{s^2\,(C_m/2+C_c)\,L_s\,(1-k^2)+1}=0 \Leftrightarrow \tag{3.18}$$

$$C_m{=}2C_c\left(\frac{1}{k}-1\right). \tag{3.19}$$

This is a nice property as it shows that by careful selection of C_m it is possible to obtain good phase and magnitude match even though the coupled spirals are not as specified above. Also note that the match is broadband as it does not depend directly on frequency, but on parameters which ideally should be frequency independent.

The even and odd mode input impedances can be found, by terminating the even- and odd-mode circuits in Figure 3.8 with Z_{P2}, as

$$Y_{even}{=}\frac{1}{Z_{even}}=s\,(C_s+C_c)+\frac{s\,(C_m/2+C_c)}{s^2\,(C_m/2+C_c)\,L_s\,(1-k^2)+1} \tag{3.20}$$

$$Y_{odd}{=}\frac{1}{Z_{odd}}=s\,(C_s+C_c)+\frac{1}{sL_s-\frac{(skL_s)^2}{sL_s+\frac{1}{s(C_s+C_c)+Y_{P2}}}} \tag{3.21}$$

where $s = j\omega$ is the complex frequency. Note that (3.20) will always be purely imaginary for lossless circuits whereas (3.21) is a general complex number having a real and a imaginary part. Inserting (3.20) and (3.21) into (3.12) gives the requirement for perfect input match. Thus to match to a real source impedance, Z_{P1}, we have

Table 3.2. Design parameters for the balun

Inductance	L_s [nH]	1.02
Inductive coupling	k	0.825
Capacitive coupling	C_c [fF]	379
Input matching capacitors	C_s [fF]	283
Balance matching capacitor	C_m [fF]	190

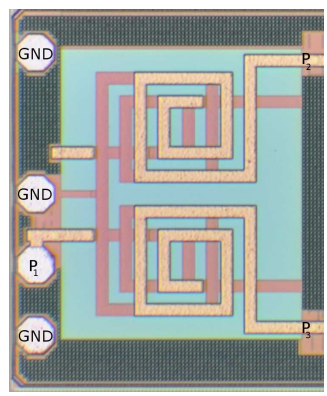

Figure 3.11. Microphotograph of on chip balun structure. Dimensions are $680\mu m \times 710\mu m$.

$Z_{odd} = \frac{1}{Y_{odd}} = 2Z_{P1} - Z_{even}$, where Z_{P1} is purely real and Z_{even} is purely imaginary. This corresponds to two real equations in C_s. Thus it is not guaranteed that there exists a C_s to fulfill the requirement for arbitrary selection of L_s, k and C_c.

Even though if the coupled spiral is not as specified by equations (3.14)-(3.16), one can try to change C_s, to obtain a better match. It is typically possible to find an acceptable match, albeit not perfect.

The implemented balun has parameters given by Table 3.2. The chip area occupied by the balun is $680\mu m \times 710\mu m$ and a microphotograph is shown in Figure 3.11. The S-parameters for the balun is shown in Figure 3.12, where simulation results are compared to measurements. It is observed that there is good agreement, in general, between the simulation and experimental results. The largest discrepancy is the S_{11} curve where the second resonance behavior is shifted down from 13 GHz to 12 GHz. This shift is probably due to parasitic capacitances not included in the simulation model. At the design frequency a loss of 2.5 dB was measured. The rather high loss is mainly due to the low Q-factor of the inductors. As desired the balun is broadband with a measured 3 dB bandwidth of 6.4 GHz. Figures 3.13 and 3.14 show the phase and magnitude imbalance, respectively. Excellent magnitude and phase imbalance of 0.11 dB and 0.7°, respectively, are achieved at the design frequency. A magnitude imbalance better than 0.4 dB and a phase imbalance better than 5°, is achieved over the entire bandwidth of operation, which makes this balun suitable for double balanced mixer implementation.

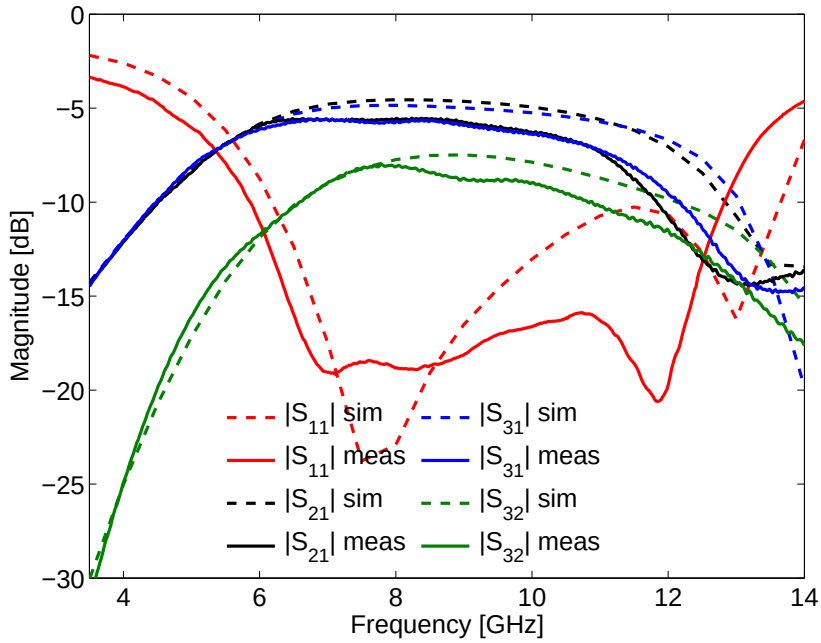

Figure 3.12. Measurements and simulation results for balun S-parameters.

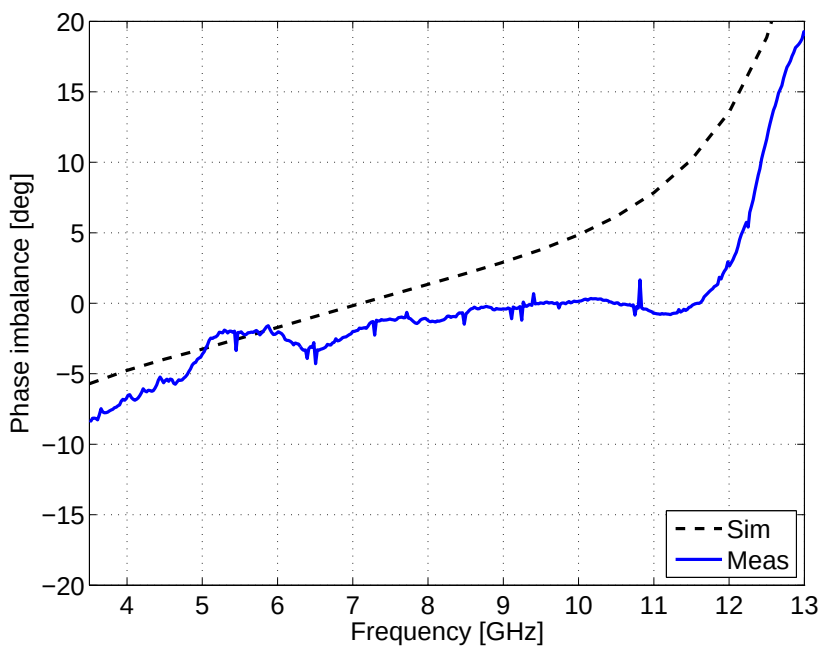

Figure 3.13. Measurement and simulation results for phase imbalance.

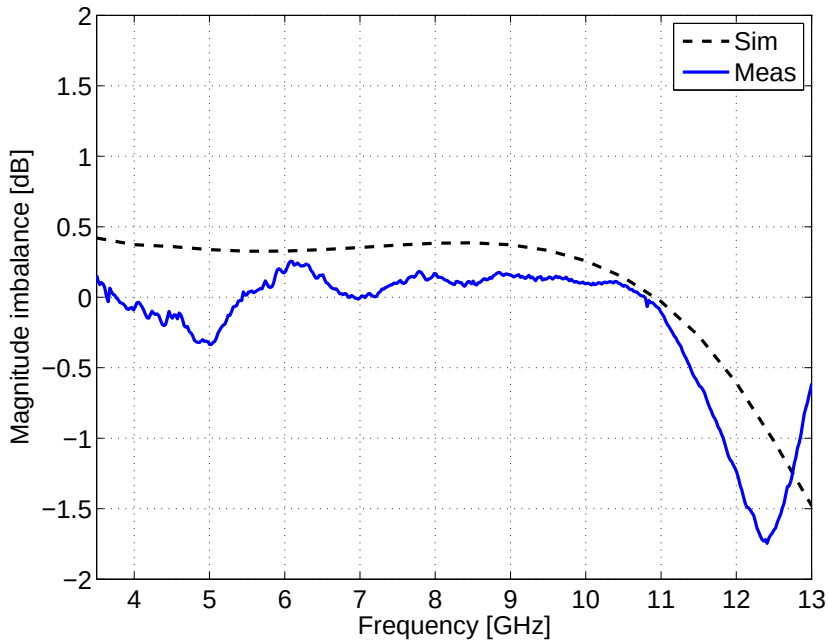

Figure 3.14. Measurement and simulation results for magnitude imbalance.

IF extraction

To get an output signal from the mixer it is necessary to have a circuit which allows to extract the IF signal, without disturbing the LO and RF baluns. The IF extraction is achieved by making a DC and low frequency return path at either the LO or RF port and extract the signal from the other. It is desirable not to have any large signal leaking out of the IF port as this might saturate or cause other unwanted effects in the low frequency circuitry following the mixer. For this reason it is chosen to use the balun at the LO port to make the DC and low frequency return path and the balun at the RF port to extract the IF signal, as the LO-signal can be several magnitudes larger than the RF signal.

Due to the low IF frequency of the mixer together with the grounded parts of the Marchand balun, the IF extraction is quite simple and follows the idea from [34]. The schematic for the IF extraction is the part of Figure 3.15 labeled 'RF balun w. IF extraction'. The DC and low frequency return path is ensured by the Marchand balun as the inductors L_s are seen as a short circuit. To avoid the ground connection in the RF balun it is blocked by large capacitors which creates an open for the IF signal and a short for the RF signal. It is important to make the IF extraction symmetric as any asymmetry will affect the balun performance. To ensure the symmetry the capacitor C_{IF} is split into three parallel 2 pF capacitors placed after both of the two inductors and in the middle where the IF signal is combined. The small influence on the balun performance from the 2 pF capacitors, can be compensated by slightly changing C_{s_2} for matching and C_{m_2} for balance.

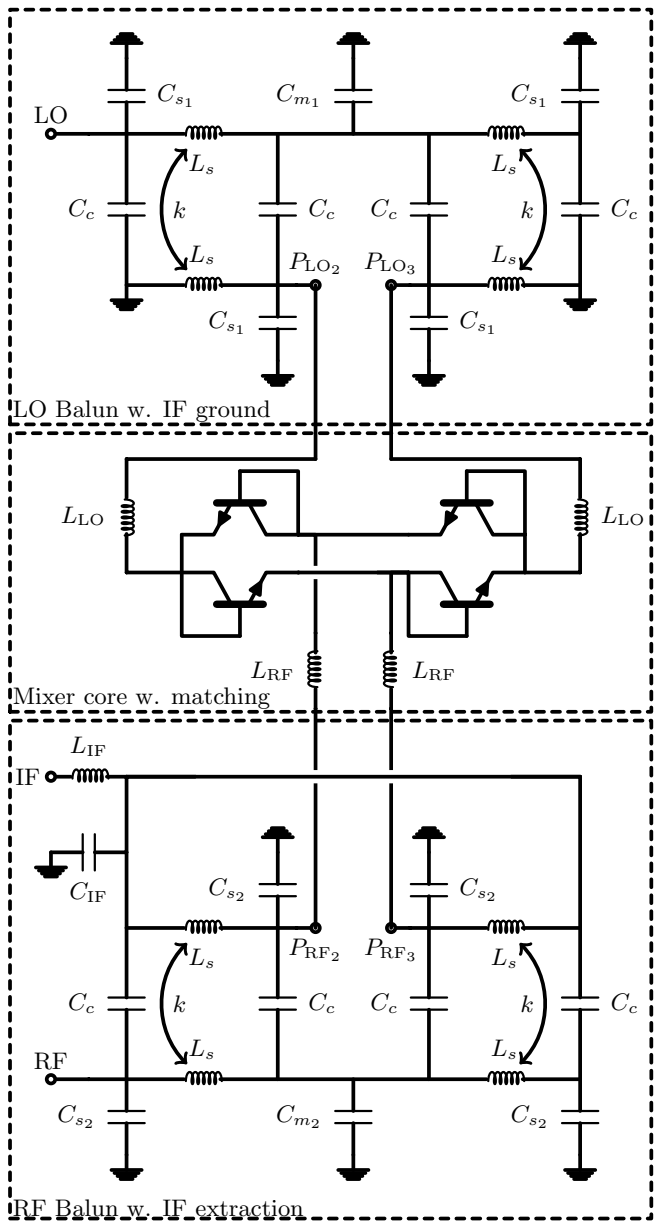

Figure 3.15. Schematic of the full mixer circuit.

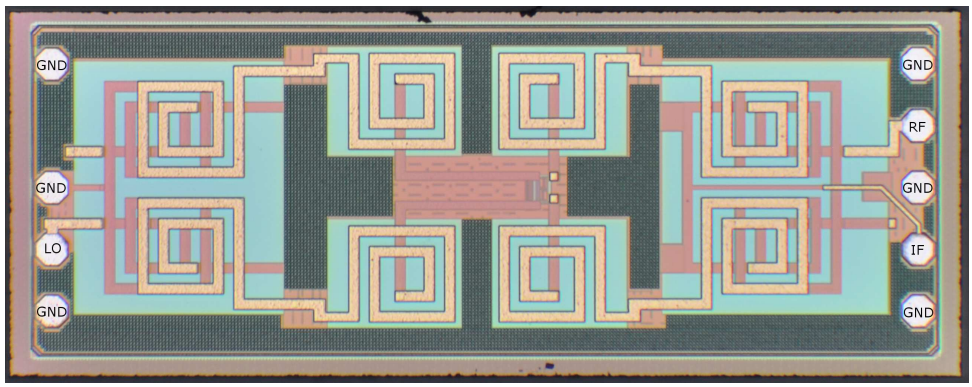

Figure 3.16. Microphotograph of passive double balanced mixer. The die size is $2200\mu m \times 800\mu m$.

Mixer core

The mixer core consists of the mixing devices and a matching circuit. Each mixing device is a diode connected HBT. There are two possible ways to make the diode connections, either by use of the base-emitter or the base-collector pn-junction. The base-emitter junction is the preferred diode junction due to the heavier doping of the n-region of the emitter compared to the collector. Simulations also show that this gives the best behavior, having a 3 dB difference in conversion loss between the two diode connections. To get the double balanced properties the ring mixer structure is used [9].

Using Harmonic Balance simulations the optimum load conditions are found to be $58 + j106\,\Omega$ and $50 + j122\,\Omega$ at 8.5 GHz for the LO and the RF ports, respectively. As a 50Ω match is required it is relatively simple to tune out the reactive part using single series inductors, L_{RF} and L_{LO}. In Figure 3.15 the schematic of the mixer core is labeled 'Mixer core w. matching'.

The die size of the manufactured mixer is $2200\mu m \times 800\mu m$. A microphotograph of the full mixer is shown in Figure 3.16.

3.2.2 Experimental Results

In this section, the experimental results are discussed. The measurements are made on-wafer using a probe station, and simple calibration is used to remove losses in cables and probes. The IF-frequency for all measurements is 100 MHz. The mixer conversion loss and single sideband noise figure is shown in Figure 3.17 as a function of frequency, with a fixed LO power of 15 dBm. At the design frequency of 8.5 GHz the conversion loss is 9.8 dB. The noise figure follows the conversion loss as expected. Due to measurement inaccuracy the noise figure is at some points lower than the conversion loss. The 3 dB bandwidth covers more than the entire X-band or more precisely the range from 7 GHz to 12 GHz, thus showing the benefit of using a broadband balun design together with the double balanced topology.

In Figure 3.18 the conversion loss and noise figure is plotted versus the LO power level at the design frequency of 8.5 GHz. It is seen that the mixer is not fully saturated

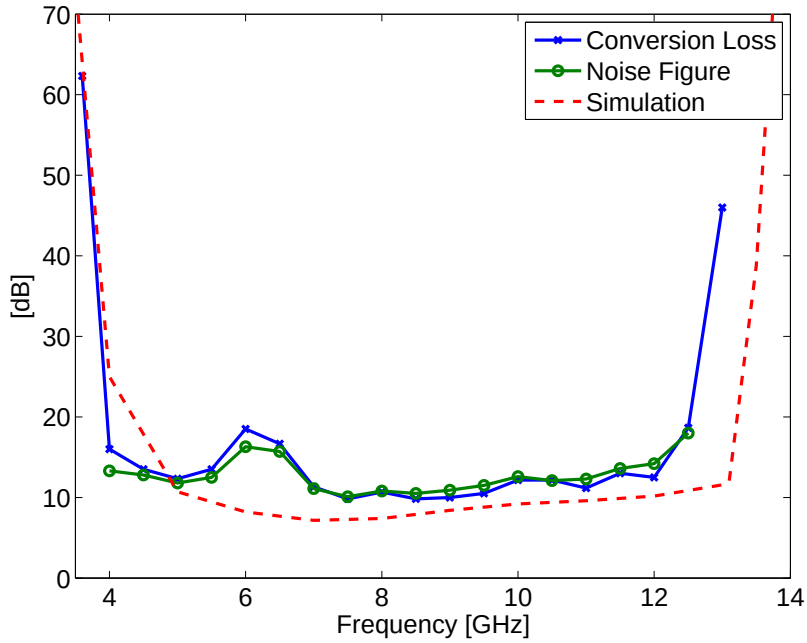

Figure 3.17. Measured conversion loss and single sideband noise figure versus frequency.

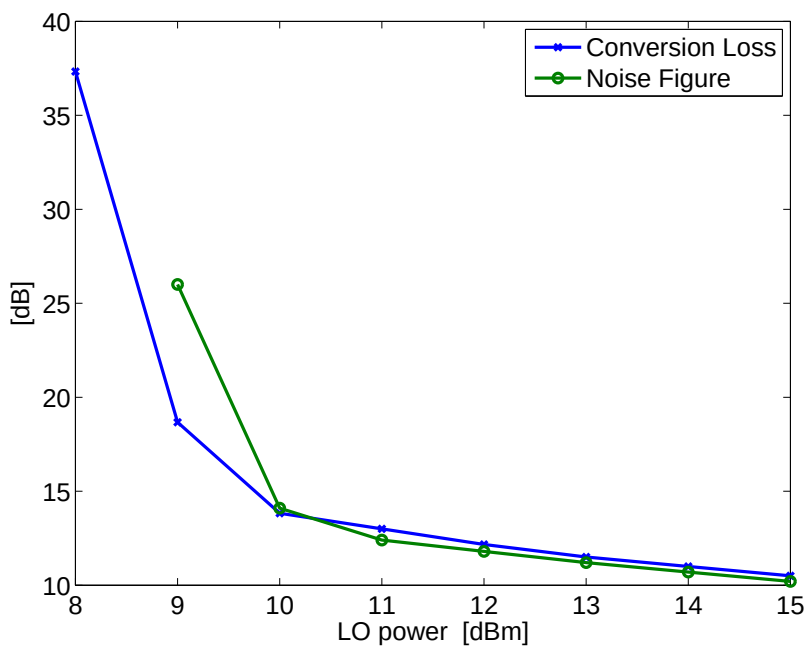

Figure 3.18. Measured conversion loss and single sideband noise figure versus LO power.

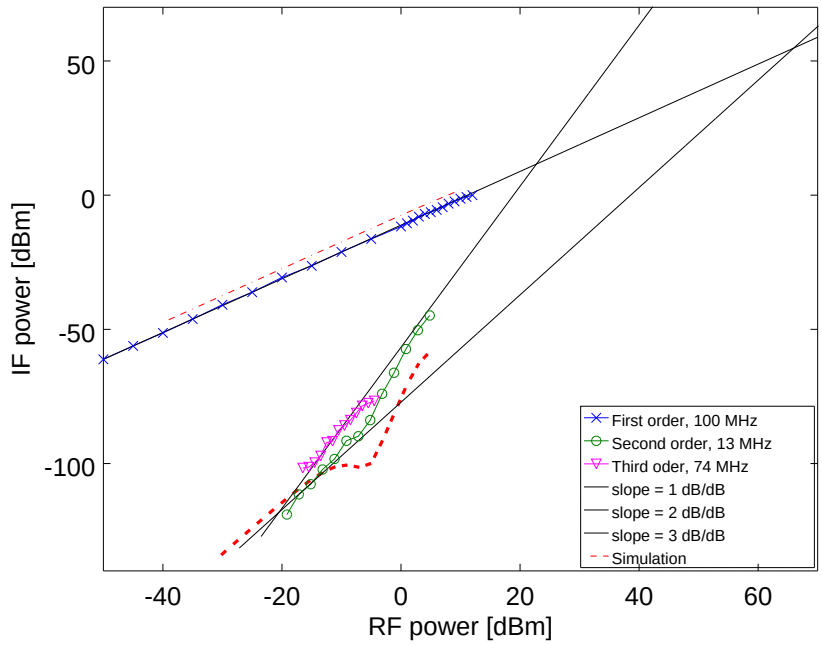

Figure 3.19. Measured IF power versus RF.

at an LO power of 15 dBm which was the limit of the measurement equipment used. To measure the linearity the IF power is measured as a function of the RF power, which is plotted in Figure 3.19. Due to equipment limitations the measurement could not be made with a RF power above 12 dBm. At this point there is measured a compression of 0.8 dB. Simulations predict the input referred 1 dB compression point to be at 12.4 dBm. Intermodulation is measured with two RF tones at frequencies of 8.4 GHz and 8.413 GHz, giving a second order product at 13 MHz and a third order product at 74 MHz. Isolators is placed after the signal generators to avoid leakage and intermodulation of the signals before they are applied to the mixer. Attenuation is added to the output of the mixer to avoid measuring the nonlinearity of the spectrum analyzer [35]. From Figure 3.19 it can be observed that not only a second and third order but also a fourth order phenomenon is observed. It is not possible to distinguish between second and fourth order by frequency selection, as a fourth order term will always be at the same frequency as the second order term. For weak signals it is the second order behavior of the mixer that is dominant whereas for powers above -5 dBm it is fourth order which is dominant. This behavior was predicted by the simulations. By extrapolation the input referred second order intercept point (IIP_2) of 66 dBm and the input referred third order intercept point (IIP_3) of 22 dBm is found. This proves that the design gives a high linearity as required.

The LO-IF, RF-IF and LO-RF isolation at the design frequency are 55 dB, 40 dB, and 58 dB, respectively. In Figure 3.20 the isolation is plotted versus frequency. In the entire band of operation the LO-IF, RF-IF, and LO-RF isolation is better than 46 dB, 36 dB, and 36 dB, respectively. The high LO to RF isolation is very important due to self-mixing issues. Self-mixing can give rise to a DC-current through the mixing

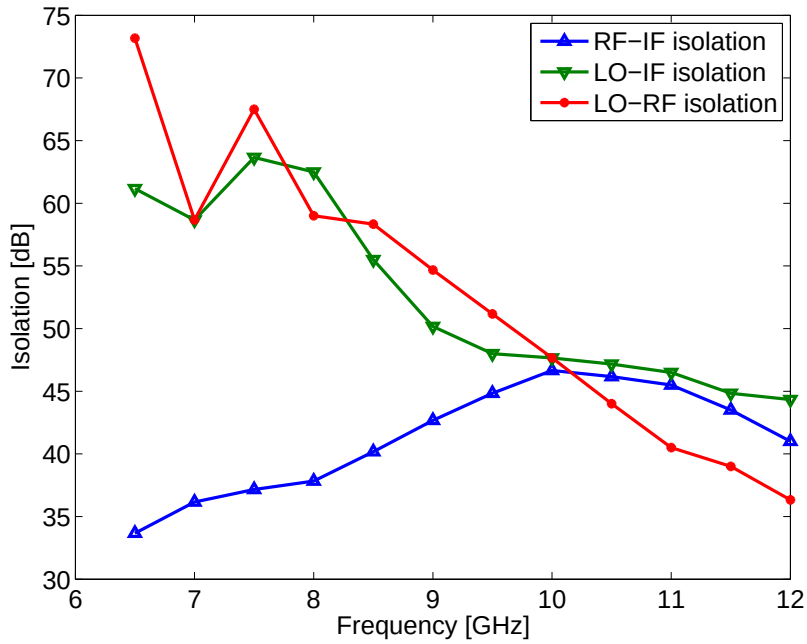

Figure 3.20. Measured LO-IF and RF-IF isolation.

Table 3.3. Comparison between this work and recent reported passive mixers.

Ref.	[30]	[34]	[36]	[37]	This work
Technology	HBT-diode	pHEMT	pHEMT	CMOS	HBT-diode
Topology	Single bal.	Double bal.	Single bal.	Double bal.	Double bal.
Frequency [GHz]	24	NA	60	2.4	8.5
BW [GHz]	22-39	11-40	NA	1.8-2.8	7-12
CG [dB]	−8	−7.2	−12	−7.5	−9.8
LO-power [dBm]	3	13	0	10	15
Isolation [dB]					
LO- IF	50	43.2	32	47.7	55
RF- IF	48	32	NA	NA	40
LO-RF	15	26.9	20	51.9	58
CP_{1dB} [dBm]	-1.5	12	-2	6.2	12

device which increases the 1/f noise, as we saw in Chapter 2.

A comparison between this work and passive mixers recently reported in the open literature is presented in table 3.3.

3.3 HBT mixer, with tunable balun

By using the tunable balun architecture from section 3.1 in the design of the HBT mixer from section 3.2 a HBT mixer with tunable LO balance is designed. In figure 3.21 is a microphotograph of the mixer. Unfortunately there is a short circuit of the tuning voltage, thus not allowing the circuit to be tuned. This was not caught by the Layout versus schematic (LVS) tool, as the MOS-varacter included a bug, which

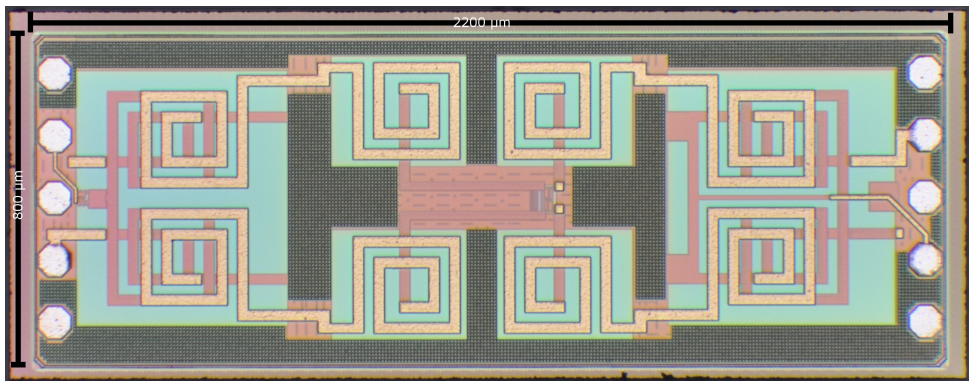

Figure 3.21. Microphotograph of tunable double balanced mixer using diode connected HBTs. The die size is $2200\mu m \times 800\mu m$.

did not allow the LVS to run while this component was used. This is unfortunate as a direct comparison between mixers with a single component change is now not possible. Due to lack of time and funds another chip was not manufactured.

3.4 Schottky Diode mixer, with tunable balun

The balancing circuits should, to get full benefit of the double balanced architecture, be well adjusted. This is challenging to achieve in practice due to process and manufacturing variances. The mixer design presented here integrates the tunable Marchand balun on the LO-port together with Schottky diodes. This allows to correct for any mismatches either in the balun design or in the mixing core itself. This should then enhance the benefits of practical implementations of double balanced mixers, where our focus will be on the properties important for direct conversion mixing, i.e. port isolation and linearity. This section is published in [JP3] and is to the authors knowledge the first time a double balanced ring mixer with balance corrections using a tunable balun is demonstrated.

3.4.1 Non-ideal double balanced mixer theory

This section will give a theoretical description of the behavior of double balanced mixers in the case of non-ideal baluns. The main focus will be on DC offset, port isolation and the intermodulation products. First we investigate the large signal conditions for the LO-voltage. This is followed by an analysis of the behavior of the ring mixer due to unbalance. The analysis takes the time-varying nature of the diodes non-linear conductances under the influence of LO balun imbalances into account. Thus it will be possible to identify the mechanisms responsible for DC offset, LO and RF leakage, conversion loss, and second-order intermodulation products.

The diode ring which will be used as the core of the double balanced mixer is depicted in Figure 3.22. The current through each Schottky diode is given by

$$I_{d_n} = I_s \left(\exp\left(\frac{V_{d_n}}{\eta V_T} \right) - 1 \right), \tag{3.22}$$

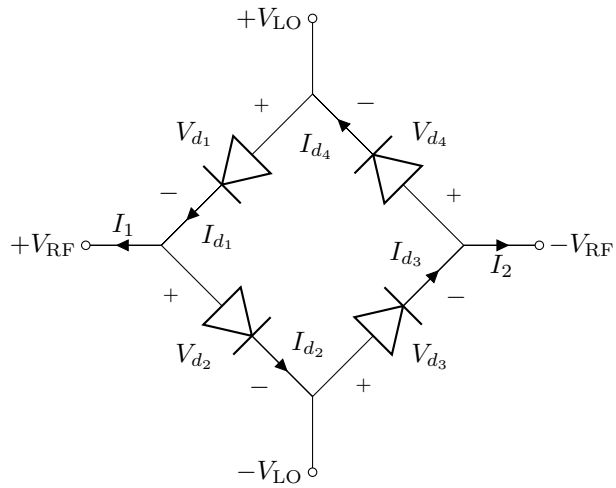

Figure 3.22. Schottky diode ring.

where I_s is the saturation current, V_{d_n} is the large signal diode voltage across diode n, η is the ideality factor and V_T is the thermal voltage.

To find the LO-voltage across a single diode in the diode ring, we look at the left and right half-circuit independently. The half-circuit is shown in Figure 3.23, where the impedance Z_m is a combination of IF, RF load and embedding network. Using the definitions on the figure, we have the following voltage relation:

$$V_a = V_{d_1} + Z_m I_m \tag{3.23}$$

$$V_b = -V_{d_2} + Z_m I_m \tag{3.24}$$

$$\textit{where } I_m = i_a + i_b = I_s \left(\exp\left(\frac{V_{d_1}}{\eta V_T}\right) - \exp\left(\frac{V_{d_2}}{\eta V_T}\right) \right). \tag{3.25}$$

The signals V_a and V_b can be given as

$$V_a = V_{\mathrm{LO}} \left(1 - \frac{\Delta A}{2}\right) \cos\left(\omega_{\mathrm{LO}} t - \frac{\Delta\phi}{2}\right) \tag{3.26}$$

$$V_b = -V_{\mathrm{LO}} \left(1 + \frac{\Delta A}{2}\right) \cos\left(\omega_{\mathrm{LO}} t + \frac{\Delta\phi}{2}\right) \tag{3.27}$$

where we have introduced a phase error, $\Delta\phi$, and a amplitude error ΔA. This allows us to investigate the consequences of imbalance on circuit performance. We will also introduce a load imbalance on the IF load given as $Z_{m_{\mathrm{left}}} = Z_m(1 + \frac{\Delta Z}{2})$ and $Z_{m_{\mathrm{right}}} = Z_m(1 - \frac{\Delta Z}{2})$ for the left and right half circuits, respectively. The term $Z_m I_m$ from (3.23), which will contribute to a voltage difference across the two diodes, is approximated by the term $\left(1 \pm A_Z \left(1 - \frac{\Delta Z}{2}\right)\right)$, where A_Z is a function of the amplitude and phase balance. A_Z reduces to zero if the amplitude and phase balance are both

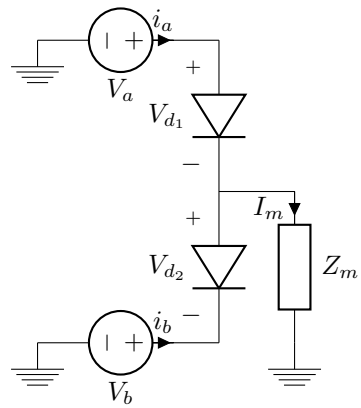

Figure 3.23. Half circuit of diode ring, left side.

zero. Then the large signal diode voltages is given as

$$V_{d_1}=V_{\mathrm{LO}}\left(1-\frac{\Delta A}{2}\right)\cos\left(\omega_{\mathrm{LO}}t-\frac{\Delta\phi}{2}\right)\left(1-A_Z\left(1+\frac{\Delta Z}{2}\right)\right) \tag{3.28a}$$

$$V_{d_2}=V_{\mathrm{LO}}\left(1+\frac{\Delta A}{2}\right)\cos\left(\omega_{\mathrm{LO}}t+\frac{\Delta\phi}{2}\right)\left(1+A_Z\left(1+\frac{\Delta Z}{2}\right)\right) \tag{3.28b}$$

$$V_{d_3}=-V_{\mathrm{LO}}\left(1+\frac{\Delta A}{2}\right)\cos\left(\omega_{\mathrm{LO}}t+\frac{\Delta\phi}{2}\right)\left(1+A_Z\left(1-\frac{\Delta Z}{2}\right)\right) \tag{3.28c}$$

$$V_{d_4}=-V_{\mathrm{LO}}\left(1-\frac{\Delta A}{2}\right)\cos\left(\omega_{\mathrm{LO}}t-\frac{\Delta\phi}{2}\right)\left(1-A_Z\left(1-\frac{\Delta Z}{2}\right)\right). \tag{3.28d}$$

From Figure 3.22 we have

$$I_1=I_{d_1}-I_{d_2} \tag{3.29}$$

$$I_2=I_{d_3}-I_{d_4}. \tag{3.30}$$

Summing these gives the currents at the IF port and the difference gives the current at the RF port

$$I_{\mathrm{IF}}=I_1+I_2 \tag{3.31}$$

$$I_{\mathrm{RF}}=I_1-I_2 \tag{3.32}$$

The current through each diode as a function of RF voltage can be expressed as a Taylor series taken around the large signal LO voltage

$$I_{d_n}(t)=I_{0_{d_n}}(t)+g_{1_{d_n}}(t)v+g_{2_{d_n}}(t)v^2+\cdots \tag{3.33}$$

where d_n denotes the diode number n, $I_{0_{d_n}}=I_d(V)\big|_{V=V_{d_n}}$, $g_1=\frac{dI_d(V)}{dV}\Big|_{V=V_{d_n}}$ and $g_2=\frac{1}{2}\,\frac{d^2I_d(V)}{dV^2}\Big|_{V=V_{d_n}}$. Using (3.33) we will investigate how the DC offset, LO and RF leakage, conversion loss and second order intermodulation depends on the unbalances.

For each diode the current will be given as

$$I_{d_1}=I_{0_{d_1}}(t)-g_{1_{d_1}}(t)v_{\mathrm{RF}}+g_{2_{d_1}}(t)v_{\mathrm{RF}}^2 \tag{3.34a}$$
$$I_{d_2}=I_{0_{d_2}}(t)+g_{1_{d_2}}(t)v_{\mathrm{RF}}+g_{2_{d_2}}(t)v_{\mathrm{RF}}^2 \tag{3.34b}$$
$$I_{d_3}=I_{0_{d_3}}(t)+g_{1_{d_3}}(t)v_{\mathrm{RF}}+g_{2_{d_3}}(t)v_{\mathrm{RF}}^2 \tag{3.34c}$$
$$I_{d_4}=I_{0_{d_4}}(t)-g_{1_{d_4}}(t)v_{\mathrm{RF}}+g_{2_{d_4}}(t)v_{\mathrm{RF}}^2. \tag{3.34d}$$

In Figure 3.24a the waveforms of the currents are plotted for each diode current, with an unbalance of $\Delta A = 0.01$, $\Delta\phi = 5^\circ$ and $\Delta Z = 0.1$. In Figure 3.24b these currents are summed to represent the current at the IF port, and compared to what is expected for the perfectly matched case. It is clear that there is a strong first order tendency, but also a contribution from DC and higher order terms. The following sections will investigate this in details.

DC offset from LO drive

From (3.33) a DC contribution comes from the first term $I_0(t)$ or the even ordered terms, for $\omega_{\mathrm{LO}} \neq \omega_{\mathrm{RF}}$. In this section we will only look at the DC that comes from the $I_0(t)$ term. In section 3.4.1 we look at the DC term coming from higher orders. It should be mentioned that other mechanisms can also add to the DC offset, such as LO self-mixing due to a parasitic path from the LO port to the RF port before the mixer core [CP1]. The zero order Fourier coefficient corresponds to the DC-current through each diode. The zero order Fourier coefficient $I_0(t)$ corresponds to the DC-current through each diode can be found as [OP1]

$$I^0_{0_{d_1}}=I_s\left[\hat{I}_0\left(\frac{V_{\mathrm{LO}}\left(1-\frac{\Delta A}{2}\right)\left(1-A_Z\left(1+\frac{\Delta Z}{2}\right)\right)}{\eta V_T}\right)-1\right] \tag{3.35a}$$
$$I^0_{0_{d_2}}=I_s\left[\hat{I}_0\left(\frac{V_{\mathrm{LO}}\left(1+\frac{\Delta A}{2}\right)\left(1+A_Z\left(1+\frac{\Delta Z}{2}\right)\right)}{\eta V_T}\right)-1\right] \tag{3.35b}$$
$$I^0_{0_{d_3}}=I_s\left[\hat{I}_0\left(\frac{V_{\mathrm{LO}}\left(1+\frac{\Delta A}{2}\right)\left(1+A_Z\left(1-\frac{\Delta Z}{2}\right)\right)}{\eta V_T}\right)-1\right] \tag{3.35c}$$
$$I^0_{0_{d_4}}=I_s\left[\hat{I}_0\left(\frac{V_{\mathrm{LO}}\left(1-\frac{\Delta A}{2}\right)\left(1-A_Z\left(1-\frac{\Delta Z}{2}\right)\right)}{\eta V_T}\right)-1\right], \tag{3.35d}$$

where $\hat{I}_0(x)$ is the modified Bessel function of zeroth order and argument x. As the deviations are all small, linearizing will give better insight. First we reformulate the nominator in 3.35a as

$$V_{\mathrm{LO}}\left(1-\frac{\Delta A}{2}\right)\left(1-A_Z\left(1-\frac{\Delta Z}{2}\right)\right)=V_{\mathrm{LO}}\left(1+a\right) \tag{3.36}$$

where $a=-\frac{\Delta A}{2}-A_Z\left(1-\frac{\Delta Z}{2}\right)+\frac{\Delta A}{2}A_Z\left(1-\frac{\Delta Z}{2}\right)$. Similar relations can be formulated for 3.35b through 3.35d. Then linearizing the Bessel function around V_{LO}, for small deviations of a, using [9.6.28] in [38], gives

$$\hat{I}_0\left(\frac{V_{\mathrm{LO}}(1+a)}{\eta V_T}\right)=\hat{I}_0\left(\frac{V_{\mathrm{LO}}}{\eta V_T}\right)+\frac{V_{\mathrm{LO}}}{\eta V_T}\hat{I}_1\left(\frac{V_{\mathrm{LO}}}{\eta V_T}\right)a \tag{3.37}$$

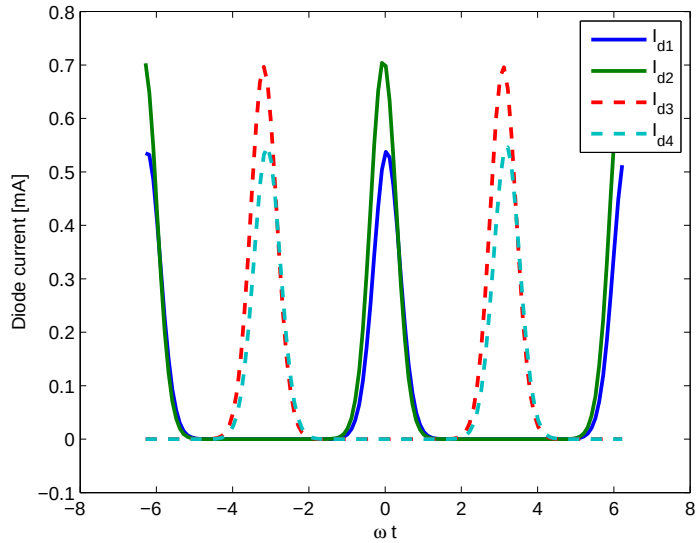

(a) Waveforms for each diode

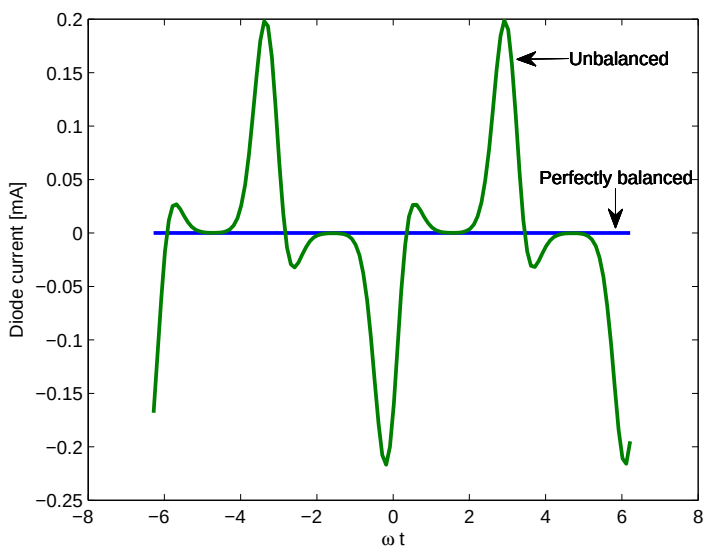

(b) Waveforms for $I_{0_{d_1}}(t) - I_{0_{d_2}}(t) + I_{0_{d_3}}(t) - I_{0_{d_4}}(t)$

Figure 3.24. Waveforms for (a) each diode and (b) the current at the IF port, both with $\Delta A = 0.01$, $\Delta\phi = 5°$ and $\Delta Z = 0.1$.

where $\hat{I}_1(x)$ is the modified Bessel function of 1st order and argument x. Using this relation in (3.35a) through (3.35d), inserting them into (3.29) and (3.30), and then into (3.31) we get

$$I_{\mathrm{IF}}=I^0_{0_{d_1}}-I^0_{0_{d_2}}+I^0_{0_{d_3}}-I^0_{0_{d_4}}=-I_s\frac{V_{\mathrm{LO}}}{\eta V_T}\hat{I}_1\left(\frac{V_{\mathrm{LO}}}{\eta V_T}\right)4A_Z\frac{\Delta Z}{2}. \tag{3.38}$$

This shows that a DC contribution comes directly from the LO signal in the mixer core due to load mismatch (ΔZ) together with LO balun imbalance (contained in A_Z). With tuning of the balun balance this can be reduced as A_Z will be zero for a perfectly balanced mixer. Also as seen in Chapter 2 a DC offset gives additional 1/f-noise, so it is important to reduce this contribution.

LO leakage

The LO leakage is found as the fundamental current running through the diodes to the IF port, corresponding to the first order term of the Fourier series of I_{0d_n}. The first order Fourier coefficients of I_{0d_n} can be found as [OP1]

$$I^1_{0_{d_1}}= I_s\left[\hat{I}_1\left(\frac{V_{\mathrm{LO}}\left(1-\frac{\Delta A}{2}\right)\left(1-A_Z\left(1+\frac{\Delta Z}{2}\right)\right)}{\eta V_T}\right)\exp\left(-j\frac{\Delta\phi}{2}\right)-1\right] \tag{3.39a}$$

$$I^1_{0_{d_2}}= I_s\left[\hat{I}_1\left(\frac{V_{\mathrm{LO}}\left(1+\frac{\Delta A}{2}\right)\left(1+A_Z\left(1+\frac{\Delta Z}{2}\right)\right)}{\eta V_T}\right)\exp\left(j\frac{\Delta\phi}{2}\right)-1\right] \tag{3.39b}$$

$$I^1_{0_{d_3}}= -I_s\left[\hat{I}_1\left(\frac{V_{\mathrm{LO}}\left(1+\frac{\Delta A}{2}\right)\left(1+A_Z\left(1-\frac{\Delta Z}{2}\right)\right)}{\eta V_T}\right)\exp\left(j\frac{\Delta\phi}{2}\right)-1\right] \tag{3.39c}$$

$$I^1_{0_{d_4}}=-I_s\left[\hat{I}_1\left(\frac{V_{\mathrm{LO}}\left(1-\frac{\Delta A}{2}\right)\left(1-A_Z\left(1-\frac{\Delta Z}{2}\right)\right)}{\eta V_T}\right)\exp\left(-j\frac{\Delta\phi}{2}\right)-1\right] \tag{3.39d}$$

The term $\exp\left(j\frac{\Delta\phi}{2}\right)$ is due to the phase mismatch, because when calculating the n'th Fourier coefficient this appears as the modified Bessel function times a factor $\exp\left(jn\frac{\Delta\phi}{2}\right)$ [OP1]. Linearizing the modified Bessel function of first order around V_{LO}, that is for small deviations, using [9.6.28] in [38], gives

$$\hat{I}_1\left(\frac{V_{\mathrm{LO}}(1+a)}{\eta V_T}\right)\approx\hat{I}_1\left(\frac{V_{\mathrm{LO}}}{\eta V_T}\right)+\frac{1}{2}\frac{V_{\mathrm{LO}}}{\eta V_T}\left(\hat{I}_0\left(\frac{V_{\mathrm{LO}}}{\eta V_T}\right)+\hat{I}_2\left(\frac{V_{\mathrm{LO}}}{\eta V_T}\right)\right)a \tag{3.40}$$

Using this relation in (3.35a) through (3.35d), inserting them into (3.29) and (3.30), and then into (3.31) we get

$$\begin{aligned}I_{\mathrm{IF}}=&-2jI_s\frac{V_{\mathrm{LO}}}{\eta V_T}\left(\hat{I}_0\left(\frac{V_{\mathrm{LO}}}{\eta V_T}\right)+\hat{I}_2\left(\frac{V_{\mathrm{LO}}}{\eta V_T}\right)\right)\\&\times\left[\cos\left(\frac{\Delta\phi}{2}\right)\left(A_Z+\frac{\Delta A}{2}\right)+j\sin\left(\frac{\Delta\phi}{2}\right)\frac{\Delta A}{2}A_Z\right].\end{aligned} \tag{3.41}$$

From (3.41) it is seen that there is a strong connection between balun imbalances and the LO leakage, but no dependence on load mismatch.

By again using (3.40) in (3.35a) through (3.35d), inserting them into (3.29) and (3.30), and then into (3.32) we get the LO to RF leakage:

$$I_{\mathrm{RF}}=-2jI_s\frac{V_{\mathrm{LO}}}{\eta V_T}\left(\hat{I}_0\left(\frac{V_{\mathrm{LO}}}{\eta V_T}\right)+\hat{I}_2\left(\frac{V_{\mathrm{LO}}}{\eta V_T}\right)\right) \times A_Z\frac{\Delta Z}{2}\left[\cos\left(\frac{\Delta\phi}{2}\right)+j\sin\left(\frac{\Delta\phi}{2}\right)\frac{\Delta A}{2}\right]. \tag{3.42}$$

From (3.42) it is seen that to have LO to RF leakage in the mixer core, there must be a load mismatch, together with a balun imbalance. As was seen in Chapter 2, it is very important to reduce this leakage as it can reflect and give a DC level by self mixing. This will again increase the the 1/f-noise.

RF leakage

The second term of (3.33) describes the linear behavior of the RF current. The RF leakage is found as the zeroth order Fourier coefficient of $g_{1_{d_n}}(t)$. This can be evaluated as [OP1]

$$G^0_{1_{d_1}}=\frac{I_s}{\eta V_T}\hat{I}_0\left(\frac{V_{\mathrm{LO}}\left(1-\frac{\Delta A}{2}\right)\left(1-A_Z\left(1+\frac{\Delta Z}{2}\right)\right)}{\eta V_T}\right) \tag{3.43a}$$

$$G^0_{1_{d_2}}=\frac{I_s}{\eta V_T}\hat{I}_0\left(\frac{V_{\mathrm{LO}}\left(1+\frac{\Delta A}{2}\right)\left(1+A_Z\left(1+\frac{\Delta Z}{2}\right)\right)}{\eta V_T}\right) \tag{3.43b}$$

$$G^0_{1_{d_3}}=\frac{I_s}{\eta V_T}\hat{I}_0\left(\frac{V_{\mathrm{LO}}\left(1+\frac{\Delta A}{2}\right)\left(1+A_Z\left(1-\frac{\Delta Z}{2}\right)\right)}{\eta V_T}\right) \tag{3.43c}$$

$$G^0_{1_{d_4}}=\frac{I_s}{\eta V_T}\hat{I}_0\left(\frac{V_{\mathrm{LO}}\left(1-\frac{\Delta A}{2}\right)\left(1-A_Z\left(1-\frac{\Delta Z}{2}\right)\right)}{\eta V_T}\right) \tag{3.43d}$$

Linearizing the Bessel function and using equations (3.34) through (3.35) we get

$$\begin{aligned}I_{\mathrm{IF}}&=(-G^0_{1_{d_1}}-G^0_{1_{d_2}}+G^0_{1_{d_3}}+G^0_{1_{d_4}})v_{\mathrm{RF}}\\&=-4v_{\mathrm{RF}}\frac{I_sV_{\mathrm{LO}}}{(\eta V_T)^2}\hat{I}_1\left(\frac{V_{\mathrm{LO}}}{\eta V_T}\right)\frac{\Delta A}{2}A_Z\frac{\Delta Z}{2}.\end{aligned} \tag{3.44}$$

As observed from (3.44), an imbalance in the LO balun will result in an RF leakage if there is also simultaneously a mismatch in the IF-load. This is not to say that this is the only way an RF-leak can occur, an imbalance in the RF-balun has a high impact on the RF-leakage, but this is outside the scope of this analysis.

Conversion loss

The desired mixing product at the IF frequency is found when the RF signal is multiplied with the fundamental tone of $g_{1_{d_n}}(t)$. The contribution can be evaluated

from the first order Fourier coefficients as

$$G^1_{1_{d_1}} = \frac{I_s}{\eta V_T}\hat{I}_1\left(\frac{V_{\mathrm{LO}}\left(1-\frac{\Delta A}{2}\right)\left(1-A_Z\left(1+\frac{\Delta Z}{2}\right)\right)}{\eta V_T}\right)\exp\left(-j\frac{\Delta\phi}{2}\right) \tag{3.45a}$$

$$G^1_{1_{d_2}} = \frac{I_s}{\eta V_T}\hat{I}_1\left(\frac{V_{\mathrm{LO}}\left(1+\frac{\Delta A}{2}\right)\left(1+A_Z\left(1+\frac{\Delta Z}{2}\right)\right)}{\eta V_T}\right)\exp\left(j\frac{\Delta\phi}{2}\right) \tag{3.45b}$$

$$G^1_{1_{d_3}} = -\frac{I_s}{\eta V_T}\hat{I}_1\left(\frac{V_{\mathrm{LO}}\left(1+\frac{\Delta A}{2}\right)\left(1+A_Z\left(1-\frac{\Delta Z}{2}\right)\right)}{\eta V_T}\right)\exp\left(j\frac{\Delta\phi}{2}\right) \tag{3.45c}$$

$$G^1_{1_{d_4}} = -\frac{I_s}{\eta V_T}\hat{I}_1\left(\frac{V_{\mathrm{LO}}\left(1-\frac{\Delta A}{2}\right)\left(1-A_Z\left(1-\frac{\Delta Z}{2}\right)\right)}{\eta V_T}\right)\exp\left(-j\frac{\Delta\phi}{2}\right). \tag{3.45d}$$

Linearizing the Bessel function and using equations (3.34) through (3.35) we get

$$\begin{aligned} I_{\mathrm{IF}} =& (-G^1_{1_{d_1}} - G^1_{1_{d_2}} + G^1_{1_{d_3}} + G^1_{1_{d_4}})v_{\mathrm{RF}} \\ =& -4v_{\mathrm{RF}}\frac{I_s}{\eta V_T}\left[\hat{I}_1\left(\frac{V_{\mathrm{LO}}}{\eta V_T}\right)\cos\left(\frac{\Delta\phi}{2}\right) + \frac{1}{2}\frac{V_{\mathrm{LO}}}{\eta V_T}\left(\hat{I}_2\left(\frac{V_{\mathrm{LO}}}{\eta V_T}\right) + \hat{I}_0\left(\frac{V_{\mathrm{LO}}}{\eta V_T}\right)\right)\right. \\ & \left.\times\left(A_Z\frac{\Delta A}{2}\cos\left(\frac{\Delta\phi}{2}\right) + j\left(A_Z + \frac{\Delta A}{2}\right)\sin\left(\frac{\Delta\phi}{2}\right)\right)\right]. \end{aligned} \tag{3.46}$$

The conversion loss is inversely proportional to the IF current. Therefore, it is observed that the conversion loss is not affected much by the phase imbalance as $\cos\left(\frac{\Delta\phi}{2}\right) \approx 1$ and the second term is negligible under the assumption of small deviations.

Second order intermodulation

The third term of (3.33) describes the second order behavior of the RF current. The zeroth order Fourier coefficient of $g_{2_{d_n}}(t)$, gives rise to the second order intermodulation and DC-contribution from the RF signal. The Fourier coefficient can be found as [OP1]

$$G^0_{2_{d_1}} = \frac{I_s}{(\eta V_T)^2}\hat{I}_0\left(\frac{V_{\mathrm{LO}}\left(1-\frac{\Delta A}{2}\right)\left(1-A_Z\left(1+\frac{\Delta Z}{2}\right)\right)}{\eta V_T}\right) \tag{3.47a}$$

$$G^0_{2_{d_2}} = \frac{I_s}{(\eta V_T)^2}\hat{I}_0\left(\frac{V_{\mathrm{LO}}\left(1+\frac{\Delta A}{2}\right)\left(1+A_Z\left(1+\frac{\Delta Z}{2}\right)\right)}{\eta V_T}\right) \tag{3.47b}$$

$$G^0_{2_{d_3}} = \frac{I_s}{(\eta V_T)^2}\hat{I}_0\left(\frac{V_{\mathrm{LO}}\left(1+\frac{\Delta A}{2}\right)\left(1+A_Z\left(1-\frac{\Delta Z}{2}\right)\right)}{\eta V_T}\right) \tag{3.47c}$$

$$G^0_{2_{d_4}} = \frac{I_s}{(\eta V_T)^2}\hat{I}_0\left(\frac{V_{\mathrm{LO}}\left(1-\frac{\Delta A}{2}\right)\left(1-A_Z\left(1-\frac{\Delta Z}{2}\right)\right)}{\eta V_T}\right). \tag{3.47d}$$

Again by linearizing the Bessel function and using equations (3.34) through (3.35) we get

$$\begin{aligned} I_{\mathrm{IF}} =& (G^0_{2_{d_1}} - G^0_{2_{d_2}} + G^0_{2_{d_3}} - G^0_{2_{d_4}}) v^2_{\mathrm{RF}} \\ =& -4 \frac{V_{\mathrm{LO}} I_s}{(\eta V_T)^3} \hat{I}_1 \left(\frac{V_{\mathrm{LO}}}{\eta V_T} \right) A_Z \frac{\Delta Z}{2} v^2_{\mathrm{RF}}. \end{aligned} \tag{3.48}$$

From (3.48) we see that second order intermodulation products will arise if there is a load mismatch together with a LO-balun imbalance.

Third order intermodulation

The fourth term of (3.33) describes the third order behavior of the RF current. To mix the frequencies to be near the IF frequency, it is neccessary for the third order RF to mix with the LO, ie. it is the first order Fourier coefficient of $g_{2_{d_n}}(t)$, which give rise to the third order intermodulation from the RF signal. The Fourier coefficient can be found as [OP1]

$$G^1_{3_{d_1}} = \frac{I_s}{(\eta V_T)^3} \hat{I}_1 \left(\frac{V_{\mathrm{LO}} \left(1 - \frac{\Delta A}{2}\right) \left(1 - A_Z \left(1 + \frac{\Delta Z}{2}\right)\right)}{\eta V_T} \right) \exp\left(-j \frac{\Delta \phi}{2} \right) \tag{3.49a}$$

$$G^1_{3_{d_2}} = \frac{I_s}{(\eta V_T)^3} \hat{I}_1 \left(\frac{V_{\mathrm{LO}} \left(1 + \frac{\Delta A}{2}\right) \left(1 + A_Z \left(1 + \frac{\Delta Z}{2}\right)\right)}{\eta V_T} \right) \exp\left(j \frac{\Delta \phi}{2} \right) \tag{3.49b}$$

$$G^1_{3_{d_3}} = -\frac{I_s}{(\eta V_T)^3} \hat{I}_1 \left(\frac{V_{\mathrm{LO}} \left(1 + \frac{\Delta A}{2}\right) \left(1 + A_Z \left(1 - \frac{\Delta Z}{2}\right)\right)}{\eta V_T} \right) \exp\left(j \frac{\Delta \phi}{2} \right) \tag{3.49c}$$

$$G^1_{3_{d_4}} = -\frac{I_s}{(\eta V_T)^3} \hat{I}_1 \left(\frac{V_{\mathrm{LO}} \left(1 - \frac{\Delta A}{2}\right) \left(1 - A_Z \left(1 - \frac{\Delta Z}{2}\right)\right)}{\eta V_T} \right) \exp\left(-j \frac{\Delta \phi}{2} \right). \tag{3.49d}$$

Linearizing the Bessel function and using equations (3.34) through (3.35) we get

$$\begin{aligned} I_{\mathrm{IF}} =& (-G^1_{3_{d_1}} - G^1_{3_{d_2}} + G^1_{3_{d_3}} + G^1_{3_{d_4}}) v^3_{\mathrm{RF}} \\ =& -4 v^3_{\mathrm{RF}} \frac{I_s}{(\eta V_T)^3} \left[\hat{I}_1 \left(\frac{V_{\mathrm{LO}}}{\eta V_T} \right) \cos\left(\frac{\Delta \phi}{2} \right) + \frac{1}{2} \frac{V_{\mathrm{LO}}}{\eta V_T} \left(\hat{I}_2 \left(\frac{V_{\mathrm{LO}}}{\eta V_T} \right) + \hat{I}_0 \left(\frac{V_{\mathrm{LO}}}{\eta V_T} \right) \right) \right. \\ & \left. \times \left(A_Z \frac{\Delta A}{2} \cos\left(\frac{\Delta \phi}{2} \right) + j \left(A_Z + \frac{\Delta A}{2} \right) \sin\left(\frac{\Delta \phi}{2} \right) \right) \right]. \end{aligned} \tag{3.50}$$

It is observed that the third order intermodulation is not affected much by the phase imbalance as $\cos\left(\frac{\Delta\phi}{2}\right) \approx 1$ and the second term is negligible under the assumption of small deviations, just like the conversion loss.

3.4.2 Design of mixer with tunable balun

This section gives a description of the design of the circuitry.

A diagram of the full mixer is shown in Figure 3.25. The mixing core consists of four Schottky diodes in a ring, to enable the double balanced properties [9]. When

Table 3.4. Design parameters for the mixer circuit

Inductance	L_s [nH]	1.02
Inductive coupling	k	0.825
Capacitive coupling	C_c [fF]	379
Input matching capacitors	C_s [fF]	283
Balance matching capacitor	C_m [fF]	190
Matching Inductor, LO	L_{LO} [nH]	0.94
Matching Inductor, RF	L_{RF} [nH]	0.94
Diode area	A_d [μm^2]	14.4

choosing the diode size, the conversion-loss degradation factor [9] is a helpful guiding parameter

$$\delta = 1 + \frac{R_s}{Z_s} + \frac{Z_s f_{\mathrm{RF}}^2}{R_s f_c^2} \tag{3.51}$$

where R_s is the series resistance, Z_s is the real diode junctions RF input resistance, and $f_c = \frac{1}{2\pi R_s C_j}$ is the cutoff frequency. Increasing the diode area will decrease the series resistance, but increase the junction capacitance, C_j, in such a manner that the cutoff frequency will decrease [10]. But as the RF frequency is relatively low, a larger diode will give better conversion-loss degradation factor as the last term of (3.51) will be almost negligible. Using Harmonic Balance simulations a size was found such that using single series inductors, L_{RF} and L_{LO} for the RF and the LO ports, respectively, was sufficient to match to $50\,\Omega$. This gave a diode area of $14.4\,\mu\mathrm{m}^2$, with corresponding series resistance of $R_s = 19\,\Omega$, junction capacitance of $C_{j_0} = 80\,\mathrm{fF}$, which results in a cutoff frequency of $f_c = 105\,\mathrm{GHz}$, and a loss degradation factor of $\delta = 1.5\,\mathrm{dB}$.

The mixer uses a tunable Marchand balun on the LO side designed after the procedure described in Section 3.1 and a conventional Marchand balun on the RF port designed after the procedure described in Section 3.2.1. The IF-extraction is similar to that described in Section 3.2. That is, the RF balun has coupling capacitors C_{IF} to its ground connection, allowing for the IF signal extraction. It is important to make the IF extraction symmetric as any asymmetry will affect the balun performance. On the LO side the balun will, by its grounding, ensure the IF-return path for the diode ring. Table 3.4 gives the design parameters.

3.4.3 Experimental Results

In this section the experimental results are discussed. The measurements are made on-wafer using a probe station, and calibration is used to remove losses in cables and probes. The Schottky diodes are not a mature part of the process and suffers from leakage current.

First measurements of the Marchand balun, measured on a separate breakout, is presented in section 3.4.3 which is followed by a presentation of the measurements of the full mixer circuit in section 3.4.3.

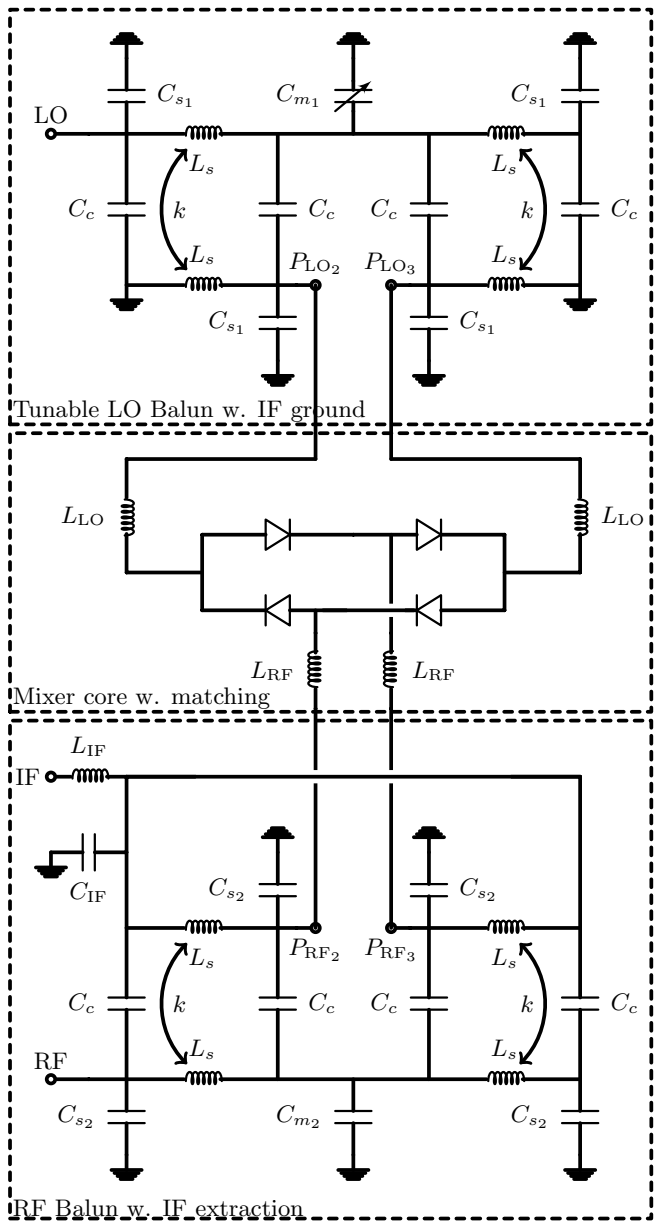

Figure 3.25. Schematic of the double balanced mixer including RF and LO baluns.

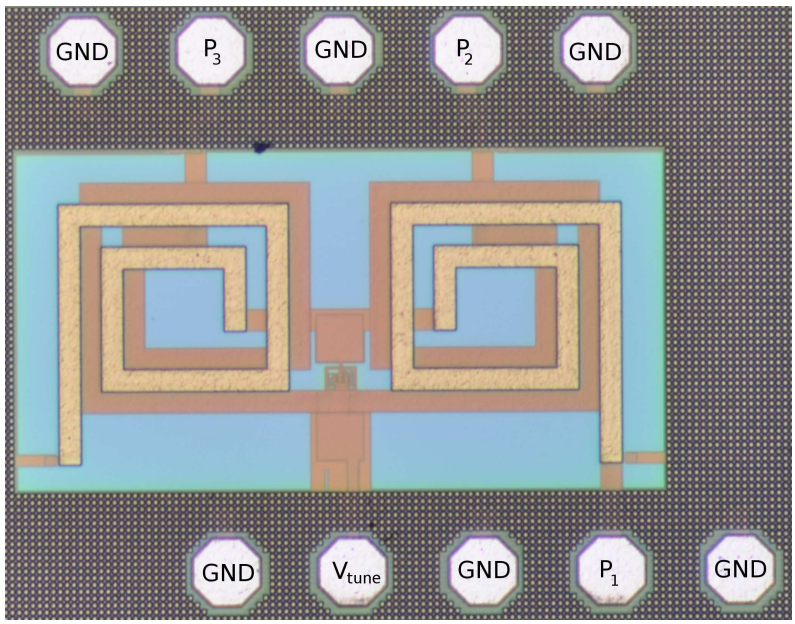

Figure 3.26. Microphotograph of the tunable Marchand balun, size 700 µm × 990 µm

Marchand balun experimental results

A break out of the circuit was manufactured, with a size of $700\mu\text{m}\times990\mu m$, which is shown in Figure 3.26. The matching capacitors, C_s is implemented as MIM capacitors and variable capacitor, C_m, is implemented using a MOS-varactor. The inductors, L_s, is implemented as broad-side coupled inductor pairs using the top two metal layers, for best Q-value. These are diagonally offset to get the desired inductive coupling, k, and capacitive coupling, C_c.

Figure 3.27 shows measurements of insertion loss, reflection and isolation of the balun structure. The insertion loss is better than 7 dB on both channels in the range from 11 GHz to 13 GHz, while having a return loss better than 14.5 dB. The magnitude balance is plotted in Figure 3.28. At the center frequency of 12 GHz the magnitude balance can be tuned by 0.8 dB, from −0.8 dB to 0 dB. In Figure 3.29 is the phase difference plotted for different bias values as a function of frequency. At the center frequency the phase difference can be tuned by 5.8°, from 171.6° to 177.4°, so a perfect match is not obtainable, but a large improvement of $\Delta\phi$ is still possible.

Full mixer circuit

In this section, measurements of the combined mixer circuit are discussed. The circuit has a size of 2050 µm×1000 µm, and in Figure 3.30 a microphotograph of the circuit is shown. For all measurements the IF-frequency is 100 MHz.

The conversion loss as a function of LO power at 11.5 GHz is plotted in Figure 3.31. It is almost saturated for a LO power level of 11 dBm with a conversion loss of 9.7 dB. Increasing the LO power level to 16 dBm will only give a small decrease in conversion

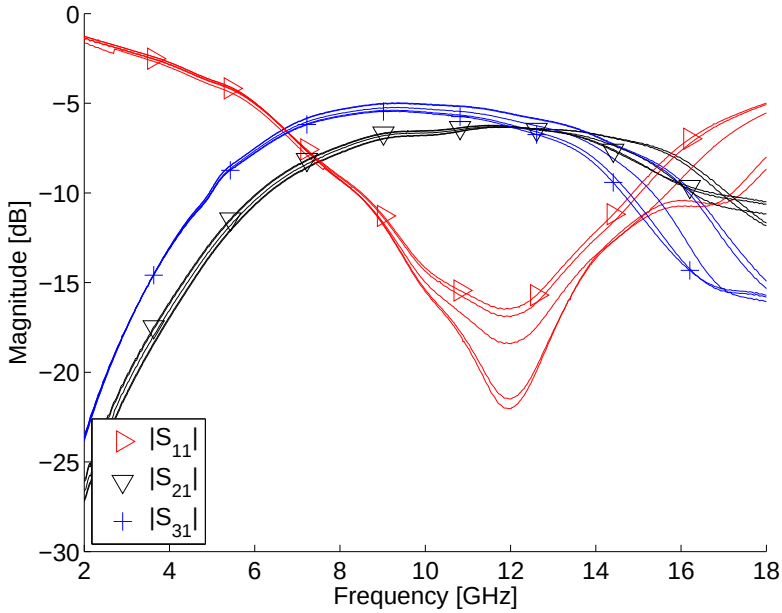

Figure 3.27. Insertion loss and input matching measured with tuning voltages ranging from −2.5 V to 2.5 V.

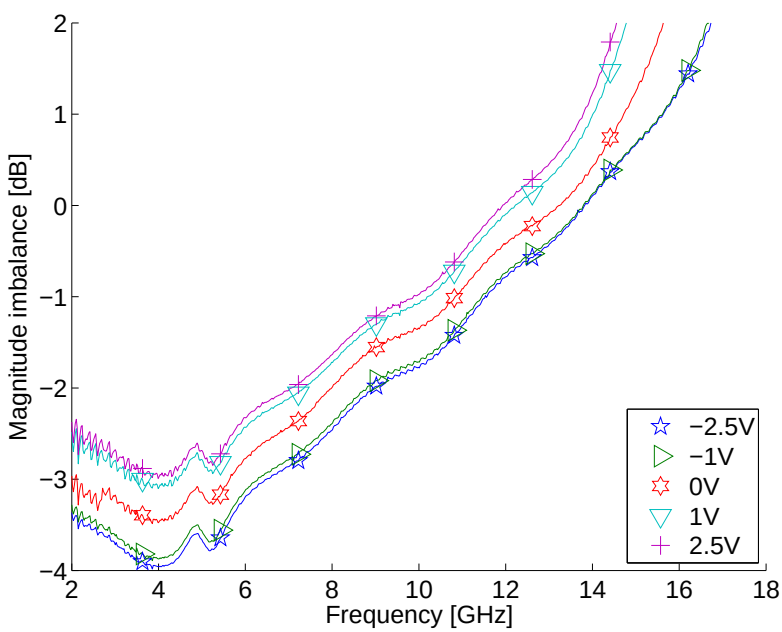

Figure 3.28. Measurement of magnitude imbalance with tuning voltages ranging from −2.5 V to 2.5 V.

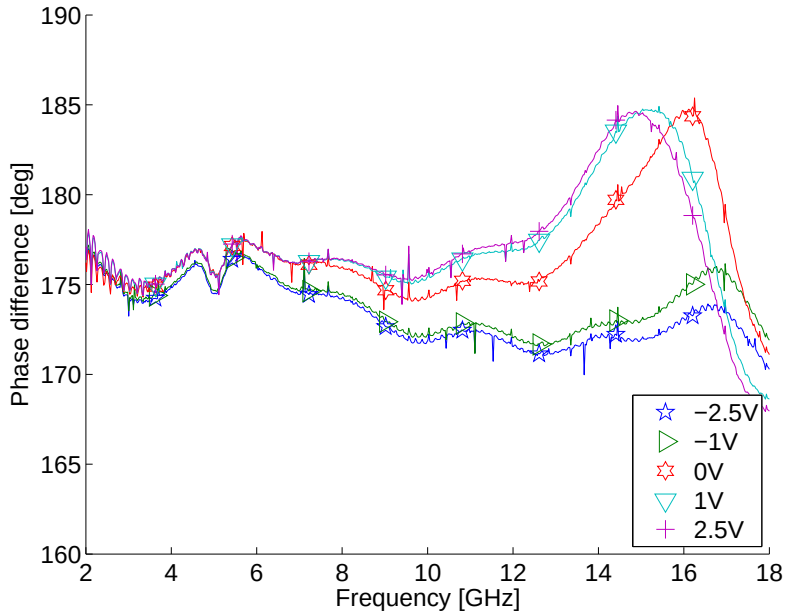

Figure 3.29. Measurement of phase difference between output ports with tuning voltages ranging from −2.5 V to 2.5 V.

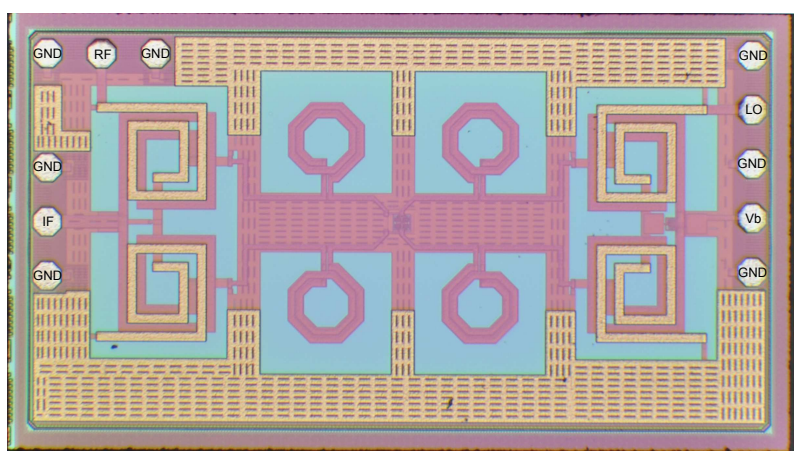

Figure 3.30. Microphotograph of the mixer circuit. Size 2050 µm×1000 µm

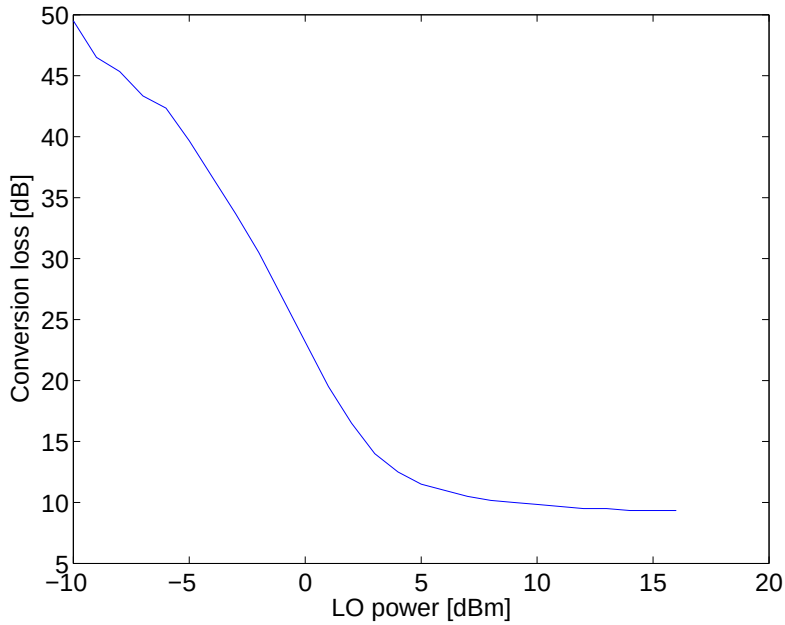

Figure 3.31. Conversion loss as a function of local oscillator power

loss to 9.3 dB. Thus for all other measurements the lower level of 11 dBm is chosen, which should give sufficiently good conversion loss. The conversion loss as a function of frequency is plotted in Figure 3.32. A conversion loss of 8.8 dB is obtained at 11 GHz. The broadband nature of the Marchand balun is seen and the 3-dB bandwidth is from 8 GHz to 13 GHz, covering more than the entire X-band. Changing the tuning capacitance has a clear influence on the isolation. At 11 GHz the LO to IF isolation can be changed from −41.3 dB at a bias voltage of −2.5 V to −48.7 dB at a bias voltage of 2.5 V. In Figure 3.33 the LO to IF isolation is plotted as a function of balun tuning voltage for different frequencies. It is possible to reduce the isolation more for the higher frequencies, but this is what is expected as the balun is more sensitive there. The LO to RF isolation is plotted versus tuning voltage at 11 GHz in figure Figure 3.34. It can be improved from −50 dB to −53.6 dB. The conversion loss is constant with the tuning, as was expected. Also the RF-IF is constant, this is due to the fact that the main contributing mechanism to the leakage is unbalance in the RF-balun which remains constant.

In Figure 3.35 the parasitic DC offset is plotted versus the tuning voltage. It is seen that it is possible to change the DC offset by a few mV, but there is a larger offset of around 9 mV which cannot be completely removed. As would be expected there is a larger swing for the higher frequencies as the balun is more sensitive there. Apart from disturbing the following circuitry the DC offset is also unwanted as it increases the flicker noise level [CP1].

The linearity is plotted in Figure 3.36. The 1dB compression point is measured to be at 8 dBm RF input power.

Intermodulation is measured with two RF tones at frequencies of 11.5 GHz and

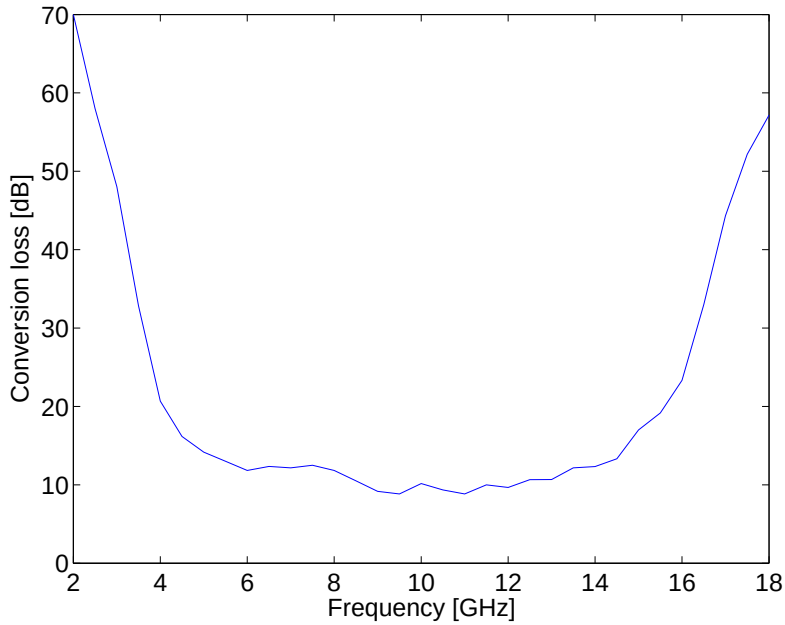

Figure 3.32. Conversion loss as a function of frequency

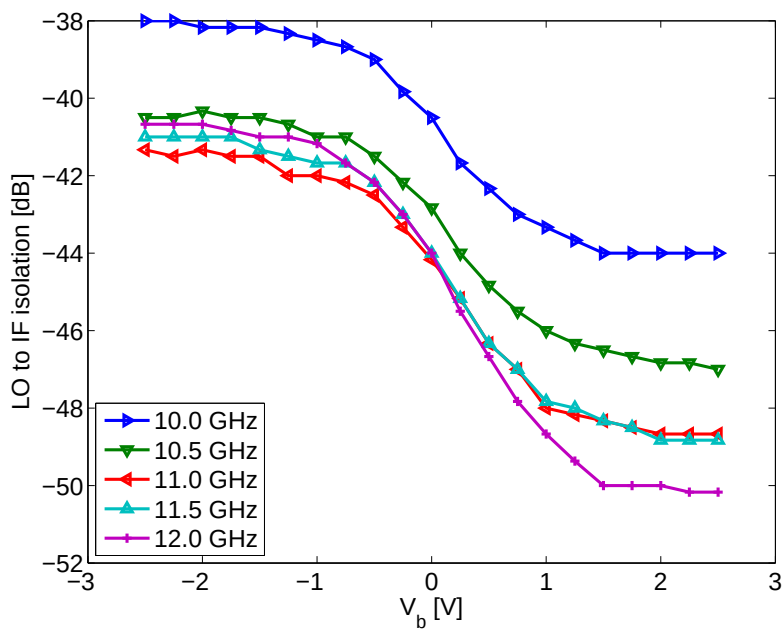

Figure 3.33. LO to IF isolation versus tuning voltage for different frequencies.

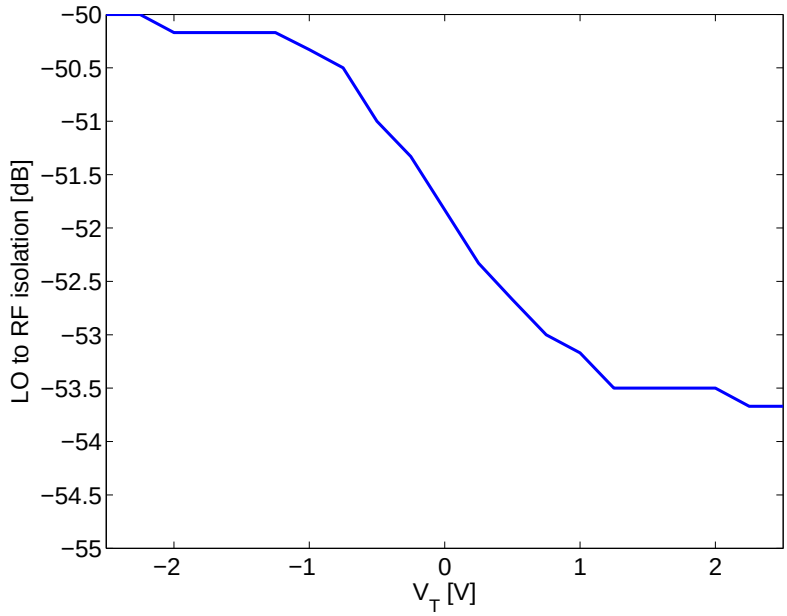

Figure 3.34. LO to RF isolation versus tuning voltage at 11 GHz.

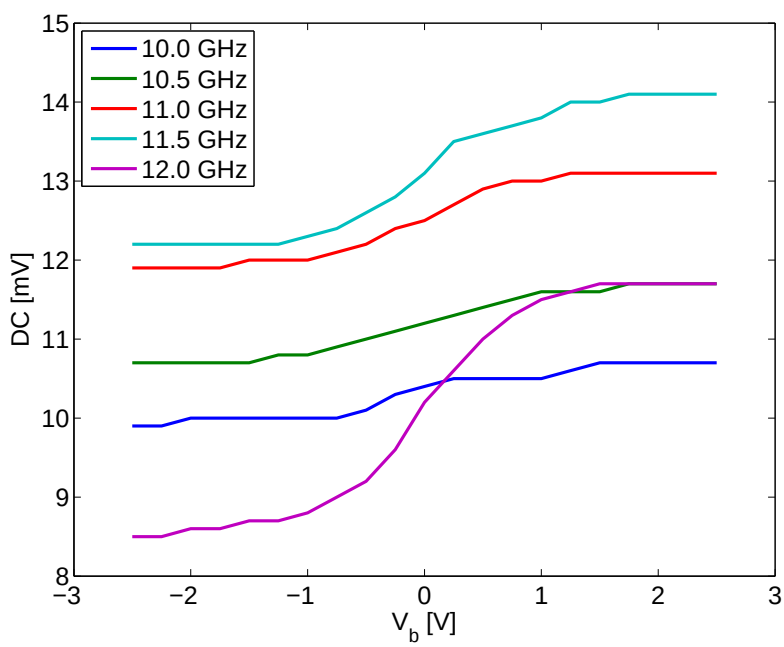

Figure 3.35. DC level versus tuning voltage for different frequencies.

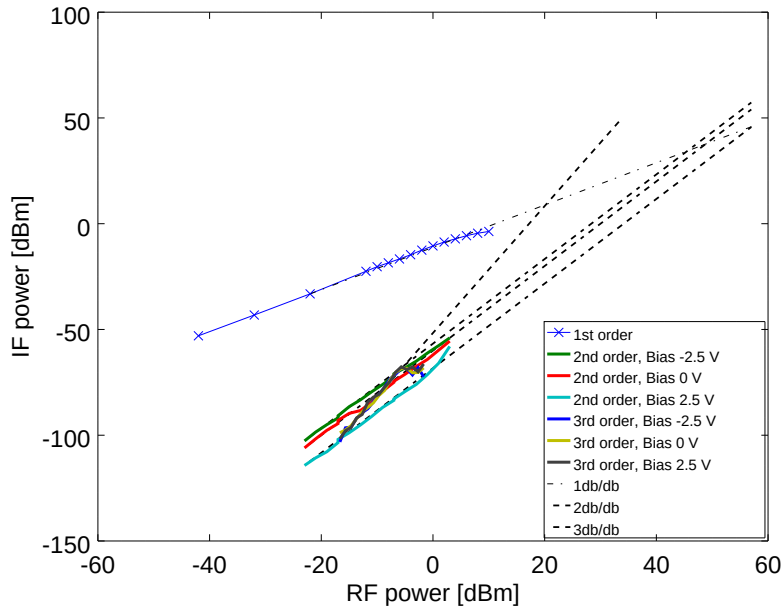

Figure 3.36. IF power versus RF power at the fundamental, second order and third order frequency for different tuning voltages. Extrapolated lines show IIP_2 and IIP_3.

Table 3.5. Comparison between this work and recent reported direct conversion mixers.

Ref.	[39]	[40]	Section 3.2	This work
Technology	SiGe HBT	SiC Schottky	SiGe HBT-diode	SiGe Schottky
Topology	Active double bal.	Double bal.	Double bal.	Double bal.
Frequency [GHz]	18	2.4	8.5	11
CG [dB]	4.5	−12	−9.8	−8.8
LO-power [dBm]	-1	24	15	11
LO-IF/RF-IF/LO-RF isolation [dB]	- / - / 31	> 30/ 7/ -	55 / 40 / 58	60.5 / 35 / 53.7
IP_{1dB} [dBm]	-12.2	23	12	8
IIP_2 [dBm]	20.3	58	66	45 - 57

11.513 GHz, giving a second order product at 13 MHz and a third order product at 74 MHz, and LO frequency of 11.4 GHz. Isolators are placed after the signal generators to avoid leakage and intermodulation of the signals before they are applied to the mixer. Attenuation is added to the output of the mixer to avoid measuring the non-linearity of the spectrum analyzer [35]. From Figure 3.36 the IIP_2 can be read as the extrapolated values to be 45.5 dBm, 48.8 dBm and 57.1 dBm for bias levels of -2.5 V, 0 V and 2.5 V respectively, giving a 11.6 dB tuning range of IIP_2. The curve corresponding to the 2.5 V bias point has a steeper slope for the last couple of points which could be a fourth order phenomenon, as the one that was observed in Section 3.2. The IIP_3 is likewise found to be 20 dBm for all bias levels. This is accordig to the theory explained in Section 3.4.1, where it was shown that the second order intermodulation is sensitive to small changes in the balance whereas the third order intermodulation is not. Thus it is experimentally shown that a tunable balun can enhance the properties of the double balanced mixer, by increasing the LO-IF isolation and the IIP_2.

In table 3.5 the mixer is compared with other state-of-the-art direct conversion mixers reported in the open literature. As would be expected it is clear that if one wants an extremely linear circuit an active topology is not suitable. Of course, the active topology comes with the benefit of having 4.5 dB gain compared with -8.8 dB or worse for the passive diode based topologies. The 1 dB compression point is lower than what is reported for [40] and Section 3.2, but these also exhibits more loss. The best IIP_2 is achieved by the mixer described in Section 3.2, but after tuning our circuit is close to this and on par with [40]. An explanation for the poorer intermodulation is that a perfect balance is not obtained anywhere in the tuning range of the balun.

3.5 Flicker noise measurements

In this section the flicker noise measurement setup will be described. This will be followed by a presentation and discussion of the results of the measurements of flicker noise on both the HBT-diode mixer and the Schottky diode mixer. Parts of this section is published in [CP4].

3.5.1 Flicker noise measurement setup

Due to the sensitive nature of the flicker noise measurements it is not possible to perform these on-wafer. Shielding the mixer from a noisy environment is much easier when packaged in a small metal case. For this purpose the mixer chips is mounted on an Arlon 25N substrate with cobber lines covered with soft gold to allow for ball bonding using gold wires. A packaged mixer is shown in Figure 3.37. Apart from the LO, RF and IF ports also a bulk bias connection to the Silicon substrate is made. This is grounded for the measurements presented here. For the tunable Schottky diode mixer, there is also a bias connection to the tunable balun.

The conversion loss is measured, at first, on a bare die using a probe station and then again after packaging. For the on wafer measurements, calibration is performed to a reference plane at the tip of the probe, ie. at the contacts of the chip. For the packaged version, calibration is done to a reference plane at the SubMiniature version A (SMA) connector.

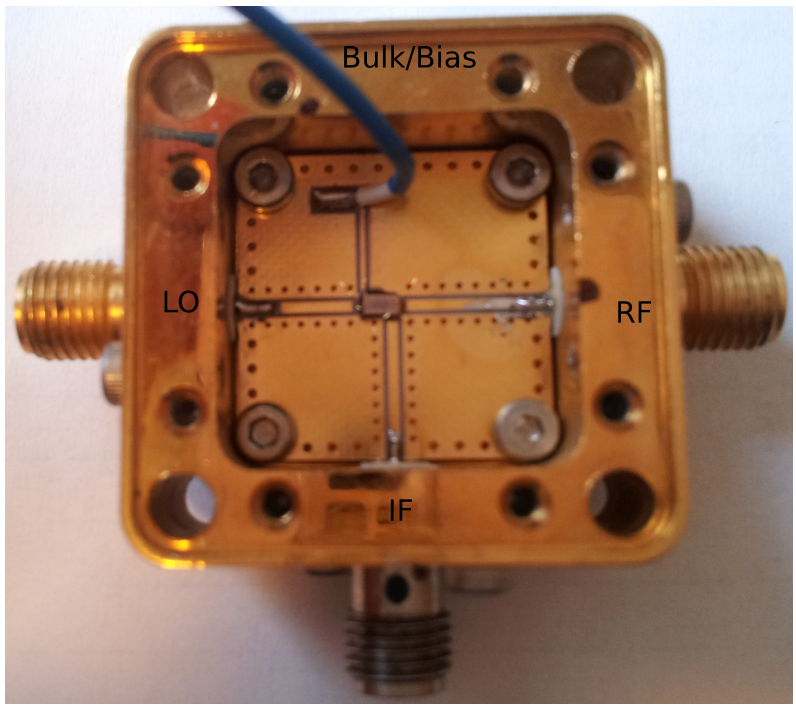

Figure 3.37. Packaged chips

The noise measurement is carried out using a spectrum analyzer together with a calibrated noise source to measure the Y-factor [9]. Then the noise figure can be calculated as

$$F = \frac{\text{ENR}}{Y - 1} \tag{3.52}$$

where ENR is the excess noise ratio of the noise diode, and Y is the power ratio of the output powers with a cold-load (diode off) and a hot-load (diode on). Two different custom made cavity resonance oscillators with a Q above 10 000 are used as LO sources. These delivers an output power around 13 dBm at 9.1 GHz and 10.4 GHz, respectively. The noise source is an Anritsu Noise diode with excess noise ratio of 14.3 dB. The IF amplifier is similar to the ones used in commercial Doppler radars manufactured by Weibel Scientific and has a gain of 80 dB. The measurement setup is shown in Figure 3.38. This measurement method gives the double sideband noise figure, and all measurement results of noise figure presented in this section will be double sideband. As the present investigation is concerned with the comparison between the two mixer circuits, there has not been done extensive measurements to determine the noise contributions from the oscillator and IF-amplifier, although quality components has been used to minimize the effect.

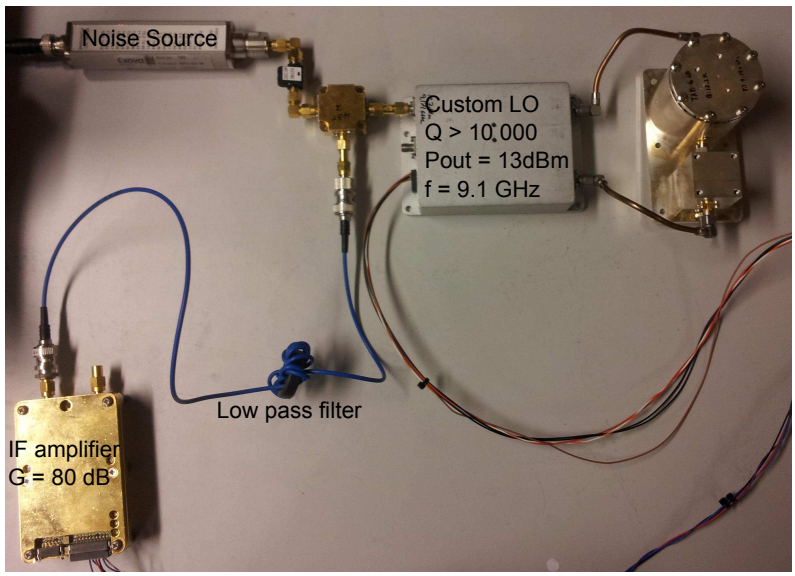

Figure 3.38. Measurements setup

3.5.2 Flicker noise measurements results and discussion

In this subsection, the measurements results are discussed. The conversion loss as a function of RF frequency for the diode connected HBT mixer is shown in Figure 3.39 both for the probed and packaged version. The conversion loss is lowest at 8.5 GHz where it is 9.8 dB for the probed and 11.2 dB for the packaged version. Around 9 GHz, where the noise is measured, the conversion loss is 10 dB for the probed and 11.7 dB for the packaged version. For the Schottky diode mixer the conversion loss is plotted as a function of frequency in Figure 3.40. The conversion loss is lowest at 11 GHz where it is 8.8 dB for the probed and 11.2 dB for the packaged version. At 10.4 GHz where the noise is measured the conversion loss is 9.3 dB for the probed and 11.4 dB for the packaged version. The additional loss of roughly 1.5 dB, which was observed for both mixers, is seen across the entire bandwidth, and is what could be expected from the bonding wires, microstrip lines and SMA to microstrip connections. Apart from additional loss, the bandwidth is also reduced by the added inductance on the input terminals.

The noise figure of the Schottky diode mixer is plotted in Figure 3.41, for IF frequencies from 20 kHz to 1 MHz on a logarithmic scale, with a LO frequency of 10.4 GHz. At higher frequencies the noise figure is 9.0 dB and rises as 1/f with a corner around 250 kHz, with a noise figure around 15 dB at 50 kHz. Changing the balun bias has no influence on the noise level. In comparison, the diode-connected HBT mixer demonstrates a noise figure of 8.8 dB with a LO frequency of 9.1 GHz. Both mixers operate with a 3-dB bandwidth covering the entire X-band, but the Schottky diode mixer operates best around 10 GHz and the diode-connected HBT mixer around 8.5 GHz. To give a realistic view of the diode-connected HBT mixer, the noise figure with a LO frequency of 9.3 GHz is plotted in Figure 3.42 on a logartihmic

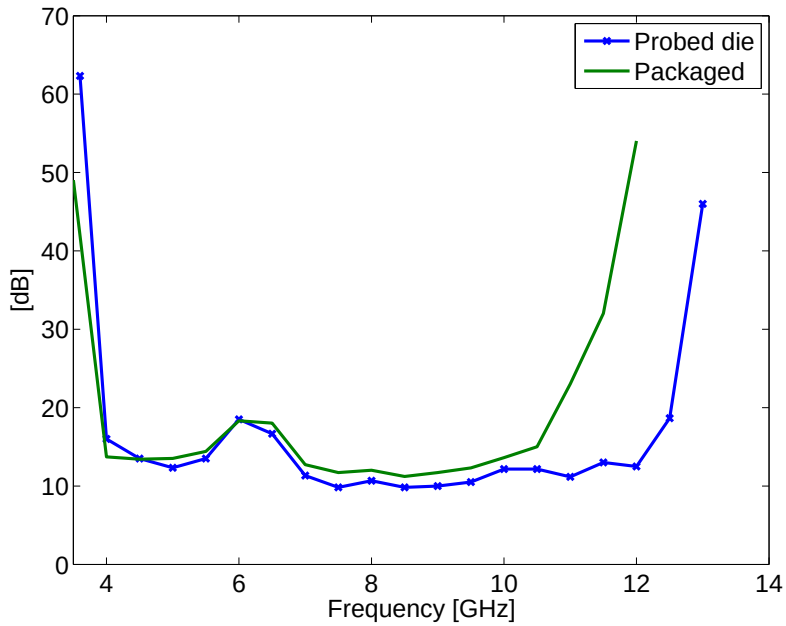

Figure 3.39. Measurement of HBT mixer conversion gain versus frequency, for probe measured die and packaged die.

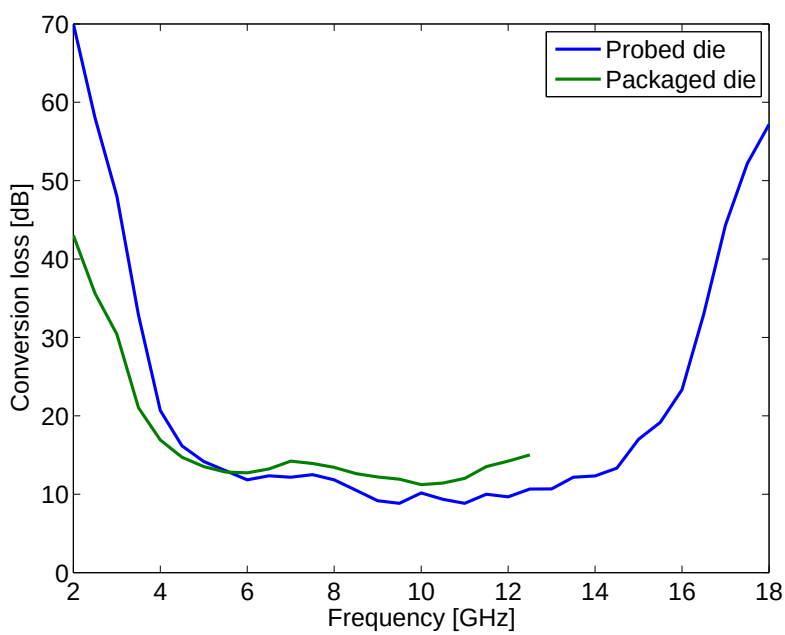

Figure 3.40. Measurement of Schottky mixer conversion gain versus frequency, for probe measured die and packaged die.

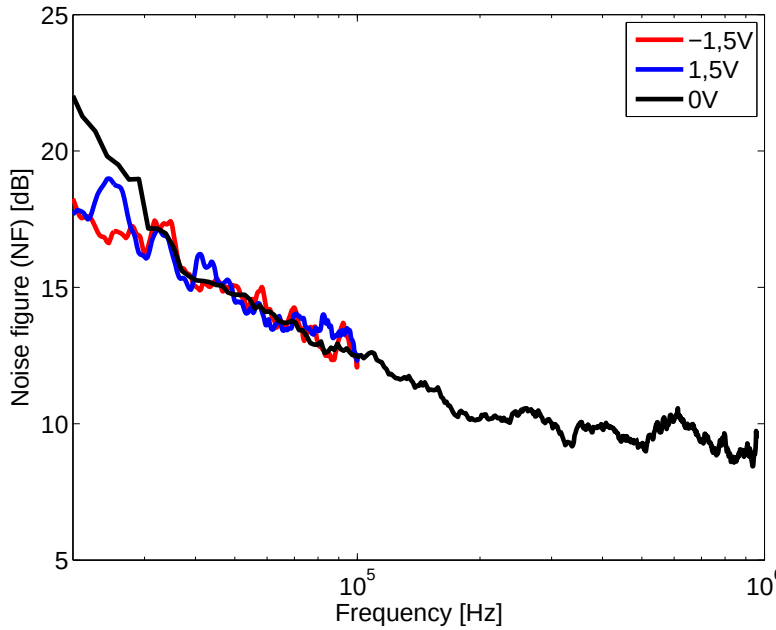

Figure 3.41. Measurement of Schottky mixer double sideband noise figure as a function IF frequency.

scale from 1 kHz to 100 kHz. Here it is seen that the diode-connected HBT mixer also have a 1/f tendency, but with a corner frequency as low as 10 kHz. Now it is clearly demonstrated that the HBT-connected diodes perform much better than the Schottky diodes in terms of low frequency noise performance. The higher low frequency noise in the Schottky diode mixer is believed to be caused by poor quality of the Schottky barrier and effect of leakage current. Together with the relative small tuning range of the DC-offset, the flicker noise reduction mechanism was masked. Again it is unfortunately that the HBT-mixer with tuning was short circuited, as it could give insight to whether the poor Schottky diodes was at fault or if it was the tuning circuitry that failed.

3.6 Conclusion

In this chapter three mixers was described and compared. Two with a tunable balance on the LO-balun, one of which is with a core of Schottky diodes and the other with a core of diode-connected HBTs. The third mixer, intended as a reference mixer, is without a tunable balun and using diode-connected HBTs for the mixer core.

A novel configuration of the Marchand balun, which allows phase tuning was constructed. A description was given which showed that variations in a shunt susceptance, to first order, gives a linear change in the phase balance, while keeping the magnitude balance constant. Measurements showed that the phase difference could be changed in the range from $-183°$ to $-175.8°$ at the design frequency of 9.4 GHz whereas the magnitude imbalance only changed with ± 0.05 dB.

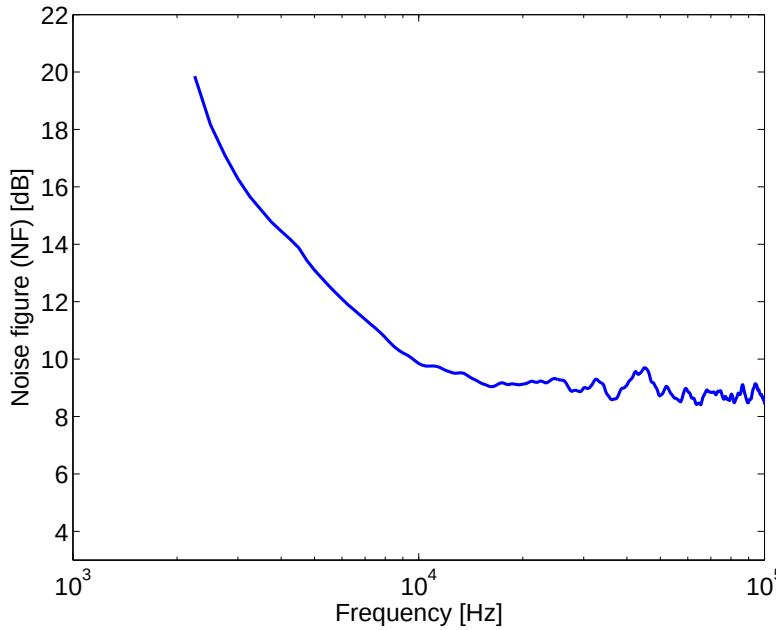

Figure 3.42. Measurement of HBT mixer double sideband noise figure as a function IF frequency.

The design of the reference HBT mixer has been presented. The mixer is a direct conversion mixer suitable for use in Doppler radars, manufactured in a $0.25\mu m$ SiGe HBT technology. The passive mixing element consists of diode connected HBTs, using the base-emitter pn-junction to realize the mixing diodes. Using the lumped element Marchand balun gives the possibility of an elegant IF-extraction together with wide bandwidth and good balance. A thorough description of the design of lumped element Marchand baluns using offset broadside coupled spiral inductors and capacitors was given. The broadband mixer has a 3 dB bandwidth from 7 - 12 GHz, covering the entire X-band, with a conversion loss of 9.8 dB at the design frequency. It requires a relatively high LO level of 15 dBm for best performance, but has a high linearity with a 1 dB compression point above 12 dBm and IIP_2 at 66 dBm. Good isolation between LO-IF, RF-IF and LO-RF ports of 55 dB, 40 dB, and 58 dB, respectively, is ensured due to the good balance of the Marchand baluns.

Analysis, design and experimental verification of mixers with a balun which is tunable to reduce leakage and enhance linearity, was also presented. The Schottky mixer manufactured in SiGe technology, has a center frequency at 11 GHz. Here it has a conversion loss of -8.8 dB with a LO power level of 11 dBm. The 3-dB bandwidth is from 8 GHz to 13 GHz, more than the entire X-band. The tuning have no influence on the conversion loss. The LO-IF isolation on the other hand can change from -51 dB to -60.5 dB, while the LO-RF isolation can change from -50 dB to -53.6 dB. The IIP_2 can be improved by the tuning from 45.5 dBm to 57.1 dBm, while the 1-dB compression point is kept constant at 6.67 dBm. Direct comparison with the HBT-mixer with tunable Marchand balun, was not possible, due to a short circuited control voltage. This is unfortunate, as it is not entirely clear which benefits come from the

change of diodes and which comes from the tuning circuitry.

To perform the low-frequency noise measurements the mixers has been mounted on an Arlon 25N substrate, gold ball bonded to soft gold transmission lines, and enclosed in a metal casing, thus shielding them from external noise sources. The experimental results showed that the Schottky diode mixer exhibits a higher 1/f noise with a corner frequency around 250 kHz, while the diode connected HBT circuit has a 1/f noise corner frequency around 10 kHz. It was not possible to reduce the noise for the Schottky mixer, by tuning of the balun balance. It is believed that it is due to small tuning range compared to the rather large noise level.

The good performance of the diode connected HBTs, encourage use of these. The next chapter will investigate techniques to use these without the rather high loss from the Marchand baluns. The idea of tuning the LO balun is abandoned as the effect on 1/f-noise could not be experimentally verified.

4

Passive diode mixers with active balun

In Chapter 3, we saw that the passive mixer suffered from a lot of loss. Much of this was due to the balun and matching circuitry. A simple solution is to replace the passive balun with an active. Another solution is to design the balun to also have impedance matching, thus the loss from the matching network is removed.

In this chapter we describe two double balanced mixers with an active balun. The block-diagram of the double-balanced mixer is shown in Figure 4.1. The mixer has the active balun placed at the RF port. A passive miniaturized Marchand balun is preferred at the LO port due to considerations about potential 1/f-noise up-conversion and bandwidth at the LO port. The IF extraction network of the mixer, shown in Figure 4.1, provides the necessary return current path from the diode ring mixer core and shields the RF from the IF port. One of the mixers uses the Marchand balun as described in Chapter 3, the other uses a Marchand balun with impedance matching. The mixer core consists of a quad ring of diode-connected HBTs as shown in Figure 4.2. The base-emitter junction is the preferred diode junction for mixer applications due to the heavier doping of the n-region of the emitter compared to the collector. The heavy doping is necessary to reduce the so-called conversion-loss degradation factor, as given in (3.51). This observation applies at least for the small-area SiGe HBT's considered here and means that the mixer core operates mainly in a resistive mode. Inductors, L_{match}, are added to the diode ring structure to provide matching to the miniaturized Marchand balun at the LO port for the mixer with conventional Marchand balun, as shown in Figure 4.2a. The mixer utilizing the matching Marchand balun has, of course, no matching circuitry added to the diode ring, as shown in Figure 4.2b.

The active balun is described in Section 4.1. In Section 4.2 is given a detailed analysis, design suggestion and experimental results of the impedance matching Marchand

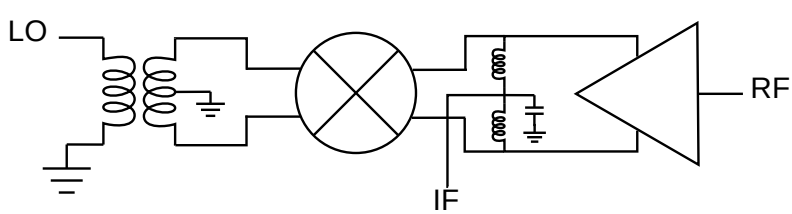

Figure 4.1. Block diagram of double-balanced mixer.

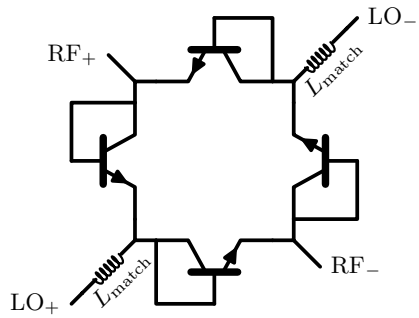

(a) Quad ring mixer using diode connected HBTs with matching for the mixer with conventional balun.

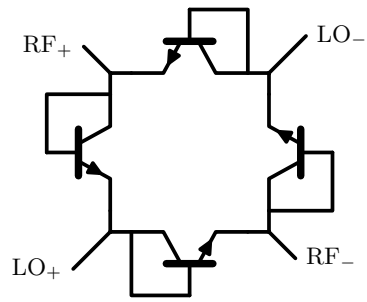

(b) Quad ring mixer using diode connected HBTs without matching for the mixer with impedance matching balun.

Figure 4.2. Quad ring mixer using diode connected HBTs.

balun. Experimental results of the mixer is given in Section 4.3. Parts of this section is published in [CP5].

4.1 Active balun

This section describes the active balun design used for the double balanced mixers. Figure 4.3 shows the schematic of the active balun. The design uses a differential cascode amplifier for high gain and good isolation. The input of one port of the differential cascode amplifier is matched using a shunt capacitor, C_{in}, and series inductor, L_{in}. The series capacitor, C_{De}, is included at the input port mainly for coupling of the AC signal. The same type of capacitor shorts the AC signal at the unused input port to ground.

This scheme allows easy biasing of the transistors through high valued resistors, R_{Bias}. The inherent high common-mode rejection ratio of the differential cascode amplifier converts the single-ended signal at the input into a differential signal at the output. The output is matched using an RF inductor, L_{VCC}, and series coupling capacitor, C_{De}. The RF inductor also serves for biasing while the series capacitor is needed for decoupling the output of the active balun from the return current flowing from the mixer core. For increased stability, a series network consisting of R_{s} and C_{s} is placed at the output. The noise and linearity of the active balun is optimized by adjusting the sizes of the HBTs and increasing the bias current and voltage supply. The bias current of the differential cascode amplifier is set through the resistor R_{DC}. This choice is better than an active current source for high-frequency integrated circuits because of the lower parasitic capacitance [41]. The value of this resistor is chosen as a trade-off between noise, common-mode rejection ratio, and required bias supply of the active balun. The nominal supply voltage, V_{cc}, is set to 6 V. The layout is EM simulated and coupled together with S-parameter and Harmonic-balance simulations to give a realistic impression of the circuit before manufacturing. According to these simulations the active balun has a gain of 16.3 dB and noise figure of 4.8 dB at the

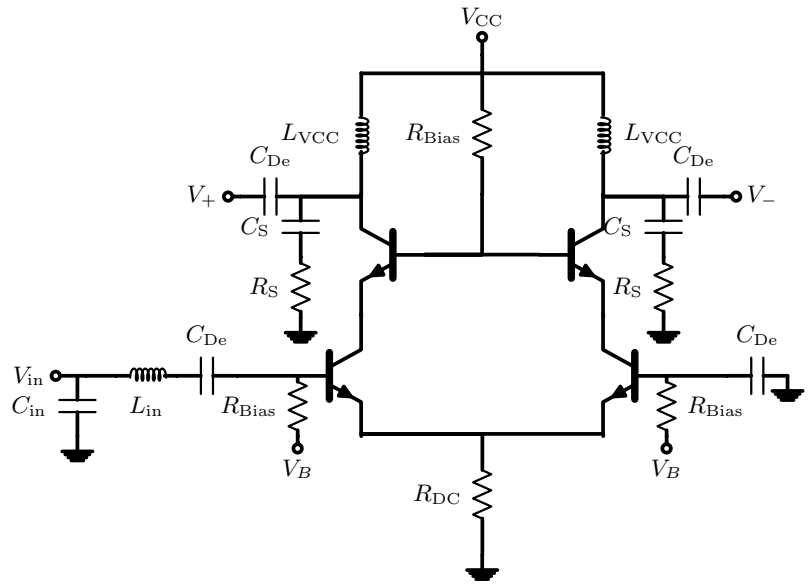

Figure 4.3. Schematic of active balun.

center frequency of 10.5 GHz. The simulated amplitude and phase mismatch is below 1.5 dB and 3 degrees, respectively, over the band from 10 GHz to 11 GHz. The input referred 1 dB compression point is −6 dBm.

4.2 Matching Marchand balun

For best performance of a mixer, the impedance of the core should be matched to the surrounding circuitry. If the matching could be incorporated in the balun design, the size of the circuit would be reduced with the space needed for the matching inductors, not only saving fabrication cost, but also reducing loss, due to the low-Q of inductors typically found in silicon based technologies.

In [42] the idea of using a coupled line, reactively loaded on the thru and coupled ports, for complex impedance matching was suggested. We will expand this idea to the Marchand balun, constructing it of two of such types of coupled lines. This allows a Marchand type balun to do impedance transformation between arbitrary complex impedances. This subsection is based on [CP3], which was the first demonstration of a Marchand balun with complex impedance transformation properties.

In this subsection an analysis of the proposed impedance transforming Marchand balun is given first. This will be followed by a design suggestion in a SiGe technology. Then we use electromagnetic (EM) simulations on the implementation to verify the analysis and design and compare it with experimental results.

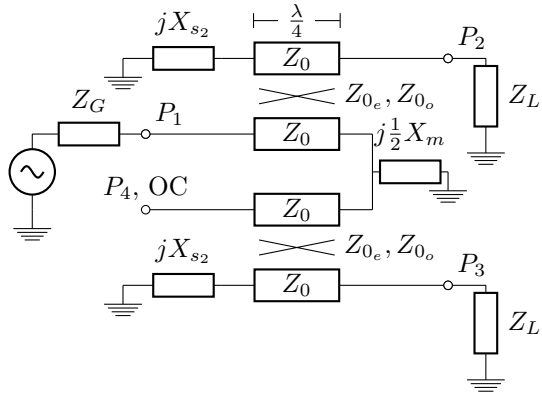

Figure 4.4. The modified Marchand balun with complex impedance matching properties.

4.2.1 Analysis

Here we will provide an analysis of the impedance matching Marchand balun. A schematic of the proposed circuit for the impedance transforming Marchand balun is shown in figure 4.4, where port 1 (P_1) is driven by a generator with impedance $Z_G = R_G + jX_G$ and port 2 (P_2) and 3 (P_3) is terminated in $Z_L = R_L + jX_L$.

The ideal balun behavior for a three port network can be described by S-parameters

$$S_{21} = -S_{31} \tag{4.1}$$

$$S_{11} = 0. \tag{4.2}$$

Ideally, there should be no reflected power from the load and the other S-parameters should not influence performance. Of course this is not the case for real world applications, but the most important ability of a balun is still as expressed above.

To analyze the Marchand balun the approach described in [32] is used. This approach uses the even-/odd-mode analysis [43] to investigate a symmetric network. The balun can be seen as a symmetric four-port with the fourth port terminated in a open circuit. In the analysis we treat the fourth port similar to port one, thus creating a plane of symmetry.

The requirement of balun behavior, i.e. (4.1) and (4.2), can be expressed from the even and odd mode circuits, as [32]

$$T_{\text{even}} = 0 \tag{4.3}$$

$$Z_{\text{even}} + Z_{\text{odd}} = 2Z_{\text{G}}^{*} \tag{4.4}$$

where T_{even} is the even mode transmission coefficient, Z_{even} and Z_{odd} is the impedance seen into the even and odd mode circuits, respectively, and Z_{G}^{*} denotes the complex conjugate of Z_{G}.

The even mode circuit of the modified Marchand balun is shown on figure 4.5. In [42] the two-port Z-parameters for a couple line loaded at the coupled and thru port

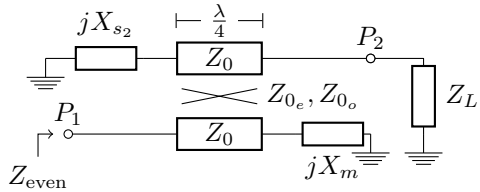

Figure 4.5. The even mode circuit.

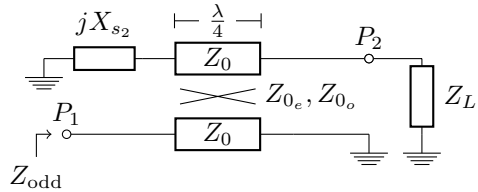

Figure 4.6. The odd mode circuit.

with Z_{s_2} and Z_m respectively is given as

$$\overline{\overline{Z}} = \begin{bmatrix} \frac{Z_{s_2}Z_+^2}{4Z_mZ_{s_2}+Z_-^2} & \frac{-jZ_-}{2} + \frac{\frac{1}{2}jZ_+^2Z_-}{4Z_mZ_{s_2}+Z_-^2} \\ \frac{-jZ_-}{2} + \frac{\frac{1}{2}jZ_+^2Z_-}{4Z_mZ_{s_2}+Z_-^2} & \frac{Z_mZ_+^2}{4Z_mZ_{s_2}+Z_-^2} \end{bmatrix} \tag{4.5}$$

where Z_+ and Z_- is $Z_{0e} + Z_{0o}$ and $Z_{0e} - Z_{0o}$, respectively, where Z_{0e} and Z_{0o} is the even and odd mode characteristic impedance of the coupled line.

The requirement of (4.3) is fulfilled if $Z_{21} = 0$, which from (4.5) can be reduced to

$$4X_mX_{s_2} - Z_-^2 + Z_+^2 = 0, \tag{4.6}$$

where it has been used that $Z_{s_2} = jX_{s_2}$ and $Z_m = jX_m$. Because of the requirement $Z_{21} = 0$ then the even mode impedance is not dependent on the load condition and we have

$$Z_{\text{even}} = \frac{Z_{s_2}Z_+^2}{4Z_mZ_{s_2} + Z_-^2}. \tag{4.7}$$

The odd mode circuit of the modified Marchand balun is shown on figure 4.6, it consists of a coupled line with a reactive load on the coupled port and a short circuit on the thru port. The two port Z-parameters for the odd mode circuit is then given as (4.5) with $Z_m = 0$,

$$\overline{\overline{Z}}\Big|_{Z_m=0} = \begin{bmatrix} \frac{Z_{s_2}Z_+^2}{Z_-^2} & j\frac{Z_+^2-Z_-^2}{2Z_-} \\ j\frac{Z_+^2-Z_-^2}{2Z_-} & 0 \end{bmatrix}. \tag{4.8}$$

The odd mode impedance can be found as the input impedance of the loaded two port

$$Z_{\text{odd}} = \frac{Z_{s_2}Z_+^2}{Z_-^2} - \frac{\left(Z_+^2 - Z_-^2\right)^2}{4Z_-^2Z_L}. \tag{4.9}$$

By inserting (4.7) and (4.9) into (4.4) and splitting the equation in a real and imaginary part gives

$$R_G = \frac{1}{8}\frac{\left(Z_+^2 - Z_-^2\right)^2 R_L}{Z_-^2\left(R_L^2 + X_L^2\right)} \tag{4.10}$$

$$X_G = \frac{1}{2}\frac{X_{s_2} Z_+^2}{Z_-^2} - \frac{1}{8}\frac{(Z_+^2 - Z_-^2)^2 X_L}{Z_-^2(R_L^2 + X_L^2)} + \frac{1}{8}\frac{X_{s_2} Z_+^2}{\frac{1}{4}Z_-^2 - X_m X_{s_2}}. \tag{4.11}$$

The condition $X_G = 0$ is chosen to simplify the following equations, but a more general approach is possible also for $X_G \neq 0$. The three equations (4.6), (4.10) and (4.11) has four design parameters, X_{s_2}, X_m, Z_{0_o} and Z_{0_e} as free variables. From (4.6) one gets

$$X_m = -\frac{1}{4}\frac{Z_+^2 - Z_-^2}{X_{s_2}}. \tag{4.12}$$

Then inserting (4.12) in (4.11) to get

$$X_{s_2} = \frac{1}{4}\frac{X_L\left(Z_+^2 - Z_-^2\right)^2}{\left(Z_-^2 + Z_+^2\right)\left(R_L^2 + X_L^2\right)} \tag{4.13}$$

Finally from (4.10) we get

$$\frac{1}{Z_{0_o}} - \frac{1}{Z_{0_e}} = \frac{1}{R_G}\sqrt{\frac{2}{\alpha}} \tag{4.14}$$

$$\text{where } \alpha = \frac{R_L^2 + X_L^2}{R_G R_L} \tag{4.15}$$

Observe that for the case of transformation to a real valued load, i.e. $X_L = 0$, (4.13) gives $X_{s_2} = 0$, a short circuit, (4.12) gives $X_m \to \infty$, an open circuit, and the impedance scaling factor becomes $\alpha = \frac{R_L}{R_G}$, which is the case for the regular Marchand balun as given by (3.13).

4.2.2 Design procedure

The lumped element Marchand balun, as seen in Section 3.2.1, is chosen to realise the circuit. This has the advantages of small size together with posibility to place capacitors where the added reactances X_{s_2} and X_m is needed. In figure 4.7 the schematic is shown. The design procedure follows what is described in Section 3.2.1,

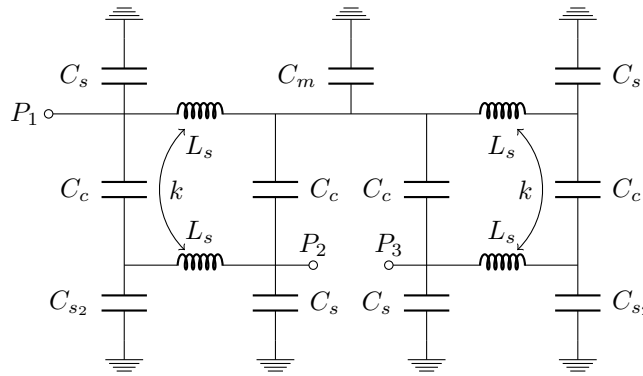

Figure 4.7. The lumped element implementation of the Marchand balun with complex matching properties.

with modification to incorporate X_{s_2} and X_m. The design equations is given as

$$L_s = \frac{Z_{0_e} + Z_{0_o}}{2\omega} \tag{4.16}$$

$$k = \frac{Z_{0_e} - Z_{0_o}}{Z_{0_e} + Z_{0_o}} \tag{4.17}$$

$$C_c = \frac{1}{2\omega}\left(\frac{1}{Z_{0_o}} - \frac{1}{Z_{0_e}}\right) \tag{4.18}$$

$$C_s = \frac{1}{\omega Z_{0_e}} \tag{4.19}$$

$$C_{s_2} = C_s - \frac{1}{X_{s_2}\omega} \tag{4.20}$$

$$C_m = 2C_s - \frac{2}{\omega X_m}. \tag{4.21}$$

4.2.3 Design example

To test the theory an X-band Marchand balun with transformation of generator impedance of $Z_g = 50\,\Omega$ to a load impedance of $Z_L = 50 - j100\,\Omega$ at 10.5 GHz is designed. The load value is chosen as it corresponds to a typical mixer diode load, being capacitive.

The size of the inductor has been the deciding factor in choosing $Z_{0_e} = 32.5\,\Omega$ giving inductor sizes of $L_s = 0.4\,\text{nH}$. In table 4.1 the design parameters for the balun are given, both the theoretical values as calculated and the realized values as implemented. Especially the implementation of the coupled inductors gives problems due to the difficulties of realization of exact k and C_c, but this can be compensated by changing C_m, C_s, and C_{s_2}.

Figure 4.8 shows layout of the proposed implementation. The two sets of coupled inductors has a total size of $423\,\mu m \times 194\,\mu m$ and the suggested breakout has a dimension of $610\,\mu m \times 930\,\mu m$. The larger dimensions of the breakout is mainly due to lines to Port 2 and 3 that have a length which makes it practical to connect the

Table 4.1. Design parameters for the balun

Description	Symbol		Calc.	Real.
Even mode characteristic impedance	Z_{0_e}	$[\Omega]$	32.5	
Odd mode characteristic impedance	Z_{0_o}	$[\Omega]$	20.9	
Reactance, side	X_{s_2}	$[\Omega]$	-5.96	
Reactance, middle	X_m	$[\Omega]$	114	
Inductance	L_s	$[nH]$	0.4	0.4
Inductive coupling	k		0.21	0.15
Capacitive coupling	C_c	$[fF]$	129	157
Side capacitor	C_s	$[fF]$	466	305
Increased side capacitor	C_{s_2}	$[pF]$	3.01	2.6
Middle capacitor	C_m	$[fF]$	667	727

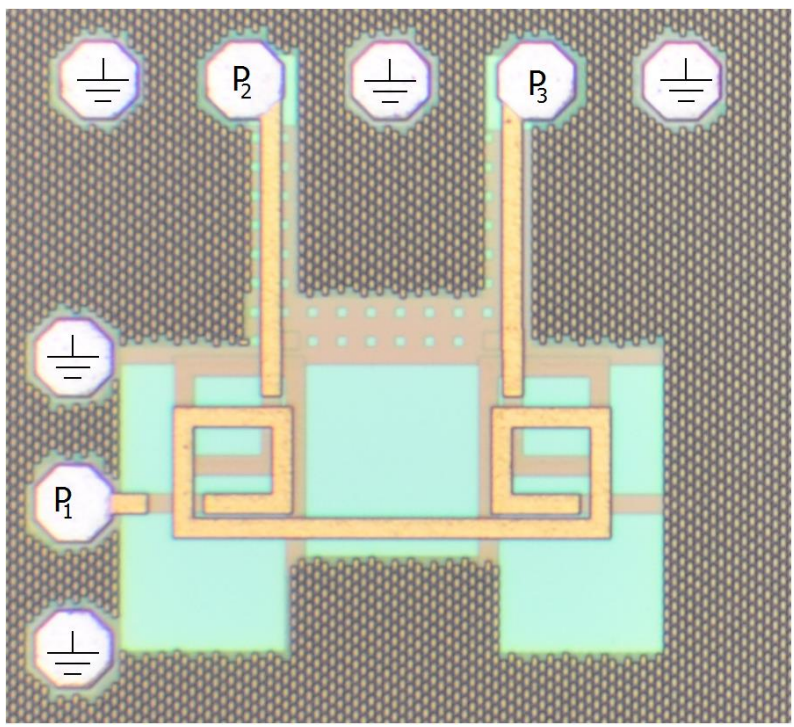

Figure 4.8. Microphotograph of manufactured breakout of proposed circuit, dimensions are $805\,\mu m \times 805\,\mu m$ including contact pads.

two set of probes for measurements. The dimensions of the breakout could also be used in a real circuit to avoid undesired coupling.

4.2.4 Experimental Results of Matching Marchand Balun

Electromagnetic simulations using Momentum in ADS has been used to verify the design implementation. Due to designkit limitations the capacitors is not part of

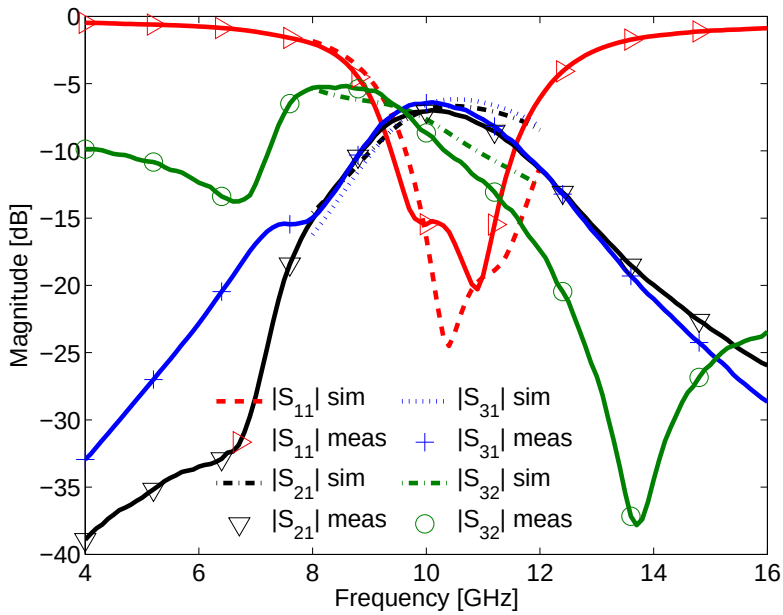

Figure 4.9. Magnitude of S-parameters for the proposed balun circuit.

the Momentum simulation, but models is included in an ADS S-parameter simulation. The experimental results are obtained using on-wafer measurements of the S-parameters. The S-parameters are plotted in Figure 4.9. At the design frequency, an insertion loss of 6.4 dB is measured, together with a reflection of -15.2 dB. The phase imbalance is 1.2° and the magnitude imbalance is 0.6 dB. Figures 4.10 and 4.11 shows plots of the magnitude and phase difference from 8 to 12 GHz. The bandwidth is limited by the matching from 9.8 GHz to 11.2 GHz if a reflection below -15 dB is desired. In this band, the insertion loss is better than 8.2 dB, the phase imbalance better than 2.4° and the magnitude imbalance better than 0.6 dB.

4.3 Experimental Results for Passive Mixers with Active Balun

In this section, the experimental results of the double-balanced mixer are discussed. The measurements are made on-wafer using a probe station. Losses in cables and probes are calibrated out. The microphotograph of the fabricated mixers is shown in Figure 4.12. The size is 1860 µm × 1020 µm for the mixer with inductor matching and 1455 µm × 830 µm for the mixer with matching Marchand balun.

The conversion gain as a function of LO drive level for supply voltages of 3V and 6V are shown in Figure 4.13a through Figure 4.13d, respectively, for both mixers. The measurements are performed on several samples with good uniformity. The LO frequency is set to 10.4 GHz and the RF frequency is set to 10.5 GHz. The current consumption for the two supply voltages are 17 mA and 38 mA, respectively, for both mixers.

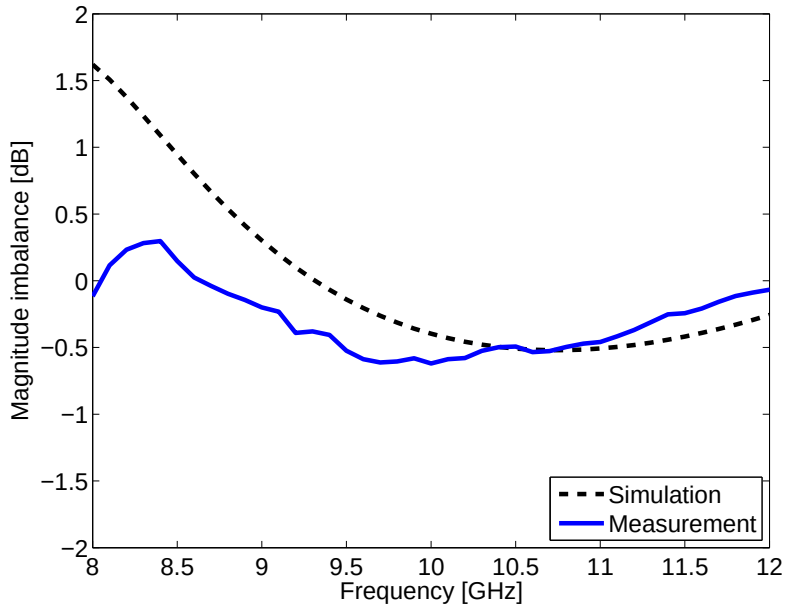

Figure 4.10. Magnitude imbalance at the output for the proposed balun circuit.

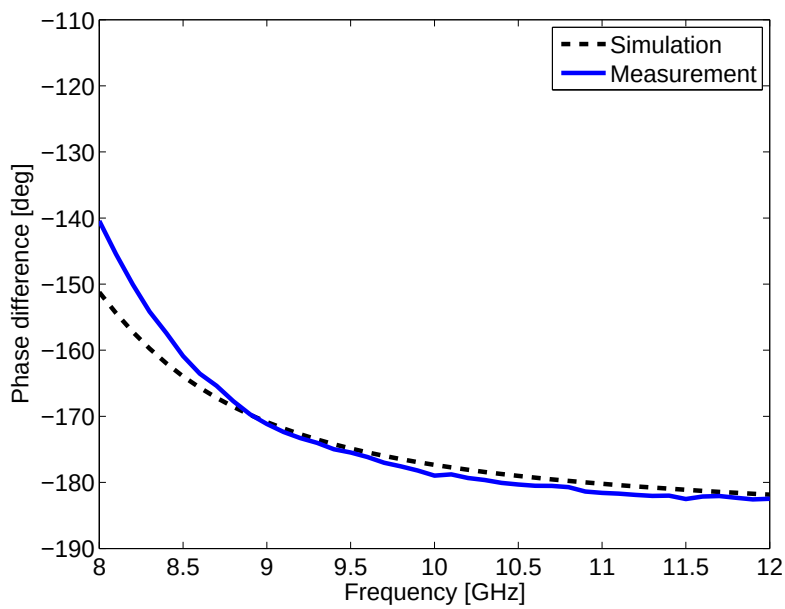

Figure 4.11. Phase difference of the two output ports of the proposed balun circuit.

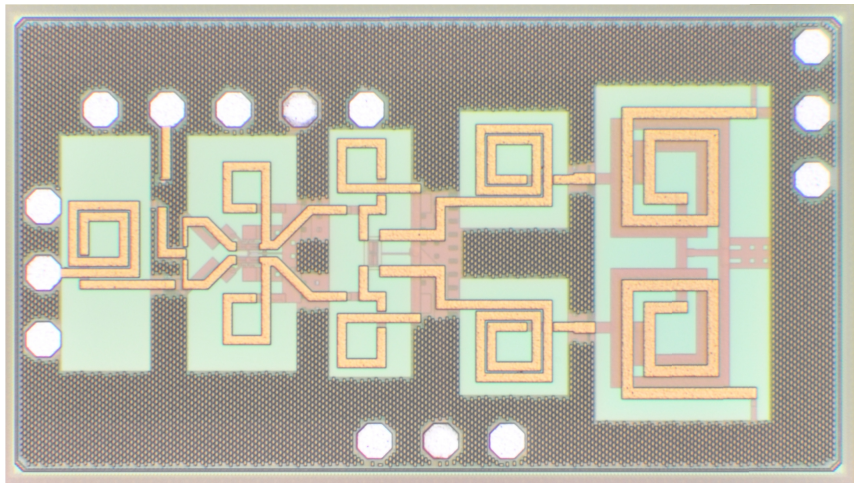

(a) Microphotograph of the double-balanced mixer with conventional Marchand balun and inductor matching, size is 1860 µm × 1020 µm.

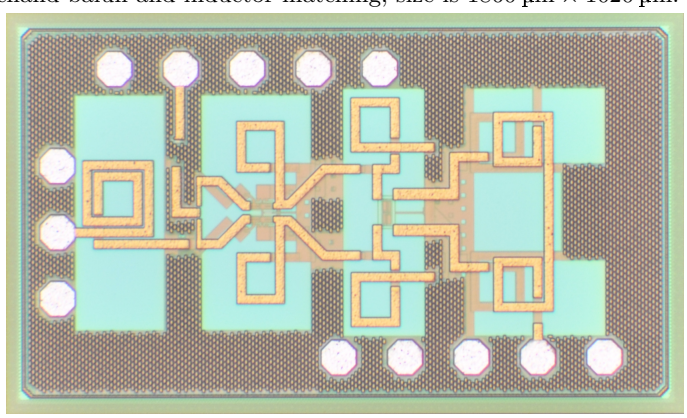

(b) Microphotograph of the double-balanced mixer with matching Marchand balun, size 1455 µm × 830 µm.

Figure 4.12. Microphotograph of the double-balanced mixers.

For the mixer with inductor matching, the conversion gain at a supply voltage of $V_{cc} = 6.0\,V$, shown in Figure 4.13a, saturates at a level around $\sim -1\,dB$ for an LO drive level above $\sim 10\,dBm$. This is significant lower than predicted by the simulation. Reducing the bias voltage to $V_{cc} = 3.0\,V$, increases the conversion gain, as shown in Figure 4.13b. The saturated level is around $\sim 4.6\,dB$, well in line with the simulation. The exact reason for the observed behavior is as yet unknown. A possible cause may be that the collector-emitter voltages across the HBTs in the active balun with a supply voltage of $V_{cc} = 6.0\,V$ are so high (close to breakdown) that the transistor model becomes inaccurate. Fortunately, the performance of the double balanced mixer is acceptable at a supply voltage of $V_{cc} = 3.0\,V$. Therefore, all the following measurements have been performed at this supply voltage. The same

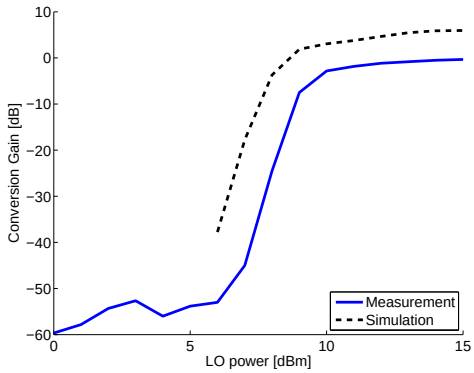

(a) Inductor matched mixer, $V_{cc} = 6.0\,\mathrm{V}$.

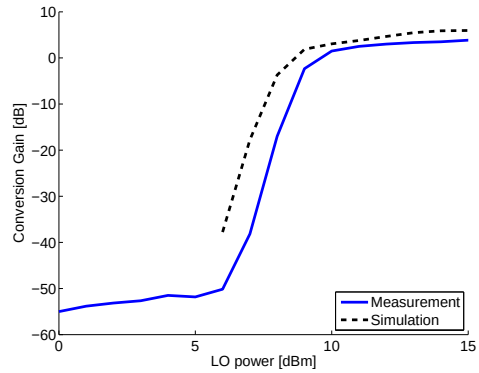

(b) Inductor matched mixer, $V_{cc} = 3.0\,\mathrm{V}$.

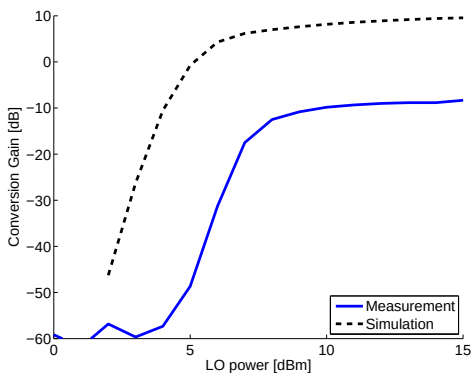

(c) Matching Marchand mixer, $V_{cc} = 6.0\,\mathrm{V}$.

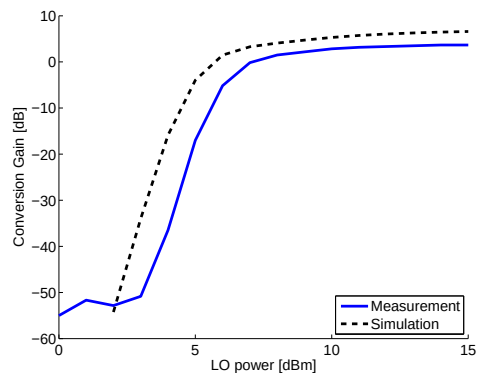

(d) Matching Marchand mixer, $V_{cc} = 3.0\,\mathrm{V}$.

Figure 4.13. Conversion gain versus LO power for both mixers at different bias voltages.

behavior is observed for the mixer with matching Marchand balun, in Figure 4.13c and Figure 4.13d. The conversion gain at a supply voltage of $V_{cc} = 3.0\,\mathrm{V}$, shown in Figure 4.13d, saturates at a level around $\sim 4.6\,\mathrm{dB}$ for an LO drive level above $\sim 7\,\mathrm{dBm}$. The reduced requirement for LO-power is due to the lack of lossy matching inductors. Thus proving the benefit of the matching Marchand balun.

Figure 4.14a and Figure 4.14b shows the conversion gain as a function of frequency at a fixed IF of 100 MHz. The LO drive level is fixed at +15 dBm. The conversion gain peak of $\sim 4.5\,\mathrm{dB}$ is around the design frequency of 10.5 GHz and the $-3\,\mathrm{dB}$ bandwidth is $\sim 2.5\,\mathrm{GHz}$. The bandwidth is mainly limited by the active balun for the mixer with conventional Marchand balun, whereas both the active balun and the impedance matching Marchand balun has the same limiting bandwidth, giving steep roll-off. In general, the frequency response of the conversion gain is well predicted by the simulation.

The LO-IF and RF-IF isolation version RF frequency is shown in Figure 4.15. In the entire band of operation the LO-IF and RF-IF isolation is better than 45 dB and 20 dB, respectively. These values indicate a good balance of both the active balun and miniaturized Marchand baluns.

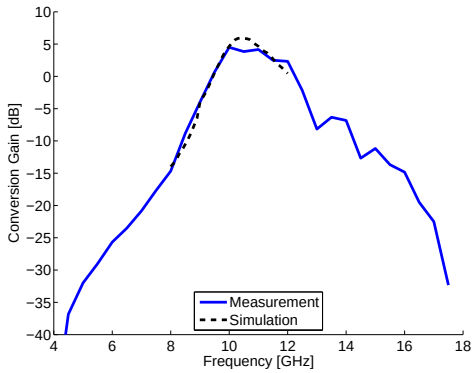

(a) Mixer with conventional Marchand balun.

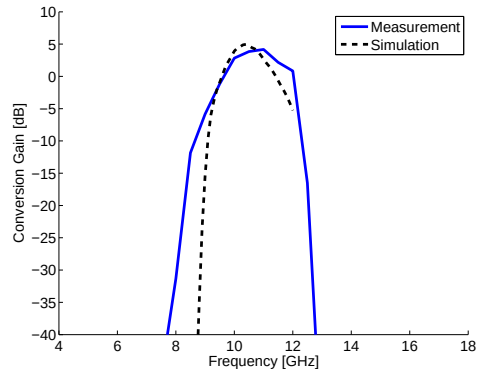

(b) Mixer with matching Marchand balun.

Figure 4.14. Conversion gain of the mixers as a function of frequency.

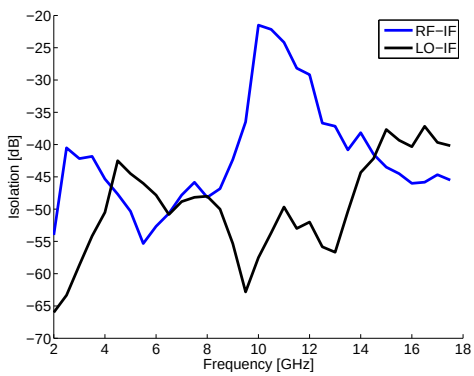

(a) Mixer with conventional Marchand balun.

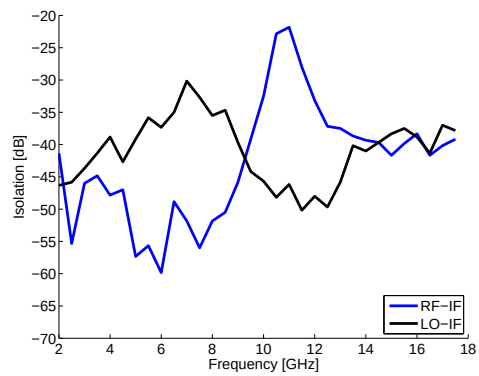

(b) Mixer with matching Marchand balun.

Figure 4.15. LO-IF and RF-IF isolation versus RF frequency.

The measured 1 dB input referred compression point of the double balanced mixers is ~ -11 dBm. This is somewhat lower than the -6 dBm simulated for the active balun alone but still acceptable for a mixer with active balun on its RF port. The IIP_2 is measured with two RF tones at frequencies of 10.5 and 10.513 GHz given a second-order product at 13 MHz. Isolators are placed after the signal generators to avoid leakage and intermodulation of the signals before they are applied to the mixer. Figure 4.16a and Figure 4.16b plots the IIP_2 at a supply voltage of 3 V for the mixer with inductor matching and the mixer with matching Marchand balun, respectively. The IIP_2 is 13 dBm for both mixers.

The double sideband noise figure versus RF frequency, shown in Figure 4.17a and Figure 4.17b, is measured under the same conditions as the conversion gain in Figure 4.14a. It reaches a minimum of $\sim$ 6.5 dB around the design frequency of 10.5 GHz, for both mixers. Compared to the purely passive X-band double balanced

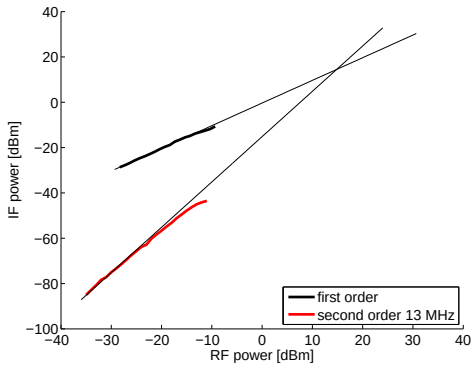

(a) IIP_2 of Mixer with inductor matching, for bias voltage of 3V

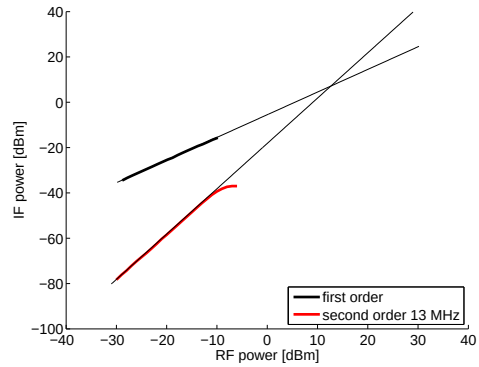

(b) IIP_2 of Mixer with matching Marchand balun, for bias voltage of 3V

Figure 4.16. IIP_2 of the two mixers.

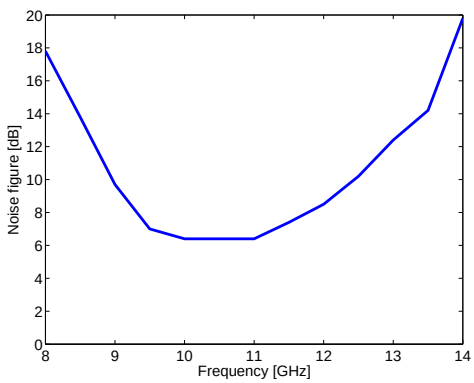

(a) Mixer with conventional Marchand balun.

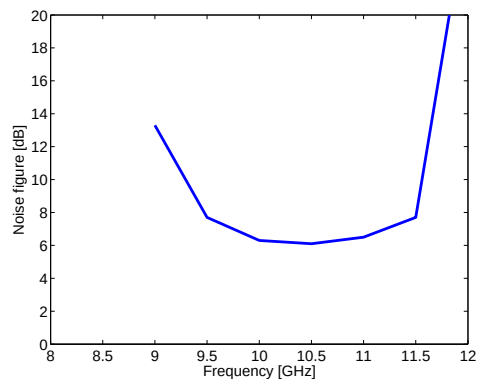

(b) Mixer with matching Marchand balun.

Figure 4.17. Double-sideband noise figure versus RF frequency.

ring mixer in Section 3.2 this represents an improvement of $\sim 3.3\,\mathrm{dB}$ due to the good noise performance of the active balun.

4.4 Conclusions

In this chapter the design of two double balanced mixers in a $0.25\,\mu\mathrm{m}$ SiGe BiCMOS technology is presented. The mixers are direct conversion mixers for use in X-band Doppler radars. The double balanced mixers integrates an active balun optimized for low noise and high linearity on the RF port and a miniaturized Marchand balun on the LO port. The mixing elements consist of diode connected HBTs.

One of the mixers uses a conventional lumped element Marchand balun on the LO-port, while the other uses a novel lumped element impedance matching Marchand balun on the LO-port. The lumped element implementation has the property

of having capacitors placed where the additional reactances should be added anyway. Thus it is possible to absorb a positive reactance by reducing a capacitor and a negative by increasing a capacitor. With this design approach, no additional inductances are needed for matching, thus reducing loss and circuit size. The matching Marchand balun matches the $Z_g = 50\Omega$ environment to the $Z_L = 50 - j100\Omega$ diodes. With a performance comparable to the conventional planar Marchand balun, except for a narrower bandwidth. This does not limit the mixer operation as the bandwidth matches the one for the active balun.

At the design frequency of 10.5 GHz the mixers have a conversion gain of $\sim 4.6\,\mathrm{dB}$ and a double-sideband noise figure of $\sim 6.5\,\mathrm{dB}$. They require a relatively high LO level of $\sim 10\,\mathrm{dBm}$ and $\sim 7\,\mathrm{dBm}$, respectively for the mixer with inductor matching and the mixer with matching Marchand balun, for best performance. The reason for the lower requirement on LO-power for the mixer with matching Marchand balun, is due to the lack of lossy matching inductors.

5

Conclusion

Mixers for direct conversion is well suited for many microwave applications, including Doppler radars and for making a simple image rejection receiver. It suffers from leakage and increased noise level due to low frequency noise or flicker noise.

The work presented here showed a method for reducing flicker noise in mixers by cancellation of the leakage signal from the LO. Reducing the DC offset on the mixer core, reduces the flicker noise. It was found that only one amplitude and phase gave full leakage cancellation, but to get zero DC-offset there is no strict limit to what the amplitude should be and there can be up to two phases for a given amplitude which gives the desired result.

An analytical description on how the balun balance influences the performance of the mixer was given. This showed that DC level, leakage and second order intercept point would benefit from a good match. This should lead to improved flicker noise performance. Using this knowledge three mixers for direct conversion was designed. Two with the property to change the phase balance on the balun circuit for the LO-port, and a control sample. One of the mixers with a quad-ring of Schottky diodes the other and the control sample with a quad-ring of diode connected HBTs. A novel configuration of the Marchand balun which allows phase tuning was described analytically and experimental results was given. A thorough description of the design of lumped element Marchand baluns was also given. The baluns are wideband, covering the entire X-band, however they suffer from low Q-factor of the integrated inductors, resulting in a rather high loss of 2.5 dB. Using these as building blocks the three mixers was designed and manufactured in a SiGe:C technology. The experimental results showed that the Schottky diode mixer exhibits a higher 1/f noise with a corner frequency around 250 kHz, while the diode connected HBT circuit has a 1/f noise corner frequency around 10 kHz. It is believed that it is due to small tuning range compared to the rather large noise level. Due to a bug in the layout versus schematic tool, a short circuit of the diode connected HBT-mixer with tunable balun was not detected before manufacturing. So, only comparison between the non-tunable diode connected HBT-mixer and the tunable Schottky diode mixer was possible.

No tuning of the noise was possible for the Schottky mixer, but other parameters could be improved. The LO-IF isolation can be changed from -51 dB to -60.5 dB. The IIP_2 can be improved by the tuning from 45.5 dBm to 57.1 dBm, while the 1-dB compression point is kept constant at 6.7 dBm. The Schottky mixer showed a conversion loss of -8.8 dB with a LO power level of 11 dBm at the center frequency of 11 GHz. The 3-dB bandwidth is from 8 GHz to 13 GHz, more than the entire X-band.

The tuning have as was expected no influence on the conversion loss. The diode connected HBT mixer showed similar results, but at a lower frequency of 8.5 GHz and with a LO power level of 15 dBm.

The good noise performance of the diode connected HBTs led to the use of these for the next iteration of the mixer circuits. To overcome the loss introduced by the low Q of the inductors an active balun is suggested. Another alternative is the novel configuration of the lumped element Marchand balun which allows for arbitrary complex impedance matching. This allows to get rid of matching inductors, thus reducing circuit size and loss from the low Q-factor inductors. A design suggestion and experimental results was presented. The matching Marchand balun has comparable performance to the conventional, but with a limited bandwidth. Two mixers was manufactured, both using the active balun on the RF side, and one using the matching Marchand balun on the LO side, while the other uses a conventional lumped element Marchand balun together with matching inductors. At the design frequency of 10.5 GHz the mixers has a conversion gain of ~ 4.6 dB and a single-sideband noise figure of ~ 6.5 dB. They require a LO level of ~ 10 dBm and ~ 7 dBm, for the mixer with inductor matching and the mixer with matching Marchand balun, for best performance. The reason for the lower requirement on LO-power for the mixer with matching Marchand balun, is due to the lack of lossy matching inductors, showing the benefit of using a balun with inherent matching.

5.1 Future work

Having no knowledge about the low frequency noise of the devices made much of the initial circuit design difficult. A thorough investigation in, and characterization of, the low frequency noise in the devices would have benefited the project and similar future projects. Therefore, it is suggested that a future project could include modeling of low frequency noise in the devices. This will allow for testing different schemes of noise reduction, without the high cost and time consuming process of manufacturing and packaging the circuit for the sensitive measurements.

Another approach to continue and enhance the work presented here is to use these circuits or parts of these circuits as building blocks for larger circuits. For example a full receiver circuit on a single MMIC. The full receiver circuit should include Low Noise Amplifier (LNA) and double I/Q mixers for FMCW radar applications. Thus allowing the radar receiver to be on a single chip.

A

Derivation of (3.2) and (3.3)

In Section 3.1 the design of a tunable Marchand balun is discussed. In this section we will derive the equations for S_{21} and S_{31}. To do this is used the Signal flow theory as described in [44].

For an ideal coupled line of length $\frac{\lambda}{4}$ the S-parameters is given as [18]

$$S_{\text{coupler}} = \begin{bmatrix} 0 & C & -j\sqrt{1-C^2} & 0 \\ C & 0 & 0 & -j\sqrt{1-C^2} \\ -j\sqrt{1-C^2} & 0 & 0 & C \\ 0 & -j\sqrt{1-C^2} & C & 0 \end{bmatrix}, \tag{A.1}$$

where C is the coupling factor. For an ideal shunt susceptive element the S-parameters is given as [44]

$$S_{\text{shunt}} = \begin{bmatrix} -\frac{jBZ_0}{2+jBZ_0} & \frac{2}{2+jBZ_0} \\ \frac{2}{2+jBZ_0} & -\frac{jBZ_0}{2+jBZ_0} \end{bmatrix}, \tag{A.2}$$

where B is the susceptance and Z_0 is the impedance of the environment in which the S-parameters are calculated or measured.

In Figure A.1 and Figure A.2 are the signal flow chart representation of the tunable Marchand balun depicted, with highlights used to calculate S_{21} and S_{31}, respectively. There are two loops, intersecting each other, these are colored a greenish-blue. One loop containing C - Γ_{SC} - C - Γ_{OC} giving the loop factor

$$K_{\text{Loop}_1} = \frac{1}{1 - \Gamma_{OC}\Gamma_{SC}C^2} \tag{A.3}$$

The total of the two loops then has a loop factor of

$$K_{\text{Loop}_2} = \frac{1}{1 - (1-C^2)\frac{jBZ_0}{2+jBZ_0}\Gamma_{OC}K_{\text{Loop}_1}}. \tag{A.4}$$

Any path going through one of these loops should have multiplied the total loop factor K_{Loop_2} to the path.

From Figure A.1 it is possible to calculate S_{21}. There are two diffent contributions to S_{21}, one following the red path and one following the blue and going through the loops. The red path gives

$$S_{21_{\text{red}}} = C\Gamma_{SC}j\sqrt{1-C^2}. \tag{A.5}$$

The blue path have two branches, one reflecting at the shunt susceptance, the other going into the loops before coming back. The blue paths give

$$S_{21_{\text{blue}}}=jC\sqrt{1-C^2}\left(-\frac{jBZ_0}{2+jBZ_0}-\left(\frac{2}{2+jBZ_0}\right)^2 K_{\text{Loop}_2}\left(1-C^2\right)\Gamma_{OC}\right). \quad \text{(A.6)}$$

Using $\Gamma_{SC}=-1$, $\Gamma_{OC}=1$ and summing (A.5) and (A.6) gives

$$S_{21}=S_{21_{\text{red}}}+S_{21_{\text{blue}}} \quad \text{(A.7)}$$

$$=C\Gamma_{SC}j\sqrt{1-C^2}+jC\sqrt{1-C^2}\left(-\frac{jBZ_0}{2+jBZ_0}-\left(\frac{2}{2+jBZ_0}\right)^2 K_{\text{Loop}_2}\left(1-C^2\right)\Gamma_{OC}\right)$$

$$=\frac{j2C\left(jBZ_0C^2+1\right)\sqrt{1-C^2}}{1+C^2+jBZ_0C^2}. \quad \text{(A.8)}$$

For S_{31} there are two path both going through the double loop, as shown in Figure A.2. They are both starting as marked with red, but are branched by the red and blue path exiting the loop. The red path gives

$$S_{31_{\text{red}}}=j\sqrt{1-C^2}\frac{2}{2+jBZ_0}K_{\text{Loop}_2}C. \quad \text{(A.9)}$$

The blue path gives

$$S_{31_{\text{blue}}}=-j\sqrt{1-C^2}\frac{2}{2+jBZ_0}K_{\text{Loop}_2}(1-C^2)\Gamma_{OC}C\Gamma_{SC}. \quad \text{(A.10)}$$

Using $\Gamma_{SC}=-1$, $\Gamma_{OC}=1$ and summing (A.9) and (A.10) gives

$$S_{31}=S_{31_{\text{red}}}+S_{31_{\text{blue}}}=j\sqrt{1-C^2}\frac{2}{2+jBZ_0}K_{\text{Loop}_2}(C-(1-C^2)\Gamma_{OC}C\Gamma_{SC}) \quad \text{(A.11)}$$

$$=\frac{j2C\sqrt{1-C^2}}{1+C^2+jBZ_0C^2}. \quad \text{(A.12)}$$

□

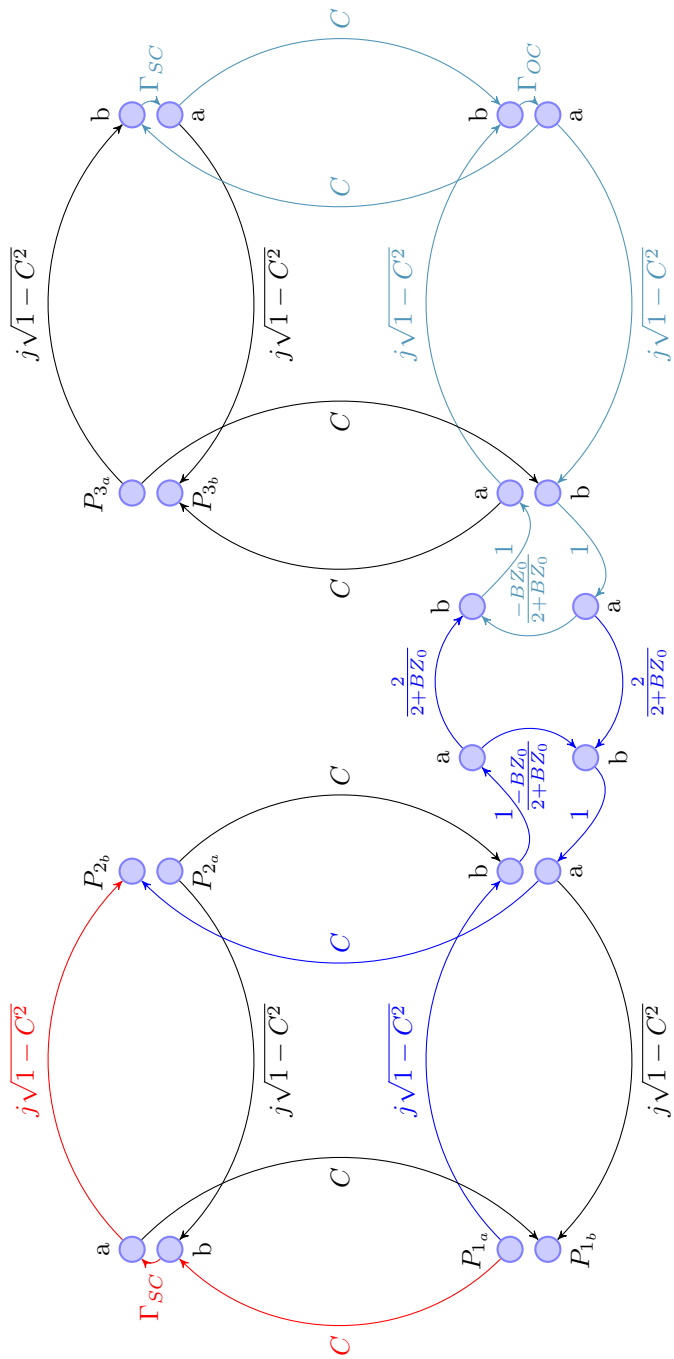

Figure A.1. Signal flow chart of the Marchand balun. Highlighted is the path for calculating S_{21}.

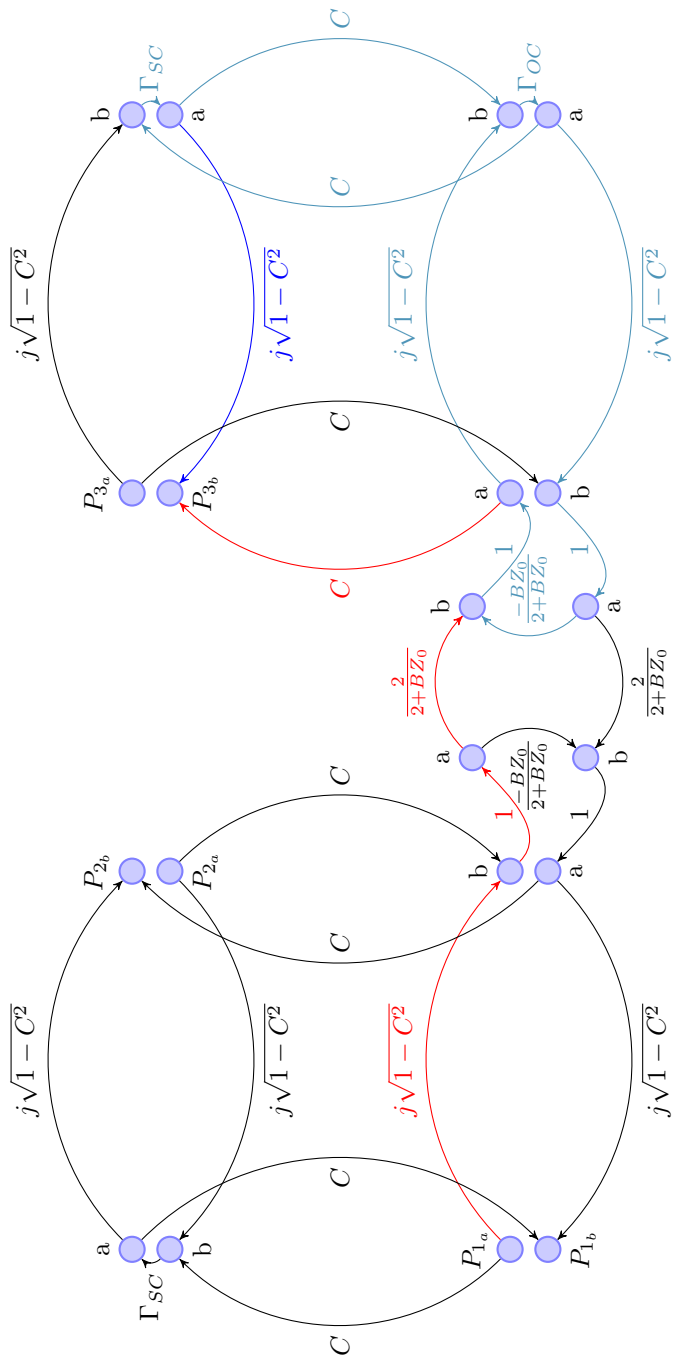

Figure A.2. Signal flow chart of the Marchand balun. Highlighted is the path for calculating S_{31}.

B

Publications

A Modified Marchand Balun Configuration With Tunable Phase Balance

Rasmus Michaelsen, *Student Member, IEEE*, Tom Johansen, *Member, IEEE*, Kjeld Tamborg, and Vitaliy Zhurbenko, *Member, IEEE*

***Abstract*—In this letter, a novel modified Marchand balun configuration with tunable phase balance is analyzed and verified experimentally. It is proposed to add a shunt susceptance in between the two couplers of the Marchand balun. This allows for a change in the phase balance which, to first order, is linear with the susceptance, while the magnitude balance is kept constant. To verify the proposed configuration, a lumped element Marchand balun has been fabricated using a SiGe BiCMOS technology. The balun design is centered around 9.4 GHz, with an insertion loss of 6.0 dB. The phase difference between the output ports can be changed from 175.8° to 183° whereas the magnitude imbalance is kept almost constant at 0.3 dB. The balun performs well in the range from 7 to 11 GHz, where it is possible to tune the phase to exactly 180°.**

***Index Terms*—Balun, lumped element, MMIC, passive devices, tunable phase.**

I. Introduction

BALUNS are used to transform an unbalanced input signal into a balanced output signal. Baluns are essential components in many microwave circuits, e.g., balanced mixers and differential amplifiers. Baluns can be split into active and passive types. Active baluns use transistors to overcome losses found in passive baluns and allow for compact circuits in MMIC processes. The main drawback of active baluns is that they limit the dynamic range of the balanced mixer or amplifier significantly.

Passive baluns can be realized using either lumped components, like capacitors and inductors or distributed elements such as transmission lines. Due to its wide band properties, the Marchand type balun finds widespread applications. Several modifications of this circuit have been reported including techniques for impedance transforming [1], tuning of center frequency [2], bandwidth enhancements [3], [4] and different types of miniaturization [2], [5]–[7].

Practical baluns suffer from imperfect phase and magnitude balance due to layout asymmetries and production variations. Only perfect phase matched baluns make it possible to exploit the full benefits of balanced configurations, i.e., for a double balanced mixer you obtain complete port-to-port isolation, rejection of LO-AM noise, spurious signals, and certain intermodulation products [8]. Therefore it would be an advantage with a balun having a tunable phase balance, allowing to correct any imbalance. Tuning of the phase balance has previously been reported for active baluns only [9].

The purpose of this letter is to introduce a novel configuration of the Marchand balun with tunable phase balance. First the general theory of the modified Marchand balun will be developed. This will be followed by the design and experimental results to verify the proposed configuration. The experimental results are obtained by producing a lumped element Marchand balun, utilizing this principle, in a SiGe BiCMOS technology. To the authors knowledge, this is the first attempt to make a Marchand balun with tunable phase balance.

Manuscript received September 20, 2012; revised November 26, 2012; accepted December 21, 2012.

R. Michaelsen is with the Electromagnetic Systems Group, DTU Elektro, Technical University of Denmark, Lyngby 2800 Kgs, Denmark and also with Weibel Scientific, Allerød 3450, Denmark (e-mail: rsmi@elektro.dtu.dk.

T. Johansen and V. Zhurbenko are with the Electromagnetic Systems Group, DTU Elektro, Technical University of Denmark, Lyngby 2800 Kgs, Denmark.

K. Tamborg is with Weibel Scientific, Allerød 3450, Denmark.

Color versions of one or more of the figures in this paper are available online at http://ieeexplore.ieee.org.

Digital Object Identifier 10.1109/LMWC.2013.2238913

II. Theory

In this section, it will be shown that by placing a shunt susceptive element between the two couplers in the Marchand balun, it is possible to tune the phase difference between Port 2 and 3 while maintaining an almost constant magnitude balance. Fig. 1 shows the proposed configuration. For an ideal coupled line of length $(\lambda)/(4)$ the S-parameters is given as [1]

$$S_{\text{coupler}} = \begin{bmatrix} 0 & C & -j\sqrt{1-C^2} & 0 \\ C & 0 & 0 & -j\sqrt{1-C^2} \\ -j\sqrt{1-C^2} & 0 & 0 & C \\ 0 & -j\sqrt{1-C^2} & C & 0 \end{bmatrix} \tag{1}$$

where C is the coupling factor. Then using the S-parameters for the two couplers and a shunted susceptance, B, the transmission from Port 1 to Port 2 and 3, respectively, can be derived to be

$$S_{21} = S_{12} = \frac{j2C(jBZ_0C^2+1)\sqrt{1-C^2}}{1+C^2+jBZ_0C^2} \tag{2}$$

$$S_{31} = S_{13} = \frac{j2C\sqrt{1-C^2}}{1+C^2+jBZ_0C^2} \tag{3}$$

where Z_0 is the reference impedance for the S-parameters. Taking the magnitude and phase of S_{21} and S_{31} from (2) and (3) gives

$$|S_{21}| = \frac{2C\sqrt{C^4Z_0^2B^2+1}\sqrt{1-C^2}}{\sqrt{C^4Z_0^2B^2+2C^2+C^4+1}} \approx \frac{2C\sqrt{1-C^2}}{C^2+1} \tag{4}$$

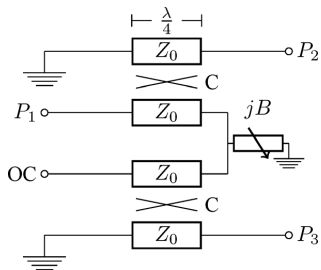

Fig. 1. Modified Marchand balun configuration, with tunable phase balance, utilizing a variable susceptance.

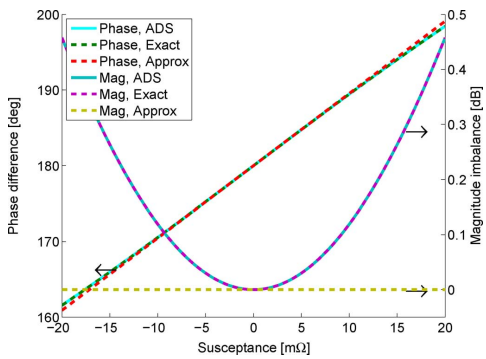

Fig. 2. Phase difference and magnitude imbalance calculated using (6) and (7) are plotted together with an ADS simulation using perfect couplers.

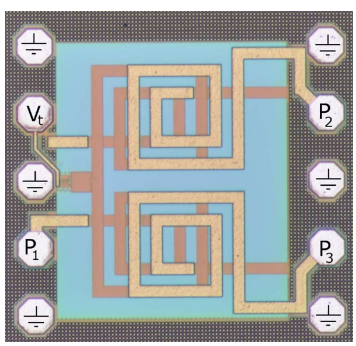

Fig. 3. Microphotograph of fabricated circuit. The size is 750 μm × 800 μm.

$$|S_{31}| = \frac{2C\sqrt{1-C^2}}{\sqrt{C^4Z_0^2B^2+2C^2+C^4+1}} \approx \frac{2C\sqrt{1-C^2}}{C^2+1} \tag{5}$$

$$\angle S_{21} = -\arctan\left(\frac{C^4Z_0^2B^2+C^2+1}{C^4Z_0B}\right) + \begin{cases} \pi & \text{for } B \geq 0 \\ 0 & \text{for } B > 0 \end{cases} \tag{6}$$

$$\approx \frac{1}{2}\pi + \frac{C^4Z_0}{C^2+1}B$$

$$\angle S_{31} = \arctan\left(\frac{C^2+1}{C^2Z_0B}\right) - \begin{cases} \pi & \text{for } B \geq 0 \\ 0 & \text{for } B > 0 \end{cases} \tag{7}$$

$$\approx -\frac{1}{2}\pi - \frac{C^2Z_0}{C^2+1}B$$

where the approximations are first order Taylor expansions valid for small B.

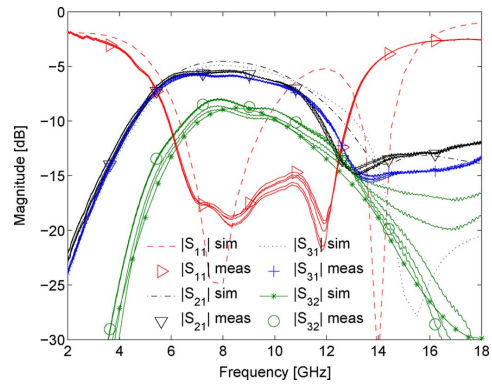

Fig. 4. Insertion loss and input matching measured with tuning voltages ranging from −2.5 to 2.5 V and simulation with tuning voltage at 0 V.

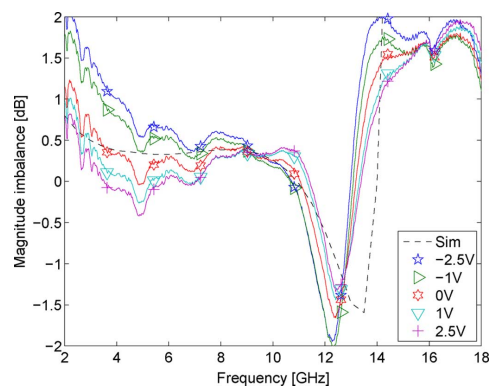

Fig. 5. Measurement of magnitude imbalance with tuning voltages ranging from −2.5 to 2.5 V and simulation with tuning voltage at 0 V.

From (4) and (5) it is seen that the magnitude is independent to changes in the susceptance and is similar to what is given in [1]. This is not the case for the phase, where both (6) and (7) shows that there is a linear relationship between the susceptance and the phase. It is thus possible to tune the phase balance of the Marchand balun by insertion of a shunt tunable susceptance. In Fig. 2 the magnitude imbalance and phase difference calculated from (4), (5), (6), and (7) are plotted together with simulation of a circuit with ideal couplers from Agilent's *Advanced Design System*, ADS. The ADS simulation results for the phase is hardly discernible from the theoretical results obtained with the Taylor expansion.

III. Design

The design procedure for a miniaturized Marchand balun utilizing lumped elements is described in [5], it uses offset coupled broadside spiral inductors together with capacitors to realize the coupled transmission lines. This configuration lend itself to easy integration of a shunt susceptance, due to the capacitor already placed as part of the couplers. This allows an effective negative susceptance by reducing this capacitance. A MOS-capacitive varactor is chosen to implement the variable susceptance with a size that allows the tuning range to be centered around

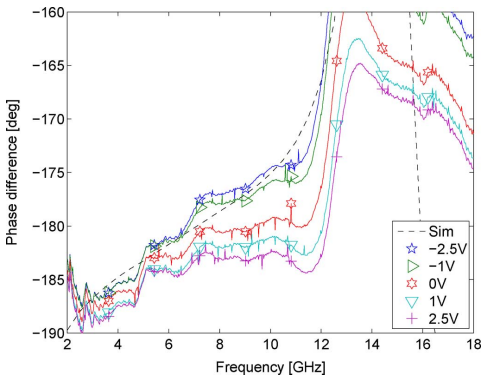

Fig. 6. Measurement of phase difference between output ports with tuning voltages ranging from −2.5 to 2.5 V and simulation with tuning voltage at 0 V.

TABLE I
PERFORMANCE COMPARISON OF PUBLISHED MARCHAND BALUNS AND THIS WORK

Ref.	Freq [GHz]	Bandwidth [GHz]	IL [dB]	Phase/Mag balance [°/dB]	Phase tune [°]
[3]	1.11-2.93	1.8	3.3	1.4 / 0.7	N/A
[4]	0.5-3.6	3.1	< 5	< 10 / < 1	N/A
[6]	23.6	24.5	5.9	< 10 / 1.5	N/A
[7]	2.09-3.06	0.97	3.8	1.6 / 0.4	N/A
[10]	4-9	5	< 4	5 / 0.5	N/A
[11]	55	10	4.14	0.9 / 1.2	N/A
This work	9.4	4	6.0	0 / 0.3	7.2

180°. The MOS-varactor, can be adjusted within a voltage range from −2.5 V 2.5 V, and the circuit is designed such that 0 V corresponds to a 180° phase difference. The circuit is realized using a SiGe BiCMOS technology with 5 metals from IHP microelectronics. Fig. 3 shows a microphotograph of the fabricated circuit.

IV. EXPERIMENTAL RESULTS

In this section, the experimental results obtained by on wafer measurements are discussed. Measurements of insertion loss, input matching, and isolation between output ports, for the full range of tuning voltages, are plotted in Fig. 4 together with the simulation results for $V_t = 0$ V, all simulations are done using Momentum in ADS. The insertion loss at the design frequency of 9.4 GHz is 6.0 dB, and remains better than 8.5 dB from 7 to 11 GHz. The rather large insertion loss is a consequence of the low Q-factor of the rectangular broadside coupled spiral structure. The measured performance of the balun is well predicted by EM simulations. The input matching stays better than −15 dB in this band and the output matching is better than −6 dB and isolation between ports 2 and 3 is better than 8 dB. Fig. 5 shows the measured magnitude imbalance versus frequency. Observe that within the band from 7.0 to 11.0 GHz the magnitude balance is better than 0.6 dB and only changes ± 0.25 dB with the bias voltage. The measured phase difference, shown in Fig. 6, can be tuned to 180° in this band. At the design frequency the phase difference can be varied from −183° to −175.8° while maintaining an almost constant magnitude imbalance of 0.3 ± 0.05 dB. As the shunted susceptance is realized by a MOS-varactor the tuning is frequency dependent. At 7 GHz it is only possible to tune the balun from −183.2° to −178.4° while at 11 GHz it can be tuned from −183.8° to −174.4°.

The nonlinearity in the phase response comes from the nonlinear relationship between the tuning voltage and the capacitance of the varactor. In Table I, this work is compared to other Marchand balun configurations recently reported in the literature [10], [11]. While being the only one with a tunable phase and thus the only with a zero phase imbalance, it also exhibits the state-of-the-art magnitude balance. The high insertion loss can be improved by using higher Q spiral transformers.

V. CONCLUSION

A novel configuration of the Marchand balun, which allows phase tuning has been presented. A description was given which showed that variations in a shunt susceptance, to first order, gives a linear change in the phase balance, while keeping the magnitude balance constant. This was verified by measurements of a lumped element Marchand balun implemented in a SiGe BiCMOS technology. Measurements showed that the phase difference could be changed in the range from −183° to −175.8° at the design frequency of 9.4 GHz whereas the magnitude imbalance only changed with ± 0.05 dB.

REFERENCES

[1] K. S. Ang, I. D. Robertson, K. Elgaid, and I. G. Thayne, "40 to 90 GHz impedance-transforming CPW Marchand balun," in *IEEE MTTS Int. Dig.*, 2000, vol. 2, pp. 1141–1144.
[2] X. Miao, W. Zhang, Y. Geng, X. Chen, R. Ma, and J. Gao, "Design of compact frequency-tuned microstrip balun," *IEEE Antennas Wireless Propag. Lett.*, vol. 9, pp. 686–688, 2010.
[3] C.-H. Tseng and Y.-C. Hsiao, "A new broadband Marchand balun using slot-coupled microstrip lines," *IEEE Microw. Wireless Compon. Lett.*, vol. 20, no. 3, pp. 157–159, Mar. 2010.
[4] J.-C. Lu, C.-C. Lin, and C.-Y. Chang, "Exact synthesis and implementation of new high-order wideband Marchand baluns," *IEEE Trans. Microw. Theory Tech.*, vol. 59, no. 1, pp. 80–86, Jan. 2011.
[5] T. Johansen and V. Krozer, "Analysis and design of lumped element Marchand baluns," in *Proc. 17th Int. Conf. Microw., Radar Wireless Commun. (MIKON'08)*, 2008, p. 4630169.
[6] M.-J. Chiang, H.-S. Wu, and C.-K. Tzuang, "A compact CMOS Marchand balun incorporating meandered multilayer edge-coupled transmission lines," in *IEEE MTT-S Int. Dig.*, 2009, pp. 125–128.
[7] C.-I. Shie, Y.-H. Pan, K.-S. Chin, and Y.-C. Chiang, "A miniaturized microstrip balun constructed with two $\lambda/8$ coupled lines and a redundant line," *IEEE Microw. Wireless Compon. Lett.*, vol. 20, no. 12, pp. 663–665, Dec. 2010.
[8] S. A. Maas, *Microwave Mixers*, 2nd ed. Norwell, MA: Artech House, 1993.
[9] H. Ma, S. J. Fang, F. Lin, and H. Nakamura, "Novel active differential phase splitters in RFIC for wireless applications," *IEEE Trans. Microw. Theory Tech.*, vol. 46, no. 12, pp. 2597–2603, Dec. 1998.
[10] A. Chen, A.-V. Pham, and R. Leoni, "A novel broadband even-mode matching network for Marchand baluns," *IEEE Trans. Microw. Theory Tech.*, vol. 57, no. 12, pp. 2973–2980, Dec. 2009.
[11] D. A. A. Mat, R. K. Pokharel, R. Sapawi, H. Kanaya, and K. Yoshida, "60 GHz-band on-chip Marchand Balun designed on flat and patterned ground shields for milimeter-wave 0.18 μm CMOS technology," in *Proc. Asia-Pacific Microwave Conf.*, 2011, pp. 884–887.

International Journal of Microwave and Wireless Technologies, page 1 of 8.
doi:10.1017/S1759078714000191

RESEARCH PAPER

Design of a broadband passive X-band double-balanced mixer in SiGe HBT technology

RASMUS S. MICHAELSEN[1,2], TOM K. JOHANSEN[1], KJELD M. TAMBORG[2] AND VITALIY ZHURBENKO[1]

In this paper, a passive double-balanced mixer in SiGe HBT technology is presented. Owing to lack of suitable passive mixing elements in the technology, the mixing elements are formed by diode-connected HBTs. The mixer uses lumped element Marchand baluns on both the local oscillator (LO) and the radio frequency (RF) port. A break out of the Marchand balun is measured. This demonstrates good phase and magnitude match of 0.7° and 0.11 dB, respectively. The Marchand baluns are broadband with a measured 3 dB bandwidth of 6.4 GHz, while still having a magnitude imbalance better than 0.4 dB and a phase imbalance better than 5°. Unfortunately with a rather high loss of 2.5 dB, mainly due to the low Q-factor of the inductors used. The mixer is optimized for use in doppler radars and is highly linear with a 1 dB compression point above 12 dBm IIP_2 of 66 dBm. The conversion gain at the center frequency of 8.5 GHz is −9.8 dB at an LO drive level of 15 dBm. The whole mixer is very broadband with 3 dB bandwidth from 7 to 12 GHz covering the entire X-band. The LO–IF, RF–IF, and RF–LO isolation is better than 46, 36, and 36 dB, respectively, in the entire band of operation.

Received 15 October 2013; Revised 17 December 2013

I. INTRODUCTION

Direct conversion receivers are used in Doppler radars for speed monitoring, vital signs detection, and measurements of ballistic targets. In these applications, using direct conversion gives the Doppler shift and thus the speed measurement directly from the received frequency. It is also common to use direct conversion to avoid complex image rejection structures in other applications [1]. The key element in a direct conversion receiver is the mixer.

Mixers for direct conversion applications must have low 1/f-noise and leakage due to LO and RF which exists at the same frequency. Two fundamental types of direct conversion mixers exist, active and passive. Active mixers have the advantage of providing conversion gain, whereas passive mixers have the advantage of higher linearity and less noise. Structures for increasing linearity of the active mixers have been proposed [2], but then suffer from increased noise. Thus, the dynamic range remains largest for a passive mixer design. The main disadvantage of the passive mixer is the loss in the signal path.

The double-balanced structure has the advantage of inherent isolation between all ports, good linearity, and broadband operation [3]. These are all desired characteristics for mixers to be used in Doppler radars. Having built-in isolation in the mixer structure is important, as normal filtering is difficult due to the proximity of the RF and LO frequencies. The drawbacks are increased circuit complexity, higher LO-power requirement, and higher conversion loss.

Using a CMOS process to realize the circuit has the advantage of low-cost mass production. Unfortunately the MOSFET suffers from traps in the oxide, which leads to an increased 1/f-noise. Bipolar devices on the other hand are bulk conduction devices, which have an order of magnitude lower 1/f noise compared to the surface channel conduction of CMOS devices [4].

In this paper, a direct conversion mixer operating at X-band that has characteristics optimized for Doppler radar applications is described. These characteristics include state-of-the-art linearity, together with good 1/f-noise performance and reasonable conversion loss. To meet these requirements, double-balanced passive mixer architecture is chosen. The circuit is fabricated using a SiGe:C BiCMOS process from Innovations for High Performance Microelectronics (IHP). It is a 0.25 μm technology, featuring high-performance npn-HBTs having a unit current gain frequency (f_T) of 110 GHz and a maximum oscillation frequency (f_{max}) of 180 GHz. The process has metal-insulator-metal (MIM) capacitors and five metal layers of which the upper two are extra thick, intended for passives or low loss interconnects [5].

As the SiGe HBT process used for implementation do not offer suitable diodes for mixing, diode-connected HBTs as in [6] are used.

[1]Department of Electrical Engineering, Technical University of Denmark, 2800 Kongens Lyngby, Denmark. Phone: + 45 45 25 38 61
[2]Weibel Scientific A/S, 3450 Allerød, Denmark
Corresponding author
R. S. Michaelsen
Email: rsmi@elektro.dtu.dk

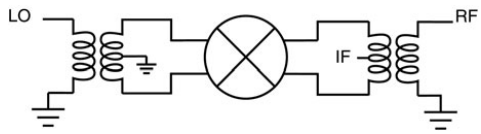

Fig. 1. Block diagram of the balanced mixer circuit. Showing LO and RF balun together with center tapped IF extraction.

II. DESIGN

This section describes the design of the proposed double-balanced ring diode mixer. Diodes are desired for the implementation of low-noise mixers in direct conversion receivers. In many SiGe HBT technologies, there are no diodes available. Using the base–emitter junction of the high-speed HBTs available as a pn-junction diode [6], it is possible to have good mixer diodes in a SiGe HBT technology. The design description is divided into three parts covering the design of the balun, the intermediate frequency (IF) extraction and the mixer core. Figure 1 shows a block diagram of the mixer circuit.

A) Marchand balun

The balun of the double-balanced mixer is implemented in the form of a lumped element Marchand balun. The Marchand balun is chosen owing to its broadband properties. The lumped element implementation allows compact size and straightforward design procedure for good phase and magnitude balance [7, 8]. The lumped element implementation uses offset broadside coupled spiral inductors together with capacitors to realize the coupled transmission lines, normally used in Marchand baluns. The schematic of the balun is shown in Fig. 2, where it is depicted as a symmetrical four port, together with the corresponding even- and odd-mode circuits. For normal operation port, four is open circuited.

For a circuit to behave like an ideal balun, it must have *S*-parameters given as

$$S_{21} = -S_{31}, \tag{1}$$

$$S_{11} = 0. \tag{2}$$

For a symmetrical four-port circuit, (1) is fulfilled if the fourth port is terminated in an open circuit to give [9]

$$T_{even} = 0, \tag{3}$$

$$Z_{in_{even}} + Z_{in_{odd}} = 2Z_{P1}, \tag{4}$$

where T_{even} is the transmission coefficient in the even-mode circuit, Z_{P1} is the system impedance at port 1, $Z_{in_{even}}$ and $Z_{in_{odd}}$ are the input impedance of the even-mode and odd-mode circuits, respectively.

The synthesis of this type of lumped balun is based on the coupled line Marchand balun [7]. Thus the synthesis starts by selecting the even- and odd-mode characteristic impedance of the lines. For a real-valued impedance scaling, α equals $Z_{P2,3}/Z_{P1}$ the relation giving the even- and odd-mode impedance is [10]

$$\frac{1}{Z_{o_{odd}}} - \frac{1}{Z_{o_{even}}} = \frac{1}{Z_{P1}}\sqrt{\frac{2}{\alpha}}, \tag{5}$$

where $Z_{o_{even}}$ and $Z_{o_{odd}}$ are the even- and odd-mode characteristic impedance of the coupled line, respectively.

From the even- and odd-mode characteristic impedance, the circuit parameters for the lumped element balun can be

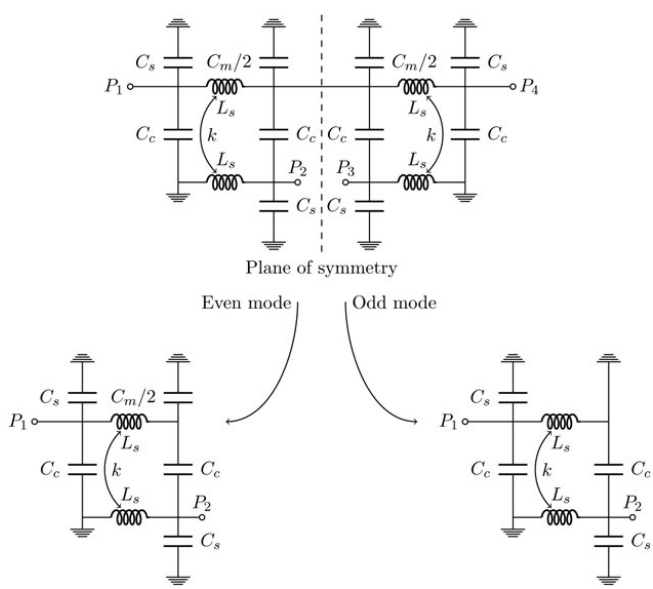

Fig. 2. Circuit diagram for the lumped Marchand balun, showing it as a symmetrical four port. Normal operation requires P_4 to be open circuited.

found. This procedure was described in [7] and the design equations are repeated here

$$L_s = \frac{Z_{o_{even}} + Z_{o_{odd}}}{2\omega}, \tag{6}$$

$$k = \frac{Z_{o_{even}} - Z_{o_{odd}}}{2\omega L_s}, \tag{7}$$

$$C_c = \frac{1}{2\omega}\left(\frac{1}{Z_{o_{odd}}} - \frac{1}{Z_{o_{even}}}\right), \tag{8}$$

$$C_s = \frac{1}{\omega Z_{o_{even}}}, \tag{9}$$

where k and C_c are the inductive coupling coefficient and the capacitive coupling, respectively, of the coupled spiral pairs. The center capacitors are given as $C_m = 2C_s$.

From (5) it is evident that there are several values of $Z_{o_{odd}}$ and $Z_{o_{even}}$, which fulfills the requirement. A higher $Z_{o_{odd}}$ gives larger bandwidth, but gives larger inductors in the realization of the lumped element balun, so a trade off between bandwidth and desired balun size must be made. In Figs. 3 and 4, are the design curves plotted for a 50 Ω environment, without scaling.

The coupled broadside spiral inductor design is limited in the realization, as it is often not possible to obtain values as dictated by equations (6)–(8). Further investigation of the structure is therefore required to reveal possible solutions or trade offs for this problem. For the even-mode circuit, shown in Fig. 2, the requirement for the transmission coefficient being zero is the same as the Y-parameter Y_{21e} become zero [8]. Thus, for (1) to be fulfilled we have

$$Y_{21e} = -\frac{(1-k)s(C_m/2 + C_c) - sC_m/2}{s^2(C_m/2 + C_c)L_s(1-k^2) + 1} = 0 \Leftrightarrow, \tag{10}$$

$$C_m = 2C_c\left(\frac{1}{k} - 1\right). \tag{11}$$

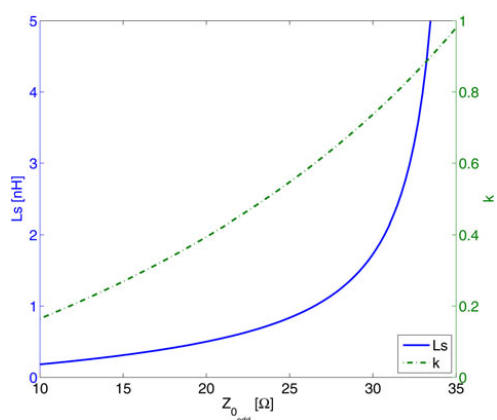

Fig. 3. Design curves for L_s and k as function of $Z_{o_{odd}}$.

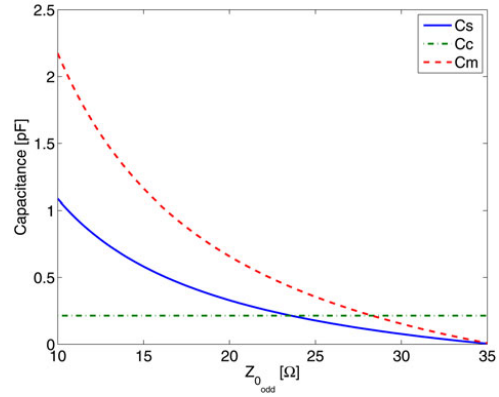

Fig. 4. Design curves for C_s, C_c and C_m as function of $Z_{o_{odd}}$.

This is a nice property as it shows that by careful selection of C_m it is possible to obtain good phase and magnitude match even though the coupled spiral is not as specified above. Also note that the match is broadband as it does not depend directly on frequency, but on parameters which ideally should be frequency independent.

The even- and odd-mode impedance can be found, by terminating the even- and odd-mode circuits in Fig. 2 with Z_{P_2}, as

$$Y_{even} = \frac{1}{Z_{even}} = s(C_s + C_c) + \frac{s(C_m/2 + C_c)}{s^2(C_m/2 + C_c)L_s(1-k^2) + 1}, \tag{12}$$

$$Y_{odd} = \frac{1}{Z_{odd}} = s(C_s + C_c) + \frac{1}{sL_s - \dfrac{(skL_s)^2}{sL_s + \dfrac{1}{s(C_s + C_c) + Y_{P_2}}}}, \tag{13}$$

where $s = j\omega$ is the complex frequency. Note that (12) will always be purely imaginary for real circuits, whereas (13) is a general complex number having a real and a imaginary part. Inserting (12) and (13) into (4) gives the requirement for the perfect input match. Thus, to match to a real source impedance, Z_{P_1}, we have $Z_{odd} = 1/Y_{odd} = 2Z_{P_1} - Z_{even}$, where Z_{P_1} is purely real and Z_{even} is purely imaginary. This corresponds to two real equations in C_s. Thus, it is not guaranteed that there exists a C_s to fulfill the requirement for arbitrary selection of L_s, k and C_c.

Even though if the coupled spiral is not as specified by equations (6)–(8), one can try to change C_s, to obtain a better match. It is typically possible to find an acceptable match, albeit not perfect.

The implemented balun has parameters given by Table 1. The chip area occupied by the balun is 680 μm × 710 μm and a microphotograph is shown in Fig. 5. The S-parameters for the balun is shown in Fig. 6, where simulation results are compared to measurements. It is observed that there is good agreement, in general, between the simulation and experimental results. The largest discrepancy is the S_{11} curve where the

Table 1. Design parameters for the balun.

Inductance	L_s (fF)	1.02
Inductive coupling	k	0.825
Capacitive coupling	C_c (fF)	379
Input matching capacitors	C_s (fF)	283
Balance matching capacitor	C_m (fF)	190

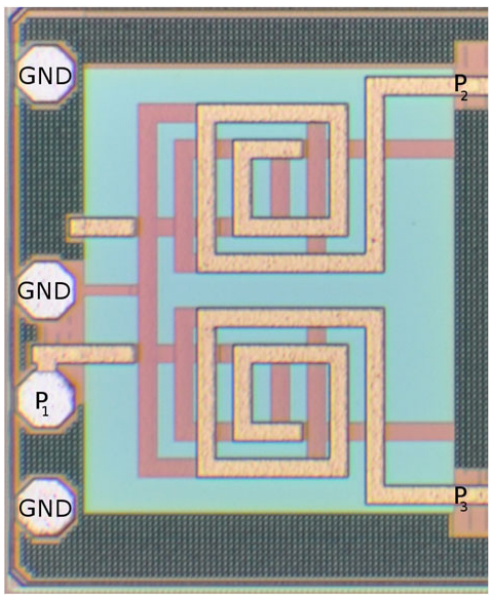

Fig. 5. Microphotograph of on chip balun structure. Dimensions are 680 μm × 710 μm.

second resonance behavior is shifted down from 13 to 12 GHz. This shift is probably due to parasitic capacitances not included in the simulation model. At the design frequency a loss of 2.5 dB was measured. The rather high loss is mainly due to the low Q-factor of the inductors. As desired the balun

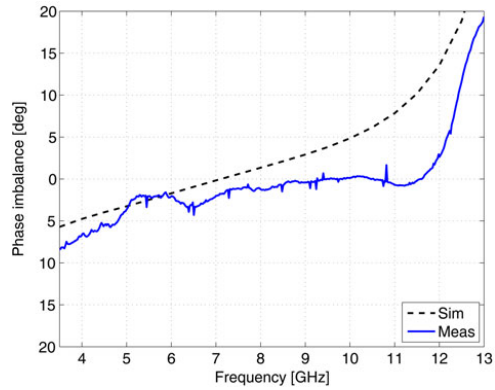

Fig. 7. Measurement and simulation results for phase imbalance.

is broadband with a measured 3 dB bandwidth of 6.4 GHz. Figures 7 and 8 show the phase and magnitude imbalances, respectively. Excellent magnitude and phase imbalance of 0.11 dB and 0.7°, respectively, are achieved at the design frequency. A magnitude imbalance better than 0.4 dB and a phase imbalance better than 5°, is achieved over the entire bandwidth of operation, which makes this balun suitable for double-balanced mixer implementation.

B) IF extraction

To get an output signal from the mixer it is necessary to have a circuit that allows to extract the IF signal, without disturbing the LO and RF baluns. The IF extraction is achieved by making a DC and low-frequency return path at either the LO or RF port and extract the signal from the other. It is desirable not to have any large signal leaking out of the IF port as this might saturate or cause other unwanted effects in the low-frequency circuitry following the mixer. For this reason, it is chosen to use the balun at the LO port to make the DC and low-frequency return path and the balun at the RF port to extract the IF signal, as the LO-signal can be several magnitudes larger than the RF signal.

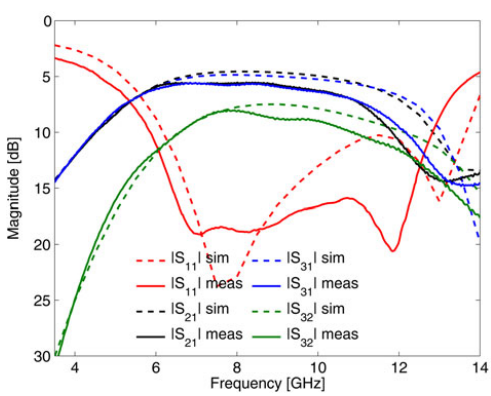

Fig. 6. Measurements and simulation results for balun S-parameters.

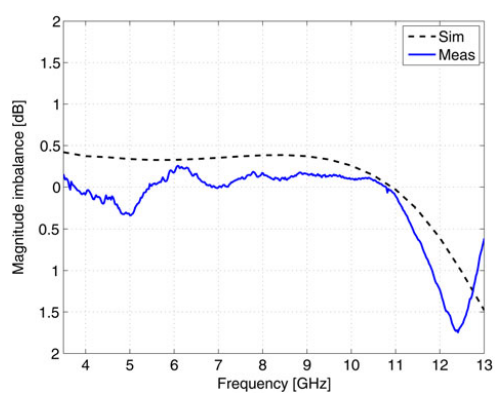

Fig. 8. Measurement and simulation results for magnitude imbalance.

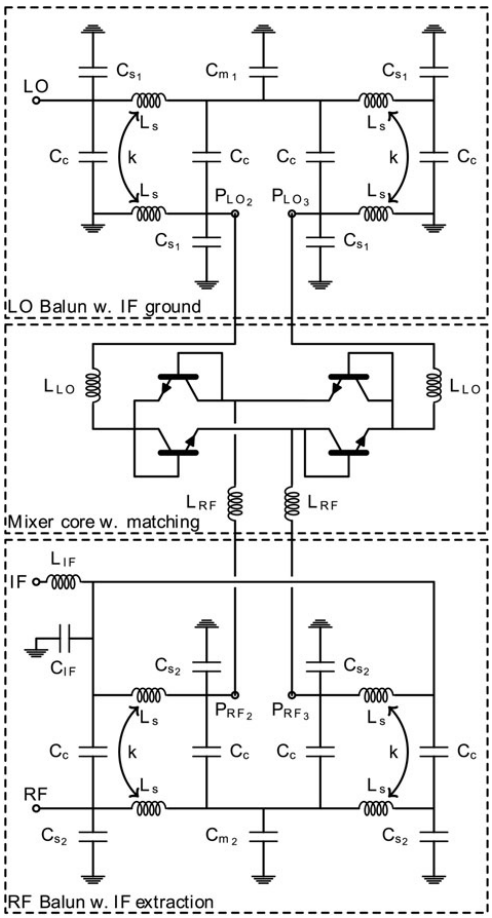

Fig. 9. Schematic representation of the full mixer circuit.

Owing to low IF frequency of the mixer together with the grounded parts of the Marchand balun, the IF extraction is quite simple and follows the idea from [11]. The schematic for the IF extraction is the part of Fig. 9 labeled 'RF balun w. IF extraction'. The DC and low-frequency return path is ensured by the Marchand balun as the inductors L_s are seen as a short circuit. To avoid the ground connection in the RF balun, it is blocked by large capacitors which creates an open for the IF signal and a short for the RF signal. It is important to make the IF extraction symmetric as any asymmetry will affect the balun performance. To ensure the symmetry the capacitor C_{IF} is split into three parallel 2 pF capacitors placed after both of the two inductors and in the middle where the IF signal is combined. The small influence on the balun performance from the 2 pF capacitors can be compensated by slightly changing C_{s2} for matching and C_{m2} for balance.

C) Mixer core

The mixer core consists of the mixing devices and a matching circuit. Each mixing device is a diode-connected HBT. There are two possible ways to make the diode connections, either by use of the base-emitter or the base-collector pn-junction. The base-emitter junction is the preferred diode junction due to the heavier doping of the n-region of the emitter compared to the collector. Simulations also show that this gives the best behavior, having a 3 dB difference in conversion loss between the two diode connections. To get the double-balanced properties the ring mixer structure is used [3].

Using Harmonic Balance simulations the optimum load conditions are found to be $58 + j106\Omega$ and $50 + j122\Omega$ at 8.5 GHz for the LO and the RF ports, respectively. As a 50Ω match is required it is relatively simple to tune out the reactive part using single series inductors, L_{RF} and L_{LO}. In Fig. 9 the schematic of the mixer core is labeled 'Mixer core w. matching'.

The mixer has been manufactured using a 0.25 μm SiGe HBT process from IHP. The die size is 2200 μm × 800 μm. A microphotograph of the full mixer is shown in Fig. 10.

III. EXPERIMENTAL RESULTS

In this section, the experimental results are discussed. The measurements are made on-wafer using a probe station, and simple calibration is used to remove losses in cables and probes. The IF-frequency for all measurements is 100 MHz. The mixer conversion loss and single sideband noise figure

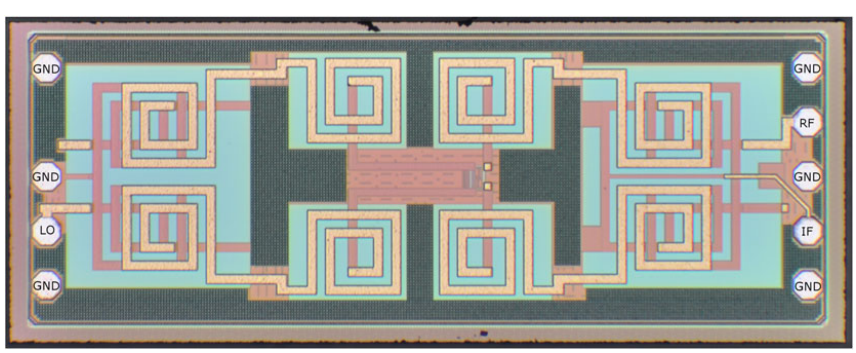

Fig. 10. Microphotograph of passive double-balanced mixer. The die size is 2200 μm × 800 μm.

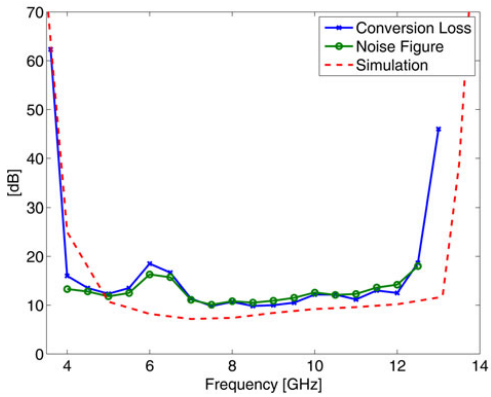

Fig. 11. Measured conversion loss and single sideband noise figure versus frequency.

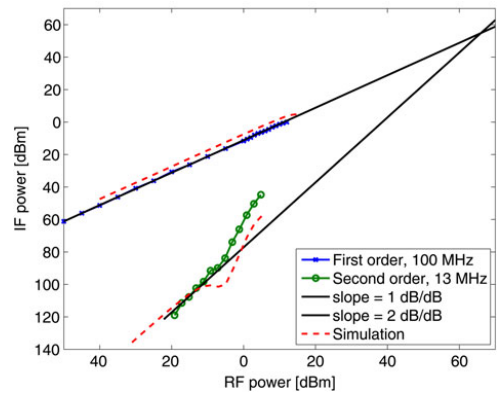

Fig. 13. Measured IF power versus RF.

is shown in Fig. 11 as a function of frequency, with a fixed LO power of 15 dBm. At the design frequency of 8.5 GHz the conversion loss is 9.8 dB. The noise figure follows the conversion loss as expected. Due to measurement inaccuracy the noise figure is at some points lower than the conversion loss. The 3 dB bandwidth covers more than the entire X-band or more precisely the range from 7 to 12 GHz, thus showing the benefit of using a broadband balun design together with the double-balanced topology.

In Fig. 12 the conversion loss and noise figure is plotted versus the LO power level, at the design frequency of 8.5 GHz. It is seen that the mixer is not fully saturated at an LO power of 15 dBm which was the limit of the measurement equipment used. To measure the linearity the IF power is measured as a function of the RF power, which is plotted in Fig. 13. Due to equipment limitations the measurement could not be made with a RF power above 12 dBm. At this point there is measured a compression of 0.8 dB. Simulations predict the input referred 1 dB compression point to be at 12.4 dBm. The input referred second-order intercept point (IIP_2) is measured with two RF tones at frequencies of 8.4 and 8.413 GHz, giving a second-order product at 13 MHz. Isolators is placed after the signal generators to avoid leakage and intermodulation of the signals before they are applied to the mixer. Attenuation is added to the output of the mixer to avoid measuring the nonlinearity of the spectrum analyzer [12]. From Fig. 13, it can be observed that not only a second order but also a fourth-order phenomenon is observed. It is not possible to distinguish between second- and fourth-order by frequency selection, as a fourth-order term will always be at the same frequency as the second-order term. For weak signals, it is the second-order behavior of the mixer that is dominant, whereas for powers above −5 dBm it is fourth-order which is dominant. This behavior was predicted by the simulations. By extrapolation an IIP_2 of 66 dBm is found. This proves that the design gives a high linearity as required.

The LO–IF, RF–IF, and LO-RF isolation at the design frequency are 55, 40, and 58 dB, respectively. In Fig. 14, the isolation is plotted versus frequency. In the entire band of operation, the LO–IF, RF–IF, and LO–RF isolation are better than 46, 36, and 36 dB, respectively. The high LO to RF isolation is very important due to self-mixing issues. Self-mixing can give rise to a DC-current through the mixing device, which increases the $1/f$ noise [13].

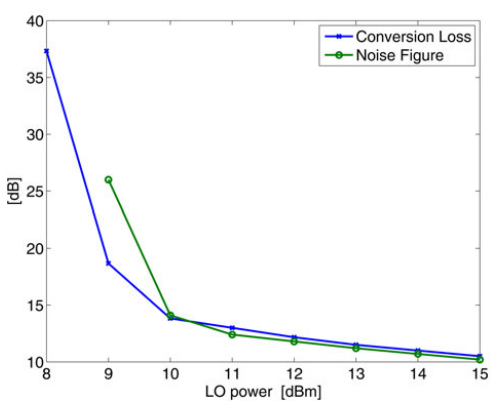

Fig. 12. Measured conversion loss and single sideband noise figure versus LO power.

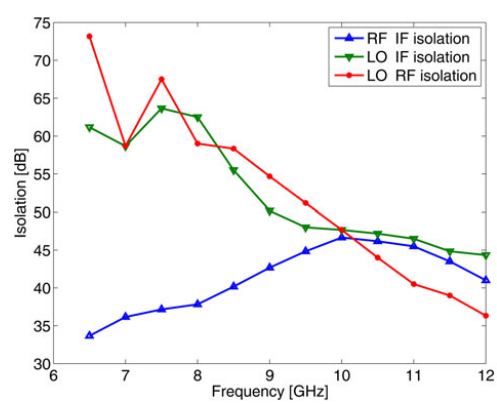

Fig. 14. Measured LO–IF and RF–IF isolation.

Table 2. Comparison between this work and recently reported passive mixers.

Ref.	Technology	Topology	Frequency (GHz)	BW (GHz)	CG (dB)	LO-power (dBm)	LO-IF/RF-IF/LO-RF isolation (dB)	IP_{1dB} (dBm)
[6]	HBT-diode	Single bal.	24	22–39	−8	3	50/48/15	−1.5
[11]	pHEMT	Double bal.	NA	11–40	−7.2	13	43.2/32/26.9	12
[14]	pHEMT	Single bal.	60	NA	−12	0	32/NA/20	−2
[15]	CMOS	Double bal.	2.4	1.8–2.8	−7.5	10	47.7/NA/51.9	6.2
This work	HBT-diode	Double bal.	8.5	7–12	−9.8	15	55/40/58	12

A comparison between this work and passive mixers recently reported in the open literature is presented in Table 2.

IV. CONCLUSION

The design of a passive double-balanced mixer in a 0.25 μm SiGe HBT technology has been presented. The mixer is a direct conversion mixer suitable for use in Doppler radars. The passive mixing element consists of diode-connected HBTs, using the base-emitter pn-junction to realize the mixing diodes. Lumped element Marchand baluns was implemented using offset broadside coupled spiral inductors and capacitors. This gives the possibility of an elegant IF-extraction together with wide bandwidth and good balance.

The lumped element Marchand baluns had an excellent phase and magnitude match of 0.7° and 0.11 dB, respectively. Being broadband they kept a magnitude imbalance better than 0.4 dB and a phase imbalance better than 5° over the entire 3 dB bandwidth of 6.4 GHz. Suffering from the low *Q*-factor of the inductors, however, they have a rather high loss of 2.5 dB.

The broadband mixer has a 3 dB bandwidth from 7–12 GHz, covering the entire X-band, with a conversion loss of 9.8 dB at the design frequency. It requires a relatively high LO level of 15 dBm for best performance, but has a high linearity with a 1 dB compression point above 12 dBm and IIP_2 at 66 dBm. Good isolation between LO–IF, RF–IF, and LO–RF ports of 55, 40, and 58 dB, respectively, is ensured due to the good balance of the Marchand baluns.

ACKNOWLEDGEMENT

The authors would like to thank the H.C. Ørsteds fond for financial support to cover the cost of chip fabrication.

REFERENCES

[1] Razavi, B.: Design considerations for direct-conversion receivers. IEEE Trans. Circuits Syst. II: Analog Digit. Signal Process., **44** (6) (1997), 428–435.

[2] Barati, M.; Yavari, M.: A highly linear mixer with inherent balun using a new technique to remove common mode currents, in Proc. – IEEE Int. Symp. on Circuits and Systems, 2011, 1884–1887.

[3] Maas, S.A.: Microwave Mixers, 2nd ed., Artec House, Norwood, MA, USA, 1993.

[4] Babcock, J.; Loftin, B.; Madhani, P.;Chen, X.; Pinto, A.; Schroder, D.: Comparative low frequency noise analysis of bipolar and MOS transistors using an advanced complementary BiCMOS technology, in IEEE Conf. on Custom Integrated Circuits, 2001, 385–388.

[5] IHP website: http://www.ihp-microelectronics.com

[6] Issakov, V.; Knapp, H.; Wojnowski, M.; Thiede, A.; Simburger, W.: A 22–39 GHz passive mixer in SiGe:C bipolar technology, in Int. Microwave Symp. (MTT-S), California, USA, 2010.

[7] Johansen, T.K.; Krozer, V.: Analysis and design of lumped element Marchand baluns, in Mikon Conf. Proc., 2008.

[8] Johansen, T. K.; Krozer, V.: A 38 to 44 GHz sub-harmonic balanced HBT mixer with integrated miniature spiral type Marchand balun. Electromagn. Waves, **135** (2013), 317–330.

[9] Ang, K.S.; Leong, Y.C.; Lee, C.H.: Analysis and design of miniaturized lumped-distributed impedance-transforming baluns. IEEE Trans. Microw. Theory Tech., **51** (2003), 1009–1017.

[10] Zhang, Z.-Y.; Guo, Y.-X.; Ong, L.; Chia, M.Y.W.: A new planar Marchand balun, in Int. Microwave Symp. (MTT-S), 2005

[11] Lee, Y.-C.; Lin, C.-M.; Hung, S.-H.; Su, C.-C.; Wang, Y.-H.: A broadband doubly balanced monolithic ring mixer with a compact intermediate frequency (IF) extraction. Progr. Electromagn. Res. Lett., **20** (2011), 175–184.

[12] Maas, S.A.: Nonlinear Microwave and RF Circuits, 2nd ed., Artec House, Norwood, MA, USA, 2003.

[13] Michaelsen, R.; Johansen, T.; Tamborg, K.: Investigation of LO leakage cancellation and dc-offset influence on flicker-noise in x-band mixers, in 7th Eur. Microwave Integrated Circuit Conf. (EuMIC), Amsterdam, 2012.

[14] Huang, F.-H.; Lin, S.-W.; Ke, P.-Y.; Chiu, H.-C.: A wide bandwidth V-band balanced resistive mixer with a miniature meandering balun. Microw. Opt. Technol. Lett., **55** (2013), 547–550.

[15] Song, C.; Boric-Lubecke, O.; Lo, I.: 0.18-m CMOS wideband passive mixer. Microw. Opt. Technol. Lett., **55** (2013), 23–27.

Vitaliy Zhurbenko received the M.Sc. degree from the Kharkiv National University of Radio Electronics in 2001, and the Ph.D. degree from the Technical University of Denmark in 2008, all in electrical engineering. From November 2000 to Jun 2005, he was a metrology engineer with the Laboratory of Metrology, Kharkiv, Ukraine.

In 2005, he joined the Technical University of Denmark, where he is currently an Associate Professor. His current research interests include microwave and millimeter wave devices and integrated circuits for instrumentation applications; microwave and millimeter wave sensing for biomedical and security applications; microwave imaging and radars; antenna and passive circuit design and characterization.

Kjeld M. Tamborg was born in Kastrup, Denmark in 1966. He received his M.Sc. degree in electronics from the Technical University of Denmark (DTU) in 1990. He was in 1990 hired by Weibel Scientific A/S, Allerød, Denmark, where he is still working. Since 2007 he has been product responsible for the Weibel radar antenna heads and components inside. During his work he has developed micro strip antenna elements, low noise amplifiers, power amplifiers, mixers, oscillators and many other components for X-band radars.

Rasmus S. Michaelsen received the M.Sc. degree in electrical engineering from the Technical University of Denmark in 2010. He is currently working toward the Ph.D. degree together with the technical University of Denmark and Weibel Scientific, Allerød, Denamark. In 2009 he joined Weibel Scientific A/S, designing and testing X-band microwave components, and later as industrial Ph.D student. In 2010 he was on an external stay at Physikalisches Institut, Johann Wolfgang Goethe-Universität, Frankfur am Main, Germany. His current research interests include microwave monolithic integrated circuit (MMIC) design, nonlinear circuits, flicker noise and direct conversion receiver circuits.

Tom K. Johansen received his M.S and Ph.D. degrees in electrical engineering from the Technical University of Denmark, Denmark, in 1999 and 2003, respectively. In 1999 he joined the Electromagnetic Systems group, DTU Elektro, Technical University of Denmark, Denmark, where he is currently an Associate Professor. From September 2001 to March 2002 he was a Visiting scholar at the center for wireless communication, University of San Diego, California, CA. From November 2012 to February 2013 he spent a sabbatical at the Ferdinand Braun Institute (FBH), in Berlin, Germany. His research areas include the modeling of HBT devices, microwave, millimeter-wave and sub-millimeter-wave integrated circuit design.

An X-band Schottky Diode Mixer in SiGe Technology with Tunable Marchand Balun

Rasmus Michaelsen, *Student Member, IEEE,* Tom Johansen, *Member, IEEE,*, Lei Yan, *Member, IEEE*, Kjeld Tamborg and Vitaliy Zhurbenko, *Member, IEEE*

***Abstract*—In this paper, we propose a double balanced mixer with a tunable Marchand balun. The circuit is designed in a SiGe BiCMOS process, using Schottky diodes. The tunability of the Marchand balun is used to enhance critical parameters for double balanced mixers. The LO-IF isolation can be changed from $-51\,\mathrm{dB}$ to $-60.5\,\mathrm{dB}$ by tuning. Similarly, the IIP_2 can be improved from $41.3\,\mathrm{dBm}$ to $48.7\,\mathrm{dBm}$ at $11\,\mathrm{GHz}$, while the input referred 1-dB compression point is kept constant at $8\,\mathrm{dBm}$. The tuning have no influence on conversion gain, which remains at $8.8\,\mathrm{dB}$ at a LO power level of $11\,\mathrm{dBm}$ at the center frequency of $11\,\mathrm{GHz}$. The mixer has a 3 dB bandwidth from $8\,\mathrm{GHz}$ to $13\,\mathrm{GHz}$, covering the entire X-band. The full mixer has a size of $2050\,\mu\mathrm{m}\times1000\,\mu\mathrm{m}$.**

***Index Terms*—Mixers, microwave integrated circuits, tunable circuits and devices.**

I. Introduction

FREQUENCY down conversion is a vital function in almost any microwave receiver. The simplest receivers are usually based on the homodyne or direct conversion architecture [**?**]. This overcomes the problem with image frequency channel and leaves only the desired signal, directly at baseband. Mixers for direct conversion are also used in Doppler radars, as the direct conversion architecture gives the Doppler shift directly from the received frequency. Mixers for direct conversion has the drawback that the RF and LO frequencies are at the same frequency, thus good isolation between the ports is important as filtering is not possible. Also, as the output frequency is low, flicker or 1/f noise might be a problem.

The double balanced mixer ideally provides infinite isolation between all ports and is therefore a good choice to use as a mixer for direct conversion. Other benefits of the double balanced mixer is rejection of LO noise and high linearity [1]. The balancing circuits should, to get full benefit of the double balanced architecture, be well adjusted. This is challenging to achieve in practice due to process and manufacturing variances.

To utilize the broadband nature of the double balanced mixer, the balun should also be broadband otherwise the bandwidth of the mixer will be limited. The Marchand balun [2] is in itself very broadband, and it s commonly used for this reason in a planar [3]–[5] or lumped-distributed [6]–[8] implementation. In [9] we presented a Marchand balun with tunable phase balance, and in [10] we presented a broad band double balanced mixer using diode connected HBTs together with lumped Marchand baluns on RF and LO ports. The mixer design presented here integrates the tunable Marchand balun on the LO-port together with Schottky diodes instead of diode connected HBTs as in [10]. This allows to correct for any mismatches either in the balun design or in the mixing core itself. This should then enhance the benefits of practical implementations of double balanced mixers, where our focus will be on the properties important for direct conversion mixing, i.e. port isolation and linearity. To the authors knowledge a double balanced ring mixer with balance corrections using a tunable balun is demonstrated here for the first time.

Manuscript received Spring, 2015.

Rasmus Michaelsen, Tom Johansen, and Vitaliy Zhurbenko are with the Electromagnetic systems group, DTU Elektro, Technical University of Denmark, 2800 Kgs. Lyngby, Denmark e-mail: rsmi@elektro.dtu.dk.

Lei Yan was with the Technical University of Denmark. He is now with HHI in Berlin, Germany

Rasmus Michaelsen is also with Weibel Scientific, 3450 Allerød, Denmark

Kjeld Tamborg is with Weibel Scientific, 3450 Allerød, Denmark

II. Non-ideal double balanced mixer theory

This section will give a theoretical description of the behavior of double balanced mixers in the case of non-ideal baluns. The main focus will be on DC offset, port isolation and the intermodulation products. First we investigate the large signal conditions for the LO-voltage. This is followed by an analysis of the behavior of the ring mixer due to unbalance. The analysis takes the time-varying nature of the diodes non-linear conductances under the influence of LO balun imbalances into account. Thus it will be possible to identify the mechanisms responsible for DC offset, LO and RF leakage, conversion loss, and second-order intermodulation products.

The diode ring which will be used as the core of the double balanced mixer is depicted in Fig. 1. The current through each Schottky diode is given by

$$I_{d_n}=I_s\left(\exp\left(\frac{V_{d_n}}{\eta V_T}\right)-1\right), \tag{1}$$

where I_s is the saturation current, V_{d_n} is the large signal diode voltage across diode n, η is the ideality factor and V_T is the thermal voltage.

To find the LO-voltage across a single diode in the diode ring, we look at the left and right half-circuit independently. The half-circuit is shown in Fig. 2, where the impedance Z_m is a combination of IF, RF load and embedding network. Using

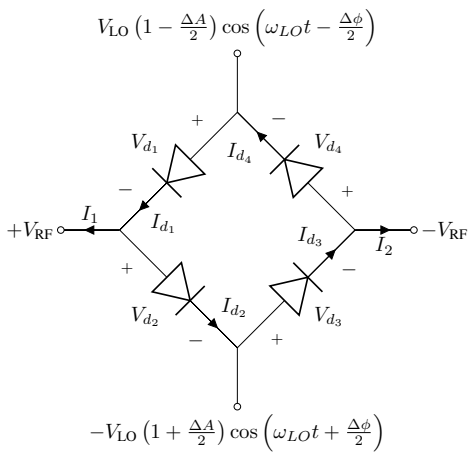

Fig. 1. Schottky diode ring.

the definitions on the figure, we have the following voltage relation:

$$V_a{=}V_{d_1}+Z_mI_m \tag{2}$$
$$V_b{=}-V_{d_2}+Z_mI_m \tag{3}$$
$$\textit{where } I_m{=}i_a+i_b=I_s\left(\exp\left(\frac{V_{d_1}}{\eta V_T}\right)-\exp\left(\frac{V_{d_2}}{\eta V_T}\right)\right) \tag{4}$$

The signals V_a and V_b can be given as

$$V_a{=}V_{\rm LO}\left(1-\frac{\Delta A}{2}\right)\cos\left(\omega_{\rm LO}t-\frac{\Delta\phi}{2}\right) \tag{5}$$
$$V_b{=}-V_{\rm LO}\left(1+\frac{\Delta A}{2}\right)\cos\left(\omega_{\rm LO}t+\frac{\Delta\phi}{2}\right) \tag{6}$$

where we have introduced an phase error, $\Delta\phi$, and a amplitude error ΔA. This allows to investigate the consequences of unbalance on circuit performance. We will also introduce an unbalance on the IF load given as $Z_{m_{\rm left}}=Z_m(1+\frac{\Delta Z}{2})$ and $Z_{m_{\rm right}}=Z_m(1-\frac{\Delta Z}{2})$ for the left and right half circuits, respectively. The term Z_mI_m from (2), which will contribute to a voltage difference across the two diodes, is approximated by the term $\left(1\pm A_Z\left(1-\frac{\Delta Z}{2}\right)\right)$, where A_Z is a function of the amplitude and phase balance. This term reduces to zero if the amplitude and phase balance are both zero. Then the large signal diode voltages is given as

$$V_{d_1}{=}V_{\rm LO}\left(1-\frac{\Delta A}{2}\right)\cos\left(\omega_{\rm LO}t-\frac{\Delta\phi}{2}\right)\times\left(1-A_Z\left(1+\frac{\Delta Z}{2}\right)\right) \tag{7a}$$
$$V_{d_2}{=}V_{\rm LO}\left(1+\frac{\Delta A}{2}\right)\cos\left(\omega_{\rm LO}t+\frac{\Delta\phi}{2}\right)\times\left(1+A_Z\left(1+\frac{\Delta Z}{2}\right)\right) \tag{7b}$$
$$V_{d_3}{=}-V_{\rm LO}\left(1+\frac{\Delta A}{2}\right)\cos\left(\omega_{\rm LO}t+\frac{\Delta\phi}{2}\right)\times\left(1+A_Z\left(1-\frac{\Delta Z}{2}\right)\right) \tag{7c}$$
$$V_{d_4}{=}-V_{\rm LO}\left(1-\frac{\Delta A}{2}\right)\cos\left(\omega_{\rm LO}t-\frac{\Delta\phi}{2}\right)\times\left(1-A_Z\left(1-\frac{\Delta Z}{2}\right)\right). \tag{7d}$$

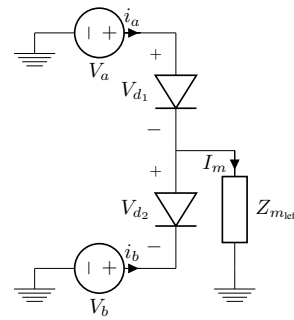

Fig. 2. Half circuit of diode ring, left side.

From Fig. 1 we have

$$I_1{=}I_{d_1}-I_{d_2} \tag{8}$$
$$I_2{=}I_{d_3}-I_{d_4}. \tag{9}$$

Summing these gives the currents at the IF port and the difference gives the current at the RF port

$$I_{\rm IF}=I_1+I_2 \tag{10}$$
$$I_{\rm RF}=I_1-I_2 \tag{11}$$

The current through each diode as a function of RF voltage can be expressed as a Taylor series taken around the large signal LO voltage

$$I_{d_n}(t)=I_{0_{d_n}}(t)+g_{1_{d_n}}(t)v+g_{2_{d_n}}(t)v^2+\cdots \tag{12}$$

where d_n denotes the diode number n, $I_{0_{d_n}}=I_d(V)\big|_{V=V_{d_n}}$, $g_1=\frac{dI_d(V)}{dV}\Big|_{V=V_{d_n}}$ and $g_2=\frac{1}{2}\frac{d^2I_d(V)}{dV^2}\Big|_{V=V_{d_n}}$. Using (12) we will investigate how the DC offset, LO and RF leakage, conversion loss and second order intermodulation depends on the unbalances. For each diode the current will be given as

$$I_{d_1}{=}I_{0_{d_1}}(t)-g_{1_{d_1}}(t)v_{\rm RF}+g_{2_{d_1}}(t)v_{\rm RF}^2 \tag{13a}$$
$$I_{d_2}{=}I_{0_{d_2}}(t)+g_{1_{d_2}}(t)v_{\rm RF}+g_{2_{d_2}}(t)v_{\rm RF}^2 \tag{13b}$$
$$I_{d_3}{=}I_{0_{d_3}}(t)+g_{1_{d_3}}(t)v_{\rm RF}+g_{2_{d_3}}(t)v_{\rm RF}^2 \tag{13c}$$
$$I_{d_4}{=}I_{0_{d_4}}(t)-g_{1_{d_4}}(t)v_{\rm RF}+g_{2_{d_4}}(t)v_{\rm RF}^2. \tag{13d}$$

In Fig. 3a the waveforms of the currents are plotted for each diode current, with an unbalance of $\Delta A=0.01$, $\Delta\phi=5^\circ$ and $\Delta Z=0.1$. In Fig. 3b these currents are summed to represent the current at the IF port, and compared to what is expected for the perfectly matched case. It is clear that there is a strong first order tendency, but also a contribution from DC and higher order terms. The following sections will investigate this in details.

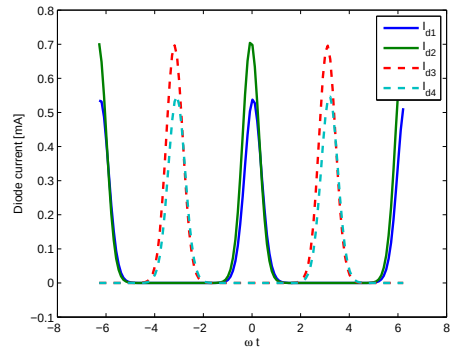

(a) Waveforms for each diode

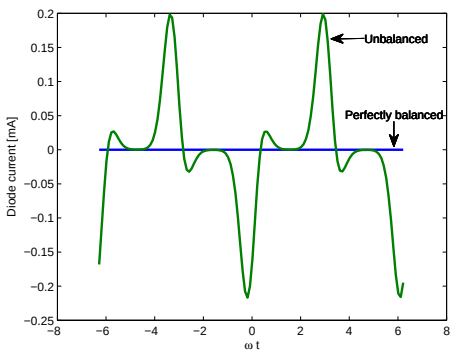

(b) Waveforms for $I_{0_{d_1}}(t) - I_{0_{d_2}}(t) + I_{0_{d_3}}(t) - I_{0_{d_4}}(t)$

Fig. 3. Waveforms for (a) each diode and (b) the current at the IF port, both with $\Delta A = 0.01$, $\Delta\phi = 5^\circ$ and $\Delta Z = 0.1$.

A. DC offset from LO drive

From (12) a DC contribution comes from the first term $I_0(t)$ or the even ordered terms, for $\omega_{\text{LO}} \neq \omega_{\text{RF}}$. In this section we will only look at the DC that comes from the $I_0(t)$ term, in section II-E we look at the DC term coming from higher orders. It should be mentioned that other mechanisms can also add to the DC offset, such as LO-self mixing due to a parasitic path from the LO port to the RF port before the mixer core [12]. The zero order Fourier coefficient corresponds to the DC-current through each diode. The zero order Fourier coefficient $I_0(t)$ corresponds to the DC-current through each diode can be found as [13]

$$I^0_{0_{d_1}} = I_s \left[\hat{I}_0 \left(\frac{V_{\text{LO}} \left(1 - \frac{\Delta A}{2}\right) \left(1 - A_Z \left(1 + \frac{\Delta Z}{2}\right)\right)}{\eta V_T} \right) - 1 \right] \tag{14a}$$

$$I^0_{0_{d_2}} = I_s \left[\hat{I}_0 \left(\frac{V_{\text{LO}} \left(1 + \frac{\Delta A}{2}\right) \left(1 + A_Z \left(1 + \frac{\Delta Z}{2}\right)\right)}{\eta V_T} \right) - 1 \right] \tag{14b}$$

$$I^0_{0_{d_3}} = I_s \left[\hat{I}_0 \left(\frac{V_{\text{LO}} \left(1 + \frac{\Delta A}{2}\right) \left(1 + A_Z \left(1 - \frac{\Delta Z}{2}\right)\right)}{\eta V_T} \right) - 1 \right] \tag{14c}$$

$$I^0_{0_{d_4}} = I_s \left[\hat{I}_0 \left(\frac{V_{\text{LO}} \left(1 - \frac{\Delta A}{2}\right) \left(1 - A_Z \left(1 - \frac{\Delta Z}{2}\right)\right)}{\eta V_T} \right) - 1 \right], \tag{14d}$$

where $\hat{I}_0(x)$ is the modified Bessel function of order 0 and argument x. As the deviations are all small, linearizing will give better insight. First we reformulate the nominator in 14a

$$V_{\text{LO}} \left(1 - \frac{\Delta A}{2}\right) \left(1 - A_Z \left(1 - \frac{\Delta Z}{2}\right)\right) = V_{\text{LO}} (1 + a) \tag{15}$$

where $a = -\frac{\Delta A}{2} - A_Z \left(1 - \frac{\Delta Z}{2}\right) + \frac{\Delta A}{2} A_Z \left(1 - \frac{\Delta Z}{2}\right)$. Similar relations can be formulated for 14b through 14d. Then linearizing the Bessel function around V_{LO}, for small deviations of a, using [9.6.28] in [**?**], gives

$$\hat{I}_0 \left(\frac{V_{\text{LO}}(1 + a)}{\eta V_T} \right) = \hat{I}_0 \left(\frac{V_{\text{LO}}}{\eta V_T} \right) + \frac{V_{\text{LO}}}{\eta V_T} \hat{I}_1 \left(\frac{V_{\text{LO}}}{\eta V_T} \right) a \tag{16}$$

where $\hat{I}_1(x)$ is the modified Bessel function of 1st order and argument x. Using this relation in (14a) through (14d), inserting them into (8) and (9), and then into (10) we get

$$\begin{aligned} I_{\text{IF}} &= I^0_{0_{d_1}} - I^0_{0_{d_2}} + I^0_{0_{d_3}} - I^0_{0_{d_4}} \\ &= -I_s \frac{V_{\text{LO}}}{\eta V_T} \hat{I}_1 \left(\frac{V_{\text{LO}}}{\eta V_T} \right) 4 A_Z \frac{\Delta Z}{2}. \end{aligned} \tag{17}$$

This shows that a DC contribution comes directly from the LO signal in the mixer core due to load mismatch (ΔZ) together with LO balun imbalance (contained in A_Z). For a properly designed circuit this contribution to the DC offset should be of a little concern.

B. LO leakage

The LO leakage is found as the fundamental current running through the diodes to the IF port, corresponding to the first order term of the Fourier series of I_{0d_n}. The first order Fourier coefficients of I_{0d_n} can be found as [13]

$$\begin{aligned} I^1_{0_{d_1}} = I_s \Bigg[& \hat{I}_1 \left(\frac{V_{\text{LO}} \left(1 - \frac{\Delta A}{2}\right) \left(1 - A_Z \left(1 + \frac{\Delta Z}{2}\right)\right)}{\eta V_T} \right) \\ & \times \exp\left(-j \frac{\Delta\phi}{2} \right) - 1 \Bigg] \end{aligned} \tag{18a}$$

$$\begin{aligned} I^1_{0_{d_2}} = I_s \Bigg[& \hat{I}_1 \left(\frac{V_{\text{LO}} \left(1 + \frac{\Delta A}{2}\right) \left(1 + A_Z \left(1 + \frac{\Delta Z}{2}\right)\right)}{\eta V_T} \right) \\ & \times \exp\left(j \frac{\Delta\phi}{2} \right) - 1 \Bigg] \end{aligned} \tag{18b}$$

$$\begin{aligned} I^1_{0_{d_3}} = -I_s \Bigg[& \hat{I}_1 \left(\frac{V_{\text{LO}} \left(1 + \frac{\Delta A}{2}\right) \left(1 + A_Z \left(1 - \frac{\Delta Z}{2}\right)\right)}{\eta V_T} \right) \\ & \times \exp\left(j \frac{\Delta\phi}{2} \right) - 1 \Bigg] \end{aligned} \tag{18c}$$

$$I^1_{0_{d_4}}=-I_s\left[\hat{I}_1\left(\frac{V_{\rm LO}\left(1-\frac{\Delta A}{2}\right)\left(1-A_Z\left(1-\frac{\Delta Z}{2}\right)\right)}{\eta V_T}\right)\times\exp\left(-j\frac{\Delta\phi}{2}\right)-1\right] \tag{18d}$$

The term $\exp\left(j\frac{\Delta\phi}{2}\right)$ is due to the phase mismatch, because when calculating the n'th Fourier coefficient this appears as the modified Bessel function times a factor $\exp\left(jn\frac{\Delta\phi}{2}\right)$ [13]. Linearizing the modified Bessel function of 1st order around $V_{\rm LO}$, that is for small deviations, using [9.6.28] in [**?**], gives

$$\hat{I}_1\left(\frac{V_{\rm LO}(1+a)}{\eta V_T}\right)=\hat{I}_1\left(\frac{V_{\rm LO}}{\eta V_T}\right)+\frac{1}{2}\frac{V_{\rm LO}}{\eta V_T}\times\left(\hat{I}_0\left(\frac{V_{\rm LO}}{\eta V_T}\right)+\hat{I}_2\left(\frac{V_{\rm LO}}{\eta V_T}\right)\right)a \tag{19}$$

Using this relation in (14a) through (14d), inserting them into (8) and (9), and then into (10) we get

$$I_{\rm IF}=-2jI_s\frac{V_{\rm LO}}{\eta V_T}\left(\hat{I}_0\left(\frac{V_{\rm LO}}{\eta V_T}\right)+\hat{I}_2\left(\frac{V_{\rm LO}}{\eta V_T}\right)\right)\times\left[\cos\left(\frac{\Delta\phi}{2}\right)\left(A_Z+\frac{\Delta A}{2}\right)+j\sin\left(\frac{\Delta\phi}{2}\right)\frac{\Delta A}{2}A_Z\right]. \tag{20}$$

From (20) it is seen that there is a strong connection between balun imbalances and the LO leakage, but no dependence on load mismatch.

C. RF leakage

The second term of (12) describes the linear behavior of the RF current. The RF leakage is found as the zeroth order Fourier coefficient of $g_{1_{d_n}}(t)$. This can be evaluated as [13]

$$G^0_{1_{d_1}}=\frac{I_s}{\eta V_T}\hat{I}_0\left(\frac{V_{\rm LO}\left(1-\frac{\Delta A}{2}\right)\left(1-A_Z\left(1+\frac{\Delta Z}{2}\right)\right)}{\eta V_T}\right) \tag{21a}$$

$$G^0_{1_{d_2}}=\frac{I_s}{\eta V_T}\hat{I}_0\left(\frac{V_{\rm LO}\left(1+\frac{\Delta A}{2}\right)\left(1+A_Z\left(1+\frac{\Delta Z}{2}\right)\right)}{\eta V_T}\right) \tag{21b}$$

$$G^0_{1_{d_3}}=\frac{I_s}{\eta V_T}\hat{I}_0\left(\frac{V_{\rm LO}\left(1+\frac{\Delta A}{2}\right)\left(1+A_Z\left(1-\frac{\Delta Z}{2}\right)\right)}{\eta V_T}\right) \tag{21c}$$

$$G^0_{1_{d_4}}=\frac{I_s}{\eta V_T}\hat{I}_0\left(\frac{V_{\rm LO}\left(1-\frac{\Delta A}{2}\right)\left(1-A_Z\left(1-\frac{\Delta Z}{2}\right)\right)}{\eta V_T}\right) \tag{21d}$$

Linearizing the Bessel function and using equations (13a) through (13d) we get

$$I_{\rm IF}=(-G^0_{1_{d_1}}-G^0_{1_{d_2}}+G^0_{1_{d_3}}+G^0_{1_{d_4}})v_{\rm RF}=-4v_{\rm RF}\frac{I_sV_{\rm LO}}{(\eta V_T)^2}\hat{I}_1\left(\frac{V_{\rm LO}}{\eta V_T}\right)\frac{\Delta A}{2}A_Z\frac{\Delta Z}{2}. \tag{22}$$

As observed from (22), an imbalance in the LO balun will result in a RF leakage if there is also simultaneously a mismatch in the IF-load. This is not to say that this is the only way a RF-leak can occur, an imbalance in the RF-balun has a high impact on the RF-leakage, but this is outside the scope of this analysis.

D. Conversion loss

The desired mixing product at the IF frequency is found when the RF signal is multiplied with the fundamental tone of $g_{1_{d_n}}(t)$. The contribution can be evaluated from the first order Fourier coefficients as

$$G^1_{1_{d_1}}=\frac{I_s}{\eta V_T}\hat{I}_1\left(\frac{V_{\rm LO}\left(1-\frac{\Delta A}{2}\right)\left(1-A_Z\left(1+\frac{\Delta Z}{2}\right)\right)}{\eta V_T}\right)\times\exp\left(-j\frac{\Delta\phi}{2}\right) \tag{23a}$$

$$G^1_{1_{d_2}}=\frac{I_s}{\eta V_T}\hat{I}_1\left(\frac{V_{\rm LO}\left(1+\frac{\Delta A}{2}\right)\left(1+A_Z\left(1+\frac{\Delta Z}{2}\right)\right)}{\eta V_T}\right)\times\exp\left(j\frac{\Delta\phi}{2}\right) \tag{23b}$$

$$G^1_{1_{d_3}}=-\frac{I_s}{\eta V_T}\hat{I}_1\left(\frac{V_{\rm LO}\left(1+\frac{\Delta A}{2}\right)\left(1+A_Z\left(1-\frac{\Delta Z}{2}\right)\right)}{\eta V_T}\right)\times\exp\left(j\frac{\Delta\phi}{2}\right) \tag{23c}$$

$$G^1_{1_{d_4}}=-\frac{I_s}{\eta V_T}\hat{I}_1\left(\frac{V_{\rm LO}\left(1-\frac{\Delta A}{2}\right)\left(1-A_Z\left(1-\frac{\Delta Z}{2}\right)\right)}{\eta V_T}\right)\times\exp\left(-j\frac{\Delta\phi}{2}\right). \tag{23d}$$

Linearizing the Bessel function and using equations (13a) through (13d) we get

$$I_{\rm IF}=(-G^1_{1_{d_1}}-G^1_{1_{d_2}}+G^1_{1_{d_3}}+G^1_{1_{d_4}})v_{\rm RF}=-4v_{\rm RF}\frac{I_s}{\eta V_T}\left[\hat{I}_1\left(\frac{V_{\rm LO}}{\eta V_T}\right)\cos\left(\frac{\Delta\phi}{2}\right)+\frac{1}{2}\frac{V_{\rm LO}}{\eta V_T}\left(\hat{I}_2\left(\frac{V_{\rm LO}}{\eta V_T}\right)+\hat{I}_0\left(\frac{V_{\rm LO}}{\eta V_T}\right)\right)\times\left(A_Z\frac{\Delta A}{2}\cos\left(\frac{\Delta\phi}{2}\right)+j\left(A_Z+\frac{\Delta A}{2}\right)\sin\left(\frac{\Delta\phi}{2}\right)\right)\right] \tag{24}$$

The conversion loss is inversely proportional to the IF current. Therefore, it is observed that the conversion loss is not affected much by the phase imbalance as $\cos\left(\frac{\Delta\phi}{2}\right)\approx 1$ and the second term is negligible under the assumption of small deviations.

E. Second order intermodulation

The third term of (12) describes the second order behavior of the RF current. The zeroth order Fourier coefficient of $g_{2_{d_n}}(t)$, gives rise to the second order intermodulation and DC-contribution from the RF signal. The Fourier coefficient can be found as [13]

$$G^0_{2_{d_1}}=\frac{I_s}{(\eta V_T)^2}\times\hat{I}_0\left(\frac{V_{\rm LO}\left(1-\frac{\Delta A}{2}\right)\left(1-A_Z\left(1+\frac{\Delta Z}{2}\right)\right)}{\eta V_T}\right) \tag{25a}$$

$$G^0_{2_{d_2}}=\frac{I_s}{(\eta V_T)^2}\times\hat{I}_0\left(\frac{V_{\rm LO}\left(1+\frac{\Delta A}{2}\right)\left(1+A_Z\left(1+\frac{\Delta Z}{2}\right)\right)}{\eta V_T}\right) \tag{25b}$$

$$G^0_{2_{d_3}}=\frac{I_s}{(\eta V_T)^2} \times\hat{I}_0\left(\frac{V_{\text{LO}}\left(1+\frac{\Delta A}{2}\right)\left(1+A_Z\left(1-\frac{\Delta Z}{2}\right)\right)}{\eta V_T}\right) \quad (25c)$$

$$G^0_{2_{d_4}}=\frac{I_s}{(\eta V_T)^2} \times\hat{I}_0\left(\frac{V_{\text{LO}}\left(1-\frac{\Delta A}{2}\right)\left(1-A_Z\left(1-\frac{\Delta Z}{2}\right)\right)}{\eta V_T}\right) \quad (25d)$$

Again by linearizing the Bessel function and using equations (13a) through (13d) we get

$$\begin{aligned} I_{\text{IF}}=&(G^0_{2_{d_1}}-G^0_{2_{d_2}}+G^0_{2_{d_3}}-G^0_{2_{d_4}})v^2_{\text{RF}} \\ =&-4\frac{V_{\text{LO}}I_s}{(\eta V_T)^3}\hat{I}_1\left(\frac{V_{\text{LO}}}{\eta V_T}\right)A_Z\frac{\Delta Z}{2}v^2_{\text{RF}}. \end{aligned} \quad (26)$$

From (26) we see that second order intermodulation products will arise if there is a load mismatch together with a LO-balun imbalance.

III. Design of mixer with tunable balun

This section gives a description of the design of the circuitry. First a description of the lumped Marchand balun design with tunable phase balance is given. This will be followed by a description of the full mixer circuit.

A. Marchand balun design

The broadband nature of the Marchand balun, makes it an ideal candidate for a double balanced mixer. The idea of the tunable Marchand balun as described in [9] is to introduce a tunable shunt susceptance between the two coupled elements of the Marchand balun. The tuning range $\Delta\phi = \angle S_{21} - \angle S_{31}$ is given as [9]

$$\Delta\phi\approx\frac{Z_0\left(C^4+C^2\right)}{C^2+1}B_m \quad (27)$$

where C is the coupling factor of the coupled line element, Z_0 is the characteristic impedance and $B_m = j\omega C_m$ is the added susceptance.

A typical planar Marchand balun is realized using coupled transmission lines, and the introduction of a negative susceptance is difficult to synthesize. Instead the exact lumped element implementation [7] is suggested, as this have already a capacitance placed where the additional susceptance is required, allowing for an effective negative susceptance by having a smaller capacitance than normally required. The design procedure follows the one given in [7], and a circuit diagram is shown in Fig. 4. The design equations are repeated here:

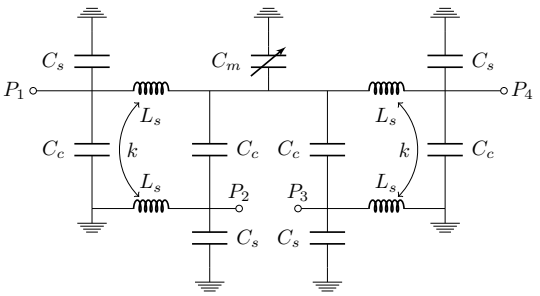

Fig. 4. Schematic of the lumped element tunable Marchand balun

$$L_s=\frac{Z_{0_{even}}+Z_{0_{odd}}}{2\omega} \quad (28)$$

$$k=\frac{Z_{0_{even}}-Z_{0_{odd}}}{2\omega L_s} \quad (29)$$

$$C_c=\frac{1}{2\omega}\left(\frac{1}{Z_{0_{odd}}}-\frac{1}{Z_{0_{even}}}\right) \quad (30)$$

$$C_s=\frac{1}{\omega Z_{0_{even}}} \quad (31)$$

$$C_m=2C_c\left(\frac{1}{k}-1\right), \quad (32)$$

where $Z_{0_{even}}$ and $Z_{0_{odd}}$ is the even and odd mode characteristic impedance of the coupled line element, respectively.

B. Mixer design

A diagram of the full mixer is shown in Fig. 5. The mixing core consists of four Schottky diodes in a ring, to enable the double balanced properties [1]. When choosing the diode size, the conversion-loss degradation factor [1] is a helpful guiding parameter

$$\delta = 1+\frac{R_s}{Z_s}+\frac{Z_s f^2_{\text{RF}}}{R_s f^2_c} \quad (33)$$

where R_s is the series resistance, Z_s is the real diode junctions RF input resistance, and $f_c = \frac{1}{2\pi R_s C_j}$ is the cutoff frequency. Increasing the diode area will decrease the series resistance, but increase the junction capacitance, C_j, in such a manner that the cutoff frequency will decrease [14]. But as the RF frequency is relatively low, a larger diode will give better conversion-loss degradation factor as the last term of (33) will be almost negligible. Using Harmonic Balance simulations a size was found such that using single series inductors, L_{RF} and L_{LO} for the RF and the LO ports, respectively, was sufficient to match to $50\,\Omega$. This gave a diode area of $14.4\,(\mu\text{m})^2$, with corresponding series resistance of $R_s = 19\Omega$, junction capacitance of $C_{j_0} = 80fF$, which results in a cutoff frequency of $f_c = 105\,\text{GHz}$, and a loss degradation factor of $\delta = 1.5dB$.

TABLE I
DESIGN PARAMETERS FOR THE MIXER CIRCUIT

Inductance	L_s [nH]	1.02
Inductive coupling	k	0.825
Capacitive coupling	C_c [fF]	379
Input matching capacitors	C_s [fF]	283
Balance matching capacitor	C_m [fF]	190
Matching Inductor, LO	L_{LO} [nH]	0.94
Matching Inductor, RF	L_{RF} [nH]	0.94
Diode area	A_d [μm^2]	14.4

The IF-extraction is similar to that described in [10]. That is, the RF balun has coupling capacitors C_{IF} to its ground connection, allowing for the IF signal extraction. It is important to make the IF extraction symmetric as any asymmetry will affect the balun performance. On the LO side the balun will, by its grounding, ensure the IF-return path for the diode ring. Table I gives the design parameters.

IV. Experimental Results

In this section the experimental results are discussed. The measurements are made on-wafer using a probe station, and calibration is used to remove losses in cables and probes.

The circuit is fabricated using a SiGe:C BiCMOS process from Innovations for High Performance Microelectronics (IHP). It is a $0.25\mu m$ technology, featuring high-performance npn-HBTs having a unit current gain frequency (fT) of 110 GHz and a maximum oscillation frequency (fmax) of 180 GHz. The Schottky diodes are not a mature part of the process and suffers from leakage current. The process has metal-insulator-metal (MIM) capacitors, metal-oxide-semiconductor (MOS)-varactors and five metal layers of which the upper two are extra thick, intended for passives or low loss interconnects.

First measurements of the Marchand balun, measured on a separate breakout, is presented in section IV-A which is followed by a presentation of the measurements of the full mixer circuit in section IV-B.

A. Marchand balun experimental results

A break out of the circuit was manufactured, with a size of 700μm×990μm, which is shown in Fig. 6. The matching capacitors, C_s is implemented as MIM capacitors and variable capacitor, C_m, is implemented using a MOS-varactor. The inductors, L_s, is implemented as broad-side coupled inductor pairs using the top two metal layers, for best Q-value. These are diagonally offset to get the desired inductive coupling, k, and capacitive coupling, C_c.

Fig. 7 shows measurements of insertion loss, reflection and isolation of the balun structure. The insertion loss is better than 7 dB on both channels in the range from 11 GHz to 13 GHz, while having a return loss better than 14.5 dB. The magnitude balance is plotted in Fig. 8. At the center frequency of 12 GHz the magnitude balance can be tuned by 0.8 dB, from -0.8 dB to 0 dB. In Fig. 9 is the phase difference plotted for different bias values as a function of frequency. At the center frequency the phase difference can be tuned by 5.8°, from 171.6° to 177.4°, so a perfect match is not obtainable, but a large improvement of $\Delta\phi$ is still possible.

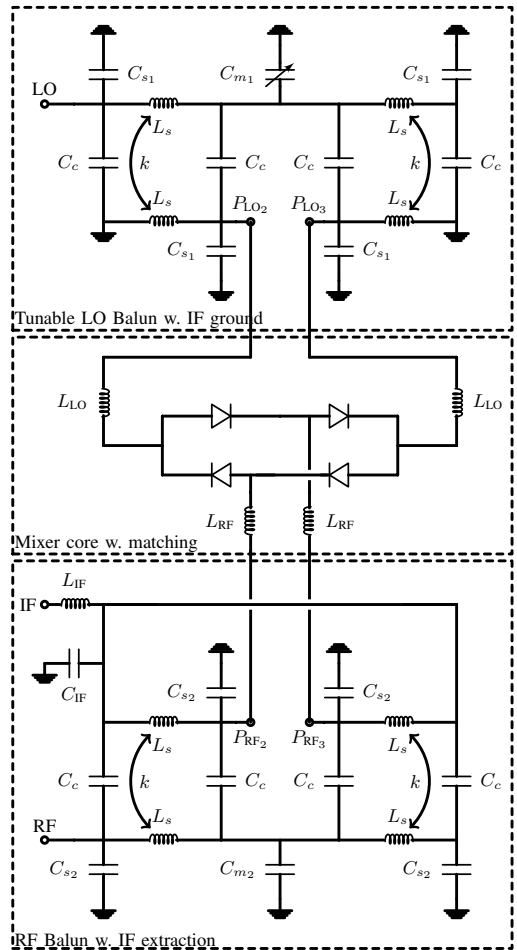

Fig. 5. Schematic of the double balanced mixer including RF and LO baluns.

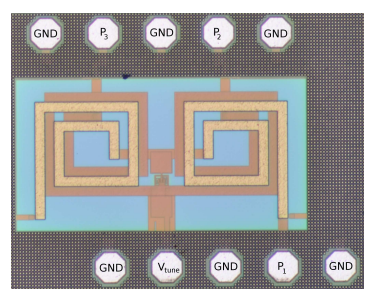

Fig. 6. Microphotograph of the tunable Marchand balun, size 700 µm × 990 µm

B. Full mixer circuit

In this section, measurements of the combined mixer circuit is discussed. The circuit has a size of 2050 µm×1000 µm,

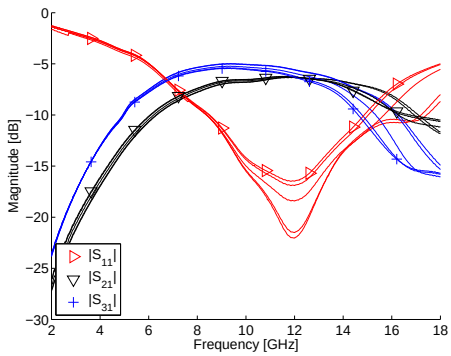

Fig. 7. Insertion loss and input matching measured with tuning voltages ranging from $-2.5\,\mathrm{V}$ to $2.5\,\mathrm{V}$.

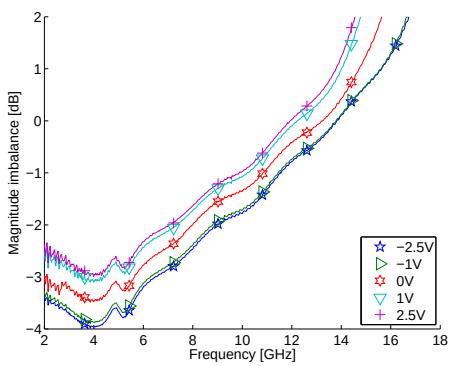

Fig. 8. Measurement of magnitude imbalance with tuning voltages ranging from $-2.5\,\mathrm{V}$ to $2.5\,\mathrm{V}$.

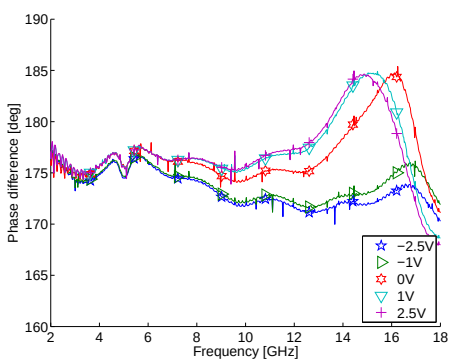

Fig. 9. Measurement of phase difference between output ports with tuning voltages ranging from $-2.5\,\mathrm{V}$ to $2.5\,\mathrm{V}$.

and in Fig. 10 is a microphotograph of the circuit. For all measurements the IF-frequency is 100 MHz.

The conversion loss as a function of local oscillator power

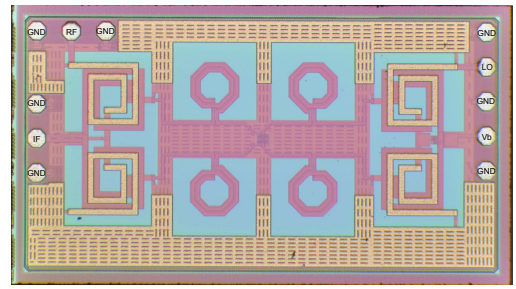

Fig. 10. Microphotograph of the mixer circuit. Size $2050\,\mu\mathrm{m} \times 1000\,\mu\mathrm{m}$

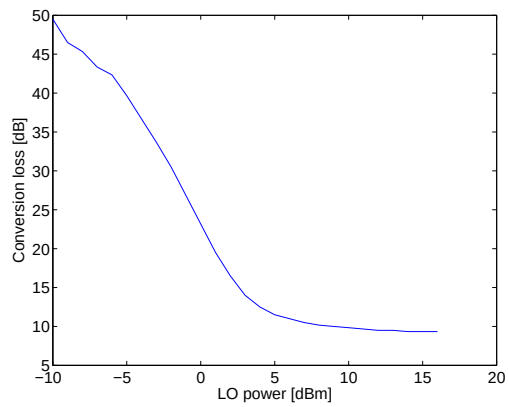

Fig. 11. Conversion loss as a function of local oscillator power

at a $11.5\,\mathrm{GHz}$ is plotted in Fig. 11. It is almost saturated for a LO power level of 11 dBm with a conversion loss of $9.7\,\mathrm{dB}$. Increasing the LO power level to $16\,\mathrm{dBm}$ will only give a small decrease in conversion loss to $9.3\,\mathrm{dB}$. Thus for all other measurements is the lower level of $11\,\mathrm{dBm}$ chosen, which should give sufficiently good conversion loss. The conversion loss as a function of frequency is plotted in Fig. 12. A conversion loss of $8.8\,\mathrm{dB}$ is obtained at $11\,\mathrm{GHz}$. The broadband nature of the Marchand balun is seen and the 3-dB bandwidth is from $8\,\mathrm{GHz}$ to $13\,\mathrm{GHz}$, covering more than the entire X-band. Changing the tuning capacitance has a clear influence on the LO to IF isolation. At $11\,\mathrm{GHz}$ it can be changed from $-41.3\,\mathrm{dB}$ at a bias voltage of $-2.5\,\mathrm{V}$ to $-48.7\,\mathrm{dB}$ at a bias voltage of $2.5\,\mathrm{V}$. In Fig. 13 the LO to IF isolation is plotted as a function of balun tuning voltage for different frequencies. It is possible to reduce the isolation more for the higher frequencies, but this is what is expected as the balun is more phase sensitive there and the magnitude balance is better at higher frequencies as was seen in Figs. 8 and 9. The conversion loss is constant with the tuning, as was expected. Also the RF-IF is constant, this is due to the fact that the main contributing mechanism to the leakage is unbalance in the RF-balun which remains constant.

In Fig. 14 the parasitic DC offset is plotted versus the tuning

TABLE II
COMPARISON BETWEEN THIS WORK AND RECENT REPORTED DIRECT CONVERSION MIXERS.

Ref.	Technology	Topology	Frequency [GHz]	CG [dB]	LO-power [dBm]	LO-IF/RF-IF/LO-RF isolation [dB]	IP_{1dB} [dBm]	IIP2 [dBm]
[?]	SiGe HBT	Active double bal.	18	4.5	-1	- / - / 31	-12.2	20.3
[?]	SiC Schottky	Double bal	2.4	−12	24	> 30/ 7/ -	23	58
[10]	SiGe HBT-diode	Double bal.	8.5	−9.8	15	55 / 40 / 58	12	66
This work	SiGe Schottky	Double bal.	11	−8.8	11	60.5 / 35 / 53.7	8	45 - 57

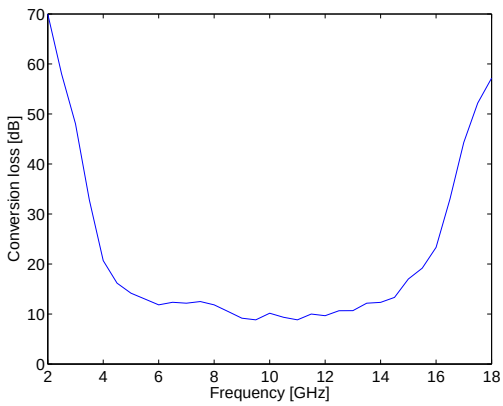

Fig. 12. Conversion loss as a function of frequency

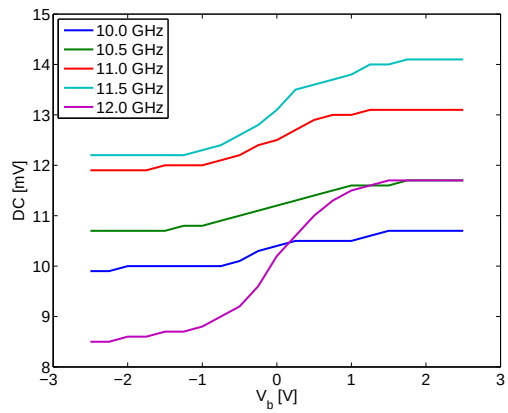

Fig. 14. DC level versus tuning voltage for different frequencies.

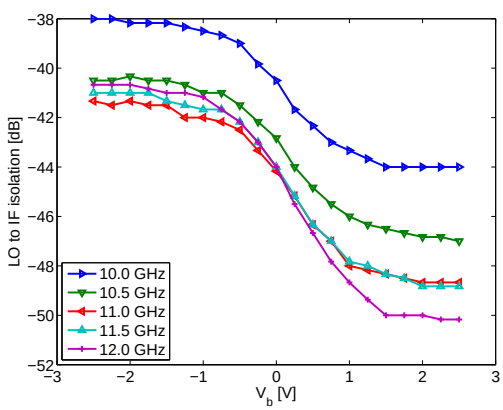

Fig. 13. LO to IF isolation versus tuning voltage for different frequencies.

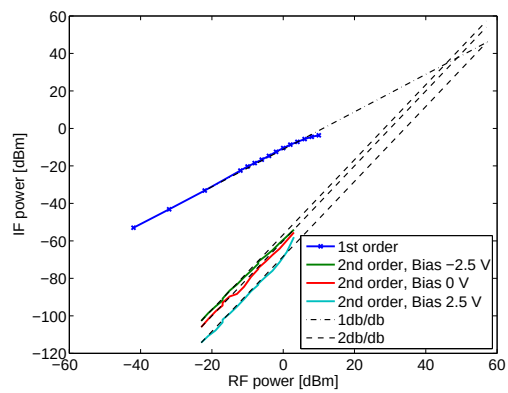

Fig. 15. IF power versus RF power at the fundamental and second order frequency for different tuning voltages. Extrapolated lines show IIP2.

voltage. It is seen that it is possible to change the DC offset by a few mV, but there is a larger offset of around 9 mV which cannot be completely removed. As would be expected there is a larger swing for the higher frequencies as the balun is more sencitive here. Apart from disturbing the following circuitry the DC offset is also unwanted as it increases the flicker noise level [12].

The linearity is plotted in Fig. 15. The 1dB compression point is measured to be at 8 dBm RF input power. The input referred second intercept point (IIP_2) is measured with two RF tones at frequencies of 11.5 GHz and 11.513 GHz, giving a second order product at 13 MHz, and LO frequency of 11.4 GHz. Isolators are placed after the signal generators to avoid leakage and intermodulation of the signals before they are applied to the mixer. Attenuation is added to the output of the mixer to avoid measuring the non-linearity of the spectrum analyzer [15]. From Fig. 15 the IIP_2 can be read as the extrapolated values to be 45.5 dBm, 48.8 dBm and 57.1 dBm

for bias levels of $-2.5\,\mathrm{V}$, $0\,\mathrm{V}$ and $2.5\,\mathrm{V}$ respectively, giving a $11.6\,\mathrm{dB}$ tuning range of IIP_2. The curve corresponding to the $2.5\,\mathrm{V}$ bias point has a steeper slope for the last couple of points which could be a fourth order phenomenon, as the one that was observed in [10]. Thus it is experimentally shown that a tunable balun can enhance the properties of the double balanced mixer, by increasing the LO-IF isolation and the IIP2.

In table II the mixer is compared with other state-of-the-art direct conversion mixers reported in the open literature. As would be expected it is clear that if one wants an extremely linear circuit an active topology is not suitable. Of course, the active topology comes with the benefit of having $4.5\,\mathrm{dB}$ gain compared with $-8.8\,\mathrm{dB}$ or worse for the passive diode based topologies. The 1 dB compression point is lower than what is reported for [**?**] and [10], but these also exhibits more loss. The best IIP2 is achieved by [10], but after tuning our circuit is close to this and on par with [**?**]. An explanation for the poorer intermodulation is that a perfect balance is not obtained anywhere in the tuning range of the balun.

V. Conclusion

We have presented and analyzed a Schottky mixer design in a SiGe technology, with a balun which is tunable to reduce leakage and enhance linearity. A breakout of the balun was measured. The full mixer has a size of $2050\,\mu\mathrm{m}\times1000\,\mu\mathrm{m}$. The center frequency of the mixer is $11\,\mathrm{GHz}$. Here it has a conversion loss of $-8.8\,\mathrm{dB}$ with a LO power level of $11\,\mathrm{dBm}$. The 3-dB bandwidth is from $8\,\mathrm{GHz}$ to $13\,\mathrm{GHz}$, more than the entire X-band. The tuning have no influence on the conversion loss. The LO-IF isolation on the other hand can change from $41.3\,\mathrm{dBm}$ to $48.7\,\mathrm{dBm}$ at $11\,\mathrm{GHz}$. The IIP_2 can be improved by the tuning from $45.5\,\mathrm{dBm}$ to $57.1\,\mathrm{dBm}$, while the 1-dB compression point is kept constant at 6.67 dBm.

References

[1] S. A. Maas, *Microwave Mixers*, 2nd ed. Artec House, 1993.

[2] N. Marchand, "Transmission-line conversion transformers," *Electronics*, vol. 17, pp. 142–145, 1944.

[3] Z.-Y. Zhang, Y.-X. Guo, L. Ong, and M. Y. W. Chia, "A new planar marchand balun," in *Microwave Symposium Digest, 2005 IEEE MTT-S International*, 2005, pp. 4 pp.–.

[4] K. S. Ang, I. D. Robertson, K. Elgaid, and I. G. Thayne, "40 to 90 GHz impedance-transforming CPW Marchand balun," *IEEE MTT-S International Microwave Symposium digest*, vol. 2, pp. 1141–1144, 2000.

[5] T.-G. Ma, C.-C. Wang, and C.-H. Lai, "Miniaturized Distributed Marchand Balun Using Coupled Synthesized CPWs," *IEEE Microwave and Wireless Components Letters*, vol. 21, no. 4, pp. 188–190, 2011.

[6] K. S. Ang, Y. C. Leong, and C. H. Lee, "Analysis and design of miniaturized lumped-distributed impedance-transforming baluns," *Microwave Theory and Techniques, IEEE Transactions on*, vol. 51, no. 3, pp. 1009 – 1017, mar 2003.

[7] T. Johansen and V. Krozer, "Analysis and Design of Lumped Element Marchand Baluns," in *2008 MIKON CONFERENCE PROCEEDINGS*. IEEE, 2008, pp. 672–675.

[8] X. Miao, W. Zhang, Y. Geng, X. Chen, R. Ma, and J. Gao, "Design of Compact Frequency-Tuned Microstrip Balun," *IEEE Antennas and Wireless Propagation Letters*, vol. 9, pp. 686–688, 2010.

[9] R. Michaelsen, T. Johansen, K. Tamborg, and V. Zhurbenko, "A Modified Marchand Balun Configuration With Tunable Phase Balance," *IEEE Microwave and Wireless Components Letters*, vol. 23, no. 2, pp. 66–68, 2013.

[10] ——, "Design of a broadband passive X-band double-balanced mixer in SiGe HBT technology," *International Journal of Microwave and Wireless Technologies*, vol. 6, no. 3-4, pp. 235–242, 2014.

[11] K. Kivekas, A. Parssinen, and K. Halonen, "Characterization of iip2 and dc-offsets in transconductance mixers," *IEEE TRANSACTIONS ON CIRCUITS AND SYSTEMS II-EXPRESS BRIEFS*, vol. 48, no. 11, pp. 1028–1038, 2001.

[12] R. Michaelsen, T. Johansen, and K. Tamborg, "Investigation of LO-leakage cancellation and DC-offset influence on flicker-noise in X-band mixers," in *7th European Microwave Integrated Circuit Conference (EuMIC)*, 2012, pp. 99–102.

[13] R. Michaelsen, T. Johansen, and V. Krozer, "Design of a 4 subharmonic sub-millimeter wave diode mixer, based on an analytic expression for small-signal conversion admittance parameters," in *2013 Microwave & Optoelectronics Conference (IMOC)*. IEEE, 2013.

[14] R. M. Rassel, J. B. Johnson, B. A. Orner, S. K. Reynolds, M. E. Dahlstrom, J. S. Rascoe, A. J. Joseph, B. P. Gaucher, J. S. Dunn, and S. A. St. Onge, "Schottky barrier diodes for millimeter wave sigebicmos applications," *PROCEEDINGS OF THE 2006 BIPOLAR/BICMOS CIRCUITS AND TECHNOLOGY MEETING*, pp. 255–258, 2006.

[15] S. A. Maas, *Nonlinear Microwave and RF Circuits*, 2nd ed. Artec House, 2003.

[16] V. Issakov, H. Knapp, M. Wojnowski, A. Thiede, and W. Simburger, "A 22-39 GHz Passive mixer in SiGe:C bipolar technology," in *Microwave Symposium Digest (MTT), 2010 IEEE MTT-S International*, may 2010, pp. 1012 –1015.

[17] Y.-C. Lee, C.-M. Lin, S.-H. Hung, C.-C. Su, Y.-H. Wang, and Y.-H. Wang, "A broadband doubly balanced monolithic ring mixer with a compact intermediate frequency (IF) extraction," *Progress In Electromagnetics Research Letters*, vol. 20, pp. 175–184, 2011.

[18] F.-H. Huang, S.-W. Lin, P.-Y. Ke, and H.-C. Chiu, "A wide bandwidth V-band balanced resistive mixer with a miniature meandering balun," *Microwave and Optical Technology Letters*, vol. 55, no. 3, pp. 547–550, 2013.

[19] C. Song, O. Boric-Lubecke, and I. Lo, "0.18-m CMOS wideband passive mixer," *Microwave and Optical Technology Letters*, vol. 55, no. 1, pp. 23–27, 2013.

Investigation of LO-leakage cancellation and DC-offset influence on flicker-noise in X-band mixers

Rasmus Michaelsen[1,2], Tom Johansen[1], Kjeld Tamborg[2]
[1]Technical University of Denmark, Department of Electrical Engineering
2800 Kongens Lyngby, Denmark
Email: rsmi@elektro.dtu.dk
[2]Weibel Scientific A/S
3450 Allerød, Denmark

***Abstract*—This paper describes an investigation on the influences in 1/f noise of LO-leakage and DC-offset cancellation for X-band mixers. Conditions for LO-leakage cancellation and zero DC-offset is derived. Measurements on a double balanced diode mixer shows an improvement in noise figure from 14.3dB to 12.1dB at 10KHz, while maintaining a noise figure of 6.2dB at 1MHz. LO-RF isolation is improved from 18dB to 60dB. The 1/f noise is shown to increase with increasing DC-offset.**

***Index Terms*—Receivers, Mixers, 1/f noise**

I. Introduction

Direct-conversion receivers are used in Doppler radars, for defense and space applications [1] or for measuring human vital signs [2]. Another common application is to use direct-conversion to avoid complex image rejection structures [3]. Direct-conversion systems comes with drawbacks. One significant drawback is leakage, since the LO-signal and RF-signal is at the same frequency and isolation between those is in many applications an important criteria. Another problem is that the intermediate frequency is now at baseband and 1/f noise can be a great issue. There have been many proposals to reduce mixer 1/f noise in active mixers, common for many is that the steps used to reduce 1/f noise is to reduce the DC-bias current through the switching transistors. This either through a static principle [4] or using dynamic current injection [5], [6]. Also in passive transistor mixers a DC-offset results in an increased 1/f noise [7], [8]. In passive mixers where no bias is applied there still will be a DC-offset due to self mixing of the LO-signal that leak to the RF port.

In [9] a LO-leakage and DC-offset cancellation techniques is presented for direct conversion systems, and tested at 2.4GHz. In this paper the idea of this technique is expanded and used at X-band and tested using a 10.5GHz system. There will be derived conditions for when LO-leakage cancellation is obtained and when zero DC-offset is obtained. With this knowledge improved direct-conversion designs can be a possibility.

II. LO cancellation and DC offset

In a direct conversion system the LO and RF signal is at roughly the same frequencies. As the isolation between the LO an RF port of the mixer must be finite, there will be some leakage from one to the other. In passive mixers the LO drive level is typically quite high (many operates with a LO power of 7dBm or above [10]), this leads to a significant component of the LO signal at the RF-port. Instead of mixing the RF with the LO signal, actually it will be a sum of the RF and a leakage signal that is mixed with the LO signal. This self-mixing of the LO signal will give higher harmonic components and a DC off-set.

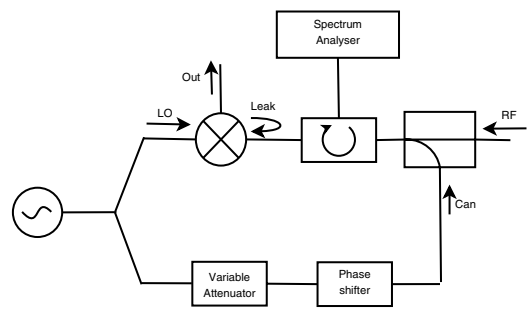

Fig. 1. Block diagram of the LO-leakage cancellation setup.

It is proposed in [9], to use a cancellation signal to remove the leakage signal. Figure 1 shows a block diagram of the method and defines the signals. The output signal, due to leakage and cancellation signals, at the IF port will then be given by (1)

$$\begin{aligned} S_{\text{out}} = & A_{\text{LO}} \cos(\omega t) \cdot \left[A_{\text{Leak}} \cos(\omega t + \phi_{\text{Leak}}) \right. \\ & \left. + A_{\text{Can}} \cos(\omega t + \phi_{\text{Can}}) \right] \qquad (1) \\ = & \frac{A_{\text{LO}} A_{\text{Leak}}}{2} \left(\cos(\phi_{\text{Leak}}) + \cos(2\omega t + \phi_{\text{Leak}}) \right) \\ & + \frac{A_{\text{LO}} A_{\text{Can}}}{2} \left(\cos(\phi_{\text{Can}}) + \cos(2\omega t + \phi_{\text{Can}}) \right) \qquad (2) \end{aligned}$$

From (2) it is seen that the output is a signal with a DC part and a part with the frequency of the second harmonic. The second harmonic parts of (2) is easily removed by low pass

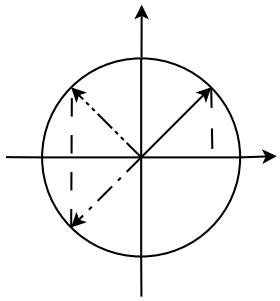

Fig. 2. Phasor of Leakage signal (solid arrow) and two possibilities of cancellation signals (dashed arrows). Only the single dotted cancels the leakage, whereas both cancel the DC-offset.

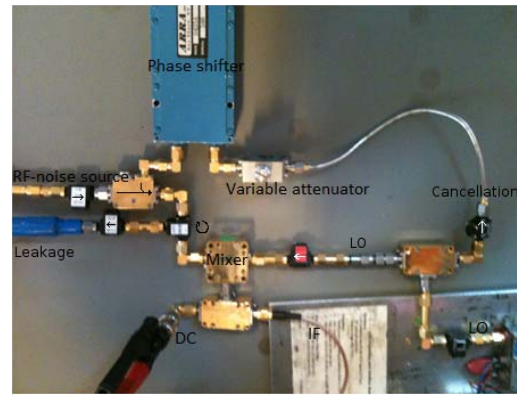

Fig. 3. Measurement setup

filtering, and the output is then given as (3)

$$S_{\text{out, lowpass}} = \frac{A_{\text{LO}}}{2}\Big(A_{\text{Leak}}\cos\left(\phi_{\text{Leak}}\right) + A_{\text{Can}}\cos\left(\phi_{\text{Can}}\right)\Big) \quad (3)$$

The criteria for cancellation of the leakage signal at the RF port is found from the part of (1) with the brackets. When this sum to zero, the cancellation signal will remove the leakage signal.

$$A_{\text{Leak}}\cos\left(\omega t + \phi_{\text{Leak}}\right) + A_{\text{Can}}\cos\left(\omega t + \phi_{\text{Can}}\right) = 0 \Leftrightarrow \quad (4)$$

$$A_{\text{Leak}} = A_{\text{Can}} \quad (5)$$

and

$$\phi_{\text{Leak}} - \phi_{\text{Can}} = \pm\pi \quad (6)$$

The criteria for a DC offset of zero can be found by setting (3) equal to zero.

$$\frac{A_{\text{LO}}}{2}\left(A_{\text{Leak}}\cos\left(\phi_{\text{Leak}}\right) + A_{\text{Can}}\cos\left(\phi_{\text{Can}}\right)\right) = 0 \Leftrightarrow \quad (7)$$

$$-\frac{A_{\text{Leak}}}{A_{\text{Can}}} = \frac{\cos\left(\phi_{\text{Can}}\right)}{\cos\left(\phi_{\text{Leak}}\right)} \quad (8)$$

Observe that to cancel the leakage the cancellation signal must have the exact same amplitude as the leakage signal and be out of phase, whereas to cancel the DC offset there is no such strict limit. Even when the amplitudes are equal there are two choices for the phase of the cancellation signal, such that the DC offset will be zero. Figure 2 illustrates this with phasors.

III. Measurements

A. Measurement setup

To test the cancellation technique two double balanced mixers each utilizing a MACOM MA4E2532L ring diode is used. One denoted 'Mixer 1' and the other 'Mixer 2', the difference between the two is in the matching circuitry. The X-band LO source is a custom made 10.52GHz oscillator. To measure the noise, a spectrum analyzer is used with a calibrated noise-diode, this setup uses the Y-factor method to measure the noise figure for the mixer [10].

In figure 3 the cancellation setup is shown. The LO-signal is split in two parts using a matched T-split, one part is used to drive the mixer (the actual LO signal), the other part is used to generate the cancellation signal. To control the phase and amplitude of the cancellation signal a variable attenuator and phase shifter is used. The cancellation signal is coupled to the RF/Noise signal from the noise source, using a directional coupler with coupling of -15dB.

The DC offset is measured using a voltmeter, which is disconnected during noise measurements, to ensure that instrument noise is not influencing the measurement. A circulator is placed at the RF port of the mixer, this allows to measure the LO-leakage during measurements. After the circulator an isolator is used to ensure that reflections or noise from the instrument is not coupled to the setup. Isolators is used between all critical components to remove reflections and limit unwanted coupling in the system.

When starting a measurement the attenuator and phase shifter is tuned such that the measured leakage is as low as possible. This is done to set the cancellation amplitude equal to the leakage amplitude, which is the case when they cancel, as was predicted in (5). When the amplitude is set, the phase is swept to see the change in DC-offset, leakage, and noise figure.

B. Results

The mixer is measured to have an LO-RF isolation of 18dB and a noise figure of 14.3dB and 6.2dB at frequencies 10KHz and 1MHz respectively. Using the LO-cancellation technique the LO-RF isolation could be improved to 60dB. Figure 4 shows the LO-RF isolation and the DC-offset as a function of phase change in the cancellation signal. As was predicted in section II only one phase gives a leakage minima while there is two phases which gives a DC-offset of zero. The leakage minima and DC-offset is not located at the same phase, which according to (5), (6) and (8) is the case when the amplitudes are equal. After the full sweep there

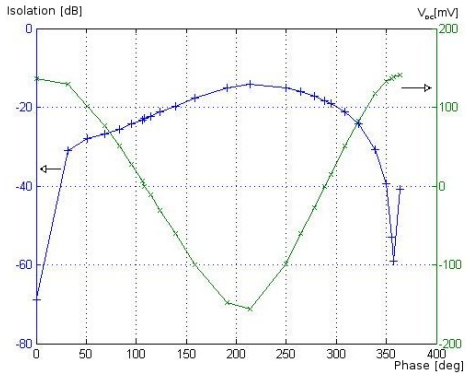

Fig. 4. LO-RF Isolation and DC-offset vs phase change.

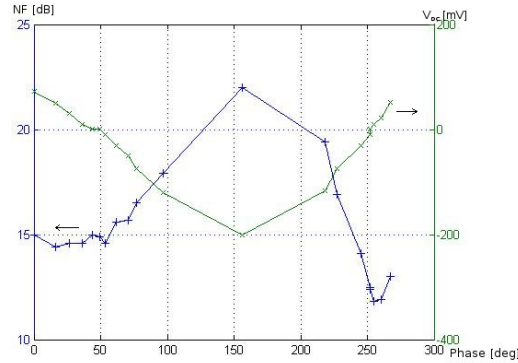

Fig. 6. Noise figure (10KHz) and DC-offset vs phase change, 'Mixer 2'.

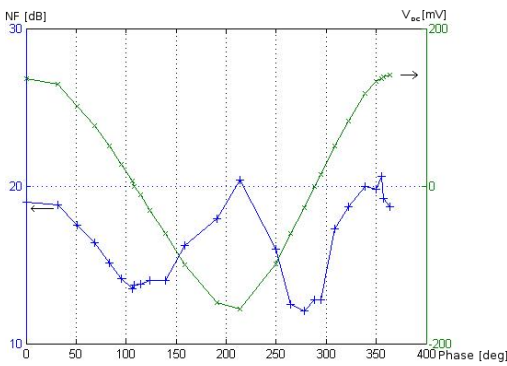

Fig. 5. Noise figure (10KHz) and DC-offset vs phase change, 'Mixer 1'.

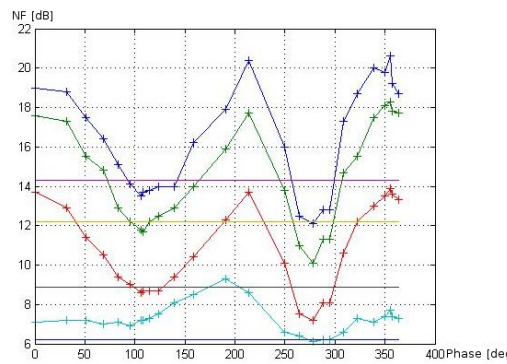

Fig. 7. Noise figure at different frequencies vs phase change, 'Mixer 1'. From top to bottom: Blue @10KHz, Green @20KHz, Red @100KHz, Cyan @1MHz (Straight line is without cancellation signal applied).

was measured an amplitude difference of 1.5dB between the cancellation signal and the leakage signal, this is the reason for the difference in phase of the DC-offset zero and leakage minima.

If one wants the minimum LO leakage while achieving a DC-offset of zero, special care should be taken to match the cancellation signal amplitude to the leakage amplitude.

Using this technique can reduce the noise figure from 14.3dB to 12.1dB at 10KHz. In figures 5 and 6 the noise figure and DC-offset is plotted as a function of phase change in the cancellation signal. It can be observed that the noise figure is proportional to the magnitude of the DC offset, having minima when the DC offset is zero. Using the cancellation signal with a wrong phase will severely damage the mixers noise figure.

While the noise figure can be improved with 2dB at 10KHz there is no significant improvement at 1MHz. Rather at one of the zeros the noise figure is worse. In figures 7 and 8 the noise figure is plotted as a function of phase change in the cancellation signal for IF frequencies of 10KHz, 20KHz, 100KHz and 1MHz. It can be seen that for the low frequencies the improvement is largest, thus there must be a correspondence between the DC-offset and the 1/f noise. Comparing figure 5 and 7 it is clearly that the DC-offset increases the 1/f noise, thus one should try to avoid the DC-offset to get a better mixers regarding 1/f noise. Comparing figure 4 and 7 there is observed no correspondence between the noise figure and the leakage, thus it is concluded that the leakage has no influence on the 1/f noise except to generate the DC-offset.

IV. Conclusion

A investigation on how LO-leakage and DC-offset effects 1/f-noise was conducted, using a LO-leakage cancellation method. For this method conditions for LO-leakage cancellation was derived together with conditions for zero DC-offset. It was shown that for leakage cancellation only one amplitude and phase will give full cancellation, whereas for zero DC-offset there is no strict limit to what the amplitude should be

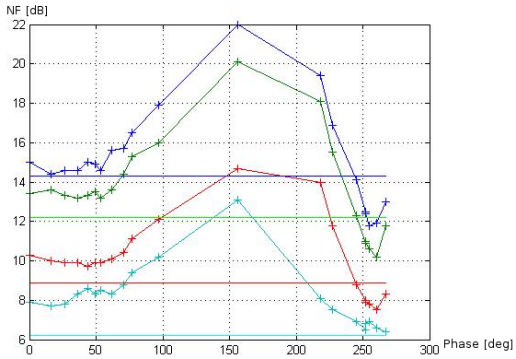

Fig. 8. Noise figure at different frequencies vs phase change, 'Mixer 2'. From top to bottom: Blue @10KHz, Green @20KHz, Red @100KHz, Cyan @1MHz (Straight line is without cancellation signal applied.)

and there can be up to two phases for a given amplitude which gives the desired result.

The cancellation method was tested using a double balanced ring diode mixer. LO-RF isolation was improved from 18dB to 60dB. Noise figure could be improved from 14.3dB to 12.1dB at 10KHz, while maintaining a noise figure of 6.2dB at 1MHz. It was shown that the 1/f noise increases as the absolute DC-offset is increased. While the LO-leakage does not effect the 1/f noise.

LO-RF isolation and zero DC-offset was in the measurement not obtained using the same cancellation signal. This was due to a amplitude mismatch between the cancellation signal and the leakage signal. In future designs utilizing this method one should take special care to match the amplitudes.

REFERENCES

[1] www.weibel.dk, "Earth, horizon, space... weibel scientific reaches further."

[2] B. S. Jensen, T. Jensen, V. Zhurbenko, and T. K. Johansen, "Noise considerations for vital signs cw radar sensors," *Proceedings of the 5th European Conference on Antennas and Propagation, EUCAP 2011*, pp. 2805–2809, 2011.

[3] Razavi, "Design considerations for direct-conversion receivers," *IEEE Transactions on Circuits and Systems II: Analog and Digital Signal Processing*, vol. 44, no. 6, pp. 428–435, 1997.

[4] S. Yang, H. Forstner, G. Haider, H. Kainmueller, K. Aufinger, L. Maurer, and R. Hagelauer, "A low noise, high gain, highly linear mixer for 77 ghz automotive radar applications in sige:c bipolar technology," *Proceedings of ESSCIRC*, pp. 312–315, 2009.

[5] Darabi and Chiu, "A noise cancellation technique in active rf-cmos mixers," *IEEE Journal of Solid-State Circuits*, vol. 40, no. 12, pp. 2628–2632, 2005.

[6] U. Alvarado, R. Berenguer, I. Adn, I. Mayordomo, A. Vaz, and G. Bistu, "Low-frequency noise analysis and minimization in gilbert-cell-based mixers for direct-conversion (zero-if) low-power front-ends," *International Journal of Circuit Theory and Applications*, vol. 38, no. 2, pp. 123–129, 2010.

[7] S. Chehrazi, R. Bagheri, and A. Abidi, "Noise in passive fet mixers: A simple physical model," *Proceedings of the Custom Integrated Circuits Conference*, pp. 375–378, 2004.

[8] Margraf and Boeck, "Analysis and modeling of low-frequency noise in resistive fet mixers," *IEEE Transactions on Microwave Theory and Techniques*, vol. 52, no. 7, pp. 1709–1718, 2004.

[9] S. Yamada, O. Boric-Lubecke, and V. M. Lubecke, "Cancellation techniques for lo leakage and dc offset in direct conversion systems," *IEEE MTT-S International Microwave Symposium digest*, pp. 1191–1194, 2008.

[10] S. A. Maas, *Microwave Mixers*, 2nd ed. Artec House, 1993.

A Passive X-Band Double Balanced Mixer Utilizing Diode Connected SiGe HBTs

Rasmus Michaelsen[1,2], Tom Johansen[1], Kjeld Tamborg[2], Vitaliy Zhurbenko[1]
[1]Technical University of Denmark, Department of Electrical Engineering
2800 Kongens Lyngby, Denmark
Email: rsmi@elektro.dtu.dk
[2]Weibel Scientific A/S
3450 Allerød, Denmark

***Abstract*—In this paper, a passive double balanced mixer in SiGe HBT technology is presented. Due to lack of suitable passive mixing elements in the technology, the mixing elements are formed by diode connected HBTs. The mixer is optimized for use in doppler radars and is highly linear with 1 dB compression point above 12 dBm. The conversion gain at the center frequency of 8.5 GHz is -9.8 dB with an LO drive level of 15 dBm. The mixer is very broadband with 3 dB bandwidth from 7-12 GHz covering the entire X-band. The LO-IF and RF-IF isolation is better than 46 dB and 36 dB, respectively, in the entire band of operation.**

***Index Terms*—Mixer, double balanced, MMIC, passive devices.**

I. Introduction

Direct conversion receivers are used in Doppler radars for speed monitoring, vital signs detection, and measurements of ballistic targets. They can also be configured to implement a simple image rejection system. The key element in a direct conversion receiver is the mixer.

Mixers for direct converison applications suffer from low frequency, 1/f, noise and leakage due to LO and RF being at the same frequency. Two fundamental types of direct conversion mixers exists, active and passive. Active mixers have the advantage of providing a conversion gain, whereas passive mixers have the advantage of higher linearity and less noise. Therefor, passive mixers provide a larger dynamic range, but at the cost of loss in the signal path.

In this paper a direct conversion mixer operating at X-band which has characteristics optimized for doppler radar applications, to be used for vital signs detection. These characteristics include, state-of-the-art linearity, reasonable conversion loss, and noise performance. To meet these requirements a double balanced passive mixer architecture is chosen. As the SiGe HBT process used for implementation do not offer suitable diodes for mixing, we use diode connected HBTs as in [1].

II. Design

This section describes the design of the proposed double balanced ring diode mixer. The double balanced structure has the advantage of inherent isolation between all ports, good linearity and broadband operation [2]. These are all wanted characteristics for mixers to be used in doppler radars. The drawbacks are increased circuit complexity, higher LO-power requirement, and higher conversion loss. Diodes are desired for the implementation of low-noise mixers in direct conversion receivers. In many SiGe technologies there are no diodes available. Using the base-emitter junction of the high-speed HBTs available as a pn-junction diode [1], it is possible to have diodes in a SiGe technology. The design description is divided into three parts covering the design of the balun, the IF extraction and the mixer core. Figure 1 shows the complete mixer schematic, divided into corresponding parts.

A. Marchand balun

The balun of the double balanced mixer is implemented in a form of a lumped element Marchand balun. The Marchand balun is chosen due to its broadband properties. The lumped element implementation allows compact size and straightforward design for good phase and magnitude balance [3], [4]. The lumped element implementation uses offset broadside coupled spiral inductors together with capacitors to realize the coupled transmission lines, normally used in Marchand baluns. The schematic for the balun can be viewed as the part of Figure 1 labelled 'LO balun w. IF ground'.

For any balun, perfect phase and magnitude match is obtained if [5]

$$T_{\text{even}} = 0, \tag{1}$$

where T_{even} is the even mode transmission coefficient. In [4] it is shown that this corresponds to the requirement that

$$C_m = 2C_c\left(\frac{1}{k} - 1\right), \tag{2}$$

where C_c and k are the capacitive and inductive coupling respectively. Thus it is possible to obtain good phase and magnitude match by careful selection of C_m, even though the coupling between the inductances is not as required for the standard Marchand balun.

The S-parameters for the balun alone is shown in Figure 2, where simulation results are compared to measurements. It is observed that there is good agreement, in general, between the simulation and experimental results, except for the S_{11} curve where an additional resonance behavior is observed in the experimental results. At the design frequency a loss of 2.5 dB was measured. The rather high loss is mainly due

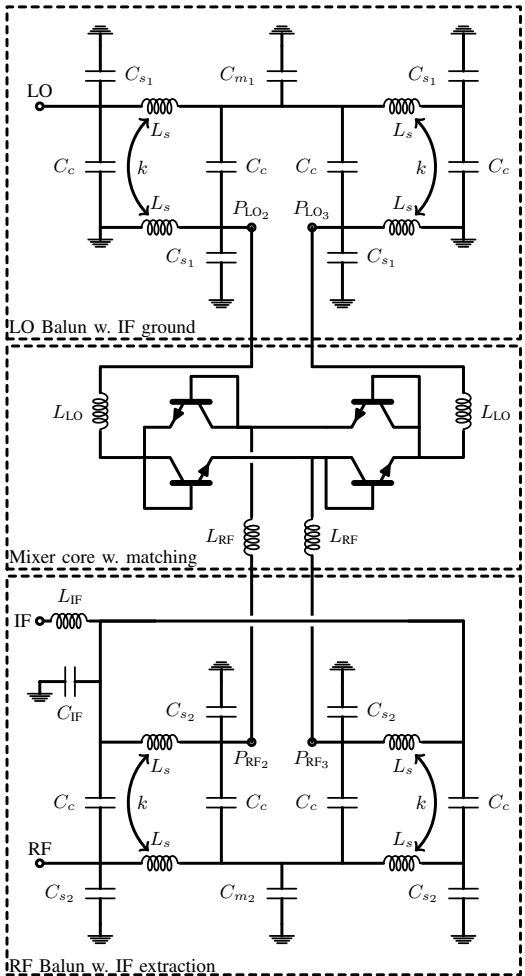

Fig. 1. Schematic of the full mixer circuit.

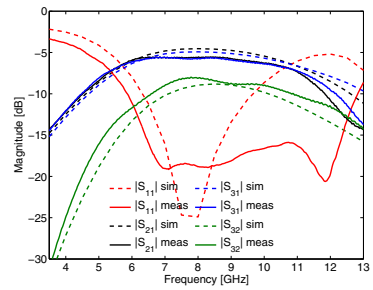

Fig. 2. Measurements and simulation results for balun S-parameters.

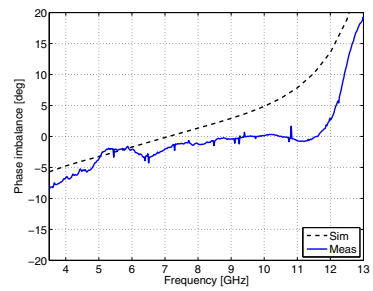

Fig. 3. Measurement and simulation results for phase imbalance.

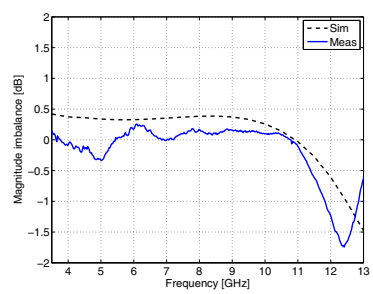

Fig. 4. Measurement and simulation results for magnitude imbalance.

to the low Q-factor of the inductors. As desired the balun is broadband with a measured 3 dB bandwidth of 6.4 GHz. Figures 3 and 4 shows the phase and magnitude imbalance, respectively. Excellent magnitude and phase imbalance of 0.11 dB and 0.7°, respectively, are achieved at the design frequency. A magnitude imbalance better than 0.4 dB and a phase imbalance better than 5°, achieved over the entire bandwidth, which makes this balun suitable for a double balanced mixer application.

B. IF extraction

To get an output signal from the mixer it is necessary to have a circuit wich allows to extract the IF signal, without disturbing the LO and RF baluns. The IF extraction is achieved by making a low frequency ground at either the LO or RF port and extract the signal from the other. It is desirable not to have any large signal leaking out of the IF port as this might saturate or cause other unwanted effects in the low frequency circuitry following the mixer. For this reason it is chosen to use the balun at the LO port to make the low frequency ground connection and the balun at the RF port to extract the IF signal, as the LO-signal can be several magnitudes larger than the RF signal.

Due to the low IF frequency of the mixer together with the grounded parts of the Marchand balun, the IF extraction is quite simple and follows the idea from [6]. The schematic for the IF extraction is the part of Figure 1 labelled 'RF balun w. IF extraction'. The low frequency grounding is ensured by the Marchand balun as the inductors L_s are seen as a

short. To avoid this short in the RF balun it is blocked by large capacitors which creates an open for the IF signal and a short for the RF signal. It is important to make the IF extraction symmetric as any asymmetry will affect the balun performance. To ensure the symmetry the capacitor C_{IF} is split into three parallel 2 pF capacitors placed after both of the two inductors and in the middle where the IF signal is combined. The small influence on the balun performance from the 2 pF capacitors, can be compensated by slightly changing C_{s_2} for matching and C_{m_2} for balance.

C. Mixer core

The mixer core consists of the mixing elements and a matching circuit. Each mixing element consists of a diode connected HBTs. There are two possible ways to make the diode, either use the base-emitter or the base-collector pn-junction. The base-emitter junction is the preferred diode junction due to the heavier doping of the n-region of the emitter compared to the collector. Simulations also shows that this gives the best behavior having a 3 dB difference between the two diode connections. To get the double balanced properties the ring mixer structure is used [2].

Using Harmonic Balance simulations the optimum load conditions are found to be $58+j106\,\Omega$ and $50+j122\,\Omega$ for the LO and the RF ports, respectively. With a conversion gain of -8.7 dB, 1 dB compression point of 8 dB and IIP2 of 53 dBm. As a 50Ω match is required it is relatively simple to tune out the reactive part using single series inductors, L_{RF} and L_{LO}. In Figure 1 the schematic of the mixer core is labelled 'Mixer core w. matching'.

The mixer has been manufactured using a $0.25\mu m$ SiGe process. The die size is $2200\mu m \times 800\mu m$. A microphotograph of the full mixer is shown in Figure 5.

III. Experimental Results

In this section, the experimental results are discussed. The measurements are made on-wafer using a probe station and simple calibration is used to remove losses in cables and probes. The IF-frequency for all measurements is 100 MHz. The mixer conversion loss and single sideband noise figure is shown in Figure 6 as a function of frequency, with a fixed LO power of 15 dBm. At the design frequency of 8.5 GHz the conversion loss is 9.8 dB. The noise figure follows the conversion loss as is expected. Due to measurement inaccuracy the noise figure is at some points lower than the conversion loss. The 3 dB bandwidth covers more than the entire X-band or more precisely the range from 7 GHz to 12 GHz, thus showing the benefit of using a broadband balun design together with the double balanced topology.

In Figure 7 the conversion loss and noise figure is plotted versus the LO power level, at the design frequency of 8.5 GHz. It is seen that the mixer is not fully saturated at an LO power of 15 dBm which was the limit of the measurement equipment used.

To measure the linearity the IF power is measured as a function of the RF power, which is plotted in Figure 8.

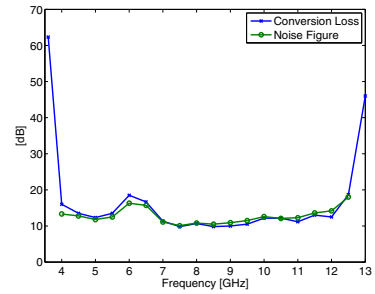

Fig. 6. Measured conversion loss and single sideband noise figure versus frequency.

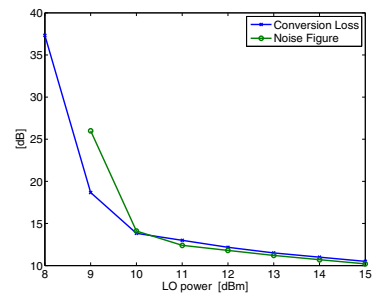

Fig. 7. Measured conversion loss and single sideband noise figure versus LO power.

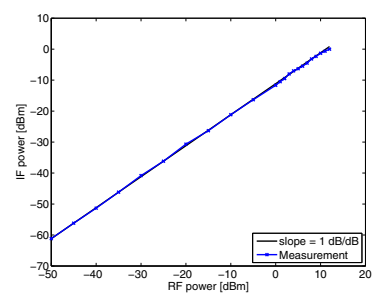

Fig. 8. Measured IF power versus RF.

Due to equipment limitations the measurement was not made with a RF power above 12 dBm. At this point there is a compression of 0.8 dB measured. The 1 dB compression point must therefore be well above 12 dBm. This proves that the design gives a high linearity as required.

The LO-IF and RF-IF isolation at the design frequency are 55 dB and 40 dB, respectively. In Figure 9 the isolation is plotted versus frequency. In the entire band of operation the LO-IF and RF-IF isolation is better than 46 dB and 36 dB, respectively. A comparison between this work and passive mixers recently reported in the open literature is presented

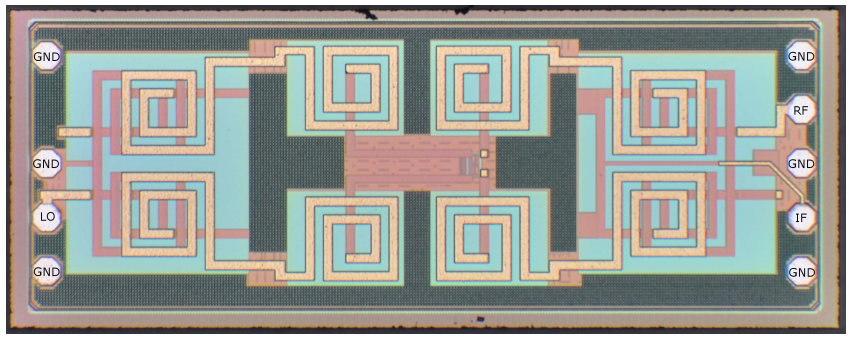

Fig. 5. Microphotograph of passive double balanced mixer. The die size is $2200\mu m \times 800\mu m$

TABLE I
COMPARISON BETWEEN THIS WORK AND RECENT REPORTED PASSIVE MIXERS.

Ref.	Technology	Topology	Frequency [GHz]	BW [GHz]	CG [dB]	LO-power [dBm]	LO/RF-IF isolation [dB]	IP_{1dB} [dBm]
[1]	HBT-diode	Single bal.	24	22-39	-8	3	50 / 48	-1.5
[6]	pHEMT	Double bal.	NA	11-40	-7.2 to -12.4	13	43.2 / 32	12
[7]	pHEMT	Single bal.	60	NA	-12 to -16	0	32 / NA	-2
[8]	CMOS	Double bal.	2.4	1.8-2.8	-7.5	10	47.7 / NA	6.2
This work	HBT-diode	Double bal.	8.5	7-12	-9.8	15	55/40	12

in table I.

IV. CONCLUSION

The design of a passive double balanced mixer in a $0.25\mu m$ SiGe HBT technology has been presented. The mixer is a direct conversion mixer suitable for use in doppler radars for vital signs detection. The passive mixing element consists of diode connected HBTs, using the base-emitter pn-junction to realize the mixing diodes. Lumped element Marchand baluns was implemented using offset broadside coupled spiral inductors and capacitors. This gives the possibility of an elegant IF-extraction together with wide bandwidth and good balance.

The broadband mixer has a 3 dB bandwidth from 7 - 12 GHz, covering the entire X-band, with a conversion loss of 9.8 at the design frequency. It requires a relatively high LO level of 15 dBm for best performance, but has a high linearity with a 1 dB compression point over 12 dB. Good isolation between LO-IF and RF-IF ports of 55 dB and 40 dB, respectively, is ensured due to the good balance of the Marchand baluns.

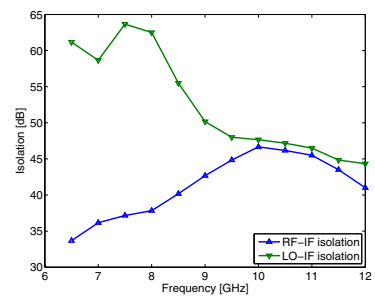

Fig. 9. Measured LO-IF and RF-IF isolation.

V. ACKNOWLEDGMENT

The authors would like to thank the H.C. Ørsteds fond for financial support to cover the cost of chip fabrication.

REFERENCES

[1] V. Issakov, H. Knapp, M. Wojnowski, A. Thiede, and W. Simburger, "A 22-39 GHz Passive mixer in SiGe:C bipolar technology," in *Microwave Symposium Digest (MTT), 2010 IEEE MTT-S International*, pp. 1012 – 1015.

[2] S. A. Maas, *Microwave Mixers*, 2nd ed. Artec House, 1993.

[3] T. Johansen and V. Krozer, "Analysis and Design of Lumped Element Marchand Baluns," in *2008 MIKON CONFERENCE PROCEEDINGS*, pp. 672–675.

[4] T. K. Johansen and V. Krozer, "A 38 to 44GHz sub-harmonic balanced HBT mixer with integrated miniature spiral type marchand balun," *Electromagnetic Waves (Progress in electromagnetics research)*, vol. 135, pp. 317–330, 2013.

[5] K. S. Ang, Y. C. Leong, and C. H. Lee, "Analysis and design of miniaturized lumped-distributed impedance-transforming baluns," *Microwave Theory and Techniques, IEEE Transactions on*, vol. 51, no. 3, pp. 1009 – 1017, mar 2003.

[6] Y.-C. Lee, C.-M. Lin, S.-H. Hung, C.-C. Su, Y.-H. Wang, and Y.-H. Wang, "A broadband doubly balanced monolithic ring mixer with a compact intermediate frequency (IF) extraction," *Progress In Electromagnetics Research Letters*, vol. 20, pp. 175–184, 2011.

[7] F.-H. Huang, S.-W. Lin, P.-Y. Ke, and H.-C. Chiu, "A wide bandwidth V-band balanced resistive mixer with a miniature meandering balun," *Microwave and Optical Technology Letters*, vol. 55, no. 3, pp. 547–550, 2013.

[8] C. Song, O. Boric-Lubecke, and I. Lo, "0.18-m CMOS wideband passive mixer," *Microwave and Optical Technology Letters*, vol. 55, no. 1, pp. 23–27, 2013.

Analysis and Design of Complex Impedance Transforming Marchand Baluns

Rasmus S. Michaelsen[1,2], Tom K. Johansen[1], Kjeld M. Tamborg[2],
[1]Technical University of Denmark, Department of Electrical Engineering
2800 Kongens Lyngby, Denmark
Email: rsmi@elektro.dtu.dk
[2]Weibel Scientific A/S
3450 Allerød, Denmark

***Abstract*—A new type of Marchand balun is presented in this paper, which has the property of complex impedance transformation. To allow the Marchand balun to transform between arbitrary complex impedances, three reactances should be added to the circuit. A detailed analysis of the circuit gives the governing equations. To verify the theory, a design and electromagnetic simulation of a lumped element Marchand balun is made in a SiGe BiCMOS technology. The lumped element impementation is favorable because capacitors are placed where the additional reactances should be added. Thus it is possible to absorb a positive reactance by reducing a capacitor. At the design frequency of 10.5 GHz it matches 50Ω to $50 - j66\Omega$. It has an insertion loss of 5.1 dB, an input reflection of -20.8 dB, as well as phase and magnitude imbalance better than 0.2° and 0.12 dB, respectively.**

***Index Terms*—Balun, Marchand balun, Complex impedance transformation, MMIC.**

I. Introduction

Baluns are used to transform an unbalanced input signal to a balanced output signal. This is an essential functionality in many microwave circuits, e.g. differential amplifiers and balanced mixers. Baluns can be characterized by a group of parameters. Magnitude balance and phase balance describes how well the balun performs the task of transforming an unbalanced signal to a balanced signal. As for all microwave circuits, input reflection must also be considered. For active baluns gain, noise and linearity is also important parameters. The passive baluns do not suffer from noise or linearity issues, but may suffer from excessive loss. The passive balun has a larger dynamic range, as it does not contribute with neither noise nor decreased linearity.

One type of passive balun structure is the so-called Marchand balun [1]. The Marchand balun consists of two sets of coupled lines connected together. The Marchand type balun has found widespread application, due to its wide bandwidth. Several modifications and enhancements has been reported, among these are techniques for bandwidth enhancement [2], miniturization [3], tuning of phase balance [4] or center frequency [5] and impedance scaling [6]. The impedance scaling is only suggested between real valued generator and load impedances.

The purpose of this paper is to give a suggestion for a Marchand type balun that can do impedance transformation between arbitrary complex impedances. By having the complex impedance matching as part of the balun circuit the total circuit size is minimized, as there is no need for additional matching inductors to the active devices. Also the low-Q of inductors typically found in silicon based technologies make it desirable to avoid them due to added loss.

In [7] the idea of using a coupled line, reactively loaded on the thru and coupled ports, for complex impedance matching was suggested. We will expand this idea to the Marchand balun, constructing it of two of such types of coupled lines. To the authors knowledge, this is the first demonstration of a Marchand balun with complex impedance transformation properties.

This paper will first give an analysis of the proposed impedance transforming Marchand balun. This will be followed by a design suggestion in a SiGe technology. Then we use electromagnetic (EM) simulations on the implementation to verify the analysis and design.

II. Analysis

In this section we will provide an analysis of the impedance matching Marchand balun. A schematic of the proposed circuit for the impedance transforming Marchand balun is shown in figure 1, where port 1 (P_1) is driven by a generator with impedance $Z_G = R_G + jX_G$ and port 2 (P_2) and 3 (P_3) is terminated in $Z_L = R_L + jX_L$.

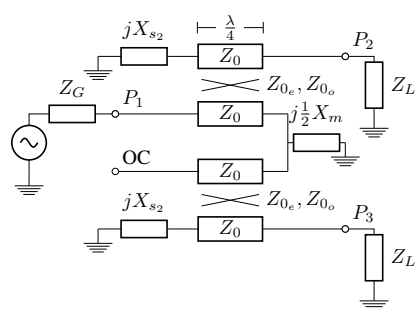

Fig. 1. The modified Marchand balun with complex impedance matching properties.

The ideal balun behavior for a three port network can be described by S-parameters

$$S_{21}{=}{-}S_{31} \tag{1}$$

$$S_{11}{=}0. \tag{2}$$

Ideally, there should be no reflected power from the load and the other S-parameters should not influence performance. Of course this is not the case for real world applications, but the most important ability of a balun is still as expressed above.

To analyze the Marchand balun the approach described in [6] is used. This approach uses the even-/odd-mode analysis [8] to investigate a symmetric network. The balun can be seen as a symmetric four-port with the fourth port terminated in a open circuit. In the analysis we treat the fourth port similar to port one, thus creating a plane of symmetry.

The requirement of balun behavior, i.e. (1) and (2), can be expressed from the even and odd mode circuits, as [6]

$$T_{\text{even}}{=}0 \tag{3}$$

$$Z_{\text{even}} + Z_{\text{odd}}{=}2Z_{\text{G}}^{*} \tag{4}$$

where T_{even} is the even mode transmission coefficient, Z_{even} and Z_{odd} is the impedance seen into the even and odd mode circuits, respectively, and Z_{G}^{*} denotes the complex conjugate of Z_{G}.

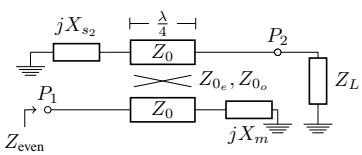

Fig. 2. The even mode circuit.

The even mode circuit of the modified Marchand balun is shown on figure 2. In [7] the two-port Z-parameters for a couple line loaded at the coupled and thru port with Z_{s_2} and Z_m respectively is given as

$$\overline{\overline{Z}} = \begin{bmatrix} \frac{Z_{s_2}Z_+^2}{4Z_mZ_{s_2}+Z_-^2} & \frac{-jZ_-}{2} + \frac{\frac{1}{2}jZ_+^2Z_-}{4Z_mZ_{s_2}+Z_-^2} \\ \frac{-jZ_-}{2} + \frac{\frac{1}{2}jZ_+^2Z_-}{4Z_mZ_{s_2}+Z_-^2} & \frac{Z_mZ_+^2}{4Z_mZ_{s_2}+Z_-^2} \end{bmatrix} \tag{5}$$

where Z_+ and Z_- is $Z_{0e}{+}Z_{0o}$ and $Z_{0e}{-}Z_{0o}$, respectively, Z_{0e} and Z_{0o} is the even and odd mode characteristic impedance of the coupled line.

The requirement of (3) is fulfilled if $Z_{21} = 0$, which from (5) can be reduced to

$$4X_mX_{s_2} - Z_-^2 + Z_+^2 = 0, \tag{6}$$

where it has been used that $Z_{s_2} = jX_{s_2}$ and $Z_m = jX_m$. Because of the requirement $Z_{21} = 0$ then the even mode impedance is not dependent on the load condition and we have

$$Z_{\text{even}} = \frac{Z_{s_2}Z_+^2}{4Z_mZ_{s_2} + Z_-^2}. \tag{7}$$

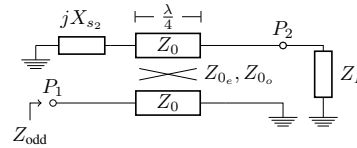

Fig. 3. The odd mode circuit.

The odd mode circuit of the modified Marchand balun is shown on figure 3, it consists of a coupled line with a reactive load on the coupled port and a short circuit on the thru port. The two port Z-parameters for the odd mode circuit is then given as (5) with $Z_m = 0$,

$$\overline{\overline{Z}}\Big|_{Z_m=0} = \begin{bmatrix} \frac{Z_{s_2}Z_+^2}{Z_-^2} & j\frac{Z_+^2-Z_-^2}{2Z_-} \\ j\frac{Z_+^2-Z_-^2}{2Z_-} & 0 \end{bmatrix}. \tag{8}$$

The odd mode impedance can be found as the input impedance of the loaded two port

$$Z_{\text{odd}} = \frac{Z_{s_2}Z_+^2}{Z_-^2} - \frac{\left(Z_+^2 - Z_-^2\right)^2}{4Z_-^2Z_L}. \tag{9}$$

By inserting (7) and (9) into (4) and splitting the equation in a real and imaginary part gives

$$R_G{=}\frac{1}{8}\frac{\left(Z_+^2 - Z_-^2\right)^2 R_L}{Z_-^2\left(R_L^2 + X_L^2\right)} \tag{10}$$

$$X_G{=}\frac{1}{2}\frac{X_{s_2}Z_+^2}{Z_-^2} - \frac{1}{8}\frac{(Z_+^2 - Z_-^2)^2X_L}{Z_-^2(R_L^2 + X_L^2)} + \frac{1}{8}\frac{X_{s_2}Z_+^2}{\frac{1}{4}Z_-^2 - X_mX_{s_2}}. \tag{11}$$

The condition $X_G = 0$ is chosen to simplify the following equations, but a more general approach is possible also for $X_G \neq 0$. The three equations (6), (10) and (11) has four design parameters, X_{s_2}, X_m, Z_{0_o} and Z_{0_e} as free variables. From (6) one gets

$$X_m{=}{-}\frac{1}{4}\frac{Z_+^2 - Z_-^2}{X_{s_2}}. \tag{12}$$

Then inserting (12) in (11) to get

$$X_{s_2}{=}\frac{1}{4}\frac{X_L\left(Z_+^2 - Z_-^2\right)^2}{\left(Z_-^2 + Z_+^2\right)\left(R_L^2 + X_L^2\right)} \tag{13}$$

Finally from (10) we get

$$\frac{1}{Z_{0_o}} - \frac{1}{Z_{0_e}}{=}\frac{1}{R_G}\sqrt{\frac{2}{\alpha}} \tag{14}$$

$$\text{where } \alpha{=}\frac{R_L^2 + X_L^2}{R_GR_L} \tag{15}$$

Observe that for the case of transformation to a real valued load, i.e. $X_L = 0$, (13) gives $X_{s_2} = 0$, a short circuit, (12) gives $X_m \to \infty$, an open circuit, and the impedance scaling factor becomes $\alpha = \frac{R_L}{R_G}$, which is the case for the regular Marchand balun [9].

III. Design procedure and simulation results

In this section we will describe the design procedure for the balun. This is followed by a design example and simulations of the design.

A. Design procedure

The lumped element Marchand balun is chosen to realise the circuit [10]. This has the advantages of small size together with posibility to place capacitors where the added reactances X_{s_2} and X_m is needed. In figure 4 the schematic is shown. The design procedure follows what is described in [9], with modification to incorporate X_{s_2} and X_m. The design equations is given as

$$L_s = \frac{Z_{0_e} + Z_{0_o}}{2\omega} \tag{16}$$

$$k = \frac{Z_{0_e} - Z_{0_o}}{Z_{0_e} + Z_{0_o}} \tag{17}$$

$$C_c = \frac{1}{2\omega}\left(\frac{1}{Z_{0_o}} - \frac{1}{Z_{0_e}}\right) \tag{18}$$

$$C_s = \frac{1}{\omega Z_{0_e}} \tag{19}$$

$$C_{s_2} = C_s - \frac{1}{X_{s_2}\omega} \tag{20}$$

$$C_m = 2C_s - \frac{2}{\omega X_m}. \tag{21}$$

B. Design example

To test the theory a X-band Marchand balun with transformation of generator impedance of $Z_g = 50\Omega$ to a load impedance of $Z_L = 50 - j60\Omega$ at 10.5 GHz is designed. The load value is chosen as it corresponds to a typical mixer diode load, being capacitive.

The circuit is designed using a designkit from Innovations for High Performance Microelectronics (IHP) for their 0.25 μm SiGe:C BiCMOS process. The process has metal-insulator-metal (MIM) capacitors and five metal layers.

The size of the inductor has been the deciding factor in choosing $Z_{0_e} = 32.5\Omega$ giving inductor sizes of $L_s = 0.4nH$. In table I the design parameters for the balun are given, both the theoretical values as calculated and the compensated values as implemented. Especially the implementation of the coupled inductors gives problems due to the difficulties of realization of exact k and C_c, but this can be compensated by changing C_m, C_s, and C_{s_2}.

Figure 5 shows layout of the proposed implementation. The two sets of coupled inductors has a total size of $423\,\mu m \times 194\,\mu m$ and the suggested breakout has a dimension of $610\,\mu m \times 930\,\mu m$. The dimensions of the breakout could also be used in a real circuit to avoid undesired coupling.

C. Simulation Results

Electromagnetic simulations using Momentum in Agilent ADS has been used to verify the design implementation. Due to designkit limitations the capacitors is not part of the Momentum simulation, but models is included in an Agilent ADS S-parameter simulation. The resulting S-parameters are plotted in Figure 6. At the design frequency, an insertion loss of 5.1 dB is simulated, together with a reflection of -20.8 dB. The phase imbalance is 0.2° and the magnitude imbalance is 0.12 dB. Figures 7 and 8 shows plots of the magnitude and phase difference from 8 to 14 GHz. The bandwidth is limited by the matching from 10.1 GHz to 10.8 GHz if a reflection below -15 dB is desired. In this band the insertion loss is better than 5.5 dB, the phase imbalance better than 0.3°, and the magnitude imbalance better than 0.16 dB.

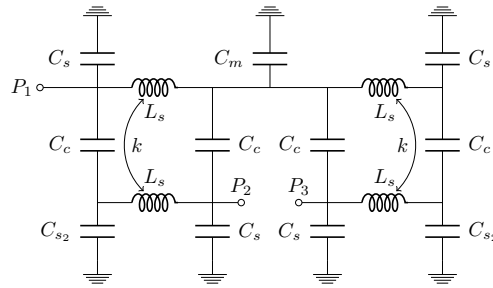

Fig. 4. The lumped element implementation of the Marchand balun with complex matching properties.

TABLE I
Design parameters for the balun

Description	Symbol		Calc.	Comp.
Even mode characteristic impedance	Z_{0_e}	$[\Omega]$	32.5	
Odd mode characteristic impedance	Z_{0_o}	$[\Omega]$	20.9	
Reactance, side	X_{s_2}	$[\Omega]$	-5.96	
Reactance, middle	X_m	$[\Omega]$	114	
Inductance	L_s	$[nH]$	0.4	0.4
Inductive coupling	k		0.21	0.15
Capacitive coupling	C_c	$[fF]$	129	157
Side capacitor	C_s	$[fF]$	466	305
Increased side capacitor	C_{s_2}	$[pF]$	3.01	2.6
Middle capacitor	C_m	$[fF]$	667	727

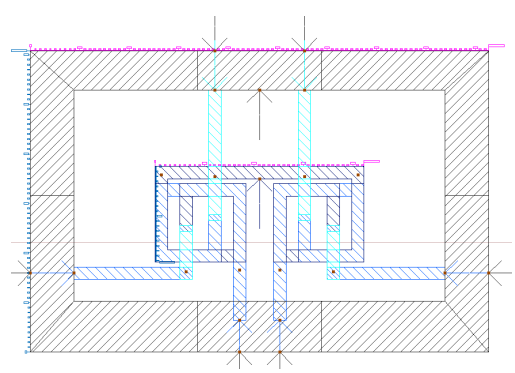

Fig. 5. Layout of proposed circuit, dimensions are $610\,\mu m \times 930\,\mu m$.

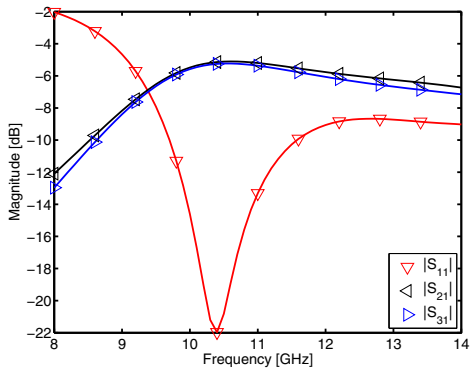

Fig. 6. Magnitude of S-parameters for the proposed balun circuit.

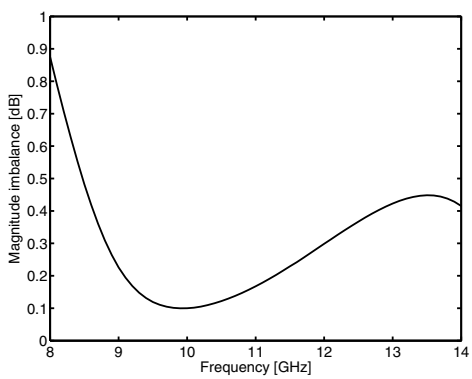

Fig. 7. Magnitude imbalance at the output for the proposed balun circuit.

IV. Conclusion

In this paper the novel idea of a complex impedance transforming Marchand balun was discussed. A detailed analysis gives the governing equations for realization of such a circuit. It was shown, that by addition of three reactances together with careful selection of even and odd mode characteristic impedance an arbitrary complex impedance match can be obtained.

A lumped element implementation of the complex impedance transforming Marchand balun was designed and EM-simulated. The lumped element impementation has the property of having capacitors placed where the additional reactances should be added anyway. Thus it is possible to absorb a positive reactance by reducing a capacitor and a negative by increasing a capacitor. With this design approach no additional inductances are needed for matching, thus reducing loss and circuit size.

The simulation showed that matching to a $50 - j66\Omega$ load

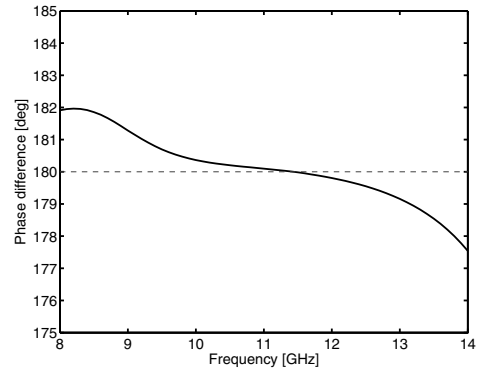

Fig. 8. Phase difference of the two output ports of the proposed balun circuit.

impedance was possible. An input reflection of -20.8 dB at the design frequency of 10.5 GHz, and a insertion loss of 5.1 dB was simulated. The phase and magnitude imbalance was better than 0.2° and 0.12 dB, respectively. The bandwidth is limited to the range from 10.1 GHz to 10.8 GHz for a input reflection better than -15 dB. In this band the insertion loss is better than 5.5 dB, the phase imbalance better than 0.2°, and the magnitude imbalance better than 0.16 dB.

References

[1] N. Marchand, "Transmission-line conversion transformers," *Electronics*, vol. 17, pp. 142–145, 1944.

[2] J.-C. Lu, C.-C. Lin, and C.-Y. Chang, "Exact Synthesis and Implementation of New High-Order Wideband Marchand Baluns," *IEEE Transactions on Microwave Theory and Techniques*, vol. 59, no. 1, pp. 80–86, 2011.

[3] L. Xu, H. Sjoland, M. Tormanen, T. Tired, T. Pan, and X. Bai, "A Miniaturized Marchand Balun in CMOS With Improved Balance for Millimeter-Wave Applications," *IEEE Microwave and Wireless Components Letters*, vol. 24, no. 1, 2014.

[4] R. Michaelsen, T. Johansen, K. Tamborg, and V. Zhurbenko, "A Modified Marchand Balun Configuration With Tunable Phase Balance," *I E E E Microwave and Wireless Components Letters*, vol. 23, no. 2, pp. 66–68, 2013.

[5] X. Miao, W. Zhang, Y. Geng, X. Chen, R. Ma, and J. Gao, "Design of Compact Frequency-Tuned Microstrip Balun," *IEEE Antennas and Wireless Propagation Letters*, vol. 9, pp. 686–688, 2010.

[6] K. S. Ang, Y. C. Leong, and C. H. Lee, "Analysis and design of miniaturized lumped-distributed impedance-transforming baluns," *Microwave Theory and Techniques, IEEE Transactions on*, vol. 51, no. 3, pp. 1009 – 1017, mar 2003.

[7] T. Jensen, V. Zhurbenko, V. Krozer, and P. Meincke, "Coupled Transmission Lines as Impedance Transformer," *IEEE Transactions on Microwave Theory and Techniques*, vol. 55, no. 12, pp. 2957–2965, 2007.

[8] J. Reed and G. Wheeler, "A Method of Analysis of Symmetrical Four-Port Networks," *IRE Transactions on Microwave Theory and Techniques*, vol. 4, no. 4, pp. 246–252, 1956.

[9] R. Michaelsen, T. Johansen, K. Tamborg, and V. Zhurbenko, "Design of a Broadband Passive X-Band Double Balanced Mixer in SiGe HBT technology," *To appear in International Journal of Microwave and Wireless Technologies*, 2014.

[10] T. Johansen and V. Krozer, "Analysis and Design of Lumped Element Marchand Baluns," in *2008 MIKON CONFERENCE PROCEEDINGS*. IEEE, 2008, pp. 672–675.

Flicker Noise Comparison of Direct Conversion Mixers using Schottky and HBT Dioderings in SiGe:C BiCMOS Technology

Rasmus S. Michaelsen[1,2], Tom K. Johansen[1], Kjeld Tamborg[2], Michele Squartecchia[1]

[1]Department of Electrical Engineering, Technical University of Denmark, 2800 Kgs. Lyngby, Denmark

[2]Weibel Scientific A/S, 3450 Allerød, Denmark

Abstract—In this paper, we present flicker noise measurements of two X-band direct conversion mixers implemented in a SiGe:C BiCMOS technology. Both mixers use a ring structure with either Schottky diodes or diode-connected HBTs for double balanced operation. The mixers are packaged in a metal casing on an Arlon 25N substrate to shield the sensitive noise measurement. Conversion loss measurements of both mixers is performed both for on-wafer and packaged versions. The experimental results shows that the Schottky diode mixer exhibits a 1/f noise corner frequency of 250 kHz, while the diode connected HBT circuit demonstrates a 1/f noise corner frequency around 10 kHz.

Index Terms — Mixer, flicker (1/f) noise, MMIC, Schottky diode, diode connected HBT.

I. Introduction

Every microwave receiver circuit needs some sort of frequency conversion circuit. Direct conversion has the benefit of giving the modulated signal directly at baseband without the need for complex image rejection structures [1]. For Doppler radars, direct conversion is beneficial as it gives the Doppler shift and thus the speed measurement directly from the received frequency. The key element in a direct conversion receiver is the mixer. The direct conversion mixer has some drawbacks, which comes from the fact that the incoming radio frequency (RF) and local oscillator (LO) frequency is very close. Isolation between LO and RF ports cannot easily be enhanced by using filters so the mixer architecture must have an inherent isolation between these ports. Another drawback is that, due to the low 'intermediate frequency' (IF), it has an increased noise level due to low frequency noise. The low frequency noise is also called flicker noise and is caused by generation-recombination processes in the solid-state mixing devices.

Passive mixers are recognized for their excellent low frequency noise performance. The low frequency noise is influenced by the LO pump signal in a non-linear manner [2] and is generally believed to be present in passive mixers only if an non-zero net average current flows through the mixing core. In double balanced mixers, flicker noise is believed to be caused by unavoidable asymmetries in the diode ring and balun structures. By employing an LO leakage cancelation scheme to the direct conversion mixer, flicker noise can be significantly improved as previously demonstrated by the authors [3].

In general, Schottky diodes is preferred for implementing passive mixers because they are majority carrier devices and hence leads to lower conversion loss at higher frequencies than mixers built using pn-junction diodes [4]. Schottky diodes, however, are not standard elements in high performance Silicon technologies. Structures with low reverse leakage current have been proposed in a SiGe:C BiCMOS technology [5], but little information is generally available about their noise performance at low frequencies. In this paper, we will experimentally investigate the difference in low noise performance between two X-band double balanced direct conversion mixers implemented in SiGe:C BiCMOS technology. One using Schottky diodes, the other using diode connected HBTs.

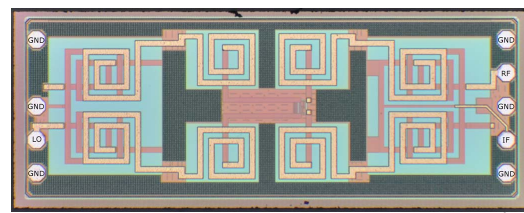

a) Microphotograph of HBT mixer, size 2200 × 800 µm^2

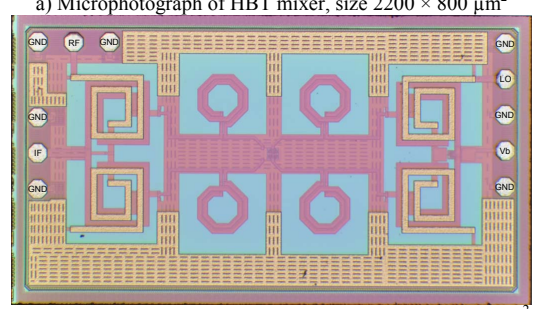

b) Microphotograph of Schottky mixer, size 2050 × 1000 µm^2

Fig. 1. Microphotograph of the two manufactured chips.

II. Doubled Balanced Mixer Design

The double balanced mixers employs lumped element spiral type Marchand baluns on the RF and LO ports due to the good balance achievable over a large bandwidth with this structure. The devices in the diodering are sized to allow easy matching to the Balun structures by placing additional series inductors.

A thorough description of the mixer circuit using diode connected HBTs is given in [6]. The Schottky diode mixer circuit is similar, but uses a ring of Schottky diodes as the mixer core. A microphotograph of the two manufactured chips is shown in figure 1. Due to the sensitive nature of the flicker noise measurements it is not possible to perform these on-wafer. Shielding the mixer from a noisy environment is much easier when packaged in a small metal case. For this purpose the mixer chips is mounted on a Arlon 25N substrate with cobber lines covered with soft gold to allow for ball bonding using gold wires. A packaged mixer is shown in figure 2. Apart from the LO, RF and IF ports also a bulk bias connection to the Silicon substrate is made. This is grounded for the measurements presented here circuits.

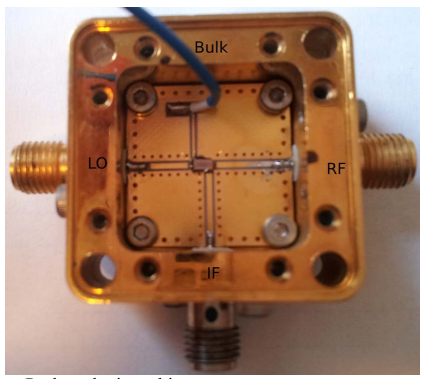

Fig. 2. Packaged mixer chip.

III. Experimental Results

In this section the measurement setup will be described. This will be followed by a presentation and discussion of the results of the measurements of flicker noise.

A. Measurement Setup

The conversion loss is measured, at first, on a bare die using a probe station and then again after packaging. For the on-wafer measurements, calibration is performed to a reference plane at the tip of the probe, ie. at the contacts of the chip. For the packaged version, calibration is done to a reference plane at the SMA-connectors. The noise measurement is carried out using a spectrum analyzer together with a calibrated noise source to measure the Y-factor [4]. Two different custom made cavity resonance oscillators with a Q above 10 000 are used as LO sources. These deliver an output power around 13dBm at 9.1 GHz and 10.4 GHz, respectively. The noise source is an Anritsu Noise diode with excess noise ratio of 14.3 dB. The IF amplifier is similar to the ones used in commercial Doppler radars manufactured by Weibel Scientific and has a gain of 80 dB. The measurement setup is shown in figure 3. As the present investigation is concerned with the comparison between the two mixer circuits, there has not been done extensive measurements to determine the noise-contributions from the oscillator and IF-amplifier, although quality components has been used to minimize the effect.

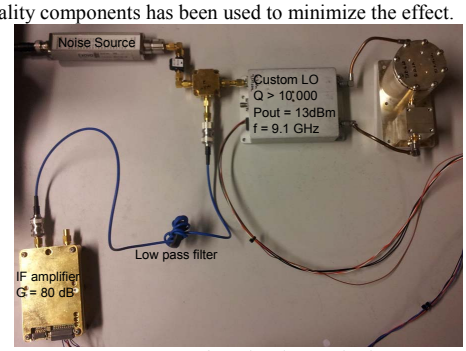

Fig. 3. Measurement setup for noise characterization.

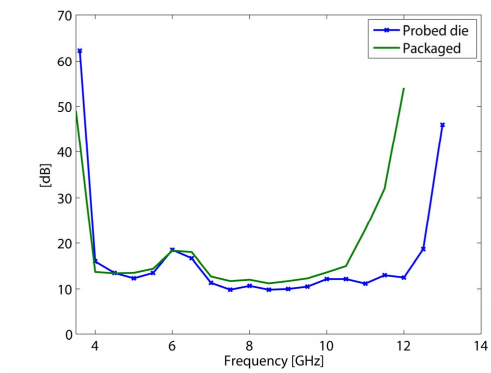

Fig. 4. Measurement of diode-connected HBT mixer conversion gain versus frequency, for probe measured die and packaged die.

B. Measurements Results and Discussion

In this subsection, the measurements results are discussed. The conversion loss as a function of RF frequency for the diode connected HBT mixer is shown in figure 4 both for the probed and packaged version. The conversion loss is lowest at 8.5 GHz where it is 9.8 dB for the probed and 11.2 dB for the packaged version. Around 9 GHz where the noise is measured the conversion loss is 10 dB for the probed and 11.7 dB for the packaged version. For the Schottky diode mixer the conversion loss is plotted as a function of frequency in figure 5. The conversion loss is lowest at 11 GHz where it is 8.8 dB for the probed and 11.2 dB for the packaged version. At 10.4 GHz where the noise is measured the conversion loss is 9.3 dB for the probed and 11.4 dB for the packaged version. The additional loss of roughly ~1.5 dB, which was observed for both mixers, is seen across the entire bandwidth, and is what could be expected from the bonding wires, microstrip lines

and SMA to microstrip connections. Apart from additional loss, the bandwidth is also reduced by the added inductance on the input terminals.

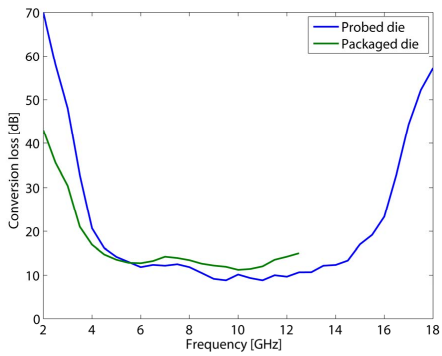

Fig. 5. Measurement of Schottky mixer conversion gain versus frequency, for probe measured die and packaged die.

The noise figure of the Schottky diode mixer is plotted in figure 6, for IF frequencies from 50 kHz to 1 MHz , with a LO frequency of 10.4 GHz. At higher frequencies the noise figure is 9.0 dB and rises as 1/f with a corner around 250 kHz, with a noise figure around 22 dB at 50 kHz. In comparison, the diode-connected HBT mixer demonstrates a noise figure of 8.5 dB with a LO frequency of 9.1 GHz. Both mixers operate with a 3-dB bandwidth covering the entire X-band, but the Schottky diode mixer operates best around 10 GHz and the diode-connected HBT mixer around 8.5 GHz. To give a realistic view of the diode-connected HBT mixer, the noise figure with a LO frequency of 9.1 GHz is plotted in figure 7 on a logartihmic scale from 1-100 KHz. Here it is seen that the diode-connected HBT mixer also have a 1/f tendency, but with a corner frequency as low as 10 kHz. Now it is clearly demonstrated that the HBT-connected diodes perform much better than the Schottky diodes in terms of low frequency noise performance. The higher low frequency noise in the Schottky diode mixer is believed to be caused by poor quality of the Schottky barrier and effect of leakage current.

IV. Conclusion

We have presented measurement of low-frequency noise of two mixers in SiGe:C BiCMOS technology, one utilizing Schottky diodes the other diode connected HBTs. To perform the measurements the mixers has been mounted on an Arlon 25N substrate, gold ball bonded to soft gold transmission lines, and enclosed in a metal casing, thus shielding them from external noise sources. The noise measurements are performed using the Y-factor method. The experimental results showed that the Schottky diode mixer exhibits a higher 1/f noise with a corner frequency around 250 kHz, while the diode connected HBT circuit has a 1/f noise corner frequency around ~10 kHz.

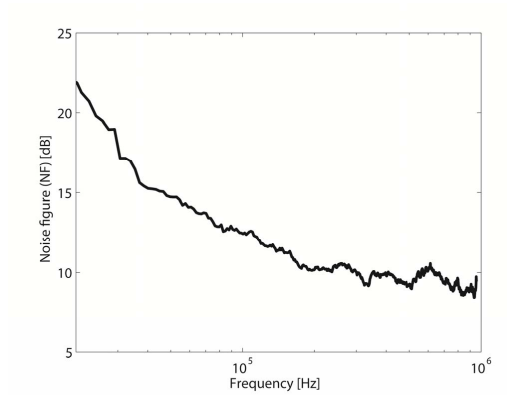

Fig. 6. Measurement of Schottky mixer noise figure as a function of IF frequency.

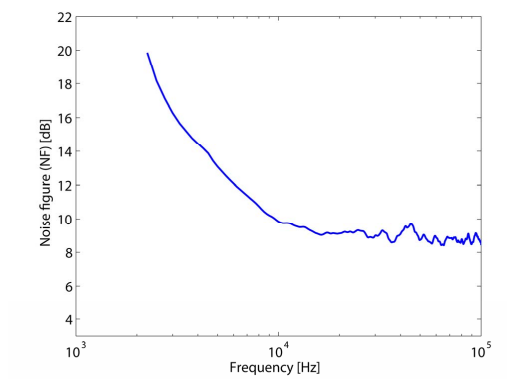

Fig. 7. Measurement of HBT mixer noise figure as a function of IF frequency.

References

[1] B. Razavi, "Design consideration for direct-conversion receivers," IEEE Trans. Circuits and Systems II: Analog and Digital Signal Processing, vol. 44, no. 6, pp. 428-435, 1997.

[2] M. Rudolph and F. Bonani, "Low-Frequency Noise in Nonlinear Systems", IEEE Microwave Magazine, pp. 84-92, Feb. 2009.

[3] R. S. Michaelsen, T. K. Johansen, and K. Tamborg, "Investigation of LO-leakage cancellation and DC-offset influence on flicker-noise in X-band mixers," in 7th European Microwave Integrated Circuit Conference, 2012, pp. 99-102.

[4] S. A. Maas, Microwave Mixers, 2nd ed. Artech House, 1993.

[5] R. M. Rassel et al., "Schottky Barrier Diodes for Millimeter Wave SiGe BiCMOS Applications," in IEEE BCTM, 2006. 2014.

[6] R. S. Michaelsen, T. K. Johansen, K. Tamborg, and V. Zhurbenko, "Design of a broadband X-band double-balanced mixer in SiGe HBT technology," Int. Jour. Microwave and Wireless Tech., vol. 6, no. 3-4, pp. 235.242, 2014.

A SiGe BiCMOS Double-Balanced Mixer with Active Balun for X-Band Doppler Radar

Rasmus S. Michaelsen[(1,2)], Tom K. Johansen[(1)], Kjeld M. Tamborg[(2)], and Vitaliy Zhurbenko[(1)]
(1) Technical University of Denmark, Department of Electrical Engineering
2800 Kgs. Lyngby, Denmark
Email: tkj@elektro.dtu.dk
(2) Weibel Scientific A/S, 3450 Allerød, Denmark

***Abstract*— In this paper, we present an X-band double-balanced mixer in SiGe BiCMOS technology. The mixer core consists of a LO matched quad diode ring using diode-connected Heterojunction Bipolar Transistors (HBTs). The mixer is integrated with a low-noise, high-linearity active balun on the RF port and a miniaturized Marchand balun on the LO port. Experimental results show a conversion gain of +4 dB at 10.5 GHz for LO drive levels > 10 dBm. The LO-IF and RF-IF isolation is better than 36 dB and 22 dB, respectively, in the entire band of operation. The input referred 1 dB compression point is better than -11 dBm. The IIP2 is +13 dBm at a supply voltage of 3 V. The measured noise figure is found to be ~6.5 dB at 10.5 GHz.**

Keywords*— Active balun, Marchand balun; mixer; MMIC; diode connected HBTs;

I. Introduction

High precision Doppler radars can be used for a high number of applications ranging from vital signs detection, tracking of aircrafts, UAVs, satellites, and space-shuttles to velocity tracking radars for artillery. The requirements to the dynamic range in the Doppler radar receivers continue to evolve as new applications emerge. The trend towards multiple receivers for phased array Doppler radars means that a monolithically integrated receiver with high dynamic range must be developed.

One of the most critical components in the Doppler radar receiver is the mixer. As the Doppler shift falls in the range from a few Hz to approximately 1 KHz, direct conversion mixers must be employed. It is well-known that direct conversion mixers suffers from DC offset problems and high 1/f-noise [1]. This has led to research into passive double-balanced mixers using either CMOS resistive mixers [2] or diode-ring mixers [3]. In a SiGe BiCMOS technology, the 1/f-noise properties are believed to be best for the bipolar transistors compared to the MOSFETs. This is because the MOSFET suffers from traps in the oxide, which leads to an increase in 1/f-noise. The bipolar transistors on the other hand are bulk conduction devices and have an order of magnitude lower 1/f-noise compared to the surface channel conduction of CMOS devices [4]. Recently, the authors compared the 1/f-noise performance of passive double-balanced mixers using diode-connected HBTs and Schottky diodes implemented in a SiGe BiCMOS technology. It was found that the diode-connected HBTs lead to much lower 1/f-noise corner frequency than the Schottky diodes. Therefore, the diode-connected HBT in a ring structure is believed to be the most suitable mixer configuration for Doppler radar receivers. The use of passive baluns on the ports of the mixer, however, introduces significant losses which also increase the noise figure. Modifying the double-balanced mixer to include an active balun on the RF port should lead to radar receivers with lower noise figure. It is well known, however, that active baluns may lead to poor linearity. Therefore, techniques to improve the linearity of the active baluns should be employed in their design.

In this paper, the design of an X-band double balanced mixer with active balun on its RF port and passive balun on the LO port is reported. The mixer is fabricated in a 0.25 µm SiGe:C BiCMOS process from Innovations for High Performance Microelectronics (IHP) in Germany. The technology features high-performance npn-transistors with a f_T of 110 GHz and f_{max} of 180 GHz. The technology has metal-insulator-metal (MIM) capacitors and five metal layers for passives and low-loss interconnects [5].

II. Circuit Design

The block-diagram of the double-balanced mixer is shown in Fig. 1. The mixer has the active balun placed at the RF port. A passive miniaturized Marchand balun is preferred at the LO port due to considerations about potential 1/f-noise up-conversion and bandwidth at the LO port. The IF extraction network of the mixer, shown in Fig. 1, provides the necessary return current path from the diode ring mixer core and shields the RF from the IF port.

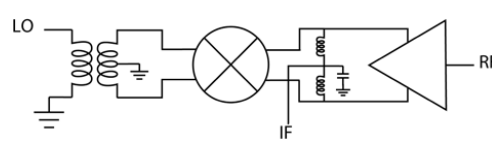

Fig. 1. Block diagram of double-balanced mixer.

A. Active Balun

Fig. 2 shows the schematic of the active balun. The design uses a differential cascode amplifier for high gain and good isolation. The input of one port of the differential cascode amplifier is matched using a shunt capacitor, C_{in}, and series

inductor, L_{in}. The series capacitor, C_{De}, is included at the input port mainly for coupling of the AC signal. The same type of

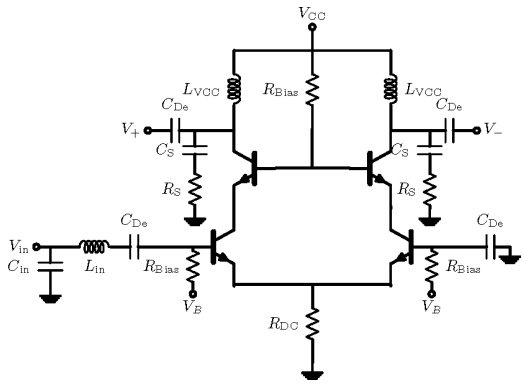

Fig. 2. Schematic of active balun.

capacitor shorts the AC signal at the unused input port to ground. This scheme allows easy biasing of the transistors through high valued resistors, R_{Bias}. The inherent high common-mode rejection ratio of the differential cascode amplifier converts the single-ended signal at the input into a differential signal at the output. The output is matched using an RF inductor, L_{VCC}, and series coupling capacitor, C_{De}. The RF inductor also serves for biasing while the series capacitor is needed for decoupling the output of the active balun from the return current flowing from the mixer core. For increased stability, a series network consisting of R_s and C_s is placed at the output. The noise and linearity of the active balun is optimized by adjusting the sizes of the HBTs and increasing the bias current and voltage supply. The bias current of the differential cascode amplifier is set through the resistor R_{DC}. This choice is better than an active current source for high-frequency integrated circuits because of the lower parasitic capacitance [6]. The value of this resistor is chosen as a trade-off between noise, common-mode rejection ratio, and required bias supply of the active balun. The nominal supply voltage, V_{cc}, is set to 6 V. The layout is EM simulated and coupled together with S-parameter and Harmonic-balance simulations to give a realistic impression of the circuit before manufacturing. According to these simulations the active balun has a gain of 16.3 dB and noise figure of 4.8 dB at the center frequency of 10.5 GHz. The simulated amplitude and phase mismatch is below 1.5 dB and 3 degrees, respectively, over the band from 10 to 11 GHz. The input referred 1 dB compression point is -6 dBm.

B. Mixer Core

The mixer core consists of a quad ring of diode-connected HBTs as shown in Fig. 3. The base-emitter junction is the preferred diode junction for mixer applications due to the heavier doping of the n-region of the emitter compared to the collector. The use of diode-connected HBTs with base and collector tied together also prevents substrate injection [7, pp. 477]. The heavy doping is necessary to reduce the so-called conversion-loss degradation factor [8]:

$$\delta = 1 + \frac{R_s}{Z_s} + \frac{Z_s f_{RF}^2}{R_s f_c^2} \qquad (1)$$

where R_s is the series resistance, Z_s is the real diode junction input resistance (depends on pump power), and $f_c=1/(2\pi R_s C_j)$ is the cut-off frequency of the diode. From the high doping in the emitter, the diode capacitance, C_j, is expected to be high but simulations shows that the ratio of the design frequency to cut-off frequency f_{rf}/f_c remains low even at X-band frequencies. This observation applies at least for the small-area SiGe HBT's considered here and indicates that the mixer core operates mainly in a resistive mode. Inductors, L_{match}, are added to the diode ring structure to provide matching to the miniaturized Marchand balun at the LO port.

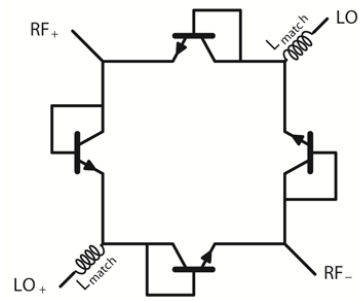

Fig. 3. Quad ring mixer using diode connected HBTs.

C. Marchand Balun

As mentioned above, a miniaturized Marchand balun is used at the LO port of the double-balanced mixer. The lumped-element representation of the Marchand balun is shown in Fig. 4. In this representation the input port is called P_1 and the two complementary output ports are called P_2 and P_3. The lumped element representation uses offset broadside coupled spiral inductors, L_s, together with external capacitors, C_s and C_m, to realize the quarter-wave coupled lines needed in the distributed Marchand balun. The inductive and capacitive coupling between the spirals is represented by k and C_c, respectively.

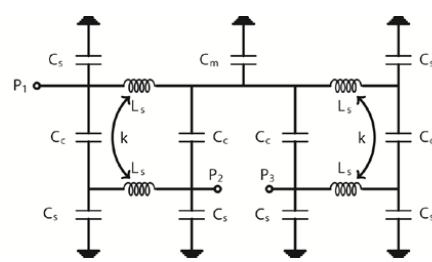

Fig. 4. Schematic of lumped element Marchand balun.

For equivalence with the distributed Marchand balun at the design frequency, ω_{LO}, the following design formulas are applied [9]:

$$L_s = \frac{Z_{oe} + Z_{oo}}{2\omega_{LO}} \quad (2a)$$

$$k = \frac{Z_{oe} - Z_{oo}}{2\omega_{LO} L_s} \quad (2b)$$

$$C_s = \frac{1}{\omega_{LO} Z_{oe}} \quad (2c)$$

$$C_c = \frac{1}{2\omega_{LO} Z_{oo}} - 0.5C_s \quad (2d)$$

$$C_m = 2 \times \frac{C_c - kC_c}{k} \quad (2e)$$

where Z_{oe} and Z_{oo} are the even and odd mode characteristic impedances of the coupled lines in the distributed Marchand balun. In practice it proofs difficult to simultaneously fulfil equations (2a) to (2e). For a given inductive and capacitive coupling of k and C_c, respectively, detailed analysis shows that equation (2e) gives the sufficient condition for ideal balance in the Marchand balun. The most critical part for proper balun performance is thus to select C_m to fulfil equation (2e). The minituarized Marchand balun is optimized using EM simulation. The simulated insertion loss at 10.5 GHz is around 5.1 dB while the amplitude and phase mismatch is 0.18 dB and 0.7 degree, respectively. The rather high loss is caused by the low quality-factor of the broadside coupled spiral inductors.

III. Experimental Results

In this section, the experimental results of the double-balanced mixer are discussed. The measurements are made on-wafer using a probe station. Losses in cables and probes are calibrated out. The microphotograph of the fabricated mixer is shown in Fig. 5. The size is 1860 × 1020 μm^2.

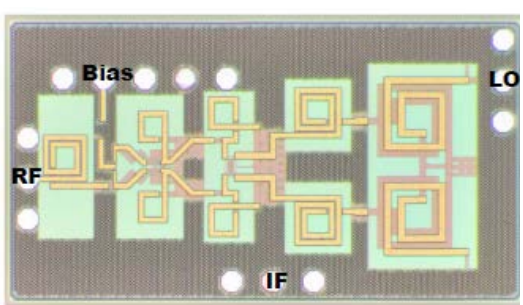

Fig. 5. Microphotograph of the double-balanced mixer, size is 1860 × 1020 μm^2.

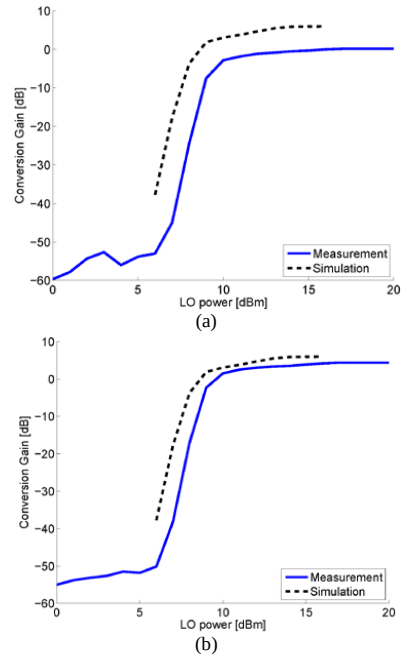

Fig. 6. Conversion gain version LO power at (a) V_{cc}=6.0 V and (b) V_{cc}=3.0 V.

The conversion gain as a function of LO drive level for supply voltages of 6V and 3V are shown in Fig. 6(a) and Fig. 6(b), respectively. The measurements are performed on several samples with good uniformity. The LO frequency is set to 10.4 GHz and the RF frequency is set to 10.5 GHz. The current consumption for the two supply voltages are 17 mA and 38 mA, respectively. The conversion gain at a supply voltage of V_{cc}=6.0 V, shown in Fig. 6(a), saturates at a level around ~-1 dB for an LO drive level above ~10 dBm. This is significant lower than predicted by the simulation. Reducing the bias voltage to V_{cc}=3.0 V, increases the conversion gain, as shown in Fig. 6(b). The saturated level is around ~4.6 dB, well in line with the simulation. The exact reason for the observed behavior is as yet unknown. A possible cause may be that the collector-emitter voltages across the HBTs in the active balun with a supply voltage of V_{cc}=6.0 V are so high (close to breakdown) that the transistor model becomes inaccurate. Fortunately, the performance of the double balanced mixer is acceptable at a supply voltage of V_{cc}=3.0 V. Therefore, all the following measurements have been performed at this supply voltage.

Fig. 7 shows the conversion gain as a function of frequency at a fixed IF of 100 MHz. The LO drive level is fixed at +15 dBm. The conversion gain peak of ~4.6 dB is around the design frequency of 10.5 GHz and the -3 dB bandwidth is ~2.5 GHz. The bandwidth is mainly limited by the active balun. In general, the frequency response of the conversion gain is well predicted by the simulation.

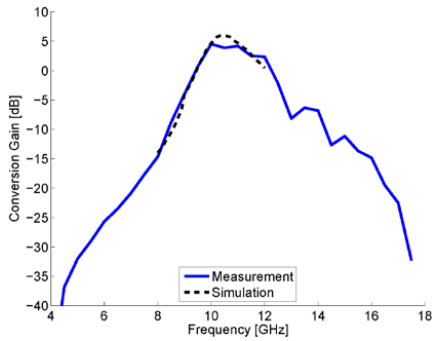

Fig. 7. Conversion gain versus RF frequency.

The LO-IF and RF-IF isolation versus RF frequency is shown in Fig. 8. In the entire band of operation the LO-IF and RF-IF isolation is better than 36 dB and 22 dB, respectively. These values indicate a good balance of both the active balun and miniaturized Marchand balun.

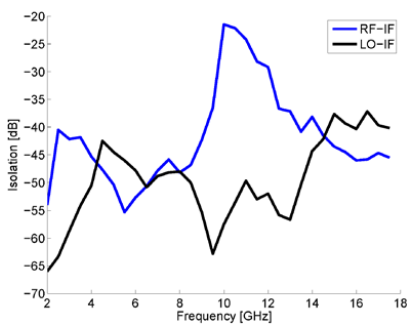

Fig. 8. LO-IF and RF-IF isolation versus RF frequency.

The measured 1 dB input referred compression point of the double balanced mixer is ~-11 dBm. This is somewhat lower than the -6 dBm simulated for the active balun alone but still acceptable for a mixer with active balun on its RF port. The input referred second-order intercept point (IIP_2) is measured with two RF tones at frequencies of 10.5 and 10.513 GHz giving a second-order product at 13 MHz. Isolators are placed after the signal generators to avoid leakage and intermodulation of the signals before they are applied to the mixer. From Fig. 9 an IIP_2 around +13 dBm is observed. This is significantly worse than the IIP_2 of +66 dBm demonstrated for the purely passive X-band double balanced ring mixer in [3].

The single sideband noise figure versus RF frequency, shown in Fig. 10, is measured under the same conditions as the conversion gain in Fig. 7. It reaches a minimum of ~6.5 dB around the design frequency of 10.5 GHz. Compared to the purely passive X-band double balanced ring mixer in [3] this represents an improvement of ~3.3 dB due to the good noise performance of the active balun.

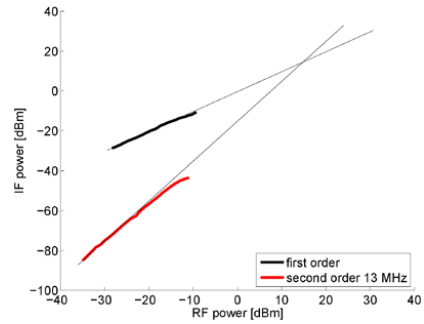

Fig. 9. IF power versus RF power.

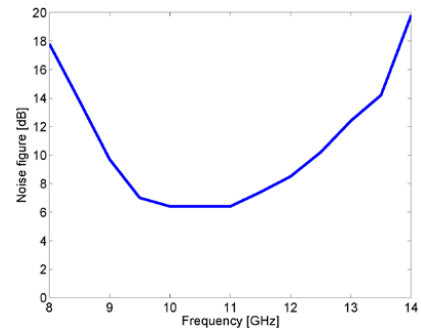

Fig. 10. Single-sideband noise figure versus RF frequency.

IV. Conclusions

The design of a double balanced mixer in a 0.25 µm SiGe BiCMOS technology has been presented. The mixer is a direct conversion mixer for use in X-band Doppler radars. The double balanced mixer integrates an active balun optimized for low noise and high linearity on the RF port and a miniaturized Marchand balun on the LO port. The mixing elements consist of diode connected HBTs.

At the design frequency of 10.5 GHz the mixer has a conversion gain of ~4.6 dB and a single-sideband noise figure of ~6.5 dB. It requires a relatively high LO level of ~15 dBm for best performance.

References

[1] B. Razavi, "Design Considerations for Direct-Conversion Receivers," IEEE Trans. Circuits Syst. II, vol. 44, no. 6, pp. 428-435, June 1997.

[2] C. Song, O. B.-Lubecke, and I. Lo, "0.18-µm CMOS Wideband Passive Mixer," Microw. Optical Tech. Letters., vol. 55, no. 1, pp. 23-27, Jan. 2013.

[3] R. S. Michaelsen, T. K. Johansen, K. M. Tamborg, and Vitaliy Zhurbenko, "Design of a broadband passive X-band double-balanced mixer in SiGe HBT technology," Int. Jour. Microw. Wireless Techn., pp. 235-242, 2014.

[4] J. Babcock, B. Loftin, P. Madhani, X. Chen, A. Pinto, and D. Schroder, "Comparative low frequency noise analysis of bipolar and MOS

transistors using an advanced complementary BiCMOS technology," in IEEE Conf. Custom Integrated Circuits, pp. 385-388, 2001.

[5] IHP website: http://www.ihp-microelectronics.com.

[6] S. Voinigescu, High-Frequency Integrated Circuits, Cambridge University Press, 2013.

[7] M. Reisch, High-Frequency Bipolar Transistors, Springer, Berlin, Germany, 2003.

[8] S. A. Mass, Microwave Mixers, 2nd edition, Artech House, Norwood, MA, USA, 1993.

[9] T. Johansen and V. Krozer, "Analysis and Design of Lumped Element Marchand Baluns," in IEEE MIKON conference proceeding, pp. 672-675, 2008.

Bibliography

[1] www.weibel.dk, *Earth, horizon, space... weibel scientific reaches further*, 2012.

[2] B. S. Jensen, T Jensen, V Zhurbenko, and T. K. Johansen, "Noise considerations for vital signs cw radar sensors", *Proceedings of the 5th European Conference on Antennas and Propagation, EUCAP 2011*, pp. 2805–2809, 2011.

[3] S. Villeval, I. Bilik, and S. Gürbuz, "Application of a 24 ghz fmcw automotive radar for urban target classification", in *Radar Conference, 2014 IEEE*, 2014, pp. 1237–1240.

[4] M. Dudek, I. Nasr, G. Bozsik, *et al.*, "System analysis of a phased-array radar applying adaptive beam-control for future automotive safety applications", *Vehicular Technology, IEEE Transactions on*, vol. 64, no. 1, pp. 34–47, 2015.

[5] Razavi, "Design considerations for direct-conversion receivers", *IEEE Transactions on Circuits and Systems II: Analog and Digital Signal Processing*, vol. 44, no. 6, pp. 428–435, 1997.

[6] M. Barati and M. Yavari, "A highly linear mixer with inherent balun using a new technique to remove common mode currents", *Proceedings - IEEE International Symposium on Circuits and Systems*, pp. 1884–1887, 2011.

[7] M. Rudolph and F. Bonani, "Low-frequency noise in nonlinear systems", *Microwave Magazine, IEEE*, vol. 10, no. 1, pp. 84–92, 2009.

[8] J. Babcock, B. Loftin, P. Madhani, *et al.*, "Comparative low frequency noise analysis of bipolar and mos transistors using an advanced complementary bicmos technology", in *Custom Integrated Circuits, 2001, IEEE Conference on.*, 2001, pp. 385–388.

[9] S. A. Maas, *Microwave Mixers*, Second. Artec House, 1993.

[10] R. M. Rassel, J. B. Johnson, B. A. Orner, *et al.*, "Schottky barrier diodes for millimeter wave sigebicmos applications", *PROCEEDINGS OF THE 2006 BIPOLAR/BICMOS CIRCUITS AND TECHNOLOGY MEETING*, pp. 255–258, 2006.

[11] (2014). Ihp website, [Online]. Available: `http://www.ihp-microelectronics.com`.

[12] S. Yang, H. Forstner, G. Haider, *et al.*, "A low noise, high gain, highly linear mixer for 77 ghz automotive radar applications in sige:c bipolar technology", *Proceedings of ESSCIRC*, pp. 312–315, 2009.

[13] Darabi and Chiu, "A noise cancellation technique in active rf-cmos mixers", *IEEE Journal of Solid-State Circuits*, vol. 40, no. 12, pp. 2628–2632, 2005.

[14] U. Alvarado, R. Berenguer, I. Adín, *et al.*, "Low-frequency noise analysis and minimization in gilbert-cell-based mixers for direct-conversion (zero-if) low-power front-ends", *International Journal of Circuit Theory and Applications*, vol. 38, no. 2, pp. 123–129, 2010.

[15] S. Chehrazi, R. Bagheri, and A. Abidi, "Noise in passive fet mixers: a simple physical model", *Proceedings of the Custom Integrated Circuits Conference*, pp. 375–378, 2004.

[16] Margraf and Boeck, "Analysis and modeling of low-frequency noise in resistive fet mixers", *IEEE Transactions on Microwave Theory and Techniques*, vol. 52, no. 7, pp. 1709–1718, 2004.

[17] S. Yamada, O. Boric-Lubecke, and V. M. Lubecke, "Cancellation techniques for lo leakage and dc offset in direct conversion systems", *IEEE MTT-S International Microwave Symposium digest*, pp. 1191–1194, 2008.

[18] K. S. Ang, I. D. Robertson, K. Elgaid, and I. G. Thayne, "40 to 90 GHz impedance-transforming CPW Marchand balun", *IEEE MTT-S International Microwave Symposium digest*, vol. 2, pp. 1141–1144, 2000.

[19] X. Miao, W. Zhang, Y. Geng, *et al.*, "Design of compact frequency-tuned microstrip balun", *IEEE Antennas and Wireless Propagation Letters*, vol. 9, pp. 686–688, 2010.

[20] C.-H. Tseng and Y.-C. Hsiao, "A new broadband marchand balun using slot-coupled microstrip lines", *IEEE Microwave and Wireless Components Letters*, vol. 20, no. 3, pp. 157–159, 2010.

[21] J.-C. Lu, C.-C. Lin, and C.-Y. Chang, "Exact synthesis and implementation of new high-order wideband marchand baluns", *IEEE Transactions on Microwave Theory and Techniques*, vol. 59, no. 1, pp. 80–86, 2011.

[22] T. Johansen and V. Krozer, "Analysis and design of lumped element marchand baluns", in *2008 MIKON CONFERENCE PROCEEDINGS*, IEEE, 2008, 672–675.

[23] M.-J. Chiang, H.-S. Wu, and C.-K. Tzuang, "A compact cmos marchand balun incorporating meandered multilayer edge-coupled transmission lines", *IEEE MTT-S International Microwave Symposium digest*, pp. 125–128, 2009.

[24] C.-I. Shie, Y.-H. Pan, K.-S. Chin, and Y.-C. Chiang, "A miniaturized microstrip balun constructed with two $\lambda/8$ coupled lines and a redundant line", *IEEE Microwave and Wireless Components Letters*, vol. 20, no. 12, pp. 663–665, 2010.

[25] L. Xu, H. Sjoland, M. Tormanen, *et al.*, "A miniaturized marchand balun in cmos with improved balance for millimeter-wave applications", *IEEE Microwave and Wireless Components Letters*, vol. 24, no. 1, 2014.

[26] H. Ma, S. J. Fang, F. Lin, and H. Nakamura, "Novel active differential phase splitters in rfic for wireless applications", *IEEE Transactions on Microwave Theory and Techniques*, vol. 46, no. 12, pp. 2597–2603, 1998.

[27] L. Boglione and J. Goodman, "Analysis of tunable marchand baluns", in *Radio Frequency Integrated Circuits Symposium, 2014 IEEE*, 2014, pp. 115–118.

[28] A. Chen, A.-V. Pham, and R. Leoni, "A novel broadband even-mode matching network for marchand baluns", *IEEE Transactions on Microwave Theory and Techniques*, vol. 57, no. 12, pp. 2973–2980, 2009.

[29] D. A. A. Mat, R. K. Pokharel, R. Sapawi, H. Kanaya, and K. Yoshida, "60 GHz-band on-chip marchand balun designed on flat and patterned ground shields for milimeter-wave 0.18 μm cmos technology", *Proceedings of the Asia-Pacific Microwave Conference 2011*, pp. 884–887, 2011.

[30] V. Issakov, H. Knapp, M. Wojnowski, A. Thiede, and W. Simburger, "A 22-39 ghz passive mixer in sige:c bipolar technology", in *Microwave Symposium Digest (MTT), 2010 IEEE MTT-S International*, 2010, pp. 1012 –1015.

[31] T. K. Johansen and V. Krozer, "A 38 to 44ghz sub-harmonic balanced hbt mixer with integrated miniature spiral type marchand balun", *Electromagnetic Waves (Progress in electromagnetics research)*, vol. 135, pp. 317–330, 2013.

[32] K. S. Ang, Y. C. Leong, and C. H. Lee, "Analysis and design of miniaturized lumped-distributed impedance-transforming baluns", *Microwave Theory and Techniques, IEEE Transactions on*, vol. 51, no. 3, pp. 1009 –1017, 2003.

[33] Z.-Y. Zhang, Y.-X. Guo, L. Ong, and M. Y. W. Chia, "A new planar marchand balun", in *Microwave Symposium Digest, 2005 IEEE MTT-S International*, 2005, 4 pp.–.

[34] Y.-C. Lee, C.-M. Lin, S.-H. Hung, *et al.*, "A broadband doubly balanced monolithic ring mixer with a compact intermediate frequency (if) extraction", *Progress In Electromagnetics Research Letters*, vol. 20, pp. 175–184, 2011.

[35] S. A. Maas, *Nonlinear Microwave and RF Circuits*, Second. Artec House, 2003.

[36] F.-H. Huang, S.-W. Lin, P.-Y. Ke, and H.-C. Chiu, "A wide bandwidth v-band balanced resistive mixer with a miniature meandering balun", *Microwave and Optical Technology Letters*, vol. 55, no. 3, pp. 547–550, 2013.

[37] C. Song, O. Boric-Lubecke, and I. Lo, " 0.18-μm cmos wideband passive mixer", *Microwave and Optical Technology Letters*, vol. 55, no. 1, pp. 23–27, 2013.

[38] M. Abramowitz and I. Stegun, *Handbook of Mathematical Functions*. Dover Publications, 1968, p. 1046.

[39] Y. Wang, J. S. Duster, K. T. Kornegay, H. Park, and J. Laskar, "An 18 ghz low noise high linearity active mixer in sige", *Proceedings - Ieee International Symposium on Circuits and Systems, Proc Ieee Int Symp Circuits Syst*, pp. 3243–3246, 2005.

[40] M. Sudow, K. Andersson, P.-A. Nilsson, and N. Rorsman, "A highly linear double balanced schottky diode s-band mixer", *IEEE MICROWAVE AND WIRELESS COMPONENTS LETTERS*, vol. 16, no. 6, pp. 336–338, 2006.

[41] S. P. Voinigescu, *High-Frequency Integrated Circuits*. Cambridge University Press, 2013.

[42] T. Jensen, V. Zhurbenko, V. Krozer, and P. Meincke, "Coupled transmission lines as impedance transformer", *IEEE Transactions on Microwave Theory and Techniques*, vol. 55, no. 12, pp. 2957–2965, 2007.

[43] J. Reed and G. Wheeler, "A method of analysis of symmetrical four-port networks", *IRE Transactions on Microwave Theory and Techniques*, vol. 4, no. 4, pp. 246–252, 1956.

[44] D. M. Pozar, *Microwave Engineering*, Second. John Wiley & Sons, Inc., 1998.